CELLULAR AND MOLECULAR MECHANISMS OF ARRHYTHMIAS IN CARDIAC FIBROSIS AND BEYOND:

FROM SYMPTOMS TO SUBSTRATES TOWARDS SOLUTIONS

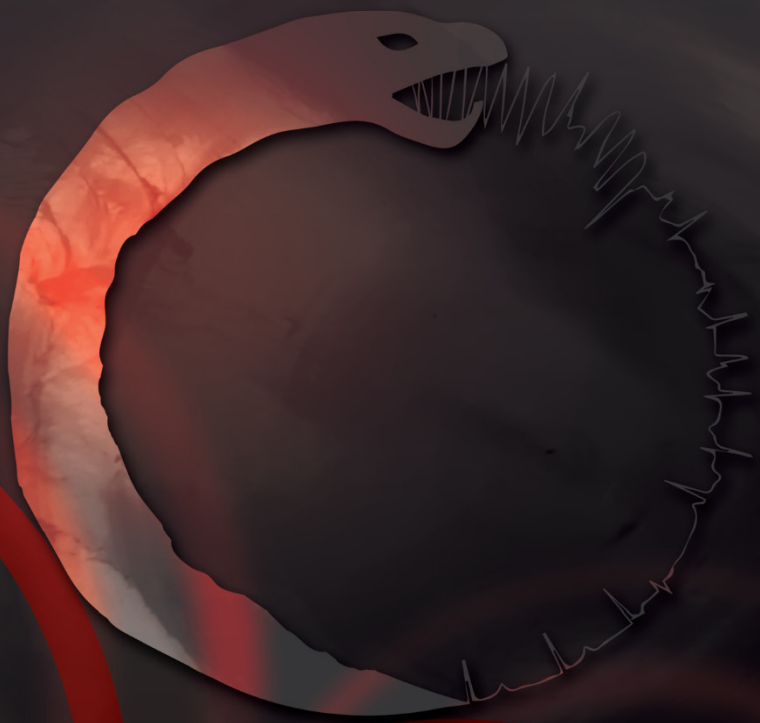

Saïd F.A. Askar

Cellular and Molecular Mechanisms of Arrhythmias in Cardiac Fibrosis and Beyond:

From Symptoms to Substrates towards Solutions

S.F.A. Askar

Colophon

The studies described in this thesis were performed at the department of Cardiology of the Leiden University Medical Center, Leiden, the Netherlands.

Thesis, Leiden University, the Netherlands

ISBN: 978-90-9027761-5
Layout: S.F.A. Askar
Cover-design: Samira Sery

Cellular and Molecular Mechanisms of Arrhythmias in Cardiac Fibrosis and Beyond:

From Symptoms to Substrates towards Solutions

PROEFSCHRIFT

Ter verkrijging van

de graad van doctor aan de Universiteit Leiden,

op gezag van Rector Magnificus prof. mr. C.J.J.M. Stolker,

volgens besluit van het College voor Promoties

te verdedigen op 11 december 2013

klokke 16:15 uur

door

Saïd Fathy Abbas Askar

Geboren te Den Haag

In 1986

Promotiecommissie:

Promotor:

Prof. Dr. M.J. Schalij

Co-Promotor:

Dr. D.A. Pijnappels

Leden:

Dr. A.A.F. de Vries

Prof. Dr. K. Zeppenfeld

Prof. Dr. H.V.M. van Rijen (Universiteit Utrecht)

Financial support by the Netherlands Heart Foundation (2008/B119) for the studies described in this thesis is gratefully acknowledged.

Financial support from Scimedia and Greiner Bio-One for the publication of this thesis is gratefully acknowledged.

Contents

Cellular and Molecular Mechanisms of Arrhythmias in Cardiac Fibrosis and Beyond:
From Symptoms to Substrates towards Solutions

Chapter I

General Introduction

Background

Cardiac disease is a leading cause of morbidity and mortality throughout the world. Strongly represented among these diseases is structural heart disease that disrupts the normally highly organized 3-dimensional cardiac architecture as well as the electrophysiological functioning of the main cardiac functional unit, the cardiomyocyte (CMC). Adequate cardiac function relies on very tight regulation of structural organization and electrophysiology and concomitantly, a significant disruption of these parameters predisposes towards potentially lethal arrhythmias that are a major cause of sudden death. Due to the lethality and burden of arrhythmias, time, effort nor money have been spared to invent and improve therapeutic strategies to prevent and treat cardiac arrhythmias. Anti-arrhythmic drugs were among the first strategies to emerge and more recently, more sophisticated anti-arrhythmic strategies have surfaced, such as implantable defibrillators and radiofrequency catheter ablation. To an extent, these efforts have been successful in reducing the incidence of arrhythmia-related sudden cardiac death by focusing on symptomatic treatment, namely treatment for the arrhythmia itself. However, the incomplete understanding of pro-arrhythmic mechanisms and suboptimal anti-arrhythmic efficacy emphasize the necessity of investigating the underlying disease process, pro-arrhythmic mechanisms and substrate to be able to treat patients more adequately in the future. As cardiac arrhythmias are highly complex phenomena, its components need to be dissected and individually studied to increase our understanding of pro-arrhythmic mechanisms and accordingly, develop novel, more effective anti-arrhythmic strategies. To accomplish such a task, it is important to comprehend the basics of cardio-electrophysiology.

Basics of Cardiac Electrophysiology

For adequate cardiac function, rhythmic contraction and forceful extrusion of blood is achieved through careful structural organization of sequential contraction.[1] Contraction of CMCs is accomplished by a process termed excitation-contraction coupling, and the electrical cascades known as action potentials that are responsible for initiating, coordinating and regulating this process therefore lie at the core of cardiac function.[2]

The action potentials are in turn mediated by voltage-gated ion channels that allow selective passage of their respective an- or cat-ionic currents across the cellular membrane down their electrochemical gradient.[3] [4]The voltage difference across

the cellular membrane is the key regulating element of the conductance of these voltage-gated ion channels and is thereby the driving force of the cardiac action potential. By subtle changes in the trans-membrane voltage, ion channel activation and inactivation ports can rapidly change their confirmation, which alters conductance of the ion channel and subsequently changes ionic currents and the transmembrane voltage.[5] This in turn influences the conductance of other ion channels and their respective ionic currents, giving rise to an electrical cascade known as an action potential. To coordinate CMC contraction throughout the entire heart, action potentials need to be propagated between CMCs through gap-junctions.[6] These gap-junctions consist of hexameres of proteins called connexins that form transmembrane hemichannels (connexons) that connect to connexons of neighboring cells.[7-9]

Such gap-junctions may consist of different subtypes of connexins, of which the expression levels are tissue and site-specific to allow for specific modulation of conduction. In mammalian hearts, ventricles mainly express Cx43 and Cx45, whereas Cx40, Cx43 and Cx45 are mainly found in the atria and conduction system.[10] [11] Each of these subtypes has its own conductance for cat- or anions and low-molecular weight compounds below 1kDa, and responds differently to environmental changes which allows for complex biophysical behavior and modulation of cardiac action potential propagation.[12,13] CMCs are generally connected by gap-junctions in a head-to-tail fashion at intercalated discs that contain a high concentration of proteins involved in intercellular communications. Although CMCs express very high levels of connexins, other cardiac cell types such as fibroblasts also express connexins, albeit in lower quantities.[14,15] Gap-junctions are essential in intercellular communication and apart from action potential propagation, have been shown to be involved in regulation of other biological processes, such as cellular differentiation and embryonic development.[16,17] To overcome the high resistance posed by cellular membranes, gap-junctions form low-resistance intercellular channels that allow passage of ions and small molecules (<1 kDa). The resistance provided by the intercalated discs roughly approximates that of the CMC cytosol.[18] Due to rapid Na^+ influx during excitation, intracellular [Na+] rises and may therefore pass to neighboring, unexcited CMCs cells that are connected by gap-junctions. This passage of Na^+ ions can depolarize the coupled unexcited CMC beyond the excitation threshold and evoke excitation in this cell, thereby realizing action potential propagation.

Through these gap-junctions, diffusion of ions occurs from the activated CMC, e.g. the source, to a coupled, resting CMC, e.g. the sink. As long as the electrical charge delivered by the source exceeds the charge required by the coupled CMC to become excited, propagation will be successful or otherwise stated the safety factor of conduction exceeds 1.[19] For cellular excitability, its capacitance that is mainly determined by cell size, its expression level of ion channels, their functional states as well as the resting membrane potential are crucial determinants. Source-sink mismatch that may cause the safety factor of conduction to fall below 1 at which conduction fails may develop by a myriad of permutations of the above mentioned factors that may exist in the source or sink cell. Without excitability of sink-cells, passive electrotonic propagation is slow and does not reach beyond 300 µm.[20] It is therefore no surprise that sodium channel expression in CMCs is highest near intercalated discs, to ensure that depolarization by Na^+ influx from an adjacent, coupled cell is sensed and responded upon as quickly as possible to maintain fast conduction.[21] Furthermore, while gap-junctional coupling can be reduced by 70% without affecting conduction velocity, even slightly reducing I_{na} slows conduction.[19,22] Beside the implications of a vast gap-junctional reserve, this also emphasizes the importance of excitability in maintaining fast conduction that in turn, is essential for proper sequential cardiac activation and contraction. Inversely, it is well established that slow conduction is a feature that predisposes towards heart rhythm disturbances known as arrhythmias.[6,18]

Arrhythmias

Cardiac electrophysiology is a complex phenomenon organized at the molecular, cellular, 2- and 3-dimensional tissue level. Therefore, alterations at any of these levels can disrupt cardiac electrophysiology and predispose towards arrhythmias. Arrhythmias comprise a wide range of conditions, each of which confers a disturbance of atrial or ventricular contraction rate. Although sinus bradycardia or tachycardia are a cause of morbidity, the most dangerous are the tachyarrhythmias that do not originate from the sinus node and exhibit exceptionally high activation frequencies that preclude diastolic filling of the atria or ventricles, which thereby may cause stroke, hemodynamic instability and sudden cardiac death. These tachyarrhythmias can be based on multiple patterns of activation, being focal, reentrant or fibrillatory.[23]

Focal tachyarrhythmias

Focal tachyarrhythmias are based on an ectopic focus or multiple foci that overrule the sinoatrial node and dominantly activate the myocardium. Clinically, the life-threatening "Torsade des Pointes" is a prime example of such an arrhythmia. A proposed mechanism of these arrhythmias is based on early afterdepolarizations (EADs). [24,25]

An EAD is reactivation of depolarizing force that may occur during phase 2 and phase 3 repolarization of the action potential and represents a potentially detrimental electrophysiological phenomenon.[24,25] Phase-2 EADs are considered to be based on reactivation of L-type calcium channels due to slow repolarization that allows the channels to de-inactivate and subsequently reactivate as the membrane voltage lingers within the so-called "window current".[26] If the criteria for a balance between de-inactivation and activation are met, this can lead to perpetual oscillations in membrane voltage and lead to a sustained focal tachyarrhythmia. Phase-3 EADs depend on Nav1.5-based mechanisms of reactivation and may play a role in EADs that are evoked by structural heterogeneity.[27] Since EADs typically occur before full repolarization, excitability is not fully recovered and therefore conduction is slowed. Moreover, apart from the decreased depolarizing force supplied by an EAD compared to normal action potentials, the downstream myocardium (sink) typically has not fully repolarized and therefore may be more difficult to excite. These changes in source and sink during EADs may therefore lead to a source-sink mismatch which may cause propagation to fail if these EADs are not generated in a synchronous fashion by sufficient amounts of CMCs. [28,29]

Thereby, heterogeneity of repolarization time throughout the cardiac tissue causes zones of conduction block, while other sites are able to propagate the EAD due to more favorable source-sink relationships because of shorter refractory periods that even in healthy hearts differ between different zones of myocardium.[30,31] This increased dispersion of repolarization is a feature that strongly predisposes towards arrhythmias.[32] As a result of increased dispersion of repolarization, unidirectional conduction block may develop, which forces activation in one direction around a refractory area that now functions as a non-conducting obstacle. If repolarization of the refractory area occurs while the activating wave front moves around this area, such critical timing would allow for the initiation of circular or reentrant activation, in which the activating front would chase its repolarizing tail.[18]

Reentrant tachyarrhythmias

Reentrant excitation is a long known phenomenon that is highly relevant to cardiac electrophysiology, as reentry is an often observed propagation pattern of tachyarrhythmias.[33] During reentry, there is a constant spatial interaction between depolarization and repolarization that is crucial for the sustainability, stability and cycle length of the arrhythmia. Although reentry was first considered to mostly rely on anatomic pathways that facilitate circular conduction such as post-myocardial infarction scars or around the pulmonary veins,[34,35] reentry was also shown to be able to exist without anatomical obstructions, giving rise to the term "functional" reentry.[36] It was later shown that functional reentry takes the form of an Archimedean spiral that continuously depolarizes the cardiac tissue.[37] The continuous depolarization is maximal at the pivot point of reentry, or core that is therefore nonexcitable[38], and decreases towards the periphery.[39,40] Since functional reentry does not rely on anatomical fixation, such reentry may meander throughout the tissue which gives rise to polymorphic electrograms.[41] Inversely, anatomical reentry is mostly considered as a highly stable form of reentry that manifests itself with a monomorphic appearance on electrograms. Although it is tempting to view functional and anatomic reentry as separate phenomena, it is becoming increasingly clear that both phenomena exist at the edges of a spectrum of reentrant arrhythmias that may often exhibit features of both reentry types. This is illustrated by the observation that functional reentrant arrhythmias can pin to anatomic obstructions.[42]

Further adding to the complexity of reentrant arrhythmias is the possible presence of multiple rotors during arrhythmias. Moreover, focal and reentrant arrhythmias can occur simultaneously during the most complex arrhythmia type known as fibrillation. During fibrillation, complex interactions between multiple activating wave fronts cause a polymorphic aspect of electrograms. But despite the seemingly chaotic nature of fibrillation, its organization is still based on spatial and temporal availability of the electrophysiological function cardiac tissue.[43]As a result, slow conduction and refractory state of cardiac tissue are key elements that modulate the time windows for multiple activation fronts to interact and predispose towards reentrant arrhythmias.[44] Therefore, these parameters are often targeted in anti-arrhythmic strategies.

Current treatment of arrhythmias

The primary tool against arrhythmias has been symptomatic treatment by pharmacological modulation of ion channel function. Most of these anti-arrhythmic drugs exhibit an ion-channel blocking function and have been categorized according to the Singh Vaughan Williams classification.[45] These agents can block Na^+ channels, K^+ and Ca^{2+} channels, which slows conduction, prolongs refractory periods or shortens refractory periods, respectively. Interestingly, despite a predictably pro-arrhythmic effect of conduction slowing by Na^+ channel blockade, anti-arrhythmic effects of such pharmacological interventions can be observed, which may be explained by attenuation of phase-3 EADs by blockade of the late sodium current. [46,47] Moreover, sodium channel blockade may induce drift of reentrant tachyarrhythmias which may terminate these arrhythmias should the arrhythmia encounter unexcitable borders of cardiac tissue. [42,48] Potassium channel is known to prolong the refractory period of cardiac tissue and thereby decrease the propensity towards reentrant arrhythmias as reentry needs a refractory period that is short enough to favor reentrant excitation.[18,49] However, prolongation of action potential duration can be pro-arrhythmic by predisposing towards EADs and increased complexity of reentrant arrhythmias.[50,51] Blockade of L-type calcium channels was also reported to yield anti-arrhythmic effects in context of acute myocardial infarctions,[52] but its effects on vascular tone and inotropy make it an undesirable agent for a large portion of patients with pro-arrhythmic substrates, that often also suffer from mechanical cardiac dysfunction and are prone to become hemodynamically comprised.[53] As all of these pharmacological agents can have either anti- or pro-arrhythmic effects, it is unfortunately unsurprising that their therapeutic efficacy at preventing sudden cardiac death is disappointingly low.[54] Such results may be explained by our incomplete understanding of pro-arrhythmic mechanisms, and provided incentive to invent different anti-arrhythmic interventions, such as the Implantable Cardioverter-Defibrillator (ICD). This implanted device monitors heart rhythm and rate and delivers electrical shocks or anti-tachy pacing to terminate arrhythmias should it detect abnormal heart rates. While effective at preventing sudden cardiac death, it constitutes a purely symptomatic treatment that does not positively affect the underlying pro-arrhythmic mechanisms. [55,56] Moreover, shocks are experienced as very stressful by patients and inappropriate shocks remain an issue with potentially lethal effects.[57,58] In addition, recurrent ventricular arrhythmias remain a problem.[59] Therefore, a technique that aims to more specifically target the underlying pro-arrhythmic substrate instead of symptoms known as radio-frequency catheter ablation was developed. During such a procedure, the aim is to damage pro-

arrhythmic tissue and prevent recurrence of arrhythmias.[60] This technique has very strong anti-arrhythmic potential, especially in arrhythmias with a clear anatomical substrate such as Wolff-Parkinson-White syndrome or post myocardial infarction.[61,62] However, high success rates are often achieved by multiple procedures.[63] Moreover, due to the invasiveness of the technique it is prone to serious complications such as cardiac perforation.[64] Although radiofrequency catheter ablation selectively targets pro-arrhythmic tissue and thereby positively affects the underlying pro-arrhythmic substrate, it does not selectively target underlying pro-arrhythmic mechanisms. By furthering our understanding of pro-arrhythmic mechanisms of underlying substrates, we may be able to increase therapeutic efficacy even further without resorting to damaging cardiac tissue to stop and prevent arrhythmias.

Pro-arrhythmic substrates as anti-arrhythmic targets

As adequate cardiac electrophysiology relies on structural integrity and optimal ion channel functionality of CMCs, it is easily conceivable that a change in any of these parameters have pro-arrhythmic consequences. The most clearly identifiable pro-arrhythmic substrates of cardiac arrhythmias lie in the domain of the genetically inherited channelopathies, which are based on mutations in ion channel genes that affect the functionality of the associated translated protein.[65] As there are a myriad of ion channel genes, the patient population affected by these channelopathies is highly heterogeneous and may require different treatments depending on the particular mutation.[66] However, most arrhythmia-prone patients do not suffer from such a clear etiology of pro-arrhythmia, as a substantially larger group of patients suffer from arrhythmias due to genetic or acquired structural cardiac disease.[67] Cardiac hypertrophy, the adaptive response of CMCs to increase their size and number of sarcomeres to compensate altered pressure and strain profiles, is not widely associated with arrhythmias if hypertrophy is adequate and physiologic.[68] However, this adaptive response may become maladaptive or pathological hypertrophy, which is marked by re-initiated activity of the fetal gene program and predisposition for arrhythmias.[69-72] Pathological hypertrophy is the result of a response that fails to properly compensate the change in cell size with increased ion channel expression and other necessary electrophysiological alterations and can result in altered CMC excitability and action potential characteristics. [73-75] In addition, changes in connexin expression levels and distributions from head-to-tail connections at intercalated discs to a more side-to-side distribution can significantly affect conduction.[76,77] Moreover, hypertrophic CMCs have been shown

to be vulnerable to formation of EADs.[78] As a result, electrical remodeling that occurs in structural cardiac disease predisposes to cardiac arrhythmias, although its exact pro-arrhythmic mechanisms are still unclear. [79] Therefore, targeting mechanisms to prevent or reverse hypertrophy may prove to also be an anti-arrhythmic strategy.[80]

A factor that further complicates our understanding of the pro-arrhythmic mechanisms of pathological hypertrophy is the often coinciding fibrosis, which consists of an increase in the amount of fibroblasts and excessive extracellular matrix deposition. Fibrosis is a healing process that occurs in response to injury and is strongly associated with arrhythmias.[81-84] Since cellular proliferation and differentiation are opposite phenomena in biology, the highly differentiated phenotype of CMCs precludes any adequate amount of proliferation of these cells, even in response to injury.[85,86] When injurious stimuli occur, fibroblasts switch their phenotype to the phenotype of myofibroblast (MFB), a proliferative and secretory cell type. These injurious stimuli can be of chemical or mechanical nature. In normal hearts, mechanical stimuli do not reach the fibroblasts that are interspersed in the stable matrix network. However, disruption of the structural integrity of the heart, strong immune response or altered myocardial strain exposes the fibroblasts to mechanical or chemical stress that can activate them to become MFBs.[82,87] Then, MFBs secrete increased amounts of ECM to compensate the mechanical stress or loss of myocardium. As a result, loss of CMCs or CMC functionality is compensated by fibrosis to maintain structural integrity to such a degree that it even prevents cardiac rupture after myocardial infarction.[88] While beneficial at first, the increased thickness of the collagen fibers effectively separate cell-cell contacts between cardiomyocytes and may therefore disrupt slow or even block conduction by increasing intercellular resistance. Indeed, the increased matrix deposition in fibrosis has been shown to be cause pro-arrhythmic conduction slowing through zigzag courses that force conduction along a longer path of activation, thereby increasing myocardial activation times and increasing the propensity towards arrhythmias.[89] Moreover, interspersion of fibroblasts between CMCs may also contribute to anatomical mechanisms of conduction slowing.[90] In addition to the anatomically based pro-arrhythmic mechanisms of fibrosis, recent evidence suggests that the phenotypical switch to MFBs may cause them to modulate CMC electrophysiology more directly.[91] More specifically, this is suggested to be mediated through heterocellular gap-junctional coupling that may slow conduction, induce ectopic activity and predispose towards reentrant arrhythmias. [20,92-94] Paracrine-[95] and mechanical coupling mediated[96,97] pro-

arrhythmic mechanisms of MFBs further complicate the pro-arrhythmic substrate of fibrosis. More importantly, this complexity hampers our understanding and the development of more effective treatment strategies against fibrosis-associated arrhythmias. Therefore, investigation and targeting of substrate-specific pro-arrhythmic mechanisms may provide a powerful future anti-arrhythmic strategy against prevalent fibrosis-associated arrhythmias.

Aim and Outline of Thesis

To be able to more effectively treat arrhythmias, it is essential to comprehend the complexity of cardiac electrophysiology and its relation to cardiac structure as discussed in **Chapter I**.

Therefore, the aim of this thesis was to develop and utilize *in vitro* models of pro-arrhythmic substrates to investigate their pro-arrhythmic mechanisms to provide a rationale for future substrate-oriented anti-arrhythmic and preventive strategies.

In cardiac fibrosis, a dramatic increase in MFBs by proliferation occurs. As MFBs are key players in highly pro-arrhythmic fibrosis, limiting their numbers may counteract pro-arrhythmic effects of fibrosis. Therefore, it is tested in **Chapter II** whether anti-proliferative treatment of MFBs may confer anti-arrhythmic effects in an *in vitro* model of fibrosis with proliferating fibroblasts in cardiac cultures.

After attainment of the MFBs phenotype, these cells express relatively high amounts of Cx43.[91] In addition, MFBs have been shown to be pro-arrhythmic in cardiac cultures and have been demonstrated to electrically couple to CMCs. **Chapter III** is therefore an investigation of the anti-arrhythmic effects of Cx43 down regulation in MFBs.

Cardiac pathophysiology is a complex agglomerate of several processes that try to compensate structural or functional changes of the myocardium. As such, cardiac fibrosis and hypertrophy often coincide. As a result, no distinction can be made between fibrosis- and hypertrophy specific mechanisms. Therefore, **Chapter IV** set out to investigate differences between pro-arrhythmic mechanisms of fibrosis and of hypertrophy, and how this may influence anti-arrhythmic strategies.

Adequate pharmacological treatment of arrhythmias remains difficult due to its high complexity and potential lack of specificity of the drugs. Although action potential duration is a common parameter to increase to terminate reentrant arrhythmias, its efficacy may provide contradictory results. Therefore, **Chapter V** aimed to investigate the effect of the minimal action potential duration in an *in vitro* and *ex vivo* model of fibrillation and how it can be utilized to destabilize and terminate reentrant arrhythmias using a wide arrangement of pharmacological agents.

Cardiac fibrosis is a process that is initiated after loss of CMCs, due to their poor proliferative capability. Therefore, regenerative medicine has focused on replenishing these lost CMCs or enhancing survival and cardiac function with an external cell source. Although mesenchymal stem cells (MSCs) show limited capability to differentiate towards CMCs, their therapeutic use in cardiac fibrosis is gaining increasing attention and more focus is placed on increasing the amount of transplanted MSCs to maximize their therapeutic potential. However, due to the complexity involved in transplanting and integrating stem cells into the heart, potentially pro-arrhythmic consequences may arise by increasing the number of MSCs transplanted. Therefore, **Chapter VI** set out to investigate the pro-arrhythmic effects and mechanisms of MSC engraftment pattern and amount.

In **Chapter VII**, a novel method to limit fibroblast arrhythmogeneity was investigated. As fibroblasts may be pro-arrhythmic by several mechanisms, anti-arrhythmic reprogramming was attempted by forcing heterocellular fusion between human ventricular scar fibroblasts and neonatal rat cardiomyocytes.

To selectively target cell-type specific pro-arrhythmic mechanisms is difficult without also unintentionally modifying other cardiac cell types. Therefore, adeno-associated-viral vectors were developed that selectively force transgene expression in either the cardiomyocyte or the fibroblast in **Chapter VIII**.

In conclusion, **Chapter IX** summarizes the findings of this thesis. Moreover, results are discussed and placed in future perspectives.

References

1. Buckberg G, Hoffman JI, Mahajan A, Saleh S, Coghlan C. Cardiac mechanics revisited: the relationship of cardiac architecture to ventricular function. *Circulation*. 2008;118:2571-2587.

2. Bers DM. Cardiac excitation-contraction coupling. *Nature*. 2002;415:198-205.

3. HODGKIN AL and HUXLEY AF. Currents carried by sodium and potassium ions through the membrane of the giant axon of Loligo. *J Physiol*. 1952;116:449-472.

4. Roden DM, Balser JR, George AL, Jr., Anderson ME. Cardiac ion channels. *Annu Rev Physiol*. 2002;64:431-475.

5. Bezanilla F. The voltage sensor in voltage-dependent ion channels. *Physiol Rev*. 2000;80:555-592.

6. Gutstein DE, Morley GE, Tamaddon H, Vaidya D, Schneider MD, Chen J, Chien KR, Stuhlmann H, Fishman GI. Conduction slowing and sudden arrhythmic death in mice with cardiac-restricted inactivation of connexin43. *Circ Res*. 2001;88:333-339.

7. Caspar DL, Goodenough DA, Makowski L, Phillips WC. Gap junction structures. I. Correlated electron microscopy and x-ray diffraction. *J Cell Biol*. 1977;74:605-628.

8. Makowski L, Caspar DL, Phillips WC, Goodenough DA. Gap junction structures. II. Analysis of the x-ray diffraction data. *J Cell Biol*. 1977;74:629-645.

9. Unwin PN and Zampighi G. Structure of the junction between communicating cells. *Nature*. 1980;283:545-549.

10. Davis LM, Kanter HL, Beyer EC, Saffitz JE. Distinct gap junction protein phenotypes in cardiac tissues with disparate conduction properties. *J Am Coll Cardiol*. 1994;24:1124-1132.

11. Beauchamp P, Yamada KA, Baertschi AJ, Green K, Kanter EM, Saffitz JE, Kleber AG. Relative contributions of connexins 40 and 43 to atrial impulse propagation in synthetic strands of neonatal and fetal murine cardiomyocytes. *Circ Res*. 2006;99:1216-1224.

12. Rackauskas M, Kreuzberg MM, Pranevicius M, Willecke K, Verselis VK, Bukauskas FF. Gating properties of heterotypic gap junction channels formed of connexins 40, 43, and 45. *Biophys J*. 2007;92:1952-1965.

13. Rohr S. Role of gap junctions in the propagation of the cardiac action potential. *Cardiovasc Res*. 2004;62:309-322.

14. Rook MB, Jongsma HJ, de JB. Single channel currents of homo- and heterologous gap junctions between cardiac fibroblasts and myocytes. *Pflugers Arch*. 1989;414:95-98.

15. Camelliti P, Green CR, Kohl P. Structural and functional coupling of cardiac myocytes and fibroblasts. *Adv Cardiol*. 2006;42:132-149.

16. Ramkisoensing AA, Pijnappels DA, Swildens J, Goumans MJ, Fibbe WE, Schalij MJ, de Vries AA, Atsma DE. Gap junctional coupling with cardiomyocytes is necessary but not sufficient for cardiomyogenic

differentiation of cocultured human mesenchymal stem cells. *Stem Cells*. 2012;30:1236-1245.

17. Reaume AG, de Sousa PA, Kulkarni S, Langille BL, Zhu D, Davies TC, Juneja SC, Kidder GM, Rossant J. Cardiac malformation in neonatal mice lacking connexin43. *Science*. 1995;267:1831-1834.

18. Kleber AG and Rudy Y. Basic mechanisms of cardiac impulse propagation and associated arrhythmias. *Physiol Rev*. 2004;84:431-488.

19. Shaw RM and Rudy Y. Ionic mechanisms of propagation in cardiac tissue. Roles of the sodium and L-type calcium currents during reduced excitability and decreased gap junction coupling. *Circ Res*. 1997;81:727-741.

20. Gaudesius G, Miragoli M, Thomas SP, Rohr S. Coupling of cardiac electrical activity over extended distances by fibroblasts of cardiac origin. *Circ Res*. 2003;93:421-428.

21. Cohen SA. Immunocytochemical localization of rH1 sodium channel in adult rat heart atria and ventricle. Presence in terminal intercalated disks. *Circulation*. 1996;94:3083-3086.

22. Shaw RM and Rudy Y. Electrophysiologic effects of acute myocardial ischemia. A mechanistic investigation of action potential conduction and conduction failure. *Circ Res*. 1997;80:124-138.

23. Pogwizd SM, Hoyt RH, Saffitz JE, Corr PB, Cox JL, Cain ME. Reentrant and focal mechanisms underlying ventricular tachycardia in the human heart. *Circulation*. 1992;86:1872-1887.

24. Cranefield PF and Aronson RS. Torsades de pointes and early afterdepolarizations. *Cardiovasc Drugs Ther*. 1991;5:531-537.

25. Cranefield PF and Aronson RS. Torsade de pointes and other pause-induced ventricular tachycardias: the short-long-short sequence and early afterdepolarizations. *Pacing Clin Electrophysiol*. 1988;11:670-678.

26. Ypey DL, van Meerwijk WP, Umar S, Pijnappels DA, Schalij MJ, van der Laarse A. Depolarization-induced automaticity in rat ventricular cardiomyocytes is based on the gating properties of L-type calcium and slow Kv channels. *Eur Biophys J*. 2012.

27. Auerbach DS, Grzda KR, Furspan PB, Sato PY, Mironov S, Jalife J. Structural heterogeneity promotes triggered activity, reflection and arrhythmogenesis in cardiomyocyte monolayers. *J Physiol*. 2011;589:2363-2381.

28. Sato D, Xie LH, Sovari AA, Tran DX, Morita N, Xie F, Karagueuzian H, Garfinkel A, Weiss JN, Qu Z. Synchronization of chaotic early afterdepolarizations in the genesis of cardiac arrhythmias. *Proc Natl Acad Sci U S A*. 2009;106:2983-2988.

29. Xie Y, Sato D, Garfinkel A, Qu Z, Weiss JN. So little source, so much sink: requirements for afterdepolarizations to propagate in tissue. *Biophys J*. 2010;99:1408-1415.

30. Fedida D and Giles WR. Regional variations in action potentials and transient outward current in myocytes isolated from rabbit left ventricle. *J Physiol*. 1991;442:191-209.

31. Myles RC, Bernus O, Burton FL, Cobbe SM, Smith GL. Effect of activation sequence on transmural patterns of repolarization and action potential duration in rabbit ventricular myocardium. *Am J Physiol Heart Circ Physiol*. 2010;299:H1812-H1822.

32. Baker LC, London B, Choi BR, Koren G, Salama G. Enhanced dispersion of repolarization and refractoriness in transgenic mouse hearts promotes reentrant ventricular tachycardia. *Circ Res*. 2000;86:396-407.

33. Wit AL and Cranefield PF. Reentrant excitation as a cause of cardiac arrhythmias. *Am J Physiol*. 1978;235:H1-17.

34. Rudy Y. Reentry: insights from theoretical simulations in a fixed pathway. *J Cardiovasc Electrophysiol*. 1995;6:294-312.

35. Mehra R, Zeiler RH, Gough WB, el-Sherif N. Reentrant ventricular arrhythmias in the late myocardial infarction period. 9. Electrophysiologic-anatomic correlation of reentrant circuits. *Circulation*. 1983;67:11-24.

36. Allessie MA, Bonke FI, Schopman FJ. Circus movement in rabbit atrial muscle as a mechanism of trachycardia. *Circ Res*. 1973;33:54-62.

37. Pertsov AM, Davidenko JM, Salomonsz R, Baxter WT, Jalife J. Spiral waves of excitation underlie reentrant activity in isolated cardiac muscle. *Circ Res*. 1993;72:631-650.

38. Karagueuzian HS, Athill CA, Yashima M, Ikeda T, Wu TJ, Mandel WJ, Chen PS. Transmembrane potential properties of atrial cells at different sites of a spiral wave reentry: cellular evidence for an excitable but nonexcited core. *Pacing Clin Electrophysiol*. 1998;21:2360-2365.

39. Athill CA, Ikeda T, Kim YH, Wu TJ, Fishbein MC, Karagueuzian HS, Chen PS. Transmembrane potential properties at the core of functional reentrant wave fronts in isolated canine right atria. *Circulation*. 1998;98:1556-1567.

40. Fast VG and Kleber AG. Role of wavefront curvature in propagation of cardiac impulse. *Cardiovasc Res*. 1997;33:258-271.

41. Ikeda T, Yashima M, Uchida T, Hough D, Fishbein MC, Mandel WJ, Chen PS, Karagueuzian HS. Attachment of meandering reentrant wave fronts to anatomic obstacles in the atrium. Role of the obstacle size. *Circ Res*. 1997;81:753-764.

42. Lim ZY, Maskara B, Aguel F, Emokpae R, Jr., Tung L. Spiral wave attachment to millimeter-sized obstacles. *Circulation*. 2006;114:2113-2121.

43. Gray RA, Pertsov AM, Jalife J. Spatial and temporal organization during cardiac fibrillation. *Nature*. 1998;392:75-78.

44. Cranefield PF and Hoffman BF. Reentry: slow conduction, summation and inhibition. *Circulation*. 1971;44:309-311.

45. Nattel S. Antiarrhythmic drug classifications. A critical appraisal of their history, present status, and clinical relevance. *Drugs*. 1991;41:672-701.

46. Persson F, Andersson B, Duker G, Jacobson I, Carlsson L. Functional effects of the late sodium current inhibition by AZD7009 and lidocaine in rabbit isolated atrial and ventricular tissue and Purkinje fibre. *Eur J Pharmacol*. 2007;558:133-143.

47. Morita N, Lee JH, Xie Y, Sovari A, Qu Z, Weiss JN, Karagueuzian HS. Suppression of re-entrant and multifocal ventricular fibrillation by the late sodium current blocker ranolazine. *J Am Coll Cardiol*. 2011;57:366-375.

48. Qu Z and Weiss JN. Effects of Na(+) and K(+) channel blockade on vulnerability to and termination of fibrillation in simulated normal cardiac tissue. *Am J Physiol Heart Circ Physiol*. 2005;289:H1692-H1701.

49. Rensma PL, Allessie MA, Lammers WJ, Bonke FI, Schalij MJ. Length of excitation wave and susceptibility to reentrant atrial arrhythmias in normal conscious dogs. *Circ Res*. 1988;62:395-410.

50. Eckardt L, Haverkamp W, Mertens H, Johna R, Clague JR, Borggrefe M, Breithardt G. Drug-related torsades de pointes in the isolated rabbit heart: comparison of clofilium, d,l-sotalol, and erythromycin. *J Cardiovasc Pharmacol*. 1998;32:425-434.

51. Starmer CF, Romashko DN, Reddy RS, Zilberter YI, Starobin J, Grant AO, Krinsky VI. Proarrhythmic response to potassium channel blockade. Numerical studies of polymorphic tachyarrhythmias. *Circulation*. 1995;92:595-605.

52. Temesy-Armos PN, Legenza M, Southworth SR, Hoffman BF. Effects of verapamil and lidocaine in a canine model of sudden coronary death. *J Am Coll Cardiol*. 1985;6:674-681.

53. Epstein SE and Rosing DR. Verapamil: its potential for causing serious complications in patients with hypertrophic cardiomyopathy. *Circulation*. 1981;64:437-441.

54. Arshad A, Mandava A, Kamath G, Musat D. Sudden cardiac death and the role of medical therapy. *Prog Cardiovasc Dis*. 2008;50:420-438.

55. Moss AJ, Hall WJ, Cannom DS, Daubert JP, Higgins SL, Klein H, Levine JH, Saksena S, Waldo AL, Wilber D, Brown MW, Heo M. Improved survival with an implanted defibrillator in patients with coronary disease at high risk for ventricular arrhythmia. Multicenter Automatic Defibrillator Implantation Trial Investigators. *N Engl J Med*. 1996;335:1933-1940.

56. Bristow MR, Saxon LA, Boehmer J, Krueger S, Kass DA, De MT, Carson P, DiCarlo L, DeMets D, White BG, DeVries DW, Feldman AM. Cardiac-resynchronization therapy with or without an implantable defibrillator in advanced chronic heart failure. *N Engl J Med*. 2004;350:2140-2150.

57. Daubert JP, Zareba W, Cannom DS, McNitt S, Rosero SZ, Wang P, Schuger C, Steinberg JS, Higgins SL, Wilber DJ, Klein H, Andrews ML, Hall WJ, Moss AJ. Inappropriate implantable cardioverter-defibrillator shocks in MADIT II: frequency, mechanisms, predictors, and survival impact. *J Am Coll Cardiol*. 2008;51:1357-1365.

58. van Rees JB, Borleffs CJ, de Bie MK, Stijnen T, van EL, Bax JJ, Schalij MJ. Inappropriate implantable cardioverter-defibrillator shocks: incidence, predictors, and impact on mortality. *J Am Coll Cardiol*. 2011;57:556-562.

59. Borleffs CJ, van EL, Schotman M, Boersma E, Kies P, van der Burg AE, Zeppenfeld K, Bootsma M, van der Wall EE, Bax JJ, Schalij MJ. Recurrence of ventricular arrhythmias in ischaemic secondary prevention implantable cardioverter defibrillator recipients: long-term follow-up of the Leiden out-of-hospital cardiac arrest study (LOHCAT). *Eur Heart J*. 2009;30:1621-1626.

60. Zeppenfeld K and Stevenson WG. Ablation of ventricular tachycardia in patients with structural heart disease. *Pacing Clin Electrophysiol*. 2008;31:358-374.

61. Van Hare GF, Lesh MD, Stanger P. Radiofrequency catheter ablation of supraventricular arrhythmias in patients with congenital heart disease: results and technical considerations. *J Am Coll Cardiol*. 1993;22:883-890.

62. Stevenson WG, Wilber DJ, Natale A, Jackman WM, Marchlinski FE, Talbert T, Gonzalez MD, Worley SJ, Daoud EG, Hwang C, Schuger C, Bump TE, Jazayeri M, Tomassoni GF, Kopelman HA, Soejima K, Nakagawa H. Irrigated radiofrequency catheter ablation guided by electroanatomic mapping for recurrent ventricular tachycardia after myocardial infarction: the multicenter thermocool ventricular tachycardia ablation trial. *Circulation*. 2008;118:2773-2782.

63. Tokuda M, Tedrow UB, Kojodjojo P, Inada K, Koplan BA, Michaud GF, John RM, Epstein LM, Stevenson WG. Catheter ablation of ventricular tachycardia in nonischemic heart disease. *Circ Arrhythm Electrophysiol*. 2012;5:992-1000.

64. Tokuda M, Kojodjojo P, Epstein LM, Koplan BA, Michaud GF, Tedrow UB, Stevenson WG, John RM. Outcomes of cardiac perforation complicating catheter ablation of ventricular arrhythmias. *Circ Arrhythm Electrophysiol*. 2011;4:660-666.

65. Cerrone M and Priori SG. Genetics of sudden death: focus on inherited channelopathies. *Eur Heart J*. 2011;32:2109-2118.

66. Lehnart SE, Ackerman MJ, Benson DW, Jr., Brugada R, Clancy CE, Donahue JK, George AL, Jr., Grant AO, Groft SC, January CT, Lathrop DA, Lederer WJ, Makielski JC, Mohler PJ, Moss A, Nerbonne JM, Olson TM, Przywara DA, Towbin JA, Wang LH, Marks AR. Inherited arrhythmias: a National Heart,

Lung, and Blood Institute and Office of Rare Diseases workshop consensus report about the diagnosis, phenotyping, molecular mechanisms, and therapeutic approaches for primary cardiomyopathies of gene mutations affecting ion channel function. *Circulation*. 2007;116:2325-2345.

67. Roberts R. Genomics and cardiac arrhythmias. *J Am Coll Cardiol*. 2006;47:9-21.

68. Bostrom P, Mann N, Wu J, Quintero PA, Plovie ER, Panakova D, Gupta RK, Xiao C, MacRae CA, Rosenzweig A, Spiegelman BM. C/EBPbeta controls exercise-induced cardiac growth and protects against pathological cardiac remodeling. *Cell*. 2010;143:1072-1083.

69. Sheehy SP, Huang S, Parker KK. Time-warped comparison of gene expression in adaptive and maladaptive cardiac hypertrophy. *Circ Cardiovasc Genet*. 2009;2:116-124.

70. Kemi OJ, Ceci M, Wisloff U, Grimaldi S, Gallo P, Smith GL, Condorelli G, Ellingsen O. Activation or inactivation of cardiac Akt/mTOR signaling diverges physiological from pathological hypertrophy. *J Cell Physiol*. 2008;214:316-321.

71. Cosin AJ, Hernandiz MA, Andres CF. Mechanisms of ventricular arrhythmias in the presence of pathological hypertrophy. *Eur Heart J*. 1993;14 Suppl J:65-70.

72. McLenachan JM, Henderson E, Morris KI, Dargie HJ. Ventricular arrhythmias in patients with hypertensive left ventricular hypertrophy. *N Engl J Med*. 1987;317:787-792.

73. Spach MS, Heidlage JF, Dolber PC, Barr RC. Electrophysiological effects of remodeling cardiac gap junctions and cell size: experimental and model studies of normal cardiac growth. *Circ Res*. 2000;86:302-311.

74. Aronson RS. Afterpotentials and triggered activity in hypertrophied myocardium from rats with renal hypertension. *Circ Res*. 1981;48:720-727.

75. Aronson RS. Characteristics of action potentials of hypertrophied myocardium from rats with renal hypertension. *Circ Res*. 1980;47:443-454.

76. Kostin S, Dammer S, Hein S, Klovekorn WP, Bauer EP, Schaper J. Connexin 43 expression and distribution in compensated and decompensated

cardiac hypertrophy in patients with aortic stenosis. *Cardiovasc Res*. 2004;62:426-436.

77. Peters NS, Green CR, Poole-Wilson PA, Severs NJ. Reduced content of connexin43 gap junctions in ventricular myocardium from hypertrophied and ischemic human hearts. *Circulation*. 1993;88:864-875.

78. Furukawa T and Kurokawa J. Potassium channel remodeling in cardiac hypertrophy. *J Mol Cell Cardiol*. 2006;41:753-761.

79. Nattel S, Maguy A, Le BS, Yeh YH. Arrhythmogenic ion-channel remodeling in the heart: heart failure, myocardial infarction, and atrial fibrillation. *Physiol Rev*. 2007;87:425-456.

80. Frey N, Katus HA, Olson EN, Hill JA. Hypertrophy of the heart: a new therapeutic target? *Circulation*. 2004;109:1580-1589.

81. Biernacka A and Frangogiannis NG. Aging and Cardiac Fibrosis. *Aging Dis*. 2011;2:158-173.

82. Chen W and Frangogiannis NG. Fibroblasts in post-infarction inflammation and cardiac repair. *Biochim Biophys Acta*. 2012.

83. Frangogiannis NG. The mechanistic basis of infarct healing. *Antioxid Redox Signal*. 2006;8:1907-1939.

84. van der Burg AE, Bax JJ, Boersma E, Pauwels EK, van der Wall EE, Schalij MJ. Impact of viability, ischemia, scar tissue, and revascularization on outcome after aborted sudden death. *Circulation*. 2003;108:1954-1959.

85. Beltrami AP, Urbanek K, Kajstura J, Yan SM, Finato N, Bussani R, Nadal-Ginard B, Silvestri F, Leri A, Beltrami CA, Anversa P. Evidence that human cardiac myocytes divide after myocardial infarction. *N Engl J Med*. 2001;344:1750-1757.

86. Ahuja P, Sdek P, MacLellan WR. Cardiac myocyte cell cycle control in development, disease, and regeneration. *Physiol Rev*. 2007;87:521-544.

87. Dobaczewski M, de Haan JJ, Frangogiannis NG. The Extracellular Matrix Modulates Fibroblast Phenotype and Function in the Infarcted Myocardium. *J Cardiovasc Transl Res*. 2012.

88. Ichihara S, Senbonmatsu T, Price E Jr, Ichiki T, Gaffney FA, Inagami T. Targeted deletion of angiotensin II type 2 receptor caused cardiac rupture after acute myocardial infarction. *Circulation*. 2002;106:2244-2249.

89. de Bakker JM, van Capelle FJ, Janse MJ, Tasseron S, Vermeulen JT, de JN, Lahpor JR. Slow conduction in the infarcted human heart. 'Zigzag' course of activation. *Circulation*. 1993;88:915-926.

90. Luke RA and Saffitz JE. Remodeling of ventricular conduction pathways in healed canine infarct border zones. *J Clin Invest*. 1991;87:1594-1602.

91. Vasquez C, Mohandas P, Louie KL, Benamer N, Bapat AC, Morley GE. Enhanced fibroblast-myocyte interactions in response to cardiac injury. *Circ Res*. 2010;107:1011-1020.

92. Miragoli M, Salvarani N, Rohr S. Myofibroblasts induce ectopic activity in cardiac tissue. *Circ Res*. 2007;101:755-758.

93. Miragoli M, Gaudesius G, Rohr S. Electrotonic modulation of cardiac impulse conduction by myofibroblasts. *Circ Res*. 2006;98:801-810.

94. Zlochiver S, Munoz V, Vikstrom KL, Taffet SM, Berenfeld O, Jalife J. Electrotonic myofibroblast-to-myocyte coupling increases propensity to reentrant arrhythmias in two-dimensional cardiac monolayers. *Biophys J*. 2008;95:4469-4480.

95. Pedrotty DM, Klinger RY, Kirkton RD, Bursac N. Cardiac fibroblast paracrine factors alter impulse conduction and ion channel expression of neonatal rat cardiomyocytes. *Cardiovasc Res*. 2009;83:688-697.

96. Thompson SA, Copeland CR, Reich DH, Tung L. Mechanical coupling between myofibroblasts and cardiomyocytes slows electric conduction in fibrotic cell monolayers. *Circulation*. 2011;123:2083-2093.

97. Rosker C, Salvarani N, Schmutz S, Grand T, Rohr S. Abolishing myofibroblast arrhythmogeneicity by pharmacological ablation of alpha-smooth muscle actin containing stress fibers. *Circ Res*. 2011;109:1120-1131.

Cellular and Molecular Mechanisms of Arrhythmias in Cardiac Fibrosis and Beyond:

From Symptoms to Substrates towards Solutions

Chapter II

Antiproliferative Treatment of Myofibroblasts Prevents Arrhythmias *In Vitro* by Limiting Myofibroblast-Induced Depolarization

Saïd F.A. Askar, MSc; Arti A. Ramkisoensing, MD, MSc; Martin J. Schalij, MD, PhD; Brian O. Bingen, MSc; Jim Swildens, MSc; Arnoud van der Laarse, PhD; Douwe E. Atsma, MD, PhD; Antoine A.F. de Vries, PhD; Dirk L. Ypey, PhD; Daniël A. Pijnappels, PhD.

Adapted from Cardiovasc Res 2011;90:295-304

Abstract

Aims: Cardiac fibrosis is associated with increased incidence of cardiac arrhythmias, but the underlying pro-arrhythmic mechanisms remain incompletely understood and antiarrhythmic therapies are still suboptimal. This study tests the hypothesis that myofibroblast (MFB) proliferation leads to tachyarrhythmias by altering the excitability of cardiomyocytes (CMCs), and that inhibition of MFB proliferation would thus lower the incidence of such arrhythmias.

Methods & Results: Endogenous MFBs in neonatal rat CMC cultures proliferated freely, or under control of different dosages of antiproliferative agents (mitomycin-C and paclitaxel). At day 4 and 9, arrhythmogeneity of these cultures was studied by optical and multi-electrode mapping. Cultures were also studied for protein expression and electrophysiological properties.

MFB proliferation slowed conduction from 15.3±3.5 cm/s (day 4) to 8.8±0.3 cm/s (day 9) (n=75, $P<0.01$), while MFB numbers increased to 37.4±1.7% and 62.0±2%. At day 9, 81.3% of these cultures showed sustained spontaneous reentrant arrhythmias. However, only 2.6% of mitomycin-C treated cultures (n=76, $P<0.0001$) showed tachyarrhythmias, and ectopic activity was decreased. Arrhythmia incidence was drug-dose dependent and strongly related to MFB proliferation. Paclitaxel-treatment yielded similar results. CMCs were functionally coupled to MFBs, and more depolarized in cultures with ongoing MFB proliferation, in which only L-type Ca^{2+} channel-blockade terminated 100% of reentrant arrhythmias, in contrast to Na^{+}-blockade.

Conclusion: Proliferation of MFBs in myocardial cultures gives rise to spontaneous, sustained reentrant tachyarrhythmias. Antiproliferative treatment of such cultures prevents the occurrence of arrhythmias by limiting MFB-induced depolarization, conduction slowing and ectopic activity. This study could provide a rationale for a new treatment option for cardiac arrhythmias.

Introduction

Cardiac arrhythmias remain a leading cause of mortality in the Western world, despite a variety of treatment options.[1] Particularly, implantable cardioverter defibrillators have shown to be effective in improving survival of patients at risk. However, the underlying arrhythmogenic substrate is left untreated and therefore the occurrence of arrhythmias is not prevented.[2] Catheter ablation therapy may serve as an alternative and potentially curative treatment modality. However, its long-term benefits and effects on survival are yet unknown.[3] Furthermore, anti-arrhythmic drug therapy appears to have no significant effect on the survival in larger groups of patients suffering from cardiac arrhythmias and is associated with significant and potentially lethal side effects.[4] The limited therapeutic efficacy and adverse effects associated with these therapies is partly explained by our insufficient understanding of the tissue substrate and pro-arrhythmic mechanisms that are responsible for the occurrence of lethal ventricular tachyarrhythmias.

Taken together, current treatment of cardiac arrhythmias, including means to prevent arrhythmias, is still suboptimal. It is therefore essential to better comprehend the underlying pro-arrhythmic tissue substrate and to provide new rationales for the development of more effective treatment options aimed at preventing arrhythmias from occurring.

Cardiac fibrosis, for example as a result of ischemic heart disease and aging, deteriorates the well-organized nature of the working myocardium due to a dramatic increase in fibroblastic cells, called myofibroblasts (MFBs).[5,6] This may increase electrical heterogeneity and the risk for lethal arrhythmias.[7,8] However, the functional role of MFBs in cardiac arrhythmias is still incompletely understood, especially the impact of their proliferative capacity on myocardial tissue. We hypothesized that MFB proliferation is a key factor in the incidence of spontaneous arrhythmias by altering the excitability of cardiomyocytes (CMCs), resulting in slow conduction and increased ectopic activity, and that inhibition of MFB proliferation may lower, or even prevent, the incidence of cardiac arrhythmias. To test this hypothesis, we studied the role of MFB proliferation in the occurrence of spontaneous reentrant arrhythmias in cardiac cultures using several antiproliferative agents, with cytological and extra- and intracellular electrophysiological techniques.

Methods

All animal experiments were approved by the Animal Experiments Committee of the Leiden University Medical Center and conform to the Guide for the Care and Use of Laboratory Animals as stated by the US National Institutes of Health. A more detailed description can be found in the Supplemental Material.

Cell isolation, cell culture and antiproliferative treatment

Neonatal rat ventricular CMCs were isolated and cultured as described previously.[9] Cells were plated on fibronectin-coated, round coverslips (15 mm) at a density of 4-8x10^5 cells/well in 24-well plates. Endogenous MFBs, present in these cultures, were allowed to proliferate freely, or under control of antiproliferative agents (mitomycin-C (0.05-10 µg/ml) and paclitaxel (0.085 mg/ml), which were added at day 1 of culture and incubated for 2h, resulting in partial or full inhibition of MFB proliferation. In addition, defined ratios of MFBs and CMCs (10/90%, 25/75%, 50/50%) were mixed and co-cultured in 24-well plates and treated with mitomycin-C as described above, to maintain initial ratio and cell density.

Immunocytological analyses

Cultures were fixed in 1% paraformaldehyde, permeabilized with 0.1% Triton X-100 and stained with 1:50-1:200 diluted primary antibodies (see Online Supplement for details on antibodies). Corresponding Alexa fluor-conjugated secondary (Invitrogen, Carlsbad, CA, USA) antibodies were used at a dilution of 1:400. Subsequently, nuclei were counterstained with Hoechst 33342. Cultures were photographed and quantified with dedicated software (Image-Pro Plus, version 4.1.0.0, Media Cybernetics, Silver Spring, MD, USA).

Western blot analyses

Homogenates were made from either 3 different purified CMC cultures, 50/50% CMC/MFB co-cultures or purified MFB cultures. Next, proteins were separated by SDS-page and transferred to Hybond PVDF membranes. Blots were blocked in 5% bovine serum albumin in TBS-T. Primary and corresponding HRP-conjugated secondary antibodies were incubated for 1 h, after which chemiluminescence was induced by ECL advance detection reagents.

Proliferation assays

Proliferation assays consisted of quantification of Ki67 expression as judged by Ki67 staining. Furthermore, MFB numbers in cardiac cultures were quantified at day 1, 4 and 9, based on collagen-I staining.

Apoptosis assay
Possible pro-apoptotic effects of the antiproliferative treatments were investigated by active caspase-3 staining, using aforementioned protocol.

Optical and multi-electrode mapping
At day 4 and 9, cardiac cultures were loaded with 16 μmol/L di-4-ANEPPS, given fresh DMEM/Ham's F12 (37ºC) and immediately mapped using the Ultima-L optical mapping setup (SciMedia, Costa Mesa, CA, USA). Throughout mapping experiments, cultures were kept at 37ºC. Optical signal recordings were analyzed using Brain Vision Analyze 0909 (Brainvision Inc, Tokyo, Japan) in order to assess conduction velocity (CV). Spontaneous ectopic activity was assessed in all groups for 24 s after unipolar electrical stimulation, so that if present, reentrant arrhythmias were eliminated, which allowed for ectopic or other spontaneous activity to resume.
For multi-electrode array (MEA) mapping, cells were cultured in glow-discharged, fibronectin-coated MEA culture dishes (Multi Channel Systems, Reutlingen, Germany) and measurements were performed in the associated data acquisition system, typically within 10 seconds after optical mapping. Electrograms were analyzed off-line using MC-Rack software (version 3.5.6, Multi-Channel Systems).

Whole-cell patch clamp and dye transfer
Measurements were performed in co-cultures of CMCs and MFBs treated with or without mitomycin-C at day 9 of culture, or co-cultures of CMCs and eGFP-labeled MFBs. After identification of CMCs by phase contrast or fluorescence microscopy, maximal diastolic potentials in CMCs were recorded in current-clamp. For data acquisition and analysis, pClamp/Clampex8 software (Axon Instruments, Molecular Devices, Sunnyvale, CA, USA) was used. To further study functional cell-cell coupling, co-cultures of calcein AM-loaded CMCs (green) and Katushka-expressing MFBs (red) were investigated for gap junction-mediated calcein transfer into MFBs by fluorescence microscopy.

Pharmacological interventions
The role of ion channel blockade in the maintenance of reentrant arrhythmias was investigated using the selective Nav1.5 blocker Tetrodotoxin (TTX, 5-10 μmol/L; TTX, Sigma-Aldrich) or verapamil (100 μmol/L; Centrafarm, Etten-Leur, the Netherlands) as Cav1.2 blocker. These blockers were added to the mapping medium, after which the cultures were studied by optical mapping.

Statistical analyses

Statistical analyses were performed using SPSS11.0 for Windows (SPSS Inc., Chicago, IL, USA). Differences were considered statistically significant if $P<0.05$. A more detailed description of the Materials and Methods can be found in the Online Supplement.

Results

Characterization of cardiac cell cultures

Cultures from neonatal rat ventricles (25 isolations) were studied for expression of cell type-specific and gap junction proteins at day 9 of culture. All cultured fibroblasts had the MFB phenotype as judged by α-smooth muscle actin (α-SMA) and vimentin expression (Figure 1). Connexin43 (Cx43) was present between adjacent CMCs, MFBs and at heterocellular junctions (Figure 1A).Dye transfer experiments demonstrated functional gap junctional MFB-CMC coupling (supplemental Figure 1). Western blot analyses revealed an inverse linear relationship between MFB percentage and Cx43 levels. In contrast, α-SMA levels showed a positive linear relationship with MFB numbers (Figure 1B-C). Of all α-SMA positive MFBs, 98.5±1.6% also expressed cytoplasmic collagen-I, centered at the nucleus (R^2=0.9921) (Figure 1D, G). CMCs did not express collagen-I, but stained positive for α-actinin (Figure 1E). Of the vimentin-positive MFBs, 98.4±1.3% also co-expressed collagen-I (R^2=0.9960) (Figure 1F, H). Immunocytological staining for collagen-I as MFB marker and cardiac α-actinin as CMC-specific marker therefore allowed us to quantify endogenous MFBs in a reliable and standardized manner.

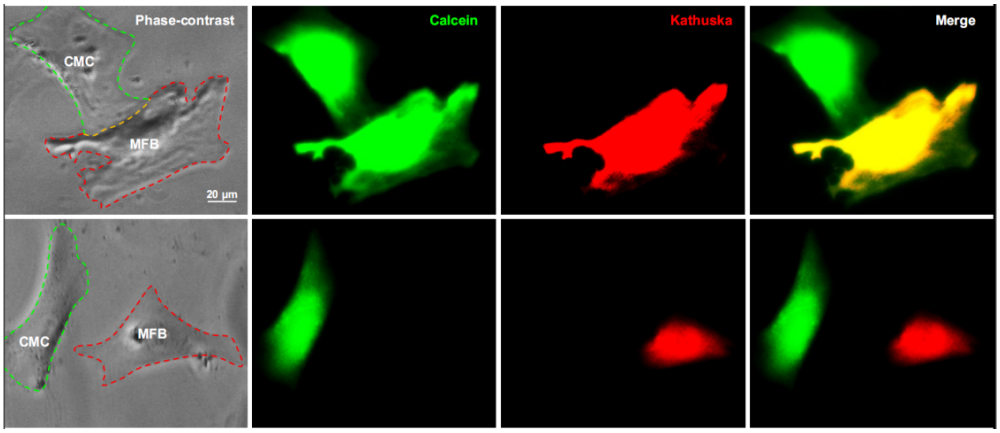

Supplemental Figure 1. *Dye transfer experiments of CMCs loaded with calcein (green) and MFBs labeled with Kathushka (red). MFBs in direct contact with calcein-loaded CMCs (top) were positive for the gap-junctional permeable green fluorescent dye calcein. In contrast, MFBs that remained separate (bottom) from CMCs were negative for this dye. These results indicate that CMCs and MFBs are functionally coupled.*

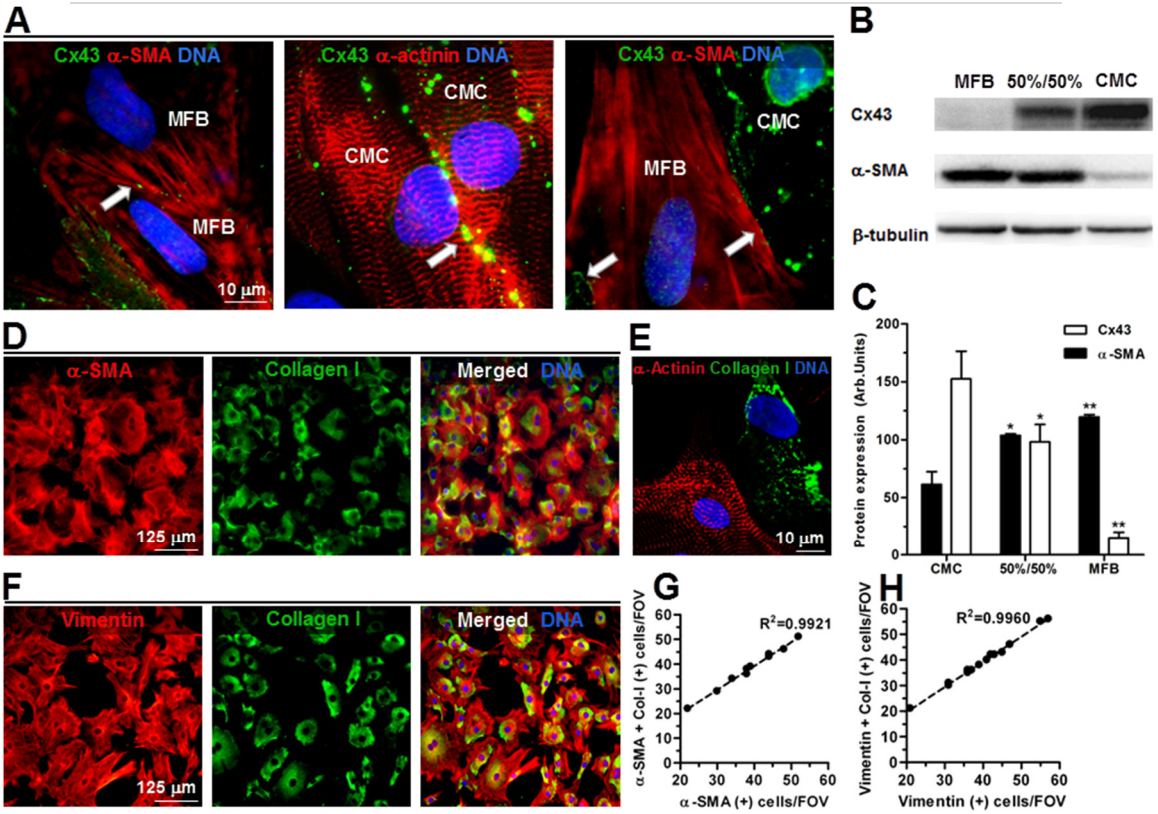

Figure 1. *Characterization of cardiac cell cultures at day 9. (A) Immunocytological double-staining for Cx43, α-SMA (MFB) or α-actinin (CMC). White arrows mark intercellular expression. (B) Western blot of primary CMC cultures, 50%/50% co-cultures of MFBs/CMCs, and purified MFB cultures. (C) Quantification of Western blots normalized for β-tubulin shows opposing trends of Cx43 and α-SMA expression related to MFB quantity. *:P<0.05 vs. CMC; **:P<0.05 vs. CMC and 50%/50%. (D) α-SMA and collagen-I double-staining in MFBs. (E) Collagen-I and α-actinin double-staining showing highly specificity for MFBs and CMCs, respectively. (F) Collagen-I and vimentin double-staining in MFBs. (G) Relationship between co-expression of α-SMA and collagen-I in MFBs, and (H) co-expression of vimentin and collagen-I in MFBs. FOV=Field of View.*

Uninhibited MFB proliferation and spontaneous reentrant arrhythmias

MFB percentage in primary cardiac cultures was 15.6±3.2% at day 1 and progressively increased to 37.4±1.7% at day 4 (P<0.0001) (Figure 2A). At day 2, a spontaneously beating confluent monolayer had formed. At day 4, 24.2% of these cultures showed sustained, spontaneous reentrant tachyarrhythmias (n=33) (Figure 2F), with an average cycle-length of 267±22 ms and conduction velocity (CV) of 15.3±3.5 cm/s. Sustained reentry was defined as repetitive circular activation lasting ≥30 s. MFB proliferation resulted in an MFB percentage of 62.2±2.0% at day 9 (P<0.0001 vs. day 1 and 4) (Figure 2B), and a decrease in CV to 8.8±0.3 cm/s (P<0.0001) (Figure 2C). At day 9, 81.3% of all spontaneously active

cultures showed reentrant activity (n=75) (Figure 2D). The cycle-lengths of these arrhythmias had increased to 365±57 ms (*P*<0.001 vs. day 4) (Figure 2E).

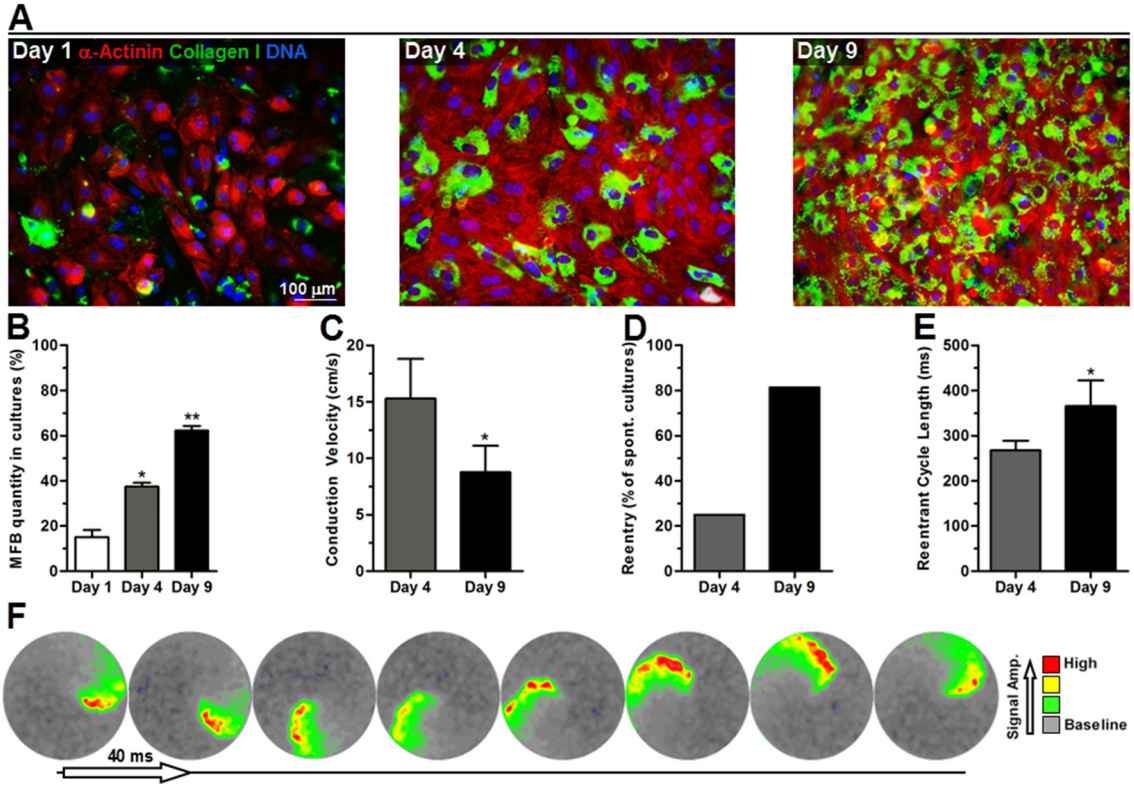

Figure 2. *Proliferation of MFBs in cardiac cultures causes conduction abnormalities. (A) Immunocytological staining for α-actinin (CMC;red) and collagen-I (MFB;green) in cardiac cultures at day 1, 4, and 9. (B) Quantification of collagen-I positive MFBs at day 1, 4 and 9. Quantities are expressed as a percentage of total number of nuclei. *:P<0.0001 vs. day 1. **:P<0.0001 vs. day 1 and 4. (C) Progressive increase in MFBs is associated with a lower CV. *:P<0.0001 vs. day 4, and (D) is also associated with an increase in the occurrence of spontaneous reentrant tachyarrhythmias and (E) an increase in cycle-length of the reentrant circuits between day 4 and 9. *:P<0.0001 vs. day 4. (F) Time-lapse (spacing: 40ms) of a typical high-pass-filtered, spatially averaged optical signal of reentrant activation. Colours represent signal intensities related to changes in membrane potential.*

Inhibition of MFB-proliferation preserves high CV, decreases ectopic activity and prevents reentrant arrhythmias

Assessment of proliferative activity of MFBs was performed by Ki67 staining (Figure 3A). Quantification showed a significant decrease in proliferating MFBs following mitomycin-C treatment (Figure 3B). In such cultures, MFB quantities remained constant throughout

follow-up (Figure 3C), with no significant increase in apoptosis compared to control (Figure 3D and Supplemental Figure 2).

Under mapping conditions, ≥60% of both treated and untreated cultures were spontaneously active at day 4 and 9. At day 4, CV of mitomycin-C treated cultures was 23±1.9 cm/s, which was significantly higher than in control cultures (~15 cm/s, *P*<0.0001) (Figure 4E). Furthermore, no arrhythmias were observed (n=17) in mitomycin-C treated cultures (Figure 4C, H). At day 9, CV in mitomycin-C treated cultures remained unaltered. Interestingly, at day 9, only 2.6% of spontaneously active mitomycin-C treated cultures showed sustained reentrant tachyarrhythmias (n=76), which is a dramatic decrease compared to proliferating control cultures (~81% arrhythmias (n=75) at day 9, Figure 4B, F-G and Movie 1).

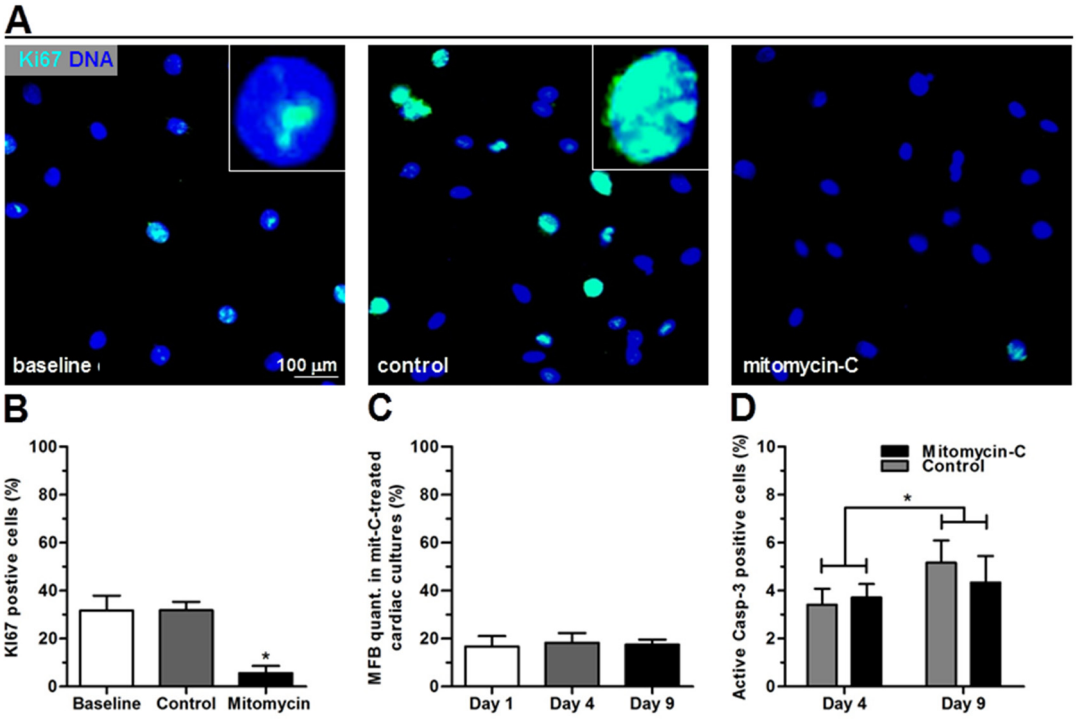

Figure 3. *Mitomycin-C is a potent inhibitor of MFB proliferation (A) Typical examples of Ki67 staining in MFBs, indicating proliferation at baseline (day 1) and 3 days later for control and mitomycin-C treated cultures. Insets show magnified nucleus positive for Ki67 staining. (B) Effect of mitomycin-C treatment on Ki67 positive staining in MFBs. *:P<0.001 vs. baseline and control. (C) MFB quantification in mitomycin-C treated cardiac cultures shows a stable MFB quantity throughout time (p=ns). (D) Quantification of active caspase-3 staining shows no significant differences in apoptosis between mitomycin-C treated and control cultures, although small but significant increases were found over time (*:P<0.05).*

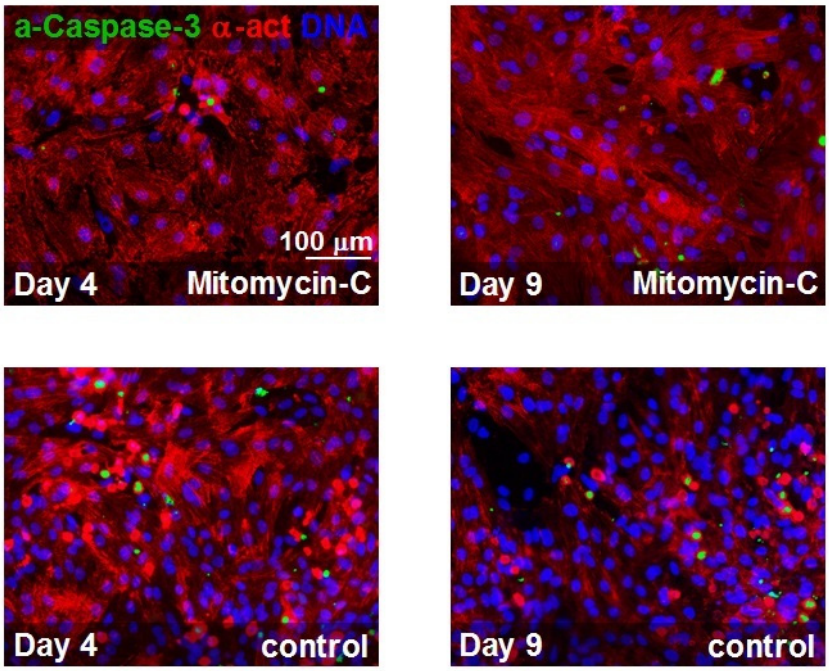

Supplemental Figure 2. *Mitomycin-C does not increase apoptosis in myocardial cultures. Representative images of immunocytochemical staining for caspase-3 in mitomycin-C treated cultures and control cultures at day 4 and 9. Nuclei were counterstained with Hoechst and caspase-3 positive nuclei were quantified and expressed as a percentage of total cell count, which was not significantly affected by mitomycin-C treatment. Total cell count was defined as the total number of viable nuclei added to the amount of caspase-3 positive cells.*

For further evaluation of arrhythmogeneity, the incidence of ectopic activity was studied in treated and untreated cultures. Ectopic activity, e.g. multiple simultaneous or alternating pacemaker sites in one culture, was observed less frequently in mitomycin-treated cultures than in untreated cultures at day 4 (25% (n=24) versus 43% (n=23)) and day 9 (8% (n=37) versus 71% (n=35), respectively (Figure 4A, D). An example of how ectopic activity can lead to reentrant arrhythmias is demonstrated in Movie 3.

Analyses of extracellular electrograms from MEA mapping experiments showed distinct differences between control cultures (n=12) and mitomycin-C treated cultures (n=11) (Figure 4I-J). Peak-to-peak electrogram amplitude was higher in mitomycin-C treated cultures (702±304 μV vs. 96±23 μV, $P<0.0001$) (Figure 4K). Spontaneous electrical activation frequency was lowered by mitomycin-C treatment compared to control (0.28±0.22HZ vs.. 3.22±0.22Hz, $P<0.0001$) (Figure 4L).

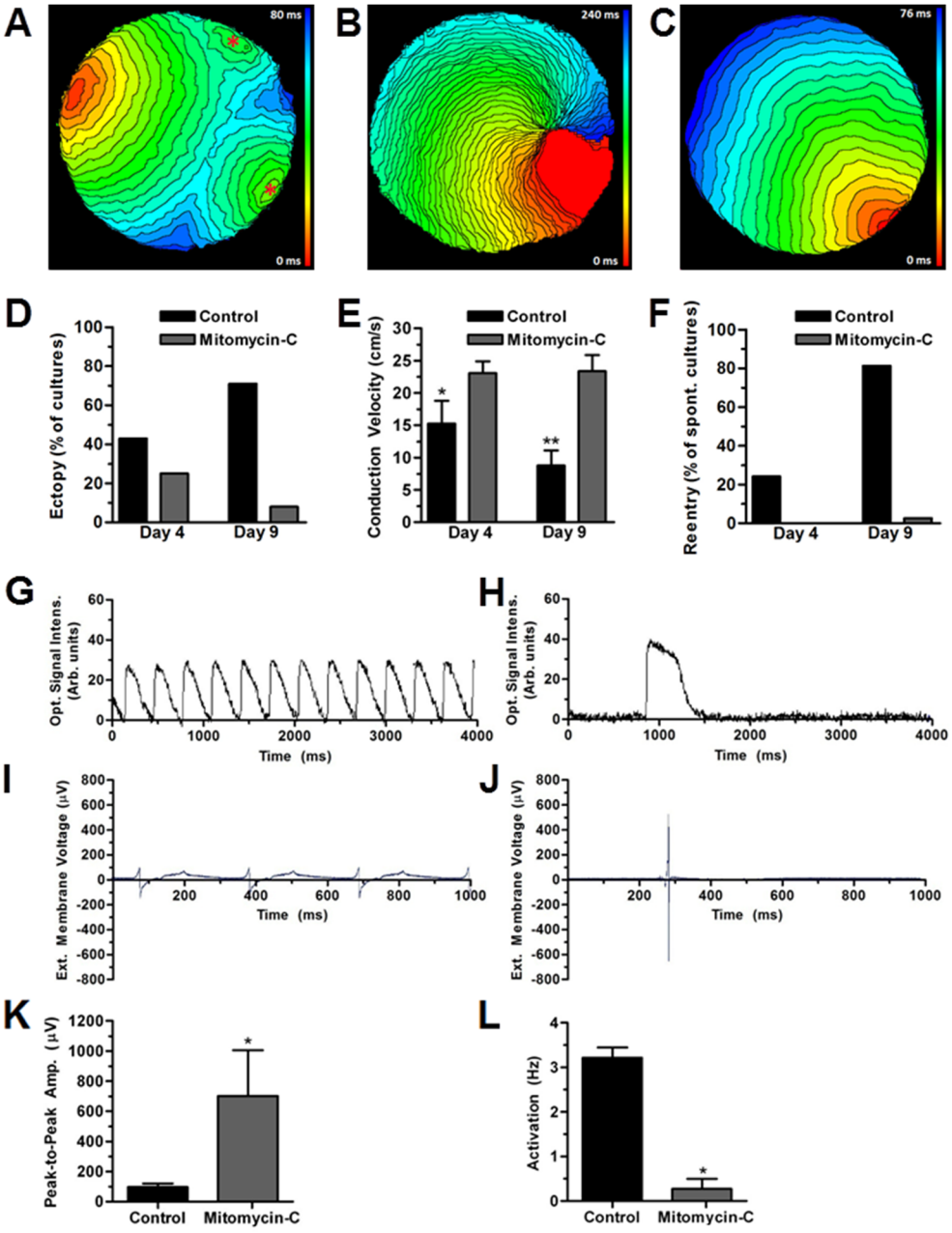

Figure 4. *Effects of mitomycin-C treatment on ectopic activity, CV and reentrant tachyarrhythmias in cardiac cultures. (A) Activation map of ectopic activity in an untreated culture at day 4 (4ms isochronal spacing). Red asterisks mark ectopic foci. (B) Activation map of a reentrant tachyarrhythmia in an untreated cardiac culture (spacing: 4ms). (C) Typical activation map of*

*uniform conduction across a mitomycin-C treated culture (spacing: 4ms). (D) Quantification of incidence of ectopic activity at day 4 and 9 reveals a substantial reduction by mitomycin-C treatment. (E) CV measured by optical mapping. *:P<0.001 vs. mitomycin-C day 4-9 and control day 9. **:P<0.001 vs. day 4-9 mitomycin-C. (F) Spontaneous reentry occurrence in mitomycin-C treated and control cultures at day 4 and 9. (G) Typical example of a non-high-pass-filtered, spatially filtered optical signal of repetitive activation in a non-treated, fibrotic culture showing reentrant tachyarrhythmias. (H) Typical example of a non-high-pass-filtered, spatially filtered optical signal of uniform conduction across a mitomycin-C treated culture. (I) Local extracellular multi-electrode array recording of a reentrant tachyarrhythmia. (J) Multi-electrode array recording of a mitomycin-C treated culture. (K) Quantification of electrical signal amplitude from multi-electrode array recordings at day 9 (P<0.0001 vs. control). (L) Beating frequency of cultures measured by such arrays at day 9. *: P<0.0001 vs. control.*

Dose-dependent effects of mitomycin-C treatment on preservation of electrophysiological parameters

As mitomycin-C treatment had such a profound impact on conduction properties of myocardial cultures, dose-dependency was studied next. Dosages administrated at day 1 of culture were 10, 5, 2.5, 0.5 and 0.05 μg/ml. At day 9, cultures were studied and subsequently stained for collagen-I (Figure 5A). Mitomycin-C decreased the amount of MFBs in a dose-dependent manner (Figure 5B). Furthermore, mitomycin-C had a strong dose-dependent effect on cell density (P<0.001). In addition, cardiomyocyte count, calculated by subtracting collagen-I positive cells from total cell count, did not change significantly (Figure 5C).

These dose-dependent changes in MFB quantities and cell density were related to significant electrophysiological changes in the cultures. At day 9, CV was 7.3±2.4 cm/s at 0.05 μg/ml mitomycin-C and significantly rose with increasing dosages (Figure 5D). MFB percentages at various mitomycin-C dosages directly correlated with CV (R^2=0.94) (Figure 5E). Furthermore, the incidence of sustained reentrant arrhythmias showed a negative mitomycin-C dose-dependent relationship, with no occurrence of arrhythmias at 10 μg/ml (n=25) and 5 μg/ml (n=20), 10% at 2.5 μg/ml (n=31), 29% at 0.5 μg/ml (n=17), 92% at 0.05 μg/ml (n=13), and 93% for control (n=27) (Figure 5F).

CMC-MFB co-cultures at predetermined cell density and MFB-dependent conduction abnormalities

Cell density is an important determinant of conduction patterns, as this directly influences cell-to-cell contacts essential for action potential propagation. To further study the quantitative effects of MFBs on conduction and arrhythmias, fixed ratios of MFBs and CMCs were plated out, while inhibiting proliferation with 10 μg/ml mitomycin-C. As a result, average cell density between the co-culture groups did not differ significantly at day 9.

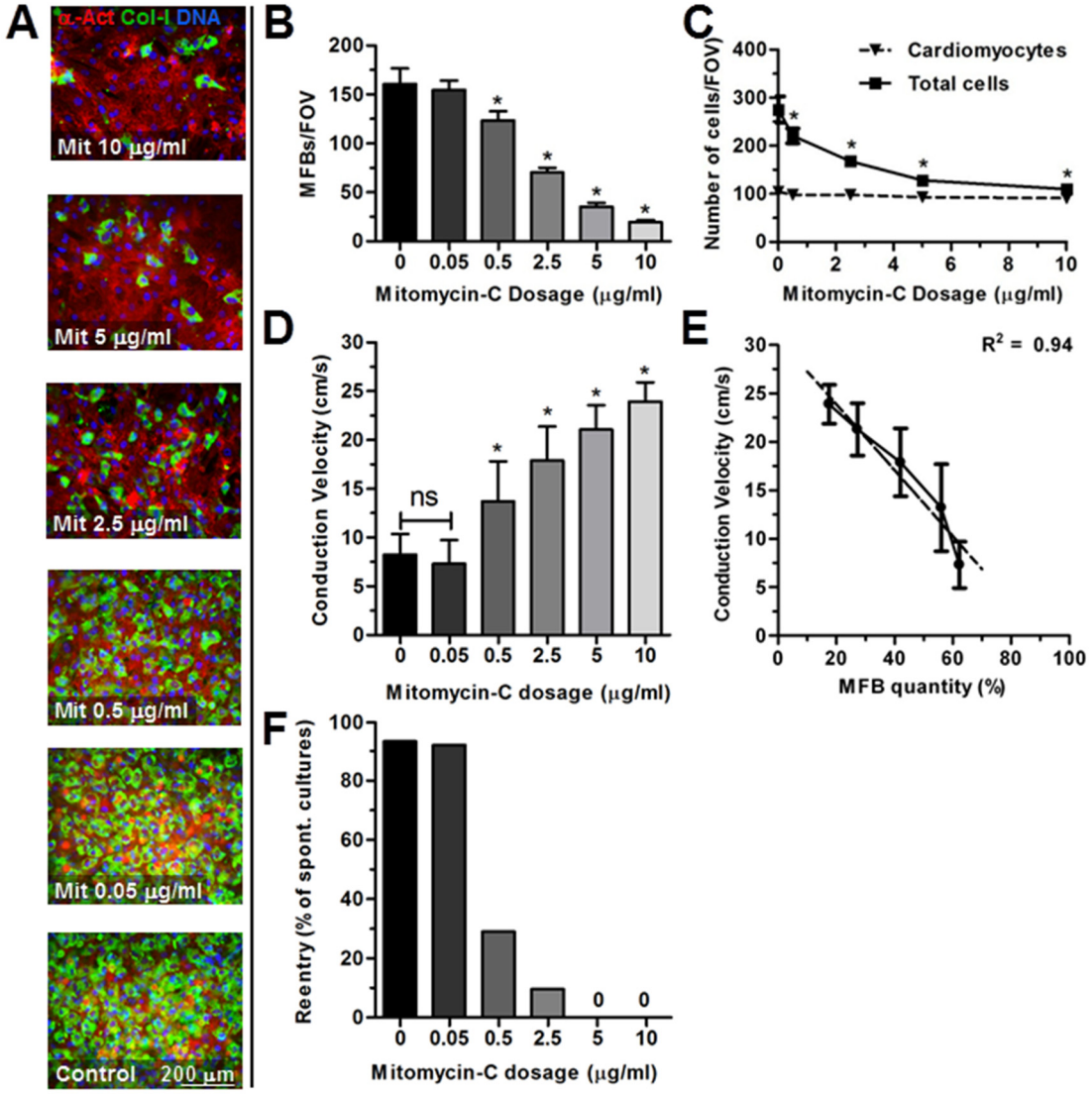

Figure 5. *Dose-dependent effect of mitomycin-C treatment on arrhythmias at day 9 of culture. (A) Immunocytological double-staining for α-actinin (CMC;red) and collagen-I (MFB;green) in cardiac cultures treated with different dosages of mitomycin-C. (B) Dose-dependent effect of mitomycin-C on MFB quantities in cardiac cultures as determined by collagen-I staining. *:P<0.001 vs. all including control (0 µg/ml). (C) Quantification of collagen-I staining shows a dose-dependent effect of mitomycin-C on total cell count without affecting CMC count. CMC count was calculated by subtract the number of MFBs from the total number of nuclei. *:P<0.01 vs. all including control. (D) Dose-dependent effect of mitomycin-C on CV (*:P<0.05 vs. all). (E) Plot of average MFB percentage found for different dosages against CV found in these groups shows a negative linear association between MFB percentage and CV. FOV: Field of View. (F) Dose-dependent effect of mitomycin-C on reentry occurrence.*

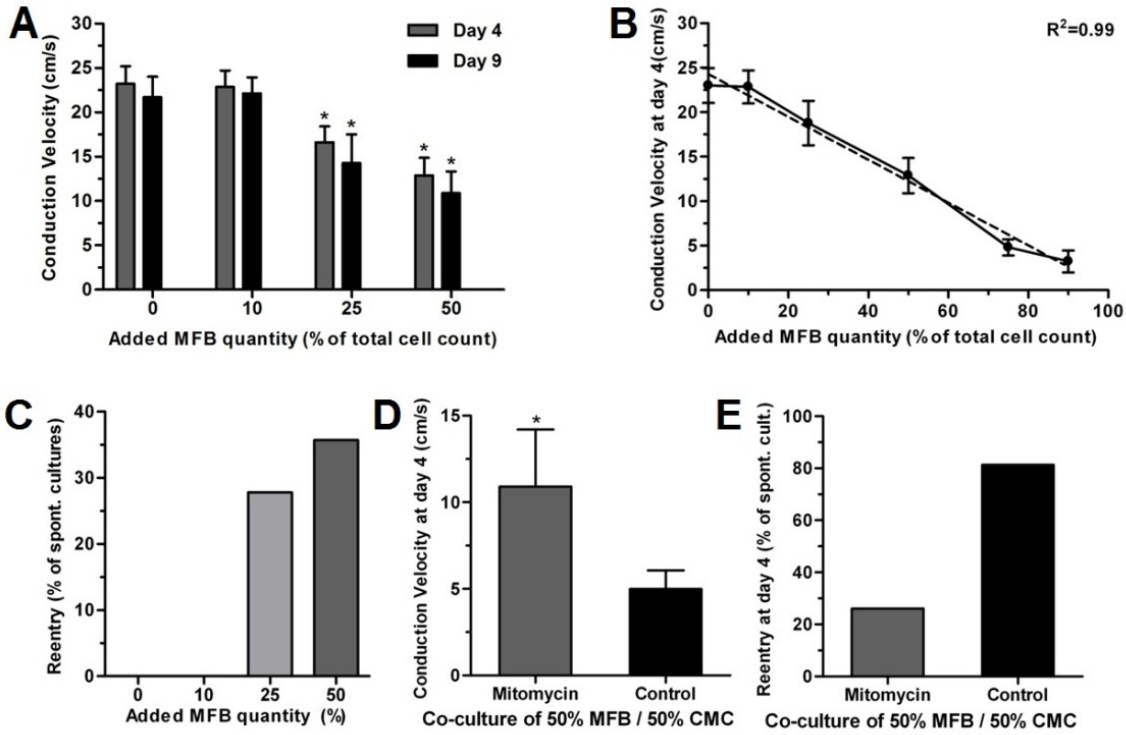

Supplemental Figure 3. *MFB-CMC co-cultures at predetermined cell density and the effects on conduction abnormalities. (A) CV slows according to plated MFB percentage, except for 10% MFBs. *:p<0.05 vs all. (B) CV at day 4 shows a strong linear association with added MFB percentage. Dotted line represents regression line. (C) Occurrence of spontaneous arrhythmias at day 9 is MFB quantity-dependent and rises with increasing added MFB percentages. (D) Mitomycin-C administration to 50%/50% MFB-CMC co-cultures results in a higher CV at day 4 compared to control. *:p<0.0001 vs control. (E) Uninhibited proliferation of MFBs in a 50%/50% CMC/MFB co-culture results in a 3.1-fold increase in reentry occurrence (n=23) compared to mitomycin-C treated cultures (n=17) of initially identical cellular composition.*

MFB quantities were 15.7±2.0% (0% added MFBs), 26.8±2.5% (10% added), 38.0±3 (25% added) and 59.0±1.6% (50% added) at day 9. CV did not differ significantly between 0% (n=18) and 10% (n=20) added MFBs (23.1±2.2 cm/s vs. 22.1±1.8 cm/s, p=0.51) at day 9. However, 25% and 50% added MFBs slowed conduction to 14.2±3.5 cm/s and 10.9±2.4 cm/s, respectively (*P*<0.05 vs.. all) (Supplemental Figure 3A). Furthermore, no arrhythmias were found in cultures containing 0% and 10% added MFBs, but at 25% and 50% added MFBs, occurrence was 27.8% (n=36) and 35.7% (n=28), respectively (Supplemental Figure 3C).

Unfortunately, cultures with added MFB percentages higher than 50% developed structural inhomogeneities from day 6 onwards and could therefore not be studied at day 9. Nevertheless, linear regression analysis revealed a strong inverse relationship between plated MFB percentages and CV at day 4 (Supplemental Figure 3B).

A potentially secondary preventive effect of mitomycin-C on the occurrence of spontaneous arrhythmias was studied in 50%/50% CMC/MFB co-cultures either treated with mitomycin-C or allowed to proliferate freely. At day 4, CV in mitomycin-C treated cultures was 10.9±3.3 cm/s with 60.2±3.8% MFBs. In contrast, in control cultures with an equally high initial number of MFBs, CV decreased to 4.9±1.1 cm/s, while MFB percentages increased to 78.8±4.7% (P<0.0001 vs. treated cultures) (Supplemental Figure 3D). Furthermore, arrhythmia occurrence was 3.1-fold higher in the non-treated cultures (26% (n=17) vs. 82% (n=23)) (Supplemental Figure 3E).

Characteristics of reentrant tachyarrhythmias

In untreated, arrhythmic cultures, cycle-length of the reentrant circuits was strongly related to CV (R^2=0.83, Figure 6A). Reentry was typically associated with a decrease in CV of 5.0±1.2 cm/s as compared to non-reentrant conduction in cultures from the same experimental group. Furthermore, administration of tetrodotoxin (TTX) to 12 untreated, arrhythmic cultures at concentrations of 5 μM and 20 μM at day 9 of culture, resulted in a significantly lower CV (Figure 6B, D-E), but had only a mild to moderate effect on terminating reentrant arrhythmias (Figure 6C). Next, 100 μM verapamil was administered to block L-type Ca^{2+}-channels, which terminated 100% of the remaining arrhythmias (Figure 6C and Movie 2). Internal PBS control did not affect arrhythmia persistence. Additionally, 12 untreated, arrhythmic cultures were immediately treated with verapamil without prior TTX administration, which also terminated all arrhythmias. In mitomycin-C treated cultures, 20 μM TTX completely blocked propagation for ≥30 seconds, after which propagation resumed at a significantly lower CV of 11.5±2.0 cm/s (n=10, previously 24.2±2.0 cm/s, P<0.0001).

To further study the role of MFB proliferation in arrhythmogeneity, CMCs were investigated for their electrophysiological properties by patch-clamp experiments in active cultures treated with or without mitomycin-C. Cultures had comparable beating frequencies (0.5-1 Hz). After 9 days of on-going MFB proliferation, the maximal negative diastolic potential of CMCs was significantly reduced (-44±9mV, n=11) as compared to those of CMCs in mitomycin-C treated cultures (-68±7mV, n=12, P<0.001) (Figure 6F).

In co-cultures of eGFP-labelled MFBs with CMCs, at equal density and ratio as day 9 of free proliferation, diastolic membrane potentials of CMCs (-48±6mV, n=8) were comparable to those derived at day 9 of free proliferation. This is in agreement with the low CV and increased ectopic activity found in such cultures and their tolerance to TTX treatment.

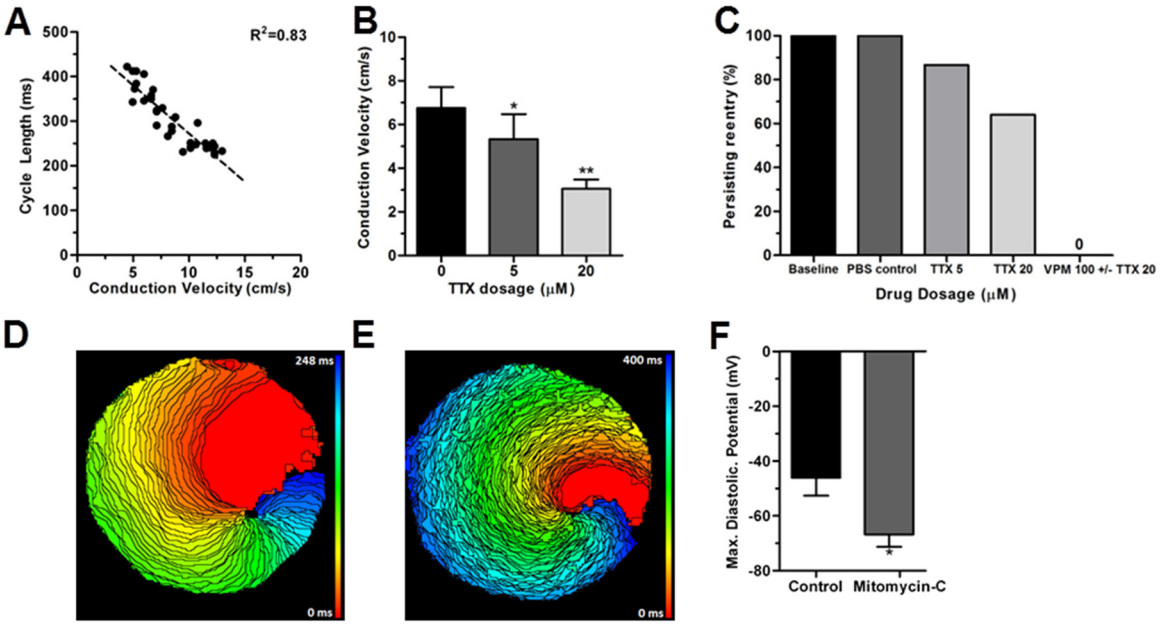

Figure 6. *Characteristics of reentrant tachyarrhythmias at day 9. (A) Linear association between cycle-length and CV (R^2=0.83, n=35). (B) TTX significantly decreased CV in a dose dependent manner (*:P<0.05 vs. baseline, **:P<0.0001 vs. 0 and 5 μM). (C) Persistence of reentrant circuits after administration of TTX and/or verapamil. (D) Activation map of a reentrant tachyarrhythmia in an untreated cardiac culture (spacing: 4ms). (E) Activation map of the same reentrant tachyarrhythmia shown in panel E after 5 min of incubation with 20 μM TTX. Of note is the increased number of isochronal lines (4 ms), indicating conduction slowing. (F) Maximal diastolic potential measured in CMCs from control and mitomycin-C treated cultures at day 9.*

Prevention of arrhythmias by paclitaxel, another antiproliferative agent

Cultures were treated with 0.085 mg/ml paclitaxel and studied identically to mitomycin-C treated cultures. In paclitaxel-treated MFB cultures, less Ki67 positive cells were found (Supplemental Figure 4B-C) and apoptosis was not significantly increased compared to vehicle-control (0.9% DMSO) treated cultures (Supplemental Figure 4D, 5). Interestingly, vehicle treatment alone also inhibited proliferation. Spontaneous activity under optical mapping conditions was >60% for both treated and untreated groups. CV at day 4 was 17.3±1.6 (vs. 11.1±3.6 cm/s in control), without reentry (n=27) in the paclitaxel-treated group, whereas 61.5% (n=13) of controls showed reentry (Supplemental Figure 4E-F). At

day 9, paclitaxel-treated cultures contained 33.3±2.9% MFBs (Supplemental Figure 4A), and CV was 15.0±1.5 cm/s (*P*<0.01 vs. day 4 and control), while arrhythmias were observed in 5% of spontaneously active cultures (n=23). In control cultures at day 9, CV was 6.5±1.4 cm/s, with a reentry incidence of 93% (n=15) (Supplemental Figure 4E-F).

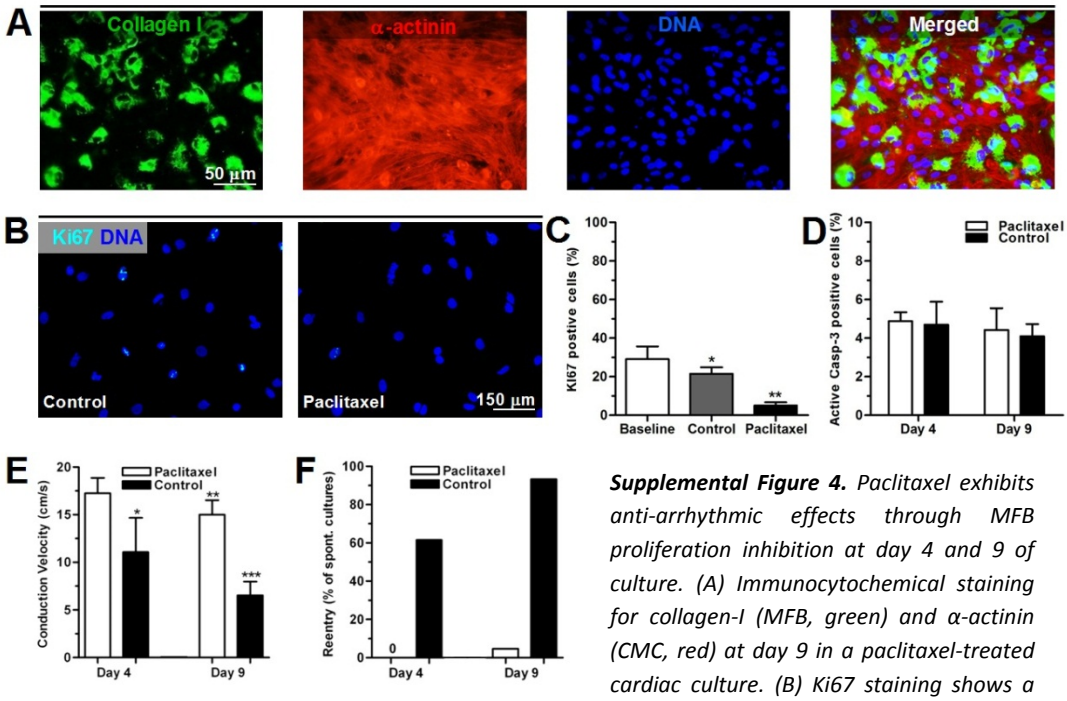

Supplemental Figure 4. *Paclitaxel exhibits anti-arrhythmic effects through MFB proliferation inhibition at day 4 and 9 of culture. (A) Immunocytochemical staining for collagen-I (MFB, green) and α-actinin (CMC, red) at day 9 in a paclitaxel-treated cardiac culture. (B) Ki67 staining shows a substantial reduction in positive cells by paclitaxel administration. (C) Quantification of Ki67-positive MFBs before and after paclitaxel treatment. *:p<0.05 vs baseline, **:p<0.05 vs baseline and control. (D) Quantification of apoptotic cells by active caspase-3 staining shows no significant increase in apoptosis by 10 μmol/L paclitaxel. (E) Paclitaxel-treated cultures maintain a higher CV compared to control cultures. *:p<0.05 vs paclitaxel at day 4. **:p<0.05 vs paclitaxel at day 4 and control at day 9. ***:p<0.05 vs control at day 4 and paclitaxel at day 9. (F) Paclitaxel treatment dramatically decreased reentry occurrence compared to control at both day 4 and 9 of culture.*

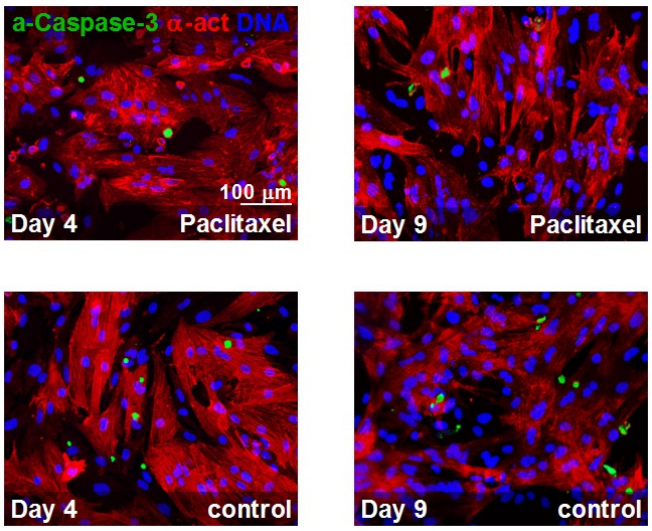

Supplemental Figure 5. *Representative images of active caspase-3 immunocytochemical staining in paclitaxel-treated cultures and control cultures at day 4 and 9. Nuclei were counterstained with Hoechst and active caspase-3 positive nuclei were quantified and expressed as a percentage of total cell count, which was not significantly affected by paclitaxel treatment. Total cell count was defined as the total number of viable nuclei added to the amount of caspase-3 positive cells.*

Discussion

Key findings of this study are (1) proliferation of myofibroblasts in myocardial cultures results in a highly pro-arrhythmogenic substrate, in which CMCs are depolarized, conduction is slow and mainly Ca^{2+}-driven, and ectopic activity is increased, thereby giving rise to spontaneous, sustained reentrant tachyarrhythmias, and (2) antiproliferative treatment of these cultures prevents or substantially reduces the occurrence of arrhythmias by limiting myofibroblasts-induced depolarization and preserving uniform, rapid, Na^{+}-driven impulse propagation in CMCs, with less ectopic activity, but without noticeable adverse effects on electrophysiological properties and without increased apoptosis in the treated cultures.

Myofibroblasts and Cardiac Arrhythmogeneity

In vitro studies indicate that MFBs could play a role in modulating electrophysiological properties in remodeled hearts, and thereby contribute to arrhythmogenesis. Rook *et al*. showed that cardiac fibroblasts and CMCs are able to form functional heterocellular gap junctions.[9] Gaudesius *et al*.,[10] and previous studies by our group,[11,12] demonstrate that fibroblasts coupled to CMCs are able to slowly conduct electrical impulses through electrotonic interaction. Paracrine activity of cardiac fibroblasts may also contribute to a reduction in CV.[13] Besides their effects on CV, MFBs may also induce ectopic activity in cardiac cultures as demonstrated by Miragoli *et al*.[14] Recently, a study by Zlochiver *et al*. showed that MFBs are able to contribute to rhythm disturbances in cardiac cultures,[15] which was further investigated in a number of *in silico* studies.[16,17] Novel in the present study is the finding that ongoing proliferation of endogenous MFBs in neonatal rat CMC

cultures results in the creation of a highly arrhythmogenic substrate, and that antiproliferative treatment of cardiac cultures prevents spontaneous reentrant tachyarrhythmias.

Reentrant tachyarrhythmias in cardiac cultures with ongoing MFB proliferation

In previous studies, functional reentry was induced by rapid electrical pacing of the cultures.[15,18,19] In the present study the focus was on the ability of myocardial cultures to spontaneously generate such reentrant arrhythmias. MFBs are known to contribute to both automaticity and slow conduction,[10,14,20] therefore reentry may occur in the absence of externally applied electrical impulses. We confirmed this by showing that ~81% of all cultures with ongoing MFB proliferation and without apparent anatomical obstacles, showed spontaneous, sustained reentrant tachyarrhythmias at day 9 of culture.

By allowing MFBs to proliferate freely in CMC cultures, CMCs became increasingly depolarized due to increasing MFB-CMC interactions. The present study shows that this eventually leads towards a depolarized resting membrane potential at which voltage-gated fast Na^+-channels are largely inactivated and propagation becomes mainly dependent on activation of Ca^{2+}-channels. It is known that Ca^{2+}-driven propagation contributes to slow conduction.[7] In line with this observation, all arrhythmias in the present study were terminated when L-type Ca^{2+}-channels were blocked. In contrast, most arrhythmias sustained after Na^+-channel blockade, indicating that electrical propagation in such conditions appears to be mainly Ca^{2+}-driven. Recently, Chang *et al*. showed similar results in another *in vitro* model of reentry, using non-fibroblastic cells.[19] Moreover, as these CMCs become depolarized by increasing numbers of MFB, they could become active as local pacemaker site through depolarized-induced automaticity,[21] and thereby add to the pro-arrhythmogenic nature of fibrotic cultures. The present study shows that around 50% of all fibrotic cultures, which did not show reentrant arrhythmias at the time of mapping, showed multiple simultaneous or alternating pacemaker sites.

Ongoing MFB proliferation also had an effect on the cycle-length of the tachyarrhythmias. At day 4, average cycle-length was 267±22 ms at a CV of 15.3±3.5 cm/s, whereas at day 9, the cycle-length increased to 365±57 ms at a CV of only 8.8±3 cm/s. These data may explain how different degrees of fibrosis during various stages of cardiac remodelling could both determine the vulnerability to arrhythmias and the rate of atrial or ventricular arrhythmias. Therefore, future *in vivo* studies are required to better understand the role of MFBs in the arrhythmic heart.

Antiproliferative treatment of endogenous myofibroblasts

In the present study, two different antiproliferative agents were used to study the role of MFB proliferation in arrhythmogeneity. One of these agents is mitomycin-C, a potent DNA-crosslinking agent. After proliferation inhibition by mitomycin-C, CV remained stable

from day 4 to day 9, and spontaneous reentry occurrence decreased from 81.3% to 2.6%. Concerning the underlying mechanisms, in cultures treated with mitomycin-C the resting membrane potential of CMCs remained more negative. Therefore propagation remained fast and mainly Na^+-driven, as was shown by addition of TTX to these cultures, in contrast to cultures with ongoing MFB proliferation. In addition, less ectopic activity was observed in cultures treated with mitomycin-C, which most likely resulted from limited MFB-induced depolarization and a subsequent reduction of the occurrence of depolarization-induced automaticity. As a consequence of fast propagation and less ectopic activity the occurrence of reentrant arrhythmias is expected to decrease, which was confirmed in the present study.

By inhibition of MFB proliferation, not only MFB-induced depolarization of CMCs is minimized, but also disruption of low-resistant gap junctional coupling between CMCs by infiltrating MFBs may be prevented, thereby preserving rapid propagation. Calculations on cell densities indicated that antiproliferative treatment does coincide with a lower total cell density while maintaining the same number of CMCs as the non-treated cultures. In addition, any negative, paracrine effect of MFBs on CV in cardiac cultures will be stabilized after inhibition of proliferation; as such an effect is expected to be cell number-dependent.

To exclude a mitomycin-C specific effect and to establish that proliferation is the key factor in this study, another antiproliferative agent was studied. Paclitaxel, a member of the taxanes drug category, interferes with breakdown of microtubules during cell division. Park *et al*. used the antiproliferative potential of paclitaxel to inhibit coronary restenosis and neo-intimal hyperplasia in the myocardium.[22] We show that paclitaxel is also suited as agent to reduce the incidence of reentrant tachyarrhythmias in myocardial cultures. Control experiments for paclitaxel included incubation with DMSO (0.9%). DMSO is known to have several effects on cells,[23] and therefore may explain the high incidence of reentry at day 4 in these cultures. The lower CV found in paclitaxel-treated cultures may also be explained by its mechanism of action.[24] Nevertheless, no reentry was observed in paclitaxel-treated cultures with DMSO as vehicle. Importantly, both agents did not result in increased apoptosis, which is in agreement with earlier studies.[25,26]

In vivo translation

The present study provides new insights in the way cardiac fibrosis may result in arrhythmias, and how this may provide a rationale for a preventive strategy, which currently does not exist. In the clinical setting, myocardial fibrosis increases arrhythmia vulnerability in diseased and aged hearts, and finds its basis in proliferation of MFBs and matrix deposition by these cells. Although functional MFB-CMC coupling remains to be proven *in vivo*, the key role of MFBs in cardiac fibrosis suggests a high significance for *in vivo* arrhythmogeneity of these cells. Measures to control MFB proliferation may

therefore counteract different pro-arrhythmic aspects at once. Naturally, *in vivo* studies are necessary to determine whether progressive fibrosis (e.g. in post myocardial infarction or aging) and its pro-arrhythmic consequences can be limited by reducing MFB proliferation. Considering the role of cell proliferation in different physiological processes in the heart,[5,27,28] and possible cardiotoxic effects of antiproliferative agents,[29] careful consideration of the time-frame, location and strength of intervention seems of importance. Still, the strong *in vitro* evidence from this study suggests that approaches to limit MFB proliferation in hearts vulnerable to fibrosis-related conduction disturbances may have profound effects on arrhythmia vulnerability.

Study limitations

The use of adult human CMCs and MFBs may have been more clinically relevant, but these CMCs cannot be kept in culture for longer periods and the proliferation rate of such MFBs *in vitro* does not allow a study like this within a reasonable time-frame. Furthermore, cardiac MFBs are also involved in secretion of extracellular matrix components, which could contribute to deleterious effects on conduction in fibrotic cardiac tissue. These aspects were not studied in detail and need more dedicated studies in the future. However, it may be expected that with inhibition of MFB proliferation, the secretion of such components is indirectly lowered.

Conclusions

Proliferation of MFBs in myocardial cultures gives rise to spontaneous, sustained reentrant tachyarrhythmias. However, antiproliferative treatment of such cultures prevents the occurrence of arrhythmias significantly by preserving a physiological membrane potential and rapid, Na^+-driven propagation in CMCs. Hence, our study indicates that MFB proliferation may be a novel target for future anti-arrhythmic strategies.

Funding

This work was supported by the Dutch Heart Foundation (2008/B119). D.A.P. is a recipient of the Netherlands Organization for Scientific Research (NWO) VENI grant.

Acknowledgements

We thank Huybert J.F. van der Stadt for excellent technical support.

Conflict of Interest

None.

Supplemental Material

Methods

All animal experiments were approved by the Animal Experiments Committee of the Leiden University Medical Center and conform to the Guide for the Care and Use of Laboratory Animals as stated by the US National Institutes of Health.

Cell isolation and culture

Primary neonatal rat cardiomyocytes (CMCs) and cardiac fibroblasts were isolated and cultured as described previously[30,31]. Immediately following isolation, cell suspensions were spinned down, resuspended and filtered through a 20 μm cell-strainer to remove cell-aggregates. Subsequently, cells were counted and plated out on fibronectin-coated round coverslips (15 mm) at a cell density of 4-8x10^5 cells/well in 24-well plates (Corning Life Sciences, Amsterdam, the Netherlands), depending on the experiment.

For co-culture experiments with fixed myofibroblast (MFB) quantities (0%, 10%, 25%, 50%, 75%, and 90%), primary CMCs, and MFBs obtained from an earlier isolation (passage 3-4), were counted and mixed in specific, pre-determined ratios before plating. Co-cultures were treated with mitomycin-C (Sigma-Aldrich, St. Louis, MO, USA) to maintain original CMC-fibroblast ratios. All cultures were refreshed daily and cultured in a humidified incubator at 37ºC and 5% CO_2.

Antiproliferative treatment

Antiproliferative treatment of cultures was performed at day 1 of culture. The choice of different types of antiproliferative agents was based on their specific mechanisms of action, thereby allowing a more accurate study of the role of proliferation in arrhythmogeneity, rather than an agent-specific effect.

Different dosages of the antiproliferative agent of interest (mitomycin-C dissolved in PBS; ranging from 10 μg/ml to 0.05 μg/ml or paclitaxel dissolved in DMSO; 0.085 mg/ml, both from Sigma-Aldrich) were diluted in growth medium (Ham's-F10 supplemented with 10% fetal bovine serum (FBS, Invitrogen, Carlsbad, CA, USA), 10% horse serum (HS, Invitrogen), and penicillin (100 U/ml) and streptomycin (100 μg/ml, P/S; Bio-Whittaker, Carlsbad, CA, USA)) and incubated for 2 hours. Cultures were then rinsed twice in PBS and once in a 1:1 mixture of Dulbecco's modified Eagle's medium (DMEM, Invitrogen) and Ham's F10 medium (ICN Biomedicals, Irvine, CA, USA) supplemented with 5% HS and P/S, before being kept on this medium throughout the experiment. Non-treated controls were rinsed identically.

Immunocytochemical analyses

Following mapping experiments, cultures were stained for proteins of interest, or cultures were stained parallel to mapping experiments, as described in earlier studies[30]. Cultures were stained for α-smooth muscle actin (α-SMA) and vimentin expression to study fibroblasts phenotype (Sigma-Aldrich), collagen-I expression to quantify myofibroblast (MFB) numbers (Abcam, Cambridge, MA, USA), Ki67 expression to identify actively proliferating cells (Abcam) and α-actinin as cardiomyocyte-specific marker (Sigma-Aldrich). Furthermore, cultures were also stained for connexin 43 (Cx43) (Sigma-Aldrich) to study gap junction formation between CMCs and MFBs. Alexa donkey-anti-mouse IgG 568 and Alexa donkey-anti-rabbit IgG 488 secondary (Invitrogen) antibodies were used at a dilution of 1:400. For all staining, nuclei were counterstained using Hoechst 3342 (Invitrogen). A fluorescent microscope equipped with a digital camera (Nikon Eclipse, Nikon Europe, Badhoevedorp, the Netherlands) and dedicated software (Image-Pro Plus, version 4.1.0.0, Media Cybernetics, Silver Spring, MD, USA) was used to analyze the cultures. All proteins of interest were studied in at least 6 different cultures from a specific group, from which at least 20 representative images were taken at different magnifications (10, 40, 100x). All cultures were stained using the same solutions and captured using equal exposure times for the protein of interest.

Western-blot analyses

Cx43 expression was studied in a MFB-density dependent manner and correlated with α-SMA expression. Homogenates were made from 3 different purified CMC cultures, 50%/50% CMC/MFB co-cultures and purified MFB cultures, size-fractionated on NuPage 12% Tris-Acetate NuPage gels (Invitrogen) and transferred to Hybond PVDF membranes (GE Healthcare, Waukesha, WI, USA). These membranes were incubated with antibodies against Cx43 or α-SMA (both from Sigma-Aldrich) for 1 h followed by incubation with corresponding HRP-conjugated secondary antibodies (Santa Cruz Biotechnologies,Santa Cruz, CA, USA). β-tubulin (Millipore, Billerica, MA, USA) expression was determined to check for equal protein loading. Chemiluminescence was induced by ECL advance detection reagents (GE Healthcare) and caught on Hyperfilm ECL (GE Healthcare), after which the intensity of Cx43 and α-SMA bands were quantified by Scion Image analysis software (Scion Corporation, Frederick, MD, USA).

Proliferation assays

To assess the effect of antiproliferative treatments on MFB proliferation, MFB cultures were seeded at $5x10^4$ cells/well in a 24-wells plate and stained for Ki67 (Abcam). Ki67 is a cellular marker for cell proliferation, and was quantified for positive staining in MFBs, before and 3 days after treatment. Quantification was performed on 6 cultures from

which 8 images were taken per culture at 40x magnification. These cultures were kept on DMEM/Ham's F10 + 5% HS and refreshed daily. Furthermore, collagen-I staining was performed after optical mapping experiments on at least 6 cardiac cultures to determine the number of MFBs in cultures treated with different antiproliferative agents and dosages (mitomycin-C 10 µg/ml, 5 µg/ml, 2.5 µg/ml, 0.5 µg/ml, 0.05 µg/ml) at day 1, 4 and 9. Quantification of total nuclei count, and cells expressing collagen-I was performed on at least 6 images and averaged per culture per timepoint per dosage.

Apoptosis assay

Antiproliferative treatment may lead to increased apoptosis. Therefore, we investigated the expression of active caspase-3 (Abcam), an established marker for apoptosis, in cultures treated with antiproliferative agents and appropriate controls. These cardiac cultures were seeded at $4x10^5$ cells/well in a 24-wells format. The same protocol was used as described earlier for immunocytochemical staining. Total nuclei number and cells expressing active caspase-3 were quantified within the same image and averaged for 6 images per culture for 6 different cultures at 40x magnification.

Optical and multi-electrode mapping

To investigate action potential propagation patterns on a whole-culture scale, cultures ($8x10^5$ cells/well in a 24-wells format), treated with or without antiproliferative agents, were optically mapped with the voltage-sensitive dye di-4-ANEPPS (Invitrogen), on day 4 and 9. For reasons of standardization and reproducibility, only spontaneously active cultures with high degrees of structural and functional homogeneity (determined by light-microscopy and electrophysiological mapping) were included for further analyses. As a result, 95 out of every 100 cultures (wells) were included. On days of mapping experiments, cells were incubated with culture medium (DMEM/Ham's F10 + 5% horse serum) containing 16 µmol/L di-4-ANEPPS for 15±5 minutes. Following incubation, cells were refreshed with DMEM/Ham's F12 (37ºC) and immediately mapped. Mapping experiments in a 24-well plate typically did not exceed 30 min. Excitation light (λ_{ex}=525±25nm) was delivered by a halogen arc-lamp (MHAB-150W, Moritex Corporation, San Jose, CA, USA). Fluorescent emission light (λ_{em}>590 nm) was passed through a camera lens (1x Plan-Apo, WD=15 mm; Leica, Wetzlar, Germany) and focused onto a 100 by 100 pixels (100 mm^2) CMOS camera (Ultima-L, SciMedia, Costa Mesa, CA, USA) by a 1.6x converging lens, resulting in a total field of view of 256 mm^2 and a spatial resolution of 160 µm/pixel. During measurements, cultures were kept at 37ºC. Electrical activation was recorded for at least 4 seconds at a rate of 500 frames/s, high-pass filtered and analyzed using Brain Vision Analyze 0909 (Brainvision Inc, Tokyo, Japan). The same culture was never exposed for longer than 40 s to minimize phototoxic effects. Importantly, mapping of the same culture at both day 4 and 9 appeared to be well tolerated as no structural

inhomogeneities were observed and CV did not change significantly over time in mitomyocin-C treated cultures.

Each pixels' signal was averaged in a fixed grid of 3x3 pixels. Activation time points were determined at dF/dt_{max}, which corresponds to the timepoint of maximum upstroke velocity. Conduction velocity (CV) in cultures with a uniform activation pattern was calculated between two 3 by 3 pixel grids, typically spaced 2-8 mm apart, and perpendicular to the activation wavefront. For cultures showing reentrant conduction wavefronts, CV was determined similarly at half the maximal distance from the core perpendicular to the wavefront over a length of 2-4 mm. Per culture, CV was determined in 6-fold and averaged for further comparisons. Reentrant cycle length was calculated from 3 separate cycles per culture and averaged. As this study focuses on reentry occurrence and prevention of such arrhythmias, all CV values for reentry and non reentry cultures were pooled within each different group, as this inclusion makes CV a valuable parameter in determining therapeutic effects *in vitro*.

For multi-electrode array (MEA) mapping, cells were cultured in glow-discharged, fibronectin-coated MEA culture dishes (Multi Channel Systems, Reutlingen, Germany) and measurements were performed as described previously [31], typically within 10 seconds after optical mapping.

Assessment of ectopic activity

Spontaneous ectopic activity was defined as multiple simultaneous or alternating pacemaker sites. In our cultures, 53% of fibrotic cultures (n=47) versus 23% (n=44) in mitomycin-C treated cultures showed ectopic activity spontaneously at day 4. However, at day 9 a high percentage of non-treated cultures showed spontaneous reentry, which continuously excites the cardiac tissue and thereby greatly decreases the possibility of ectopic activity. Therefore, to be able to quantify ectopic activity at day 9, reentry needed to be eliminated in a non-pharmacological manner. For this purpose, we used a custom-made epoxy-coated platinum electrode and performed unipolar stimulation with 6 V for 4 seconds using an electrical stimulus module with corresponding software (Multichannel Systems), which successfully eliminated re-entry in >90% of the cultures. This allowed for spontaneous ectopic activity to resume, which was detected by mapping of the cultures for 24 seconds directly after applying the stimulus. This allowed for quantification of ectopic activity at day 9. To provide a balanced comparative view, these experiments were performed identically at day 4 and 9 in mitomycin-C treated and control cultures.

Whole-cell patch-clamp

Whole-cell patch-clamp measurements were performed in co-cultures of CMCs and MFBs treated with or without mitomycin-C at day 9 of culture. In addition, MFBs were labeled with eGFP using lenti-viral vectors (LV.CMV.eGFP.HBVPRE; MOI 10), refreshed daily and passaged twice before these cells were co-cultured with CMCs at equal density and ratio at day 9 of free MFB proliferation. After identification of CMCs by phase contrast or fluorescence microscopy, maximal diastolic potentials in CMCs were recorded in current-clamp. Whole-cell recordings were performed at 25°C using a L/M-PC patch-clamp amplifier (3kHz filtering) (List-Medical, Darmstadt, Germany). The pipette solution contained (in mmol/L) 10 Na_2ATP, 115 KCl, 1 $MgCl_2$, 5 EGTA, 10 HEPES/KOH (pH 7.4). Tip and seal resistance were 2.0-2.5 MΩ and >1 GΩ, respectively. The bath solution contained (in mmol/L) 137 NaCl, 4 KCl, 1.8 $CaCl_2$, 1 $MgCl_2$, and 10 HEPES (pH 7.4). For data acquisition and analysis, pClamp/Clampex8 software (Axon Instruments, Molecular Devices, Sunnyvale, CA, USA) was used.

Dye transfer

To establish functional coupling between MFBs and CMCs, MFBs were labeled with a lenti-viral vector encoding kathuska (MOI 20). MFBs were kept in culture for 2 weeks and were at least passaged twice before usage in experiments. CMC cultures with a density of $1.0x10^5$ cells/well were treated with 10 μg/ml mitomycin-C to prevent endogenous MFB overgrowth. At day 4, these cultures (n=12) were loaded for 30 minutes with calcein-AM (Invitrogen) diluted in HBSS (Gibco), which once internalized is converted to the green fluorescent dye calcein. Cells were rinsed twice with PBS and kept on culture medium containing 2.5 mmol/L probenecid (Invitrogen) to block extracellular leakage. Kathuska labeled MFBs were subsequently plated out in a 1:1 ratio with the calcein-loaded CMCs. Brightfield and fluorescent images (at least 10 per culture) were captured after 24 hours.

Pharmacological interventions

To study the role of Nav1.5 and Cav1.2 channels in the maintenance of reentrant arrhythmias in cultures with high numbers of MFBs, increasing doses of Tetrodotoxin (TTX) (5 and 20 μmol/L; Sigma-Aldrich) were added to the cultures followed by administration of verapamil (100 μmol/L; Centrafarm, Etten-leur, the Netherlands) during optical mapping experiments. As internal control, PBS was administered to the mapping medium prior to pharmacological interventions. To study the role of Cav1.2 blockade exclusively, arrhythmic cultures were immediately treated with verapamil without prior TTX administration. Both 20 μM TTX and 100 μM verapamil are expected to fully block the targeted ion channels in neonatal rat CMCs[32,33]. The electrophysiological effects of these drugs were evaluated by optical mapping, directly, 1 min and 5 min after administration.

In identical fashion, TTX was administered to mitomyocin-C treated cultures at day 9, showing uniform, rapid activation, and evaluated for persistence of electrical activation.

Statistical analysis

Statistical analyses were performed using SPSS11.0 for Windows (SPSS Inc., Chicago, IL, USA). Data were compared with one-way or two-factor mixed ANOVA test with Bonferroni post-hoc correction if appropriate, and expressed as mean±SD. Linear correlation analysis was performed by calculating Pearson's correlation coefficient. Comparison between two groups was performed using the student-t test. Differences were considered statistically significant if $p<0.05$.

References

1. Huikuri HV, Castellanos A, Myerburg RJ. Sudden death due to cardiac arrhythmias. *N Engl J Med*. 2001;345:1473-1482.

2. Borleffs CJ, van EL, Schotman M, Boersma E, Kies P, van der Burg AE, Zeppenfeld K, Bootsma M, van der Wall EE, Bax JJ, Schalij MJ. Recurrence of ventricular arrhythmias in ischaemic secondary prevention implantable cardioverter defibrillator recipients: long-term follow-up of the Leiden out-of-hospital cardiac arrest study (LOHCAT). *Eur Heart J*. 2009;30:1621-1626.

3. Zeppenfeld K and Stevenson WG. Ablation of ventricular tachycardia in patients with structural heart disease. *Pacing Clin Electrophysiol*. 2008;31:358-374.

4. Arshad A, Mandava A, Kamath G, Musat D. Sudden cardiac death and the role of medical therapy. *Prog Cardiovasc Dis*. 2008;50:420-438.

5. Frangogiannis NG. The mechanistic basis of infarct healing. *Antioxid Redox Signal*. 2006;8:1907-1939.

6. Porter KE and Turner NA. Cardiac fibroblasts: at the heart of myocardial remodeling. *Pharmacol Ther*. 2009;123:255-278.

7. Kleber AG and Rudy Y. Basic mechanisms of cardiac impulse propagation and associated arrhythmias. *Physiol Rev*. 2004;84:431-488.

8. van der Burg AE, Bax JJ, Boersma E, Pauwels EK, van der Wall EE, Schalij MJ. Impact of viability, ischemia, scar tissue, and revascularization on outcome after aborted sudden death. *Circulation*. 2003;108:1954-1959.

9. Rook MB, Jongsma HJ, de JB. Single channel currents of homo- and heterologous gap junctions between cardiac fibroblasts and myocytes. *Pflugers Arch*. 1989;414:95-98.

10. Gaudesius G, Miragoli M, Thomas SP, Rohr S. Coupling of cardiac electrical activity over extended distances by fibroblasts of cardiac origin. *Circ Res*. 2003;93:421-428.

11. Pijnappels DA, van Tuyn J, de Vries AA, Grauss RW, van der Laarse A, Ypey DL, Atsma DE, Schalij MJ. Resynchronization of separated rat cardiomyocyte fields with genetically modified human ventricular scar fibroblasts. *Circulation*. 2007;116:2018-2028.

12. van Tuyn J, Pijnappels DA, de Vries AA, de V, I, van der Velde-van Dijke, Knaan-Shanzer S, van der Laarse A, Schalij MJ, Atsma DE. Fibroblasts from human postmyocardial infarction scars acquire properties of cardiomyocytes after transduction with a recombinant myocardin gene. *FASEB J*. 2007;21:3369-3379.

13. Pedrotty DM, Klinger RY, Kirkton RD, Bursac N. Cardiac fibroblast paracrine factors alter impulse conduction and ion channel expression of neonatal rat cardiomyocytes. *Cardiovasc Res*. 2009;83:688-697.

14. Miragoli M, Salvarani N, Rohr S. Myofibroblasts induce ectopic activity in cardiac tissue. *Circ Res*. 2007;101:755-758.

15. Zlochiver S, Munoz V, Vikstrom KL, Taffet SM, Berenfeld O, Jalife J. Electrotonic myofibroblast-to-myocyte coupling increases propensity to reentrant arrhythmias in two-dimensional cardiac monolayers. *Biophys J*. 2008;95:4469-4480.

16. Jacquemet V and Henriquez CS. Loading effect of fibroblast-myocyte coupling on resting potential, impulse propagation, and repolarization: insights from a microstructure model. *Am J Physiol Heart Circ Physiol*. 2008;294:H2040-H2052.

17. Xie Y, Garfinkel A, Camelliti P, Kohl P, Weiss JN, Qu Z. Effects of fibroblast-myocyte coupling on cardiac conduction and vulnerability to reentry: A computational study. *Heart Rhythm*. 2009;6:1641-1649.

18. Bian W and Tung L. Structure-related initiation of reentry by rapid pacing in monolayers of cardiac cells. *Circ Res*. 2006;98:e29-e38.

19. Chang MG, Zhang Y, Chang CY, Xu L, Emokpae R, Tung L, Marban E, Abraham MR. Spiral waves and reentry dynamics in an in vitro model of the healed infarct border zone. *Circ Res*. 2009;105:1062-1071.

20. Miragoli M, Gaudesius G, Rohr S. Electrotonic modulation of cardiac impulse conduction by myofibroblasts. *Circ Res*. 2006;98:801-810.

21. Rosenthal JE and Ferrier GR. Contribution of variable entrance and exit block in protected foci to arrhythmogenesis in isolated ventricular tissues. *Circulation*. 1983;67:1-8.

22. Park SJ, Shim WH, Ho DS, Raizner AE, Park SW, Hong MK, Lee CW, Choi D, Jang Y, Lam R, Weissman NJ, Mintz GS. A paclitaxel-eluting stent for the prevention of coronary restenosis. *N Engl J Med*. 2003;348:1537-1545.

23. Berliner DL and Ruhmann AG. The influence of dimethyl sulfoxide on fibroblastic proliferation. *Ann N Y Acad Sci*. 1967;141:159-164.

24. Casini S, Tan HL, Demirayak I, Remme CA, Amin AS, Scicluna BP, Chatyan H, Ruijter JM, Bezzina CR, van Ginneken AC, Veldkamp MW. Tubulin polymerization modifies cardiac sodium channel expression and gating. *Cardiovasc Res*. 2010;85:691-700.

25. Axel DI, Kunert W, Goggelmann C, Oberhoff M, Herdeg C, Kuttner A, Wild DH, Brehm BR, Riessen R, Koveker G, Karsch KR. Paclitaxel inhibits arterial smooth muscle cell proliferation and migration in vitro and in vivo using local drug delivery. *Circulation*. 1997;96:636-645.

26. Nieto A, Cabrera CM, Catalina P, Cobo F, Barnie A, Cortes JL, Barroso del JA, Montes R, Concha A. Effect of mitomycin-C on human foreskin fibroblasts used as feeders in human embryonic stem cells: immunocytochemistry MIB1 score and DNA ploidy and apoptosis evaluated by flow cytometry. *Cell Biol Int*. 2007;31:269-278.

27. Souders CA, Bowers SL, Baudino TA. Cardiac fibroblast: the renaissance cell. *Circ Res*. 2009;105:1164-1176.

28. Bergmann O, Bhardwaj RD, Bernard S, Zdunek S, Barnabe-Heider F, Walsh S, Zupicich J, Alkass K, Buchholz BA, Druid H, Jovinge S, Frisen J. Evidence for cardiomyocyte renewal in humans. *Science*. 2009;324:98-102.

29. Yeh ET, Tong AT, Lenihan DJ, Yusuf SW, Swafford J, Champion C, Durand JB, Gibbs H, Zafarmand AA, Ewer MS. Cardiovascular complications of cancer therapy: diagnosis, pathogenesis, and management. *Circulation*. 2004;109:3122-3131.

30. Pijnappels DA, Schalij MJ, van TJ, Ypey DL, de Vries AA, van der Wall EE, van der LA, Atsma DE. Progressive increase in conduction velocity across human mesenchymal stem cells is mediated by enhanced electrical coupling. *Cardiovasc Res*. 2006;72:282-291.

31. Pijnappels DA, Schalij MJ, Ramkisoensing AA, van TJ, de Vries AA, van der LA, Ypey DL, Atsma DE. Forced alignment of mesenchymal stem cells undergoing cardiomyogenic differentiation affects functional integration with cardiomyocyte cultures. *Circ Res*. 2008;103:167-176.

32. Motlagh D, Alden KJ, Russell B, Garcia J. Sodium current modulation by a tubulin/GTP coupled process in rat neonatal cardiac myocytes. *J Physiol*. 2002;540:93-103.

33. Verhoeven FA, Moerings EP, Lamers JM, Hennemann G, Visser TJ, Everts ME. Inhibitory effects of calcium channel blockers on thyroid hormone uptake in neonatal rat cardiomyocytes. *Am J Physiol Heart Circ Physiol*. 2001;281:H1985-H1991.

Cellular and Molecular Mechanisms of Arrhythmias in Cardiac Fibrosis and Beyond:
From Symptoms to Substrates towards Solutions

Chapter III

Connexin43 Silencing in Myofibroblasts Prevents Arrhythmias in Myocardial Cultures: Role of Maximal Diastolic Potential

Heterocellular Coupling and Arrhythmias

Saïd F. Askar, MSc; Brian O. Bingen, MD*; Jim Swildens, MSc*; Dirk L. Ypey, PhD; Arnoud van der Laarse, PhD; Douwe E. Atsma, MD, PhD; Katja Zeppenfeld, MD, PhD; Martin J. Schalij, MD, PhD; Antoine A. de Vries, PhD*; Daniël A. Pijnappels, PhD*.

*Equal contribution

Adapted from Cardiovasc Res 2012;93:434-44

Abstract

Aims: Arrhythmogenesis in cardiac fibrosis remains incompletely understood. Therefore, this study aims to investigate how heterocellular coupling between cardiomyocytes (CMCs) and myofibroblasts (MFBs) affects arrhythmogeneity of fibrotic myocardial cultures. Potentially this may lead to the identification of novel anti-arrhythmic strategies.

*Methods & Results***:** Co-cultures of neonatal rat CMCs and MFBs in a 1:1 ratio were used as a model of cardiac fibrosis, with purified CMC cultures as control. Arrhythmogeneity was studied at day 9 of culture by voltage-sensitive dye mapping. Heterocellular coupling was reduced by transducing MFBs with lentiviral vectors encoding shRNA targeting Connexin43 (Cx43) or Luciferase (pLuc) as control.

In fibrotic cultures, conduction velocity (CV) was lowered (11.2±1.6cm/s vs. 23.9±2.1cm/s $P<0.0001$), while action potential duration and ectopic activity were increased. Maximal diastolic membrane potential (MDP) of CMCs was less negative in fibrotic cultures. In fibrotic cultures, (n=30) 30.0% showed spontaneous reentrant tachyarrhythmias compared to 5% in controls (n=60). Cx43-silencing in MFBs made the MDP in CMCs more negative, increased excitability and CV by 51% ($P<0.001$), reduced action potential duration and ectopic activity ($P<0.01$), thereby reducing reentry incidence by 40%, compared to pLuc-silenced controls. Anti-arrhythmic effects of Cx43-downregulation in MFBs could be reversed by depolarization of CMCs through I_{k1} inhibition or increasing extracellular $[K^+]$.

Conclusion: Arrhythmogeneity of fibrotic myocardial cultures is mediated by Cx43 expression in MFBs. Reduced expression of Cx43 causes a more negative MDP of CMCs. This preserves CMC excitability, limits prolongation of repolarization and thereby strongly reduces the incidence of spontaneous reentrant tachyarrhythmias.

Introduction

Cardiac fibrosis is associated with an increased risk of potentially lethal tachyarrhythmias.[1] While increasing numbers of patients are suffering from such rhythm disturbances, the underlying cellular pro-arrhythmic substrate of fibrosis remains incompletely understood. In addition, there is a need for more effective treatment options.[2] This provides a strong incentive for obtaining a better understanding of the fibrotic substrate and to identify novel therapeutic targets.

One of the hallmarks of cardiac fibrosis is a substantial increase in the relative number of myofibroblasts (MFBs) that actively remodel the myocardium.[3,4] These MFBs are inexcitable, and may contribute to ectopic activity, conduction slowing and increased propensity towards reentrant tachyarrhythmias.[5-8] However, the exact mechanism through which MFBs exert their pro-arrhythmic effects remains incompletely understood. Various *in vitro* studies suggest that heterocellular coupling between cardiomyocytes (CMCs) and MFBs is potentially pro-arrhythmic. Through electrotonic interaction, CMC excitability is altered and conduction velocity (CV) and upstroke velocity are reduced while ectopic activity becomes more prevalent.[5] However, the effects of MFB-induced depolarization on repolarization dynamics remain largely unknown, especially how such alterations could be related to ectopic activity. Although heterocellular coupling has been proposed as a pro-arrhythmic mechanism, experimental down regulation of such coupling to establish its role in arrhythmogeneity has not been performed. To further define the pro-arrhythmic mechanisms in fibrotic myocardial cultures and to identify novel anti-arrhythmic targets, we investigated the effect of direct inhibition of MFB-CMC coupling on arrhythmogeneity of fibrotic myocardial cell cultures by selective down regulation of connexin43 (Cx43) expression in MFBs.

Our results demonstrate that inhibition of heterocellular coupling in co-cultures of CMCs and MFBs acts anti-arrhythmic by preserving CMC excitability and reducing prolongation of repolarization, both resulting from less MFB-induced depolarization. The maximal diastolic membrane potential (MDP) of CMCs was shown to be a key factor, as the anti-arrhythmic effects of MFB-selective Cx43 knockdown could be reversed by I_{k1} blockade-induced or high extracellular $[K^+]$-induced depolarization of CMCs.

Methods

All animal experiments were approved by the Animal Experiments Committee of the Leiden University Medical Center and conform to the Guide for the Care and Use of Laboratory Animals as stated by the US National Institutes of Health. A more detailed description can be found in the Supplemental Material.

Cell isolation and culture

Primary ventricular CMCs and cardiac fibroblasts were isolated from hearts of neonatal Wistar rats. Animals were anesthetized using 4-5% isoflurane inhalation anesthesia. Adequate anesthesia was assured by absence of reflexes prior to rapid heart excision. Next, the ventricular cardiac tissue was chopped into small pieces and enzymatically digested under agitation at 37ºC by 2 sequential 45-minute treatments with collagenase type I (450 units/ml; Worthington, NJ, USA). The resulting cell suspension was transferred to plastic dishes (Falcon Primaria; BD Biosciences, Breda, the Netherlands) to allow preferential attachment of non-CMCs (mainly cardiac fibroblasts). Seventy-five minutes later, the non-adhered cells (mostly CMCs) were passed through a nylon cell strainer with a mesh pore size of 70 µm (Becton Dickinson, Franklin Lakes, NJ, USA) to remove undigested tissue fragments and cell aggregates. Next, the cells were counted and plated on fibronectin (Sigma-Aldrich, St. Louis, MO, USA)-coated round glass coverslips (15 mm Ø) at a density of 1-8x10^5 cells/well in 24-well plates (Corning Life Sciences, Amsterdam, the Netherlands), depending on the experiment.

Fibrosis was mimicked by co-cultures of primary CMCs and MFBs obtained from an earlier isolation. Cells were counted and mixed in a 1:1 ratio before plating, as this ratio has been shown to be pro-arrhythmic and allows for adequate detection of anti-arrhythmic effects.[8] To maintain initially seeded ratios (for fibrosis and control), all cultures were treated with the anti-proliferative agent mitomycin-C (Sigma-Aldrich, St. Louis, MO, USA) at day 1 of culture.[8] All cultures were refreshed daily with DMEM/Ham's F10 in a 1:1 mixture with 5% added horse serum (HS) (all from Invitrogen, Breda, the Netherlands) and cultured in a humidified incubator at 37ºC and 5% CO_2.

Immunocytological analyses

At day 9 of culture, cultures were stained for proteins of interest.[8] Quantification of fibroblast numbers was based on collagen type I staining.

Cultures were stained with antibodies specific for Cx43 (Sigma-Aldrich) or Cx45 (Santa Cruz Biotechnology, Santa Cruz, CA, USA) and α-actinin (Sigma-Aldrich), to study gap-junction formation between CMCs and MFBs. Corresponding AlexaFluor-

568 conjugated donkey-anti-mouse IgG and AlexaFluor-488 conjugated donkey-anti-rabbit IgG secondary antibodies (Invitrogen) were used at a dilution of 1:400. Nuclei were stained with Hoechst 33342 (10 µg/mL; Invitrogen). Fluorescent images were captured by fluorescent microscopy and analyzed using dedicated software (ImageJ, National Institutes of Health, Bethesda, MA, USA).

SIN-LV production

Vesicular stomatitis virus G-protein-pseudotyped self-inactivating human immunodeficiency virus type I vectors (SIN-LVs.) were produced in 293T cells. These cells were transfected with a lentiviral vector shuttle plasmid together with psPAX2 (Addgene, Cambridge, MA, USA) and pLP/VS.VG (Invitrogen) using 25-kDa linear polyethyleneimine (Polysciences, Warrington, PA, USA) as transfection agent. After 16 hours, transfection medium was replaced by culture medium and after 64 hours, the culture fluid was collected by centrifugation and freed of cellular debris by filtration. Concentration of lentiviral vector particles was performed by ultracentrifugation through a 20% (w/V) sucrose cushion. Pellets containing vector particles were suspended in phosphate-buffered saline with 1% bovine serum albumin fraction V (Sigma-Aldrich).

Lentiviral knockdown of Cx43 expression in MFBs

To suppress Cx43 expression, MFBs were transduced by lentiviral vectors carrying a Cx43-specific shRNA (Open Biosystems, Huntsville, AL, U.S.A.). The lentiviral vectors LV.SM2C.Cx43.hPGK.eGFP targeting Cx43 and LV.SM2C.pLuc.hPGK.eGFP targeting firefly luciferase (control) have been described previously.[9] Knockdown was structurally confirmed by immunocytological and Western Blot analyses and functionally confirmed by dye transfer assay.

Western blot analyses

At day 9 of culture, cultures were rinsed in ice-cold PBS and homogenized in RIPA-buffer. Homogenates were size-fractionated on NuPage 12% Bis-Tris gels (Invitrogen) before transfer to Hybond PVDF membranes (GE Healthcare, Leiderdorp, the Netherlands). These membranes were incubated with an antibody against Cx43 (Sigma-Aldrich) for 1 h followed by incubation with a matching HRP-conjugated secondary antibody (Santa Cruz Biotechnologies, Santa Cruz, CA, USA). To check for equal protein loading, β-tubulin (Millipore, Billerica, MA, USA) expression was determined. ECL Advance Detection reagents (GE Healthcare) were used to induce chemiluminescence which was subsequently caught on Hyperfilm ECL

(GE Healthcare). Intensities of Cx43 and β-tubulin bands were quantified by Scion Image analysis software (Scion Corporation, Frederick, MD, USA).

Optical mapping

Action potential propagation patterns of purified CMC cultures and MFB-CMC co-cultures ($8x10^5$ cells/well in a 24-wells format) were studied by optical mapping with the voltage-sensitive dye di-4-ANEPPS (Invitrogen). On day 9 of culture, cells were incubated for 15±5 min with serum-free culture medium (DMEM/Ham's F10) containing 8 µmol/L di-4-ANEPPS. After incubation, cultures were refreshed with DMEM/Ham's F10 (37ºC) and subsequently mapped at 37ºC. To limit phototoxic effects, the same culture was never exposed to excitation light for ≥40s and mapping experiments typically did not exceed 30 min. Electrical activation was optically recorded (Ultima-L, SciMedia, Costa Mesa, CA, USA) and subsequently analyzed (Brain Vision Analyze 1103, Brainvision Inc, Tokyo, Japan). Action potential duration was defined as the period between the timepoint of maximal upstroke velocity and 90% repolarization (APD_{90}). Ectopic activity was defined as the presence of multiple sites of initiating activation.[8] Early afterdepolarizations (EADs) were defined as reversal of repolarization of at least 10% of the optical action potential amplitude of the initial activation, before full repolarization occurred. Pharmacological interventions were performed by directly pipetting the agent of interest into the mapping medium under mapping conditions, and effects were assessed after gentle agitation during an incubation period of 30 seconds in all groups. Tetrodotoxin (TTX) was obtained from Alomone Labs (Jerusalem, Israel).

Whole-cell patch-clamp

Whole-cell patch-clamp measurements were performed in purified CMC cultures, MFB cultures and co-cultures of CMCs and Cx43-silenced or pLuc-silenced, eGFP expressing MFBs at day 7-9 of culture. CMCs were identified by phase contrast microscopy and lack of fluorescence signal. Next, action potentials in CMCs were recorded in current-clamp at 25°C. Whole-cell recordings were performed using a L/M-PC patch-clamp amplifier (3 kHz filtering) (List-Medical, Darmstadt, Germany). Tip and seal resistance were 2.0-2.5 MΩ and >1 GΩ, respectively. For data acquisition and analysis, pClamp/Clampex8 software (Axon Instruments, Molecular Devices, Sunnyvale, CA, USA) was used. Parameters of interest were maximal diastolic potential (MDP), maximal upstroke velocity (dV/dt_{max}) and APD_{90}. In a different set of experiments, 0.5 mM $BaCl_2$ was added to the cultures to study the effect on MDP.

Dye transfer

Mitomycin-C-treated CMC cultures were loaded for 7 min with calcein-red-orange AM (Invitrogen) diluted in Hank's buffered salt solution (HBSS, Gibco, Grand Island, USA). Cells were rinsed twice and kept on culture medium containing 2.5 mmol/L probenecid (Invitrogen), which blocks multidrug resistance protein-dependent calcein efflux from the cells. Lentivirally eGFP-labeled MFBs or MFBs with Cx43 knockdown or pLuc knockdown were subsequently plated out in a 1:1 ratio with the calcein-loaded CMCs. The presence of dye transferred from CMCs to labeled MFBs and intensity of fluorescent signal were captured and subsequently quantified using dedicated software (ImageJ).

Statistical analysis

Statistical analyses were performed using SPSS11.0 for Windows (SPSS Inc., Chicago, IL, USA). Data were compared with one-way or two-factor mixed ANOVA test with Bonferroni post-hoc correction when appropriate, and expressed as mean±SD. Comparison between two groups was performed using paired or unpaired Student's-t test where appropriate. Differences were considered statistically significant if $P<0.05$.

Results

Conduction slowing, prolonged repolarization, ectopic activity and spontaneous reentrant tachyarrhythmias are commonly found in fibrotic cultures

In all cultures, >98% of all fibroblasts expressed α-SMA and collagen-I and were therefore considered MFBs as described previously.[8] In fibrotic cultures, relative MFB numbers were 53.0±0.6% at day 9, whereas purified CMC cultures contained 18.7±1.2% MFBs, as judged by quantification of collagen I/α-actinin staining (Figure 1A). To assess the arrhythmogenic potential of MFBs, fibrotic co-cultures of MFBs and CMCs and purified CMC cultures were assessed for several electrophysiological parameters using optical mapping. CV was significantly lower in fibrotic cultures compared to controls (11.2±1.6 cm/s vs. 23.9±2.1 cm/s; $P<0.0001$ n=30 and n=60) (Figure 1B). Basal spontaneous activation frequencies were 0.52±0.39Hz in controls and 0.90±0.61Hz in fibrotic cultures ($P<0.05$). Optical signal characteristics were distinctly altered in fibrotic cultures (Figure 1C). Time until 90% repolarization (APD_{90}), was significantly increased in fibrosis (Figure 1D). This signified slowing of repolarization in addition to slowed depolarization. Furthermore, prolonged repolarization was observed to precede early afterdepolarizations (EADs). EADs comprised 58% of 36 episodes of ectopic activity (Figure 1C arrow), whereas remaining episodes consisted of spatially alternating sites that initiated activation.

Consequently, of fibrotic cultures (total n=30), 53.3% showed ectopic activity as opposed to 18.3% of CMC cultures (total n=60) (Figure 1E, G). Moreover, the incidence of reentrant tachyarrhythmias was considerably higher in fibrotic cultures when compared to CMC cultures (5.0% vs. 30%) (Figure 1F, H). Of 14 episodes of spontaneous spiral wave formation, all were initiated by EADs, emphasizing their importance in arrhythmogenesis. Together, these results strongly demonstrate the pro-arrhythmogenic effects of MFBs in cardiac cultures.

Heterocellular coupling is associated with an elevated MDP of CMCs in fibrotic cultures

To study intercellular coupling between CMCs and MFBs, CMC-MFB co-cultures were stained for the gap-junctional proteins Cx43 and Cx45. Immunocytological staining revealed that Cx43 as well as Cx45 were expressed between adjacent MFBs, CMCs and MFBs adjacent to CMCs, suggesting the ability of MFBs to form homo- and heterocellular gap-junctions with both connexins (Supplemental Figure 1A). Of heterocellular junctions, 50.2% of 227 cell pairs showed expression of Cx43, whereas 25.5% of 180 cell pairs showed expression of Cx45. Furthermore, areas covered by Cx43 expression were significantly larger than areas covered by Cx45 at homocellular (Supplemental Figure 1B) and heterocellular junctions (Supplemental 1C), consistent with a dominant role of Cx43 in gap-junctional protein expression. Heterocellular gap-junction functionality was studied by calcein-red-orange dye transfer from CMCs to adjacent MFBs. Supplemental Figure 1D shows a representative image of adjacent calcein-positive MFBs and CMCs, confirming this ability, as isolated cells did not show such transfer of calcein (Supplemental Figure 1E). On an electrophysiological level, whole-cell current-clamp performed on CMCs in fibrotic cultures during spontaneous 0.5-1 Hz activation revealed a less negative MDP (-49.4±6.1 mV; n=7) compared to CMCs in control cultures (-64.8±5.9 mV; n=8; $P<0.001$) (Supplemental Figure 1F). The resting membrane potential of MFBs in homocellular cultures was -17.0±6 mV (n=9), which could explain their depolarizing effect on neighbouring CMCs after the establishment of functional heterocellular gap junctions.

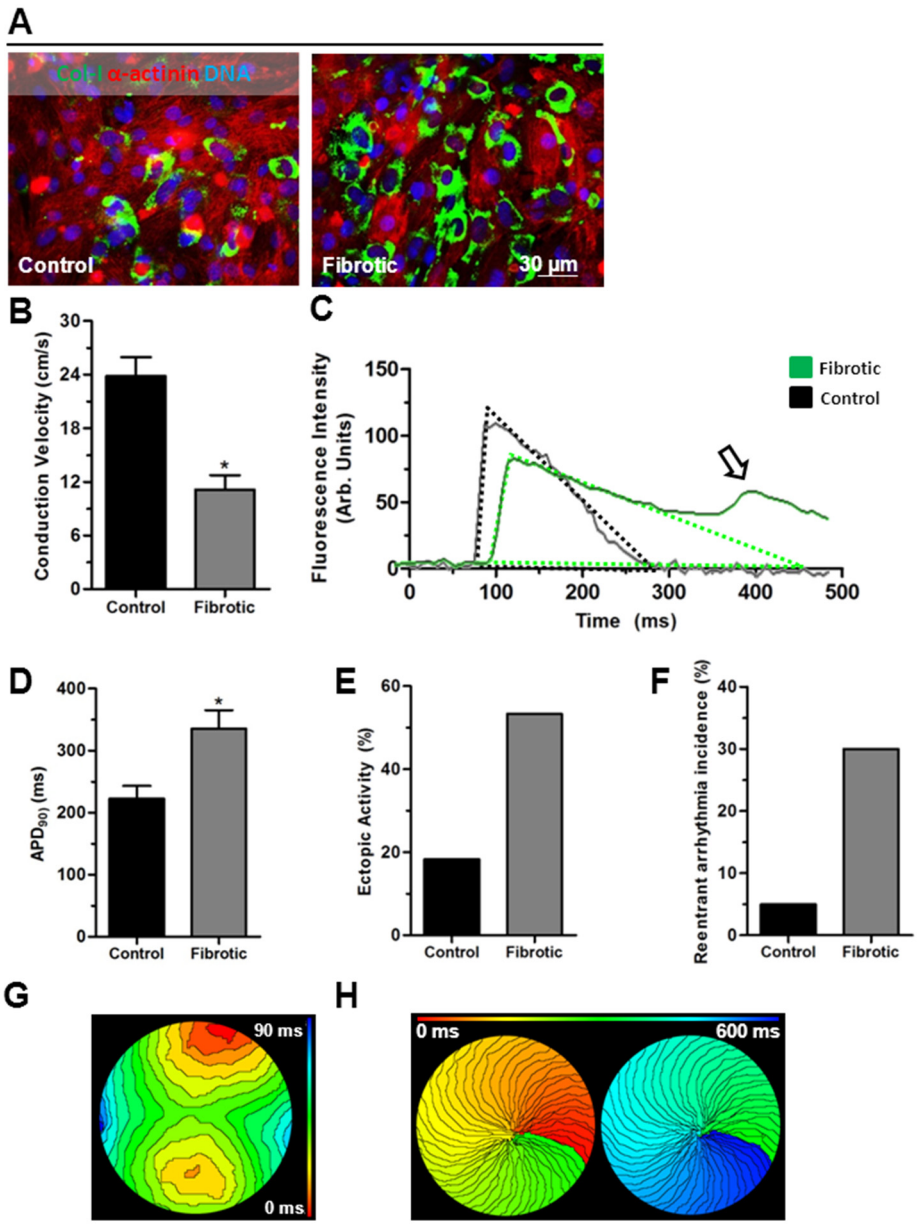

Figure 1. *Fibrotic cultures are pro-arrhythmic. (A) Typical example of a collagen I (green) and α-actinin (red) double staining showing more MFBs in fibrotic cultures compared to control cultures. Nuclei are stained blue with Hoechst 33342. (B) CV was slowed in fibrotic cultures *: P<0.001. (C) Typical optical signal trace shows prolongation of the action potential, the occurrence of an EAD in a fibrotic culture. (D) APD_{90} is increased in fibrotic culture. *:P<0.05*

vs. control. (E) Incidence of ectopic activity was significantly higher in the fibrotic group, as was the case for (F) spontaneous reentry. (G) Isochronal maps (6 ms) showing ectopic activity in a fibrotic culture and (H) 2 subsequent activations during a reentrant tachyarrhythmia in a fibrotic culture.

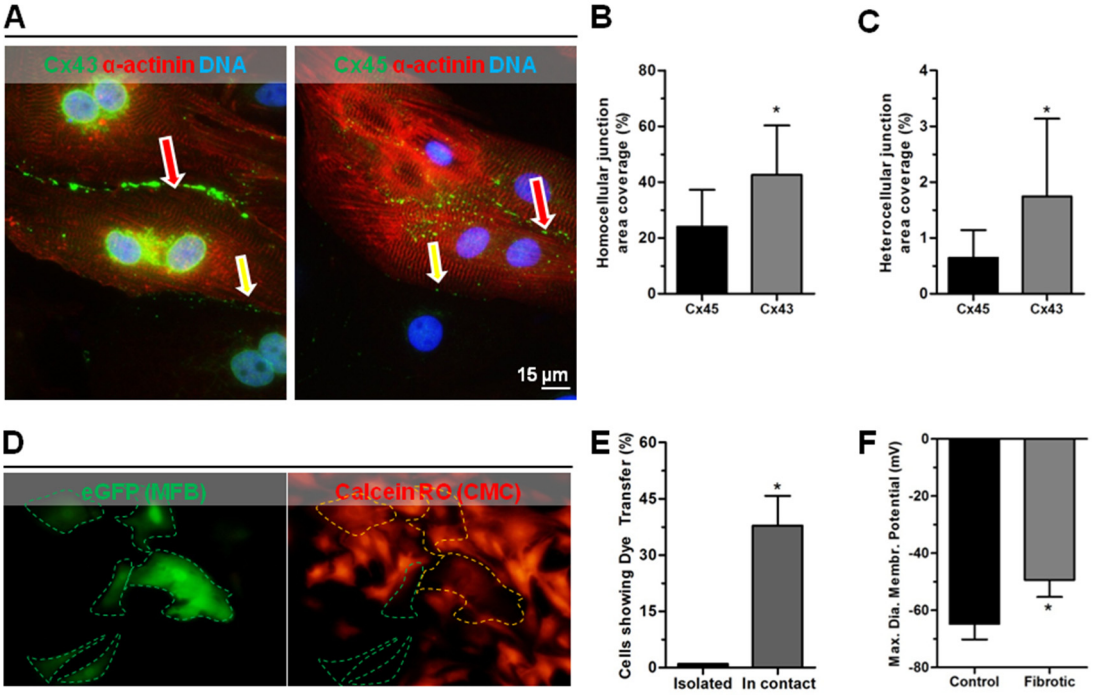

Supplemental Figure 1. Heterocellular coupling is associated with a less negative MDP of CMCs in fibrotic cultures*. (A) Cx43 and Cx45 were present at homo- and heterocellular junctions. Red arrows indicate homocellular CMC-CMC junctions. Yellow arrows indicate heterocellular MFB-CMC junctions. (B) Cx43 covers relatively larger areas at homocellular or (C) heterocellular junctions compared to Cx45. *p<0.05. (D) Typical photomicrographs of a dye transfer assay show that (E) eGFP-labeled MFBs in direct contact with calcein red-orange AM-loaded CMCs exhibit transfer of the calcein, whereas isolated MFBs showed no such transfer. (F) MDP obtained from whole-cell current-clamp recordings during 0.5-1 Hz spontaneous activity showed that CMCs in fibrotic cultures are significantly more depolarized as compared to those in purified CMC cultures (control). *: P<0.001.*

Taken together, these results implicate that MFBs and CMCs are functionally coupled and that CMCs are significantly depolarized in the proximity of MFBs, which may play a key role in the arrhythmogeneity of MFBs and may therefore represent a therapeutic target.

shRNA-mediated Cx43 silencing by viral transduction

To investigate heterocellular coupling as a potential target for anti-arrhythmic interventions, Cx43 expression in MFBs was downregulated by means of lentiviral shRNA-mediated RNA interference. After transduction with LV.SM2C.Cx43.hPGK.eGFP, Cx43 expression in MFBs was 53% lower than in LV.SM2C.pLuc.hPGK.eGFP-transduced MFBs as judged by Western blot analysis (Supplemental Figure 2A). Assessment of eGFP expression by fluorescence microscopy revealed that both SIN-LVs. had transduced the cells at equally high levels (Supplemental Figure 2B). To exclude the possibility that Cx43 knockdown solely affected the intracellular Cx43 pool, the western blot data were complemented with immunocytological analysis. After transduction with LV.SM2C.Cx43.hPGK.eGFP, Cx43 expression at MFB-MFB junctions was 74% lower in than control cells (Supplemental Figure 2B, C).

Silencing Cx43 expression in MFBs reduces functional heterocellular coupling without affecting homocellular CMC expression of Cx43

The effect of Cx43 knockdown on functional heterocellular coupling was first assessed by calcein transfer experiments. The effect of Cx43 knockdown on intercellular dye transfer between MFBs and CMCs was a lower percentage of calcein-positive LV.SM2C.Cx43.hPGK.eGFP-transduced MFBs in co-cultures when compared to Lv.SM2C.pLuc.hPGK.eGFP-transduced MFBs in co-cultures (22.4±6.5% vs. 40.8±10.6%; $P<0.01$ n=50 cell pairs across 7 photos per group) (Figure 2A and B). In addition, fluorescence intensity of the transferred dye was significantly lower in the Cx43 knockdown group than in the pLuc-silenced MFB group (Figure 2C). In 1:1 co-cultures with either pLuc- or Cx43-silenced MFBs, the MFB numbers and distribution were equal (Figure 2D). Homocellular Cx43 expression between CMCs was not affected by Cx43-silencing in MFBs. However, intercellular Cx43 expression at heterocellular junctions was 68% lower in co-cultures with Cx43-silenced MFBs than in co-cultures with pLuc-silenced MFBs (2.7±1.3 arb. units vs. 8.5±3.8 arb. units; $P<0.001$, Figure 2E, F).

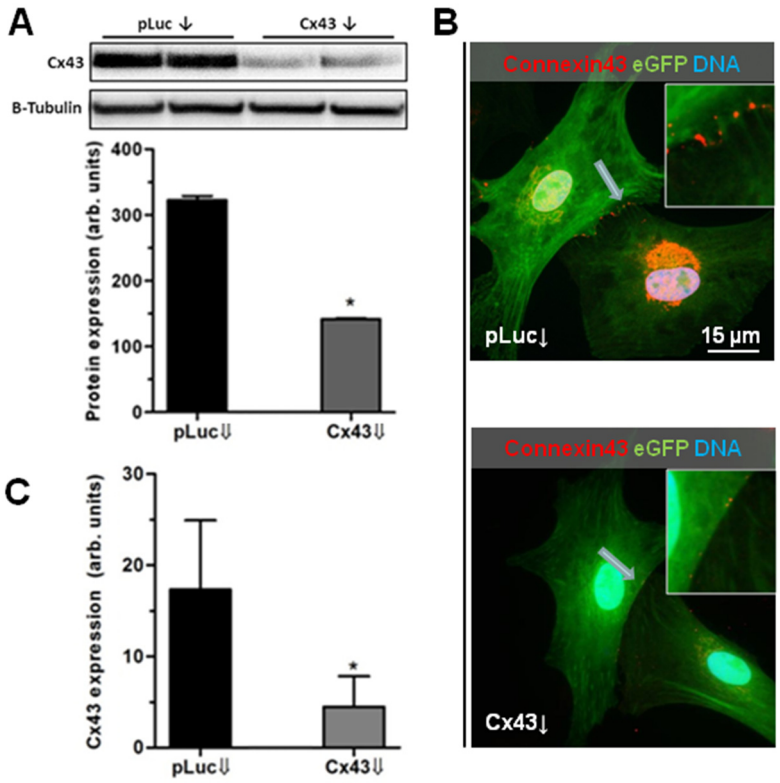

Supplemental Figure 2. *shRNA-mediated Cx43 silencing by lentiviral vectors decreases Cx43 expression in MFBs. (A) Typical example and quantification of Cx43 expression, normalized for β-tubulin expression from Western blot analysis showing significantly lower expression of Cx43 in Cx43-silenced MFBs compared to control (p<0.001). (B) Typical example of an immunocytological staining, showing less intercellular expression of Cx43 between Cx43-silenced MFBs compared to pLuc-silenced MFBs (control). (C) Quantification of intercellular Cx43 expression. *: p<0.001 vs. pLuc silencing (control).*

Preserved MDP and faster repolarization of CMCs in fibrotic cultures by heterocellular uncoupling

Next, CMCs in co-cultures were analysed by whole-cell patch-clamp to evaluate the electrophysiological consequences of Cx43 knockdown in fibrotic cultures (Supplemental Figure 3, Figure 3A). As a result of depressed heterocellular coupling, MDP was preserved in co-cultures with LV.SM2C.Cx43.hPGK.eGFP-transduced MFBs compared to co-cultures containing pLuc-silenced MFBs (-61.4±5.7 mV vs. -51.6±4.0 mV; *P*<0.05, (Figure 3B).Concomitantly, dV/dt_{max} was significantly higher in fibrotic

cultures with Cx43-silenced MFBs (Figure 3C), implying increased excitability. In addition, repolarization occurred faster in CMCs of the Cx43 knockdown group, as APD_{90} was reduced to 333±35 ms vs. 525±42 ms in the pLuc group (225±21 ms for non-fibrotic controls, Figure 3D).

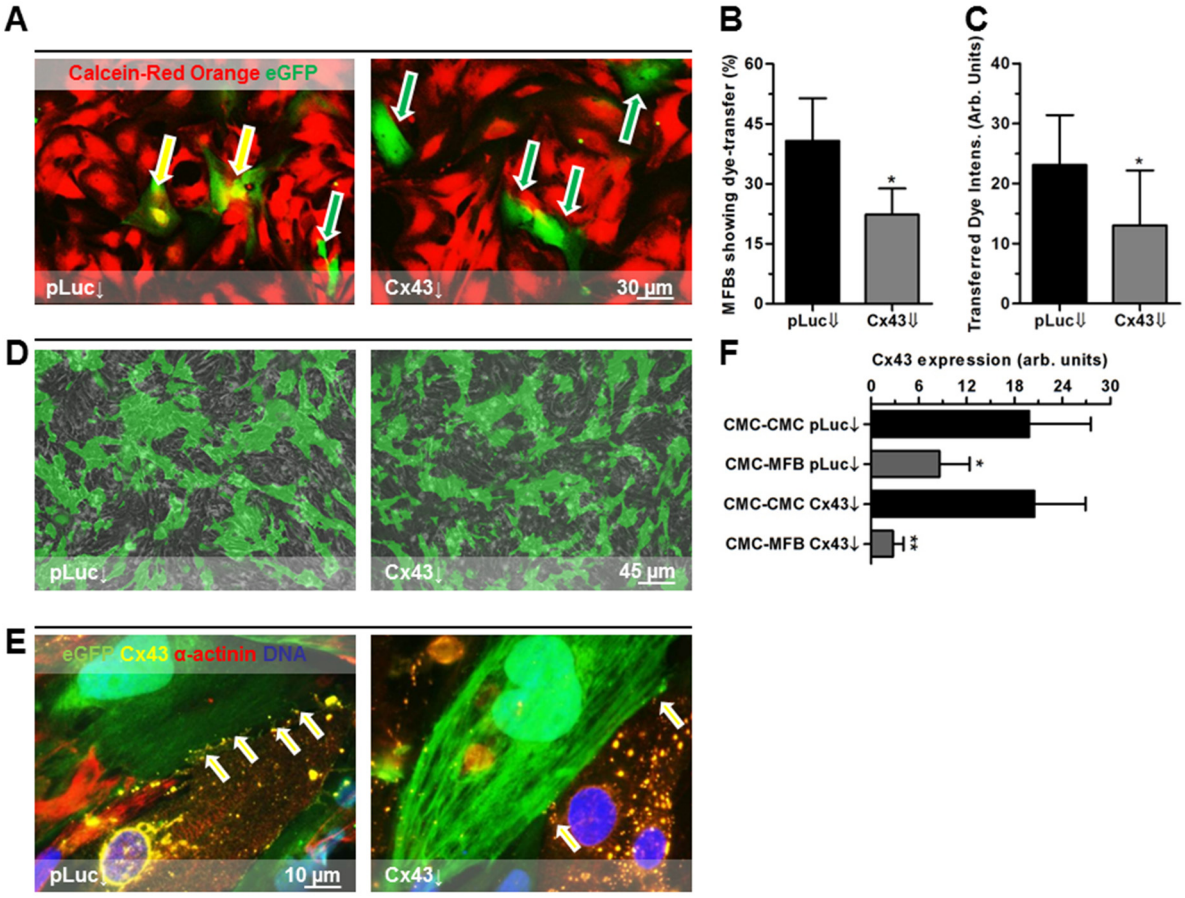

Figure 2. *Functional consequences of MFB Cx43 silencing in CMC-MFB co-cultures. (A) Typical examples of calcein Red-Orange loaded CMCs in co-culture with eGFP expressing, Cx43-silenced or pluc-silenced MFBs. Yellow arrows indicate MFBs that show transfer, whereas green arrows indicate MFBs that do not receive calcein from neighboring CMCs. (B) Quantification of the number of eGFP-positive MFBs showing transfer of calcein Red-Orange per image. *: P<0.001 (C) Fluorescence intensity of the transferred dye. *: P<0.001. (D) Typical examples of a merged image of phase-contrast and eGFP fluorescence showing equal distribution and relative numbers of Cx43-silenced or pLuc-silenced green MFBs in co-cultures. (E) Typical example of Cx43/α-actinin double staining showing decreased intercellular Cx43*

*expression in co-cultures with Cx43-silenced MFBs compared to co-cultures with pLuc-silenced MFBs (control). (F) Homo- and heterocellular Cx43 expression. *:P<0.05 vs. CMC-CMC pLuc silencing. **:P<0.05 vs. CMC-CMC Cx43 silencing and CMC-MFB pLuc silencing.*

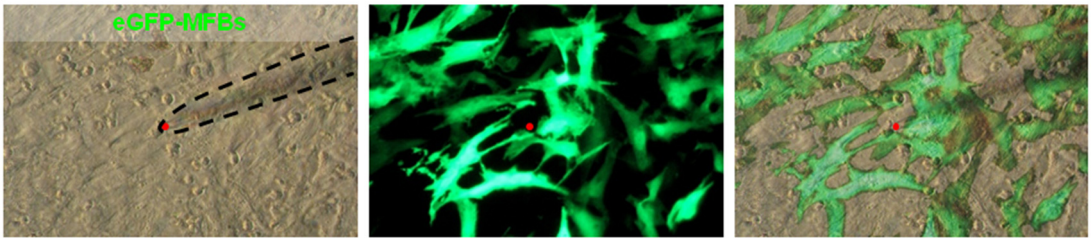

Supplemental Figure 3. *EGFP-labeling of MFBs in fibrotic co-cultures allowed for the selective intracellular measurement of CMCs.*

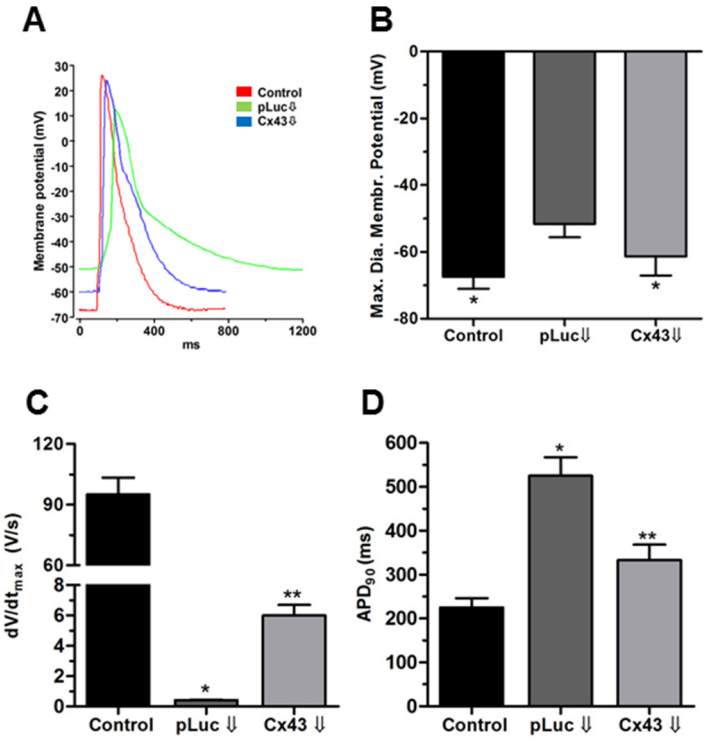

Figure 3. *Electrophysiological effects of Cx43 silencing in MFBs on CMCs at the intracellular level. (A) Typical examples of whole-cell patch-clamp recordings of CMCs in different myocardial cultures. (B) In fibrotic cultures with Cx43-silenced MFBs, the resting membrane potential of CMCs is significantly more negative as compared to CMCs in co-culture with pLuc-silenced MFBs, although not as negative as the resting membrane potential of CMCs in purified CMC cultures (control). *: P<0.05 vs. pLuc-silencing. (C) Maximal upstroke velocity in CMCs in co-culture with Cx43-silenced MFBs is significantly higher compared to CMCs in co-culture with pLuc-silenced MFBs. *:P<0.05 vs. control. **:P<0.05 vs. pLuc and Control. (D) APD_{90} is significantly decreased in fibrotic cultures with Cx43-silenced MFBs. *:P<0.05 vs. pLuc silencing.*

Cx43 knockdown in MFBs preserves excitability and prevents prolonged repolarization, ectopic activity and reentrant tachyarrhythmias in fibrotic myocardial cultures

At the tissue level, CV was significantly higher in co-cultures with Cx43-silenced MFBs than in co-cultures with pLuc-silenced MFBs (16.0±3.2 cm/s vs. 10.6±4.3 cm/s; P<0.001) (Figure 4A, B). Furthermore, Cx43-silencing in MFBs resulted in morphological changes in optical action potentials (Figure 4C). Consistent with the dV/dt_{max} - increasing effect of MFB-specific Cx43 silencing in patch-clamp experiments, the decrease in CV after I_{na} inhibition by 20 µM TTX was significantly larger in co-cultures with Cx43-silenced MFBs than in co-cultures with pLuc-silenced MFBs (Figure 4D). This indicated reduced MFB-induced depolarization and larger availability of Nav1.5 channels in CMCs by Cx43-knockdown in MFBs. This indicated reduced MFB-induced depolarization and larger availability of Nav1.5 channels in CMCs by Cx43-knockdown in MFBs.

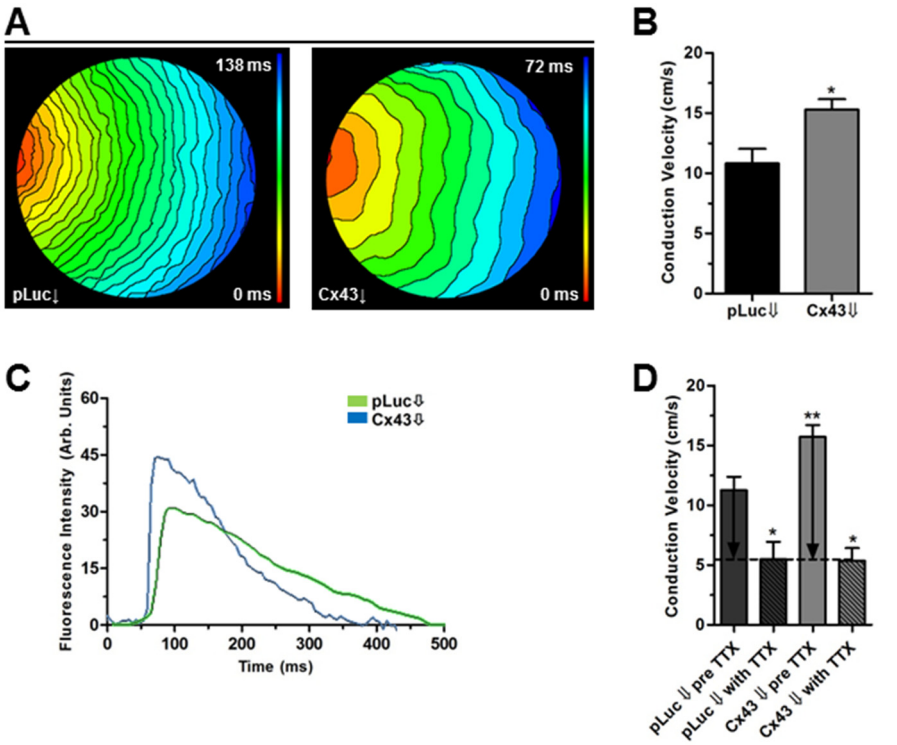

Figure 4. *Cx43-silencing in MFBs preserves culture excitability and fast conduction. (A) Typical activation maps of uniform propagation in co-cultures with Cx43-silenced MFBs and pLuc-silenced MFBs (6 ms isochrones). (B) CV was significantly higher for co-cultures with Cx43-*

*silenced MFBs than in co-cultures with pLuc-silenced MFBs. *: P<0.001 vs. fibrotic cultures with pLuc-silenced MFBs. (C) Optical signal traces show different action potential morphologies by Cx43-silencing in MFBs. (D) Nav1.5 blockade by 20 µM TTX decreases CV in both groups to similar values, although the decrease was larger for the Cx43-silenced group, indicating increased excitability. *:P<0.05 vs. pre TTX. **:P<0.05 vs. all.*

Findings of faster repolarization in patch-clamp experiments were also confirmed at the population level by optical mapping, as APD_{90} was significantly reduced by Cx43 knockdown in MFBs (Figure 5A, B, C). Furthermore, the incidence of ectopic activity in co-cultures was significantly decreased by Cx43 downregulation in MFBs. Of all co-cultures with Cx43-silenced MFBs 19.4% (total n=62) showed ectopic activity compared to 36.4% in co-cultures with pLuc-silenced MFBs (total n=33) (Figure 5D). Foremost, Cx43 knockdown in MFBs (n=55) decreased the incidence of reentrant tachyarrhythmias in co-cultures by 40% when compared to co-cultures with pLuc-silenced MFBs (n=32) (16.4% vs. 56.4%, Figure 5E). If a co-culture with Cx43-silenced MFBs exhibited a reentrant tachyarrhythmia, its reentrant cycle length was shorter than observed in a co-culture with pLuc-silenced MFBs (248±19ms vs. 296±48ms, *P*<0.05).

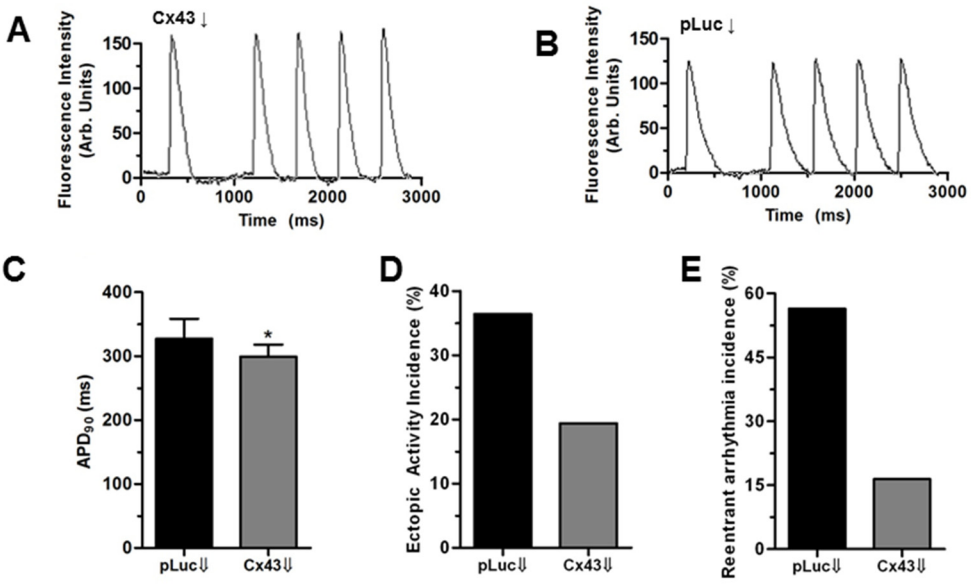

Figure 5. *Reduction of prolonged repolarization signifies a decrease in ectopic activity and spontaneous arrhythmias by Cx43-silencing in MFBs. (A) Typical optical signal trace during 1-2 Hz activation of fibrotic cultures with Cx43-silenced MFBs or (B) pLuc-silenced MFBs showing*

*that (C) APD_{90} was significantly decreased by Cx43-silencing in MFBs. *:P<0.05 vs. pLuc-silencing. (D) Co-cultures with Cx43-silenced MFBs showed less ectopic activity and (E) less spontaneous reentrant activity compared to co-cultures with pLuc-silenced MFBs (control).*

Re-induced depolarization abolishes anti-arrhythmic effects of Cx43 knockdown in MFBs in fibrotic myocardial tissue

To investigate whether the anti-arrhythmic mechanism of Cx43 knockdown was due to prevention of MFB-induced depolarization of the CMCs, depolarization was re-induced by I_{k1} inhibition with 0.5 mM $BaCl_2$. Indeed, $BaCl_2$ elevated the MDP of CMCs in co-culture with Cx43-silenced MFBs towards values found in the pLuc co-cultures (-59.0±4.7 mV (n=4) vs. -48.3±4.1 mV (n=4) before and after, respectively, P<0.05, Figure 6A). At the tissue level, this more positive MDP of CMCs caused by I_{k1} inhibition decreased CV in Cx43-knockdown cultures from 15.2±1.1 cm/s (n=62) to 9.7±1.1 cm/s (n=18), negating the higher CV normally found when compared to pLuc control cultures, which were not significantly affected (n=19, Figure 6B). Similarly, APD_{90} was increased in the Cx43 knockdown group after $BaCl_2$ (Figure 6C, D) and associated with increased ectopic activity by 27% (Figure 6E) and reentry by 36% (Figure 6F), thereby abolishing the anti-arrhythmic effects of down regulation heterocellular coupling in fibrotic myocardial cultures. To confirm these findings, CMCs in these cultures were depolarized by adding 10 mM of KCl to the mapping medium to increase the extracellular K^+ concentration to 14 mM. In accordance with the $BaCl_2$ experiments, increased extracellular [K^+] also reversed the anti-arrhythmic potential of MFB-specific Cx43 knockdown in fibrotic co-cultures, as CV was decreased, whereas APD_{90} and ectopic and arrhythmic activity were increased in these cultures (Supplemental Figure 4).

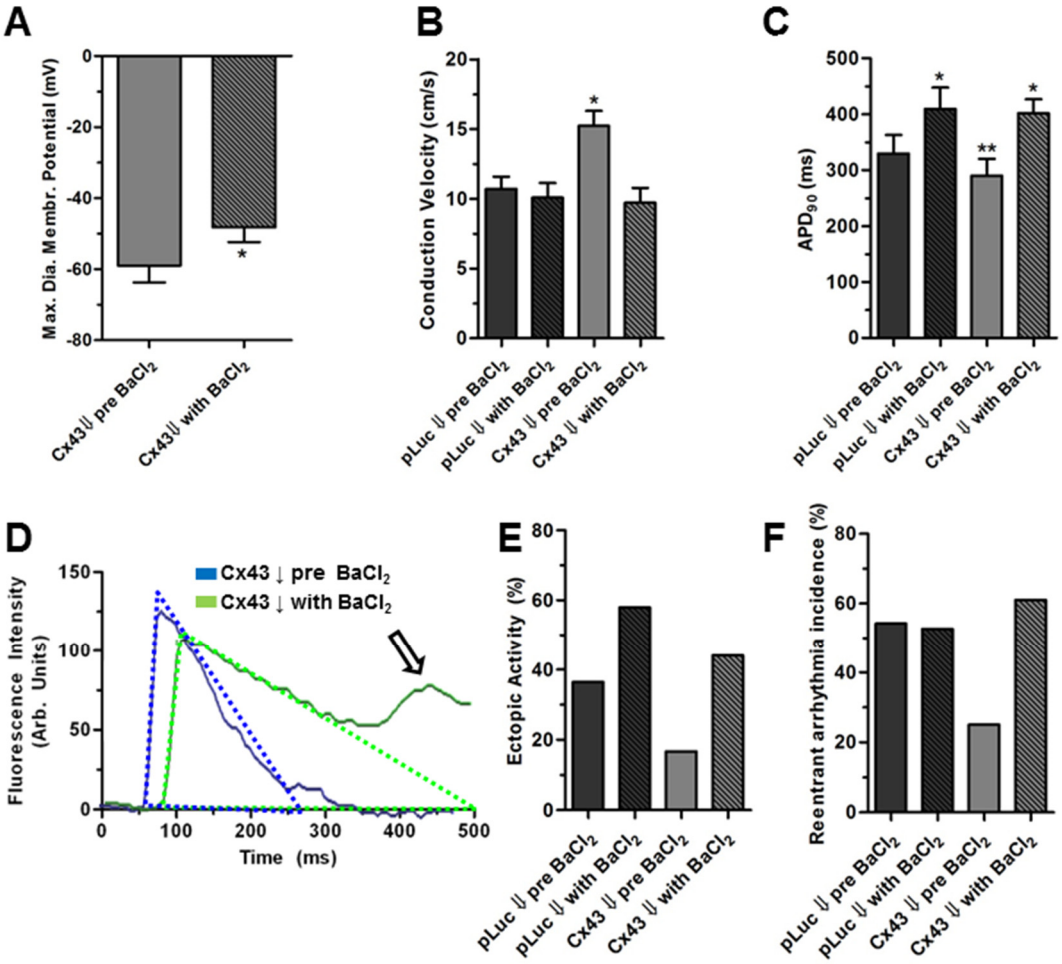

***Figure 6**. Increased excitability of CMCs after Cx43-silencing in MFBs and the preventive effect on ectopic activity and arrhythmias is reversed by depolarization of the resting membrane potential. (A) Inhibition of I_{k1} by 0.5 mM $BaCl_2$ elevated the MDP of CMCs in the Cx43-silencing group towards values of the pLuc group. The same intervention did not affect pLuc cultures. *:P<0.05 vs. all. (B) Depolarization by I_{k1} inhibition using BaCl2 slowed CV only in the Cx43 silencing group. *:P<0.05 vs. all. (C) I_{k1} inhibition cancels the effect of Cx43-silencing in MFBs on APD_{90} of optical action potentials and thus lengthens repolarization. (D) Increased APD_{90} by $BaCl_2$ increases the propensity towards EADs as marked by the arrow. (E) The preventive effect of Cx43 silencing on ectopic activity or (F) reentry is abolished by depolarization by I_{k1} inhibition.*

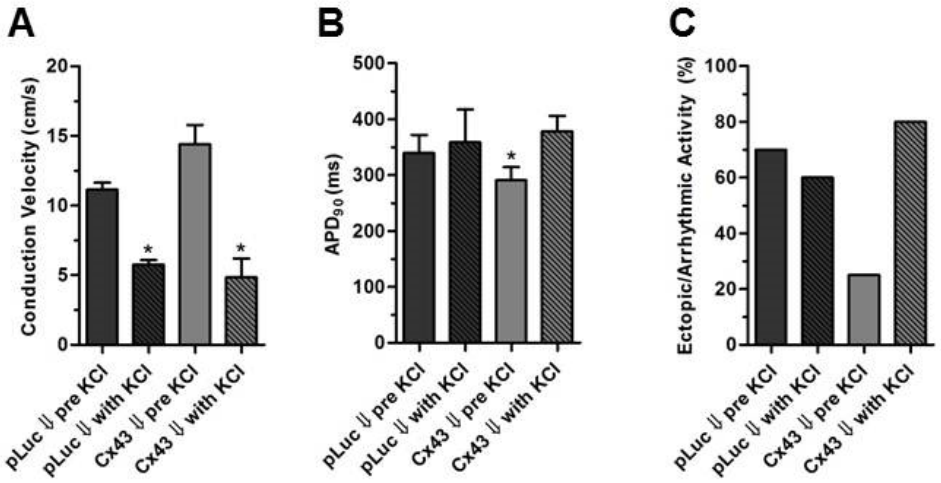

Supplemental Figure 4. *Depolarization in fibrotic myocardial cultures by increased extracellular K^+ reverses anti-arrhythmic potential of Cx43 knockdown in MFBs. Administration of 10 mM KCl to fibrotic CMC cultures has a more profound effect on (A) conduction velocity (*:p<0.05 vs pre KCl), (B) repolarization (*:p<0.05 vs all) or (C) ectopic and arrhythmic activity in co-cultures with Cx43-silenced MFBs than in those containing pLuc-silenced MFBs. The number of cultures analyzed were 10 and 10 for the pLuc group and 8 and 10 for the Cx43-knockdown group in the absence and presence of extra KCl, respectively.*

Discussion

Key findings of this study are (1) Silencing of Cx43 expression in MFBs leads to reduced heterocellular functional coupling and less MFB-induced depolarization of CMCs. 2) Preservation of the MDP of CMCs by Cx43 down regulation in MFBs leads to increased excitability and reduced prolongation of repolarization as compared to control, thereby limiting conduction slowing and decreasing ectopic activity. 3) The aforementioned changes are associated with a lower incidence of spontaneous reentrant tachyarrhythmias in fibrotic myocardial cultures. 4) MDP of CMCs is a key factor in the anti-arrhythmic effects of Cx43 down regulation in MFBs as all of the favorable changes could be reversed by depolarization of CMCs through I_{k1} inhibition or increasing extracellular $[K^+]$.

Cardiac fibrosis and abnormal impulse propagation and generation

The pro-arrhythmogenic effects of cardiac fibrosis, a process which consists of excessive MFB proliferation and extracellular matrix deposition, have been demonstrated *in vitro* and *in vivo*. Unfortunately, the exact pro-arrhythmic mechanisms are incompletely understood and the therapeutic efficacy of current anti-arrhythmic treatment options remains suboptimal. Initially, the mechanism by which cardiac fibrosis was considered to be pro-arrhythmic was that of extracellular matrix-mediated CMC separation, which leads to anatomical zigzag course of conduction and conduction block.[10,11] However, in recent years several studies have demonstrated that MFBs, independent of matrix deposition, could play a more crucial pro-arrhythmic role than initially thought. In fibrotic myocardial cultures, slow conduction, increased ectopic activity and propensity towards reentrant arrhythmias have been described, as was confirmed by the present study.[5-8]

In vitro studies have indicated that MFB-CMC coupling could be responsible for arrhythmogenesis by altering electrophysiological characteristics of CMCs. Functional heterocellular coupling between cardiac fibroblasts and CMCs was first observed by Rook *et al*.[12] The mechanism by which heterocellular coupling causes slowed conduction is thought to be based on electrotonic interaction leading to depolarization of CMCs to membrane potentials at which fast sodium channels are largely inactivated, thereby reducing excitability and CV.[13]

Besides causing conduction slowing, MFBs have also been shown to contribute to ectopic activity when seeded on top of cultured CMCs.[6] As the sarcolemma of CMCs becomes increasingly less negative with increasing numbers of adjacent MFBs, a level of depolarization can be reached that allows for depolarization-induced automaticity as basis for ectopic activity. Slowed conduction and ectopic activity are known to increase arrhythmogeneity in *in vitro* models of cardiac tissue and are both caused by heterocellular interactions.[5, 7, 14]

Anti-arrhythmic effects of Cx43 down regulation in MFBs

As electrotonic interaction is mediated through gap-junctions and has been suggested to be the basis of both conduction slowing and increased ectopic activity, this study investigated whether down regulation of this heterocellular coupling would have anti-arrhythmic effects. Although heterocellular coupling occurs through, at least, both Cx43 and Cx45-based connexons, a strong, functionally relevant reduction in heterocellular coupling could be achieved by solely down regulating Cx43 in MFBs. This can be explained by the higher expression levels of Cx43 at heterocellular junctions compared to Cx45, as was confirmed in this study.[14,15] The relatively higher occurrence of heterocellular Cx43 and Cx45

expression in this study compared to other studies can be explained by the notion that the fibroblastic cells are α-SMA positive myofibroblasts as opposed to α-SMA negative fibroblasts.[16] Conduction slowing by heterocellular coupling seems to be based on depolarization-induced inactivation of fast sodium channels, thereby reducing excitability. Indeed, the decrease in heterocellular coupling by lentiviral Cx43 knockdown in MFBs led to an increased CV and upstroke velocity. Nav1.5 blockade by 20 µM TTX yielded larger decreases in CV in the Cx43 knockdown group than in fibrotic control cultures, thereby proving that excitability was increased by reducing heterocellular coupling. Furthermore, by Cx43 knockdown in MFBs, CMCs were significantly less depolarized, also indicating increased excitability. As junctional Cx43 expression in MFBs was not completely abolished by transduction of these cells with LV.SM2C.Cx43.hPGK.eGFP, it was to be expected that CV would not be fully restored due to residual heterocellular coupling through Cx43 and Cx45. In addition, other mechanisms than heterocellular electrical coupling may contribute to arrhythmogeneity of fibrotic myocardial cultures. In a recent study, mechanical coupling and contractile forces between MFBs and CMCs were shown to affect CV and inducibility of arrhythmias in an anisotropic co-culture model.[17] However, the role of mechanical coupling may be of lesser influence in the current model, possibly because, unlike in the previous study, cells were not treated with TGF-β, different cellular ratios and tissue organizations were studied at different time-points.

Cx43 silencing in MFBs had also a pronounced effect on ectopic activity. The basis for increased ectopic activity in fibrotic cultures is still not fully understood. The current study provides a possible explanation by describing altered repolarization dynamics in fibrotic cultures. Triangulation of the action potential, or phase 3 prolongation is considered to be a highly pro-arrhythmic phenomenon as it can precede TdP *in vivo*.[18] In fibrotic cultures, APD_{90} was increased and preceded ectopic activity in the form of EADs. This is in accordance with computer simulations predicting that EADs occur more frequently in fibrotic cultures and are critical in spiral wave formation.[13,19] Prolongation of repolarization is currently thought to increase the chance of EAD generation by prolonging the time spent within the membrane potential range of the window current of L-type calcium channels, which allows for de-inactivation and subsequent reactivation.[20]

The combination of slowed conduction and increased ectopic activity is known to increase the pro-arrhythmic potential of cardiac tissue.[21] Hence, an increase in CV and a decrease in ectopic activity by Cx43 knockdown in MFBs reduce arrhythmogeneity, reflected by a lower incidence of spontaneous tachyarrhythmias. The importance of depolarization of CMCs as a key pro-arrhythmic mechanism was demonstrated by administration of $BaCl_2$, which effectively blocks I_{k1} and thereby

depolarizes CMCs independently of heterocellular coupling.[22] The dosage of $BaCl_2$ used in the present study is expected to completely and selectively block I_{K1} without significant effects on other potassium currents.[22,23] or L-type calcium current.[24] The I_{K1}-inhibition-induced depolarization immediately resulted in conduction slowing, prolonged repolarization, ectopic activity by EAD formation and spontaneous reentry in fibrotic cultures with Cx43-silenced MFBs, thereby reversing the anti-arrhythmic effect of reducing heterocellular coupling. In accordance, fibrotic cultures with pLuc knockdown as a control were not as strongly affected by $BaCl_2$-induced depolarization, suggesting that MFB-induced depolarization elevated the membrane potential towards values at which excitability was low enough to be relatively insensitive to further depolarization. Increasing extracellular $[K^+]$ confirmed the effects of $BaCl_2$ on reversing the anti-arrhythmic effect of Cx43-silencing in MFBs.
Taken together, the results of this study provide mechanistic insight into how MFBs exert their pro-arrhythmic effects on CMCs and how modulation of heterocellular coupling between CMCs and MFBs, as well as the MDP of CMCs could be targeted by anti-arrhythmic strategies.

Study limitations

Human adult CMCs are a more clinically relevant cell type than neonatal rat CMCs, but cannot be kept in culture for extended periods of time and are limited in availability. Although fibrosis consists of both an increase in MFBs and extracellular matrix, the latter was not investigated, as *in vitro* deposition of matrix of quality and quantity comparable to an in vivo situation is difficult to achieve. Although it is well established that MFBs and CMCs functionally couple *in vitro*, strong, undeniable proof of this phenomenon *in vivo* has yet to appear. Consequently, it is recognized that more *in vivo* research is necessary before *in vitro* results can be translated to clinical implications.

Conclusions

MFBs are able to form functional heterocellular gap-junctions with CMCs and are thereby able to diminish CMC excitability, reduce CV in cardiac cultures, prolong repolarization and induce ectopic activity, and give rise to spontaneous reentrant tachyarrhythmias in fibrotic myocardial cell cultures. Targeting heterocellular gap-junctional coupling by selective silencing of Cx43 expression in MFBs preserves CMC excitability, limits conduction slowing, prolonged repolarization and the incidence of ectopic activity and thereby prevents reentrant tachyarrhythmias. This effect resulted from decreased depolarization of CMCs through heterocelullar coupling as

I_{k1} inhibition or an increase in extracellular [K^+] abolished the anti-arrhythmic effects of Cx43-silencing in MFBs.

Funding
This work was supported by the Dutch Heart Foundation (2008/B119). D.A.P. is the recipient of the Netherlands Organisation for Scientific Research (NWO) VENI grant (91611070).

Acknowledgements
We thank Dr. Wilbert P.M. van Meerwijk for constructive discussions, and Huybert J.F. van der Stadt for excellent technical support.

Conflict of Interest
None declared

Supplemental Material

Methods

All animal experiments were approved by the Animal Experiments Committee of the Leiden University Medical Center and conform to the Guide for the Care and Use of Laboratory Animals as stated by the US National Institutes of Health.

Immunocytochemical analyses

Following mapping experiments at day 9 of culture, cultures were stained for proteins of interest, or cultures were stained parallel to mapping experiments as described earlier.[1] Cultures were stained for α-smooth muscle actin (α-SMA) and vimentin expression to study fibroblasts phenotype (Sigma-Aldrich, St. Louis, MO, USA), collagen-I expression to quantify MFB numbers (Abcam, Cambridge, MA, USA), and α-actinin (Sigma-Aldrich) as CMC-specific marker. In addition, cultures were also stained for connexin43 (Cx43) (Sigma-Aldrich) and connexin45 (Cx45) (Santa Cruz Biotechnology, Santa Cruz, CA, USA), to study gap junction formation between CMCs and MFBs. Corresponding AlexaFluor-568 conjugated donkey-anti-mouse IgG and AlexaFluor-488 conjugated donkey-anti-rabbit IgG secondary antibodies (Invitrogen, Breda, the Netherlands) were used at a dilution of 1:400. Nuclei were stained with Hoechst 33342 (10 µg/mL; Invitrogen). A fluorescent microscope equipped with a digital camera was used to capture images (Nikon Eclipse, Nikon Europe, Badhoevedorp, the Netherlands) and dedicated software (Image-Pro Plus, version 4.1.0.0, Media Cybernetics, Silver Spring, MD, USA) was used to analyze stained cultures. All proteins of interest were studied in at least 6 different cultures from a specific group, from which at least 20 representative images were acquired at various magnifications (10, 40, 100x). All cultures were stained using the same solutions and captured using equal exposure times for the protein of interest. Analysis of images was performed with ImageJ 1.44p (National Institutes of Health, USA). For analysis of gap-junctional Cx43 or Cx45 expression, percentual area coverage was determined in a fixed predefined area after setting a threshold value at 33% of maximal signal intensity. Fluorescent intensity levels were determined as an average pixel value within a fixed area, at least 5-fold per cell, or cell-cell junction for connexin staining.

SIN-LV production

To suppress Cx43 expression, MFBs were transduced by lentiviral vectors carrying a Cx43-specific shRNA (Open Biosystems, Huntsville, AL, U.S.A.). The lentiviral vectors LV.SM2C.Cx43.hPGK.eGFP targeting Cx43 and LV.SM2C.pLuc.hPGK.eGFP targeting firefly luciferase (control) have been described previously.[2]

Vesicular stomatitis virus G-protein-pseudotyped self-inactivating human immunodeficiency virus type I vectors (SIN-LVs.) were produced by seeding six 175 cm^2 culture flasks with 1 x 10^5 293T cells per cm^2 in DMEM (Invitrogen) supplemented with 10% fetal bovine serum (FBS, Invitrogen) and 10 µmol/L cholesterol (Sigma-Aldrich). The next day, these producer cells were transfected with either one of the lentiviral vector plasmids together with psPAX2 (Addgene, Cambridge, MA, USA) and pLP/VSVG (Invitrogen) at a 2:1:1 molar ratio using a total of 200 ng DNA/cm^2 and 3 ng polyethyleneimine (Polysciences, Warrington, USA) per ng DNA as transfection agent. Sixteen hours later, the transfection medium was replaced by DMEM containing 5% FBS, 10 mM HEPES-NaOH (pH 7.4) and 10 µmol/L cholesterol. At 64 h post-transfection, the culture fluid was collected and freed of cellular debris by centrifugation at room temperature for 10 min at 825x *g* and filtration through a 0.45 µm pore-sized cellulose acetate filter (Pall Corporation, East Hills, NY, USA). To concentrate the lentivirus vector particles, a 5 mL cushion of 20% sucrose in phosphate-buffered saline (PBS) was loaded under 30 ml of the cleared culture medium, which was then centrifuged for 90 min at 15,000 rpm and 10°C in an SW28 rotor (Beckman Coulter, Fullerton, CA, USA). Next, the supernatant was discarded and the pellets with the vector particles were suspended in 400 µL of PBS containing 1% bovine serum albumin (BSA fraction V from Sigma-Aldrich) by gentle rocking overnight at 4°C.

The gene transfer activity of the vector stocks was determined by end-point titration on HeLa indicator cells using flow-cytometric analysis of *eGFP* as read-out. The titers of the SIN-LV preparations are thus expressed in HeLa cell-transducing units (HTUs) per mL.

MFBs were transduced with SIN-LV particles at a multiplicity of infection (MOI) of 32 HTUs per cell in culture medium containing 20 µg/mL diethylaminoethyl-dextran sulfate (GE Healthcare, Diegem, Belgium). After 4 h, the cultures were washed three times with PBS and supplied with fresh culture medium. MFBs were passaged twice before application in experiments.

Western blot analyses

MFB cultures were transduced with LV.SM2C.Cx43.hPGK.eGFP or LV.SM2C.pLuc.hPGK.eGFP parallel to mapping experiments. At day 9 of culture, transduced and mock-transduced cultures were rinsed in ice-cold PBS and homogenized in RIPA-buffer consisting of 50 mmol/L Tris-HCl (pH 8.0), 150 mmol/L NaCl, 1% NP-40, 0.5% sodiumdeoxycholate, and 0.1% SDS. Homogenates were size-fractionated on NuPage 12% gels before wet transfer to Hybond PVDF membranes (GE Healthcare). These membranes were incubated with an antibody against Cx43 (Sigma-Aldrich) for 1 h followed by incubation with corresponding HRP-conjugated secondary antibody (Santa Cruz). To check for equal protein loading, β-tubulin (Millipore, Billerica, MA, USA) expression was determined. ECL Advance Detection reagents (GE Healthcare) were used to induce chemiluminescence which was subsequently caught on Hyperfilm ECL (GE Healthcare). The intensity of Cx43 and β-tubulin-specific signals were quantified by Scion Image analysis software (Scion Corporation, Frederick, MD, USA).

Optical mapping

Action potential propagation patterns of purified CMC cultures and CMC-MFB co-cultures ($8x10^5$ cells/well in 24-wells plate) were studied by optical mapping with the voltage-sensitive dye di-4-ANEPPS (Invitrogen). Structurally heterogenous cultures (<5%, determined by light microscopy or electrophysiological mapping) were all excluded for reasons of standardization and reproducibility. On day 9 of culture, cells were incubated for 15±5 min with culture medium (1:1 DMEM/Ham's F10 + 5% HS) containing 8 µmol/L di-4-ANEPPS. After incubation, cultures were refreshed with DMEM/Ham's F12 (37ºC) and subsequently mapped at 37º C. Epi-illumination excitation light (λ_{ex}=525±25 nm) was delivered by a halogen arc-lamp (MHAB-150W, Moritex Corporation, San Jose, CA, USA). To limit phototoxic effects of the mapping protocol on the cultures, the same culture was never exposed to excitation light for longer than 40s and mapping experiments in a 24-well plate typically did not exceed 30 min. Fluorescent emission light (λ_{em}>590 nm) passed through a camera lens (1x Plan-Apo, WD=15 mm; Leica, Wetzlar, Germany) and a dichroic mirror, after which it was focused onto a 100 by 100 pixels (100 mm^2) CMOS camera (Ultima-L, SciMedia, Costa Mesa, CA, USA) by a 1.6x converging lens, resulting in a total field of view of 256 mm^2 and a spatial resolution of 160 µm/pixel. Electrical activation was recorded for at least 4 s at a rate of 167 or 500 frames/s, high-pass filtered and analyzed using Brain Vision Analyze 1103 (Brainvision Inc, Tokyo, Japan). For each pixel, signals were averaged with 8 of its nearest neighboring pixels. Time point at which the rate of rise of fluorescence signal (d*F*/dt) was maximal was defined as the activation time point.

CV in cultures with a uniform activation pattern at an activation frequency of 1-2 Hz, was calculated between two 3 by 3 pixel grids, typically spaced 2-8 mm apart, and perpendicular to the activation wavefront. Per culture, CV was determined in 6-fold and averaged for further comparisons. Action potential duration, measured from the timepoint of maximal upstroke velocity (dF/dT_{max}) until 90% of repolarization (APD_{90}), was determined in 3-fold and averaged. Reentry was defined as >4 cycles of a circular activation pattern. Reentrant cycle length was calculated from 3 separate cycles per culture and averaged. Ectopic activity was defined as the presence of multiple sites of initiating activation.[1] Early after depolarizations (EADs) were defined as the reversal of repolarization of at least 10% of the optical action potential amplitude of the previous activation. Pharmacological interventions were performed by directly pipetting the agent of interest into the mapping medium under mapping conditions and effects were assessed after gentle agitation during an incubation period of 30 seconds in all groups.

Dye transfer

To investigate functional coupling between MFBs and CMCs, eGFP-labeled MFBs were kept in culture for 2 weeks and at least passaged twice before they were used in experiments. CMC cultures containing 10^5 cells/well were treated with 10 µg/ml mitomycin-C to prevent endogenous MFB overgrowth. At day 4, these cultures (n=12) were loaded for 7 min with 10 µg/mL calcein-red-orange AM (Invitrogen) in HEPES-buffered salt solution (HBSS, Gibco, Grand Island, USA), which once internalized is hydrolyzed to the orange fluorescent dye calcein-red-orange. Cells were rinsed twice with PBS and kept on culture medium containing 2.5 mmol/L probenecid (Invitrogen) which prevents calcein efflux[25]. eGFP-labeled MFBs were subsequently plated out in a 1:1 ratio with the calcein-loaded CMCs. To determine the functional effect of Cx43 downregulation in MFBs, dye transfer experiments were performed using MFBs transduced with LV.SM2C.Cx43.hPGK.eGFP or LV.SM2C.pLuc.hPGK.eGFP, and CMCs loaded with 10 µg/mL Calcein Red-Orange-AM (Invitrogen). Fluorescent images (at least 10 per culture, at least 12 cultures per group) were acquired after 7 h of co-culture under equal exposure times and magnifications. The percentage of eGFP-labeled MFBs that had received calcein from adjacent CMCs as well as the intensity of the dye-associated fluorescent signal per calcein-positive MFB were determined using ImageJ.

References

1. van der Burg AE, Bax JJ, Boersma E, Pauwels EK, van der Wall EE, Schalij MJ. Impact of viability, ischemia, scar tissue, and revascularization on outcome after aborted sudden death. *Circulation*. 2003;108:1954-1959.

2. Arshad A, Mandava A, Kamath G, Musat D. Sudden cardiac death and the role of medical therapy. *Prog Cardiovasc Dis*. 2008;50:420-438.

3. Manabe I, Shindo T, Nagai R. Gene expression in fibroblasts and fibrosis: involvement in cardiac hypertrophy. *Circ Res*. 2002;91:1103-1113.

4. Sun Y, Kiani MF, Postlethwaite AE, Weber KT. Infarct scar as living tissue. *Basic Res Cardiol*. 2002;97:343-347.

5. Miragoli M, Gaudesius G, Rohr S. Electrotonic modulation of cardiac impulse conduction by myofibroblasts. *Circ Res*. 2006;98:801-810.

6. Miragoli M, Salvarani N, Rohr S. Myofibroblasts induce ectopic activity in cardiac tissue. *Circ Res*. 2007;101:755-758.

7. Zlochiver S, Munoz V, Vikstrom KL, Taffet SM, Berenfeld O, Jalife J. Electrotonic myofibroblast-to-myocyte coupling increases propensity to reentrant arrhythmias in two-dimensional cardiac monolayers. *Biophys J*. 2008;95:4469-4480.

8. Askar SF, Ramkisoensing AA, Schalij MJ, Bingen BO, Swildens J, van der Laarse A, Atsma DE, de Vries AA, Ypey DL, Pijnappels DA. Antiproliferative treatment of myofibroblasts prevents arrhythmias in vitro by limiting myofibroblast-induced depolarization. *Cardiovasc Res*. 2011.

9. Pijnappels DA, Schalij MJ, van Tuyn J, Ypey DL, de Vries AA, van der Wall EE, van der Laarse A, Atsma DE. Progressive increase in conduction velocity across human mesenchymal stem cells is mediated by enhanced electrical coupling. *Cardiovasc Res*. 2006;72:282-291.

10. de Bakker JM, van Capelle FJ, Janse MJ, Tasseron S, Vermeulen JT, de JN, Lahpor JR. Slow conduction in the infarcted human heart. 'Zigzag' course of activation. *Circulation*. 1993;88:915-926.

11. Spach MS and Dolber PC. Relating extracellular potentials and their derivatives to anisotropic propagation at a microscopic level in human cardiac

muscle. Evidence for electrical uncoupling of side-to-side fiber connections with increasing age. *Circ Res*. 1986;58:356-371.

12. Rook MB, Jongsma HJ, de JB. Single channel currents of homo- and heterologous gap junctions between cardiac fibroblasts and myocytes. *Pflugers Arch*. 1989;414:95-98.

13. Xie Y, Garfinkel A, Camelliti P, Kohl P, Weiss JN, Qu Z. Effects of fibroblast-myocyte coupling on cardiac conduction and vulnerability to reentry: A computational study. *Heart Rhythm*. 2009;6:1641-1649.

14. McSpadden LC, Kirkton RD, Bursac N. Electrotonic loading of anisotropic cardiac monolayers by unexcitable cells depends on connexin type and expression level. *Am J Physiol Cell Physiol*. 2009;297:C339-C351.

15. Pedrotty DM, Klinger RY, Badie N, Hinds S, Kardashian A, Bursac N. Structural coupling of cardiomyocytes and noncardiomyocytes: quantitative comparisons using a novel micropatterned cell pair assay. *Am J Physiol Heart Circ Physiol*. 2008;295:H390-H400.

16. Vasquez C, Mohandas P, Louie KL, Benamer N, Bapat AC, Morley GE. Enhanced fibroblast-myocyte interactions in response to cardiac injury. *Circ Res*. 2010;107:1011-1020.

17. Thompson SA, Copeland CR, Reich DH, Tung L. Mechanical coupling between myofibroblasts and cardiomyocytes slows electric conduction in fibrotic cell monolayers. *Circulation*. 2011;123:2083-2093.

18. Hondeghem LM, Carlsson L, Duker G. Instability and triangulation of the action potential predict serious proarrhythmia, but action potential duration prolongation is antiarrhythmic. *Circulation*. 2001;103:2004-2013.

19. Sato D, Xie LH, Sovari AA, Tran DX, Morita N, Xie F, Karagueuzian H, Garfinkel A, Weiss JN, Qu Z. Synchronization of chaotic early afterdepolarizations in the genesis of cardiac arrhythmias. *Proc Natl Acad Sci U S A*. 2009;106:2983-2988.

20. Guo D, Zhao X, Wu Y, Liu T, Kowey PR, Yan GX. L-type calcium current reactivation contributes to arrhythmogenesis associated with action potential triangulation. *J Cardiovasc Electrophysiol*. 2007;18:196-203.

21. Kleber AG and Rudy Y. Basic mechanisms of cardiac impulse propagation and associated arrhythmias. *Physiol Rev*. 2004;84:431-488.

22. Kilborn MJ and Fedida D. A study of the developmental changes in outward currents of rat ventricular myocytes. *J Physiol*. 1990;430:37-60.

23. Giles WR and Imaizumi Y. Comparison of potassium currents in rabbit atrial and ventricular cells. *J Physiol*. 1988;405:123-145.

24. Rampaart LJ, Beekwilder JP, van Kempen GT, van den Berg RJ, Ypey DL. The local anesthetic butamben inhibits total and L-type barium currents in PC12 cells. *Anesth Analg*. 2008;106:1778-1783.

25. Feller N, Broxterman HJ, Wahrer DC, Pinedo HM. ATP-dependent efflux of calcein by the multidrug resistance protein (MRP): no inhibition by intracellular glutathione depletion. *FEBS Lett*. 1995;368:385-388.

Cellular and Molecular Mechanisms of Arrhythmias in Cardiac Fibrosis and Beyond:

From Symptoms to Substrates towards Solutions

Chapter IV

Similar Arrhythmicity in Hypertrophic and Fibrotic Cardiac Cultures Caused by Distinct Substrate-Specific Mechanisms

Substrate-Dependent Arrhythmic Mechanisms

Saïd F. A. Askar, MSc*; Brian O. Bingen, MD*; Martin J. Schalij, MD, PhD; Jim Swildens, Msc; Douwe E. Atsma, MD, PhD; Cindy I. Schutte, BSc; Antoine A. F. de Vries, PhD; Katja Zeppenfeld, MD, PhD; Dirk L. Ypey, PhD; Daniël A. Pijnappels, PhD.

*Equal contribution

Adapted from Cardiovasc Res 2013;97:171-181

Abstract

Aims: Cardiac hypertrophy and fibrosis are associated with potentially lethal arrhythmias. As these substrates often occur simultaneously in one patient, distinguishing between pro-arrhythmic mechanisms is difficult. This hampers understanding of underlying pro-arrhythmic mechanisms and optimal treatment. This study investigates and compares arrhythmogeneity and underlying pro-arrhythmic mechanisms of either cardiac hypertrophy or fibrosis in *in vitro* models.

Methods & Results: Fibrosis was mimicked by free myofibroblast (MFB) proliferation in neonatal rat ventricular monolayers. Cultures with inhibited MFB proliferation were used as control or exposed to phenylephrine to induce hypertrophy. At day 9, cultures were studied with patch-clamp and optical-mapping techniques and assessed for protein expression. In hypertrophic (n=111) and fibrotic cultures (n=107), conduction and repolarization were slowed. Triggered activity was commonly found in these substrates and led to high incidences of spontaneous reentrant arrhythmias (67.5% hypertrophic, 78.5% fibrotic vs. 2.9% in controls (n=102)) or focal arrhythmias (39.1% 51.7% vs. 8.8% respectively). Kv4.3 and Cx43 protein expression levels were decreased in hypertrophy but unaffected in fibrosis. Depolarization of cardiomyocytes (CMCs) was only found in fibrotic cultures (-48±7mV vs. -66±7mV in control, $P<0.001$). L-type calcium-channel blockade prevented arrhythmias in hypertrophy, but caused conduction block in fibrosis. Targeting heterocellular coupling by low doses of gap-junction uncouplers prevented arrhythmias by accelerating repolarization only in fibrotic cultures.

Conclusions: Cultured hypertrophic or fibrotic myocardial tissues generated similar focal and reentrant arrhythmias. These models revealed electrical remodeling of CMCs as a pro-arrhythmic mechanism of hypertrophy and MFB-induced depolarization of CMCs as a pro-arrhythmic mechanism of fibrosis. These findings provide novel mechanistic insight into substrate-specific arrhythmicity.

Introduction

Pathophysiological alterations in myocardial structure as observed in cardiac fibrosis or hypertrophy are associated with the occurrence of lethal cardiac arrhythmias.[1-3] As hypertrophy and fibrosis may occur concomitantly to varying degrees in cardiac remodeling in one patient, it remains unclear how these adaptations independently contribute to the arrhythmogeneity of remodeled tissue. Hence, the mechanisms through which hypertrophy or fibrosis cause arrhythmias remain incompletely understood. Because hypertrophy and fibrosis are characterized by specific modifications at molecular and cellular levels, these alterations could thereby provide a basis for distinct substrate-specific pro-arrhythmic mechanisms. Although treatment of cardiac arrhythmias has improved over recent years, it remains suboptimal in terms of efficacy and safety.[4-6] The notion that pharmacological anti-arrhythmic treatment does not significantly improve survival, and may in fact evoke lethal arrhythmias, could indicate that anti-arrhythmic treatment, without detailed knowledge of the underlying pro-arrhythmic mechanisms, may limit therapeutic efficacy.[7] Therefore, this study aimed to identify and compare independent mechanisms of arrhythmias in hypertrophic or fibrotic myocardial tissue and thereby determine the arrhythmogeneity per substrate. The results revealed a similar occurrence of prolongation of repolarization, triggered activity and reentrant tachyarrhythmias in fibrotic and hypertrophic myocardial cultures. However, the underlying pro-arrhythmic mechanisms in these substrates were distinct, being of intrinsic nature in cardiac hypertrophy and of extrinsic origin in cardiac fibrosis.

Materials and Methods

All animal experiments were approved by the Animal Experiments Committee of the Leiden University Medical Center and conform to the Guide for the Care and Use of Laboratory Animals as stated by the US National Institutes of Health.

Cell Isolation and culture

Isolation of primary neonatal rat ventricular myocardial cells was performed as described previously.[8] In brief, animals were anaesthetized with 4–5% isoflurane inhalation anaesthesia. Adequate anaesthesia was assured by the absence of reflexes prior to rapid heart excision. After animal sacrifice by rapid heart excision, ventricular tissue was minced and digested with collagenase I (450 units/ml; Worthington, NJ, USA) in two digestion steps of 50 and 40 minutes. After a 75-minute pre-plating step to minimize the amount of fibroblasts in cardiac cell preparation, cells were plated out on fibronectin-coated, round glass coverslips (15 mm) at a cell density of 1-8x10^5 cells/well in 24-well plates (Corning Life Sciences, Amsterdam, the Netherlands) depending on the experiment. To mimic fibrosis, endogenously present myofibroblasts (MFBs) proliferated freely. As control, proliferation was inhibited by 10 µg/mL Mitomycin-C (Sigma-Aldrich, St. Louis, MO, USA) at day 1.[9] To induce hypertrophy, control cultures were exposed to 100 µM phenylephrine (PE, Sigma) for 24h at day 3 and day 8.

Immunocytological analyses

Cultures were stained for several markers of interest after 20 minute fixation in 1% paraformaldehyde and permeabilization with 0.1% Triton X-100. Primary antibodies (1:200) and corresponding secondary Alexa fluor-conjugated antibodies (1:400, Invitrogen, Carlsbad, CA, USA) were incubated for 2 hours. Counterstaining of nuclei was performed with Hoechst 33342 (Invitrogen). Images of cultures were quantified using dedicated software (Image-Pro Plus, version 4.1.0.0, Media Cybernetics, Silver Spring, MD, USA).

Western Blot

Hypertrophic, fibrotic or control cultures were homogenized in RIPA-buffer containing 50 mmol/L Tris-HCl (pH 8.0), 150 mmol/L NaCl, 1% Triton X-100, 0.5% sodiumdeoxycholate and 0.1% SDS. Then, 10 µg of protein per sample (at least 3 samples per group) were size-fractionated on NuPage 12% gels (Invitrogen) and transferred to Hybond PVDF membranes (GE Healthcare, Diegem, Belgium). Membranes were blocked in TBS-Tween (0.1%) + 5% Bovine Serum Albumin (Sigma) for 1h. Afterwards, these membranes were incubated with primary antibodies directed against Nav1.5 (Abcam, Cambridge, UK), Cav1.2, Kv4.3, Kir2.1, Kv7.1 (all from Alomone Labs, Jerusalem, Israel) for 1h, rinsed three times in TBS-Tween and then incubated with corresponding HRP-conjugated secondary antibodies (Santa Cruz Biotechnlogy, Santa Cruz, CA, USA) for 1h. Chemiluminescence was detected and caught on

hyperfilm ECL using ECL Prime detection reagents (GE Healthcare). To check for equal protein loading, GAPDH (Millipore, Billerica, MA, USA) expression was determined. To compare fibrotic and control groups, protein expression was subsequently adjusted for CMC content by normalizing for α-actinin (Sigma).

Optical mapping

Optical mapping in 24-well plates at a density of $8x10^5$ cells/well and subsequent analyses were performed as previously described.[9] At day 9, cultures were incubated with 8 μM Di-4-ANEPPS after which cultures were refreshed with DMEM/Hams F10 (37 °C) and optically mapped immediately using the Ultima-L mapping setup (SciMedia, Costa Mesa, CA, USA). Mapping experiments typically did not exceed 30 minutes per 24-wells plate. Also, cultures were not exposed to excitation light for longer than 50 s to limit possible phototoxic effects. Parameters of interest were determined using Brain Vision Analyze 1108 (Brainvision, Inc., Tokyo, Japan). The incidence of triggered activity was assessed in all groups after eliminating reentrant conduction by electrical stimulation. Triggered activity was defined as all newly formed optical action potentials independent of initial pacing- or spontaneous frequency, with >10% of the optical amplitude of the initial paced or spontaneous action potential. An early after depolarization (EAD) was defined as a reversal of repolarization during phase 2 or 3 of the action potential of > 10% of optical amplitude. Focal tachyarrhythmias were defined as non-reentrant activation patterns >3 repetitions faster than 2 Hz. Reentrant tachyarrhythmias were defined as repetitive circular activation patterns for >3 rotations at >2 Hz.

Pro-arrhythmic mechanisms studied by pharmacological interventions

Different pharmacological agents were administered during optical mapping for investigation of pro-arrhythmic mechanisms. To reduce the net inward current, L-type Ca^{2+} current was inhibited by administration of a relatively low dose of nitrendipine (3 μM) (Sigma) or verapamil (10 μM) (Centrafarm, Etten-Leur, the Netherlands) directly into the mapping medium. To reduce heterocellular coupling, a relatively low dose of 2-Amino-ethoxy diphenyl borate (2-APB, 5 μM) (Tocris Bioscience, Bristol, United Kingdom) or carbenoxolone (100 μM) (Sigma) was incubated for 20 minutes. To investigate effects of Nav1.5 blockade, tetrodotoxin (TTX, 20 μM, Alomone Labs) was directly used. For investigation of the involvement of intracellular calcium handling in arrhythmogeneity, intracellular calcium was buffered using 10-50 μM BAPTA-AM (Sigma) which incubated for 20 minutes. To investigate the effect of action potential duration (APD) prolongation on arrhythmogeneity, 0.5 mM sotalol (Sigma) was used. For reproducibility and comparability between all pharmacological interventions, all cultures were paced with a 1 Hz supra-threshold stimulation protocol during optical mapping recordings.

Whole-cell patch-clamp

Membrane potential recordings were performed with the whole-cell patch-clamp technique in hypertrophic cultures, co-cultures of cardiomyocytes (CMCs) and eGFP labeled MFBs at equal cell quantity and density as fibrotic cultures with freely proliferating MFBs, and control cultures. At day 9, after identification of CMCs by phase contrast and fluorescence microscopy, action potential properties were determined in current-clamp. Whole-cell recordings were performed at 25°C using a L/M-PC patch-clamp amplifier (3kHz filtering) (List-Medical, Darmstadt, Germany). The pipette solution contained (in mmol/L) 10 Na_2ATP, 115 KCl, 1 $MgCl_2$, 5 EGTA, 10 HEPES/KOH (pH 7.4). Tip and seal resistance were 2.0-2.5 MΩ and >1 GΩ, respectively. The bath solution contained (in mmol/L) 137 NaCl, 4 KCl, 1.8 $CaCl_2$, 1 $MgCl_2$, and 10 HEPES (pH 7.4). In a subset of experiments, CMCs were functionally uncoupled by incubation for 20 minutes with 25 µmol/L 2-APB to investigate action potential characteristics in hypertrophic, fibrotic or control cultures. For data acquisition and analysis, pClamp/Clampex8 software (Axon Instruments, Molecular Devices, Sunnyvale, CA, USA) was used.

Statistical analysis

Statistical analyses were performed using SPSS11.0 for Windows (SPSS, Inc., Chicago, IL, USA). Differences were considered statistically significant if $P<0.05$.

Results

Cellular characterization of hypertrophic myocardial cultures

In PE-treated cultures, expression levels of ANP (126.9±8.1 vs. 93.4±5.6 arbitrary units, $P<0.001$) (Supplemental figure 1A and 1B) and α-Skeletal Muscle Actin (131.0±9.0 vs. 116.5±17.0 arbitrary units, $P<0.01$) (Supplemental figure 1C and 1D) were significantly higher compared to control cultures. Furthermore, a significant increase from 1.4±0.7 10^6 pixels to 2.6±0.6x10^6 pixels ($P<0.05$) in cell surface area was observed (Supplemental figure 1F). Non-myocytes expressed α-Smooth-Muscle-Actin and Collagen-I as determined by immunocytological staining and were therefore considered MFBs. Moreover, cellular composition of cultures was analyzed by collagen I/α-actinin double staining, suitable for distinction between MFBs and CMCs.[9] Administration of PE to cardiac cultures did not influence MFB quantities (18.6±2.8% vs. 18.1±2.0% in control cultures, p=ns) (Supplemental figure 1E) or CMC quantities. As MFB quantities were as low as control cultures, PE-treated cultures were considered primarily pathologically hypertrophic with a minimal fibrotic component.

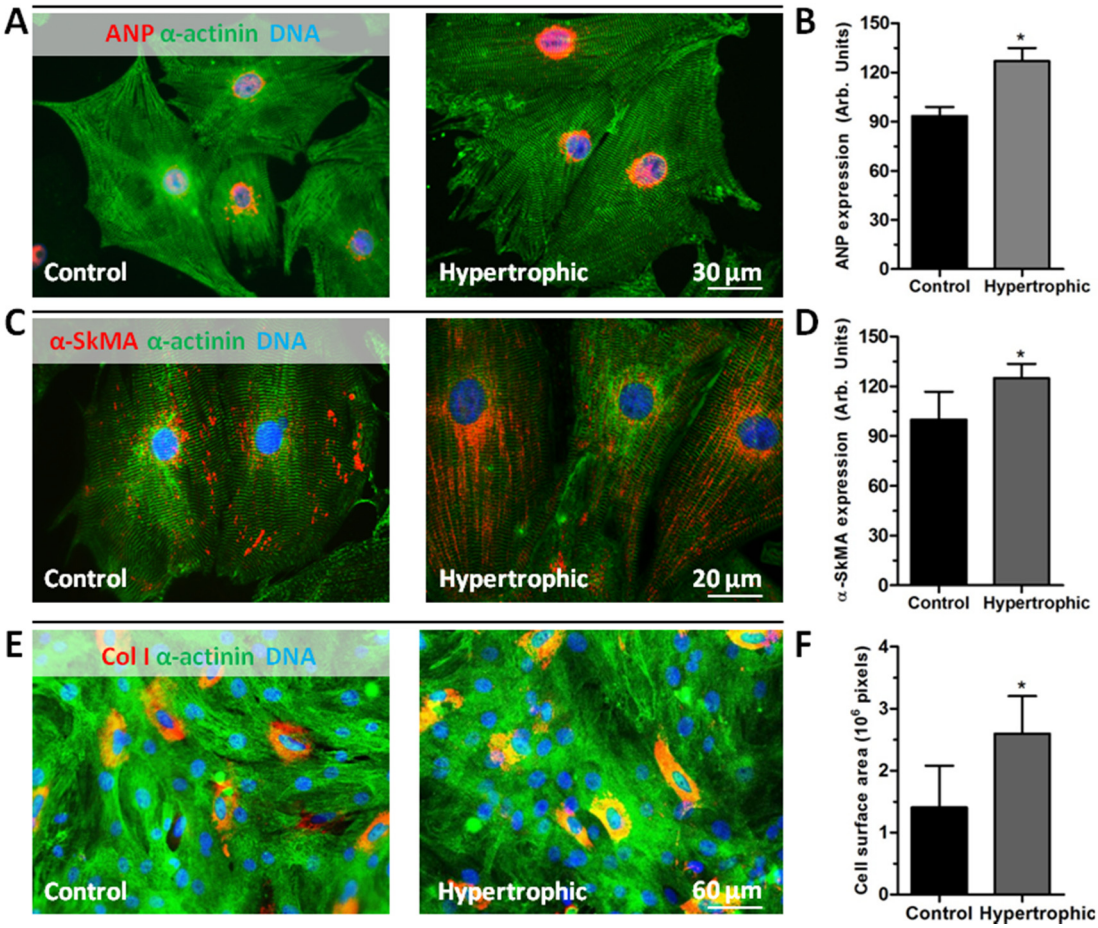

Supplemental Figure 1. *Cellular characterization of hypertrophic myocardial cultures. (A) Typical examples of immunocytological double-staining for ANP (red) and α-actinin (green). (B) Quantification of ANP signal. *:p<0.001 vs control. (C) Immunocytological double-staining for α-skeletal actin (red) and α-actinin (green). (D) Quantification of α-skeletal actin signal. *:p<0.01 vs control. (E) Immunocytological double-staining for collagen type I (red) and α-actinin (green). (F) Quantification of cell surface tracing, *:p<0.05.*

Cellular characterization of fibrotic myocardial cultures

At day 9 of culture, fibrotic cultures contained 61.5±2.6% MFBs whereas control cultures, treated with the antiproliferative agent mitomycin-C, contained 18.9±2.4% MFBs (P<0.001) (Supplemental figure 2A and B). Immunocytological staining revealed intercellular Cx43 expression at MFB-MFB, CMC-CMC and CMC-MFB junctions (Supplemental figure 2C). Heterocellular coupling was confirmed by calcein dye transfer between CMCs and MFBs (data not shown). Expression levels of Cx43 at heterocellular CMC-MFB junctions were significantly lower than at homocellular CMC-CMC junctions (35.5±12.3 vs. 7.8±3.1 arbitrary

units, *P*<0.0001) (Supplemental figure 2D). Importantly, as fibrotic cultures did not show an increase in cell surface area (1.2±0.46 10^6 pixels in control cultures vs. 1.1±0.35 10^6 pixels in fibrotic cultures) or up regulation of ANP expression (16.8±4.8 vs. 17.3±6.6 arbitrary units in control and fibrotic cultures, respectively, p=ns), absence of a hypertrophic component was confirmed (Supplemental figure 2E and 2F).

Conduction and repolarization are slowed in fibrotic and in hypertrophic cultures

Optical mapping recordings similarly showed slow conduction in uniformly propagating hypertrophic and fibrotic cultures (12.2±2.5 and 13.2±3.0 cm/s, respectively, vs. 24.5±2.1 cm/s in controls, *P*<0.0001) (Figure 1A). APD_{80} restitution curves from spontaneous optical signals showed prolonged repolarization compared to control cultures, which was most pronounced at activation frequencies ≤1 Hz (238±65 ms in control [range of 157-393 ms] vs. 721±404 ms [range of 396-1842] and 820±681 ms [range of 400-2474 ms], *P*<0.001 and *P*<0.05 respectively) (Supplemental Figure 3 and Figure 1B). Apart from AP prolongation, AP triangulation (APD_{30}-APD_{90}) was significantly increased (140±59 ms in control vs. 303±117 ms and 298±64 ms in hypertrophy and fibrosis, *P*<0.05) (Figure 1C, 1D and 1E). Furthermore, the maximal spatial APD_{80} dispersion was higher in both pathological substrates (240±92ms in hypertrophic and 233±151ms in fibrotic cultures vs. 53±36ms in controls, *P*<0.01) (Figure 1F), suggesting increased heterogeneity of repolarization in hypertrophic or fibrotic cultures.

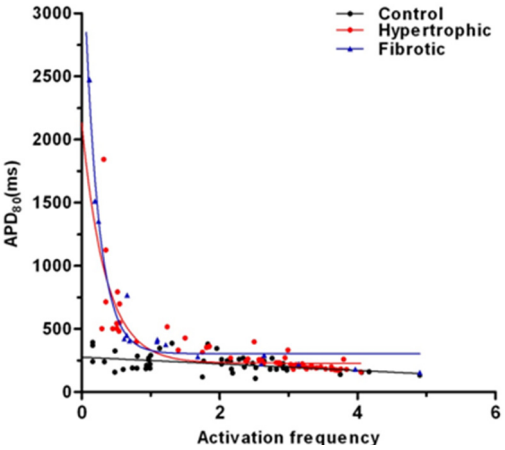

Supplemental Figure 3: *APD_{80} restitution curve shows that the slope of APD_{80} restitution strongly increases at activation frequencies below 1 Hz in hypertrophic or fibrotic cultures.*

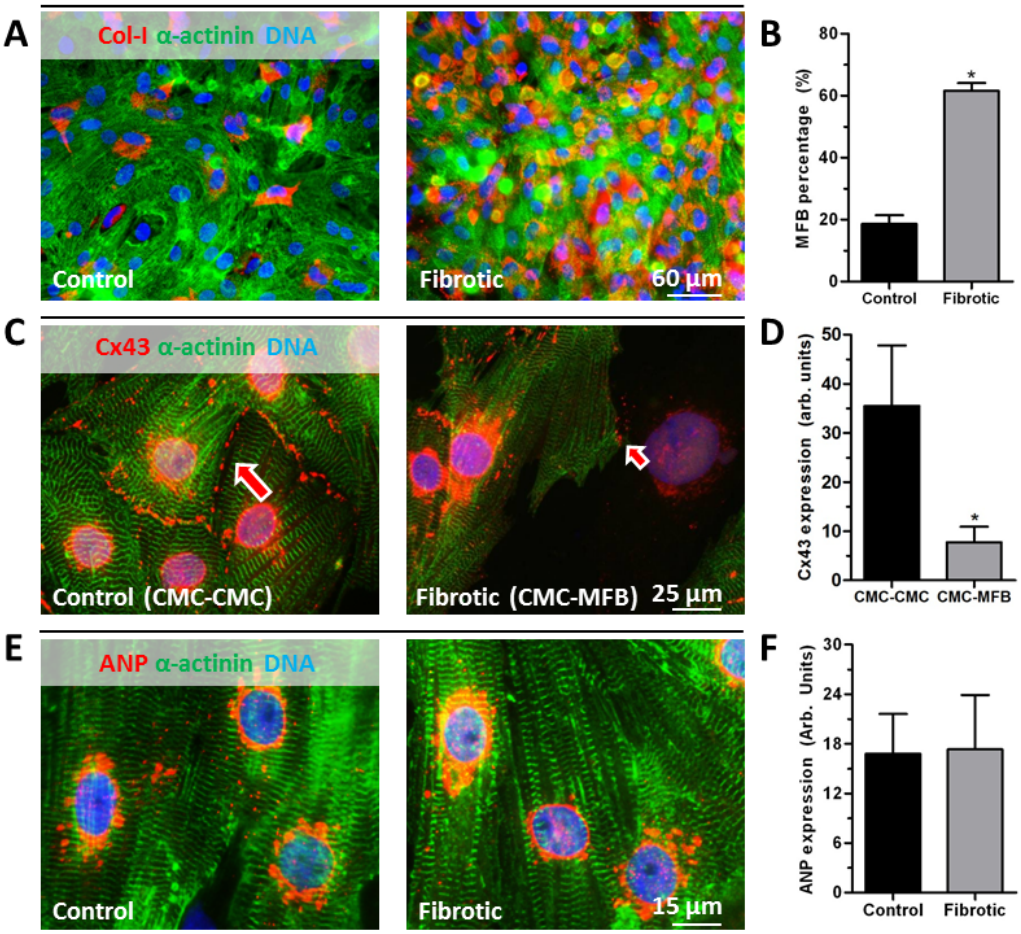

Supplemental Figure 2. *Cellular characterization of fibrotic myocardial cultures. (A) Typical examples of immunocytological double-staining for collagen-I (red) and α-actinin (green) (B) Quantification of MFB count by collagen-I signal *:p<0.0001 vs control (C) Immunocytological double-staining of Cx43 (red) and α-actinin (green) showing homocellular (red arrow) and heterocellular Cx43 expression (indicated by small red arrow) between CMCs (green) and MFBs. (D) Quantification of homocellular (CMC-CMC) and heterocellular (CMC-MFB) Cx43 expression. *:p<0.001 vs control. (E) Typical examples of ANP (red) and α-actinin (green) double-staining. (F) Quantification of ANP signal.*

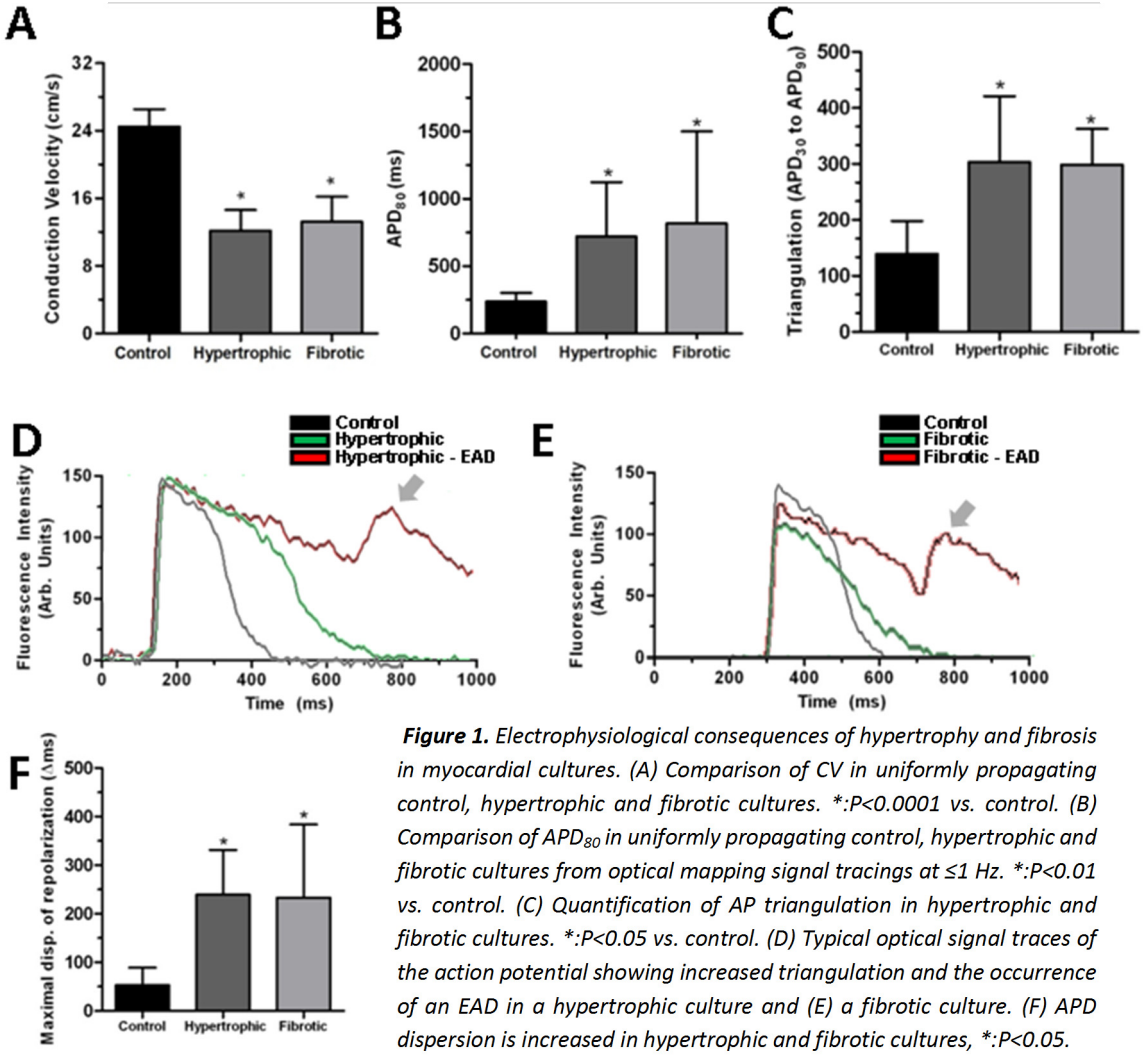

Figure 1. *Electrophysiological consequences of hypertrophy and fibrosis in myocardial cultures. (A) Comparison of CV in uniformly propagating control, hypertrophic and fibrotic cultures. *:P<0.0001 vs. control. (B) Comparison of APD_{80} in uniformly propagating control, hypertrophic and fibrotic cultures from optical mapping signal tracings at ≤1 Hz. *:P<0.01 vs. control. (C) Quantification of AP triangulation in hypertrophic and fibrotic cultures. *:P<0.05 vs. control. (D) Typical optical signal traces of the action potential showing increased triangulation and the occurrence of an EAD in a hypertrophic culture and (E) a fibrotic culture. (F) APD dispersion is increased in hypertrophic and fibrotic cultures, *:P<0.05.*

Triggered activity caused by abnormal repolarization gradients underlies focal tachyarrhythmias that occur in fibrotic and hypertrophic cultures

Apart from prolonged repolarization in fibrotic or hypertrophic cultures, triggered activity due to EADs was frequently observed. The incidence of EADs in both hypertrophy (40%, n=25) and fibrosis (65.5%, n=29) was significantly higher compared to control cultures (4.2%, n=24) (Figure 2D). The occurrence of EADs not only lengthened APD_{80}, but also dramatically increased the spatial heterogeneity of repolarization (from 197±78ms during uniform repolarization to 1570±1155ms during EADs, *P*<0.05, Supplemental Figure 4). EADs could be observed spontaneously but were also easily evoked by 1Hz stimulation in both substrates. Additionally, EADs could repeatedly oscillate.

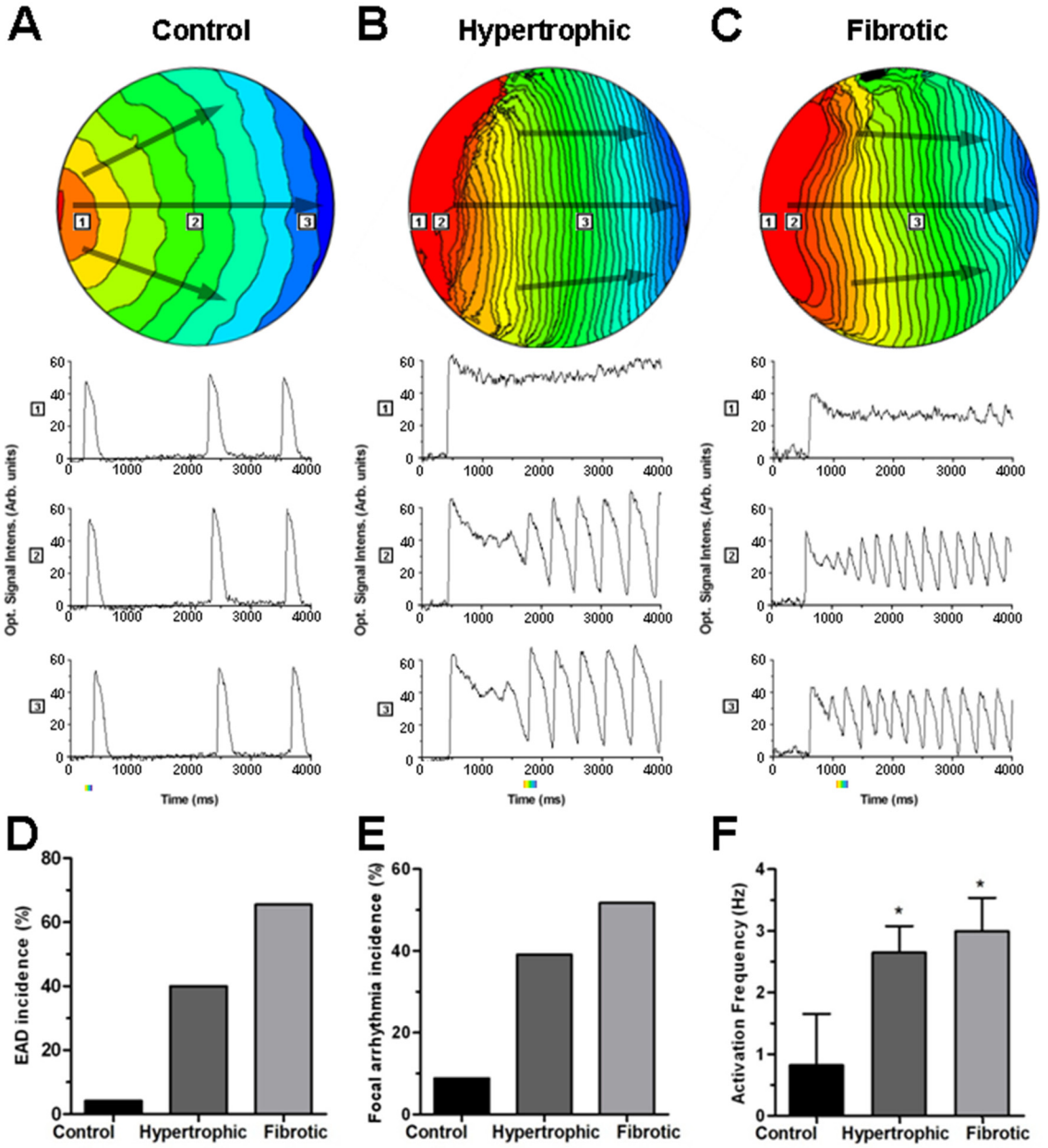

Figure 2. *Spontaneous focal tachyarrhythmias are formed in both hypertrophic and fibrotic myocardial cultures by repetitive EADs. (A) Typical example of an activation map of an uniformly propagating control culture (6 ms isochronal spacing). Corresponding non-high-pass filtered and spatially filtered optical signals indicated by numbers 1-3 show short APDs and low activation frequency. Black arrows indicate the diverging direction of AP propagation as a result of the convex waveform. (B) Activation map of focal tachy-arrhythmic activation in a hypertrophic or (C) fibrotic culture (6ms isochrones spacing). Corresponding optical signals show ceased repolarization at point 1, initiation of the first EAD*

*after slow repolarization in point 2 followed by several propagated EADs and propagation of the first and following EADs in point 3 resulting in a high activation frequency. Black arrows indicate converging/planar direction of AP propagation. (D) Incidence of EADs and (E) spontaneous focal arrhythmias. (F) Repetitive focal activation increases activation frequency in both substrates when compared with normal, uniformly propagating control cultures. *:P<0.001 vs. control.*

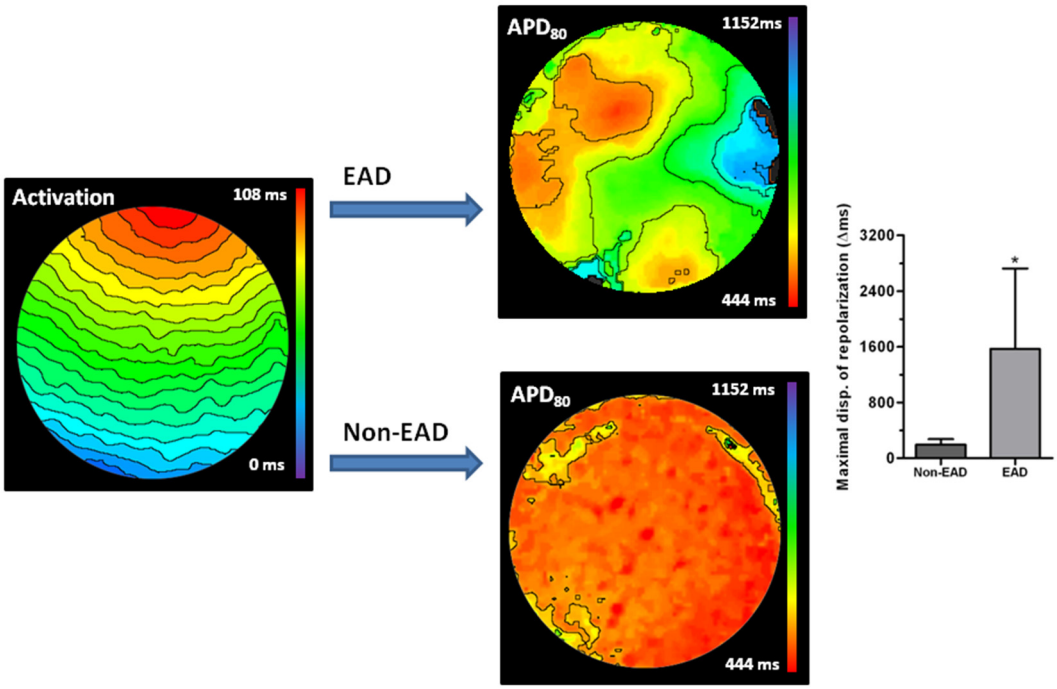

Supplemental Figure 4: *Effect of EADs on APD dispersion. Examples are taken from fibrotic cultures but are also representative for hypertrophic cultures. Uniform activation is shown on the left (6 ms isochrones). After such activation, repolarization occurs throughout the culture (bottom-right repolarization map). However, repolarization can reverse in fibrotic or hypertrophic cultures. The resulting EADs greatly lengthen local APDs (top-right repolarization map), which considerably enhances spatial APD dispersion. This creates a substrate that is vulnerable to reentrant conduction as enhanced differences in refractoriness facilitate formation of unidirectional block. The same observations were made in hypertrophic cultures.*

Triggered activity resulted in an increased activation frequency (2.64±0.42 Hz in hypertrophic or 2.99±0.54 Hz for fibrotic cultures vs. 0.82±0.83 Hz in uniformly conducting control cultures, both *P*<0.001 vs. control) (Figure 2F), thereby identifying this activation pattern as a focal tachyarrhythmia. These focal arrhythmias were infrequently observed in controls (8.8%, n=57, Figure 2A), but were prominent in both hypertrophic (39.1%, n=23) (Figure 2B) and fibrotic cultures (51.7%, n=29, Figure 2C, 2E). During focal tachyarrhythmias, repolarization locally ceased, (Figure 2B and C, point 1) resulting in a sustained depolarized

area in both substrates. As a consequence of juxtaposed repolarizing tissue and the resulting repolarization gradient, tissue at the border of the sustained depolarized area (Figure 2B, C point 2) repolarized very slowly. This translated to a diminished maximal repolarizing down stroke velocity in these areas (0.71±0.16 in controls vs. 0.26±0.04 in hypertrophic and 0.251±0.06 arbitrary optical units/ms in fibrotic cultures, $P<0.001$), thereby providing a prolonged time window for reactivation of the depolarizing force, which could lead to EAD formation. As the membrane potential of tissue distal from the constitutively depolarized area lowers again after the triggered action potential, repolarization in proximity of the depolarized area again occurs slowly. This provided an opportunity for subsequent EADs, persistently repeating the previous sequence of events.

Both hypertrophy and fibrosis cause spontaneous reentrant tachyarrhythmias by critically timed EADs

Interestingly, both hypertrophic (n=111) and fibrotic cultures (n=107) showed a high incidence of spontaneous reentrant tachyarrhythmias, whereas control cultures (n=102) exhibited uniform and fast propagation (Figure 3A, 3B and 3C). Spontaneous reentry incidence was 67.5%, 78.5% and 2.9% in hypertrophic, fibrotic and control cultures, respectively (Figure 3D). To investigate the mechanisms behind these high incidences, reentry formation was studied in these cultures. Spontaneous reentry formation in both substrates was found to be a consequence of triggered activity caused by EADs. The common determinant of reentry initiation was the critical timing of EADs, which is described hereafter. During EADs, APD was increased in both hypertrophic and fibrotic cultures compared to controls (Figure 3B and C, point 1) prior to reentrant conduction, as was the case for APD dispersion (Supplemental Figure 4). Consequentially, hypertrophic and fibrotic cultures were vulnerable to conduction block following EADs. These EADs typically formed at the edge of an area with long APD (Figure 3B and C, point 2) where down stroke velocity of repolarization was locally slowed and thus could prolong the time frame for reactivation of depolarizing current (Figure 3B and C, point 2). If an EAD was generated, this newly generated EAD propagates away from the area with the long APD, as the AP will only meet relatively well-repolarized tissue in that direction (Figure 3B and C point 3). Thereby, unidirectional conduction block was formed (Figure 3, indicated by double black lines). If repolarization occurred at the site of EAD origin before return of the wave front, reentry was enabled by such critical timing. This resulted in increased activation frequency (0.82±0.83Hz in uniformly conducting controls vs. 3.22±0.41Hz in hypertrophic or 3.93±0.66Hz in fibrotic cultures showing reentry $P<0.0001$) (Figure 3E, 3F and 3G) identifying this conduction pattern as another type of tachyarrhythmia.

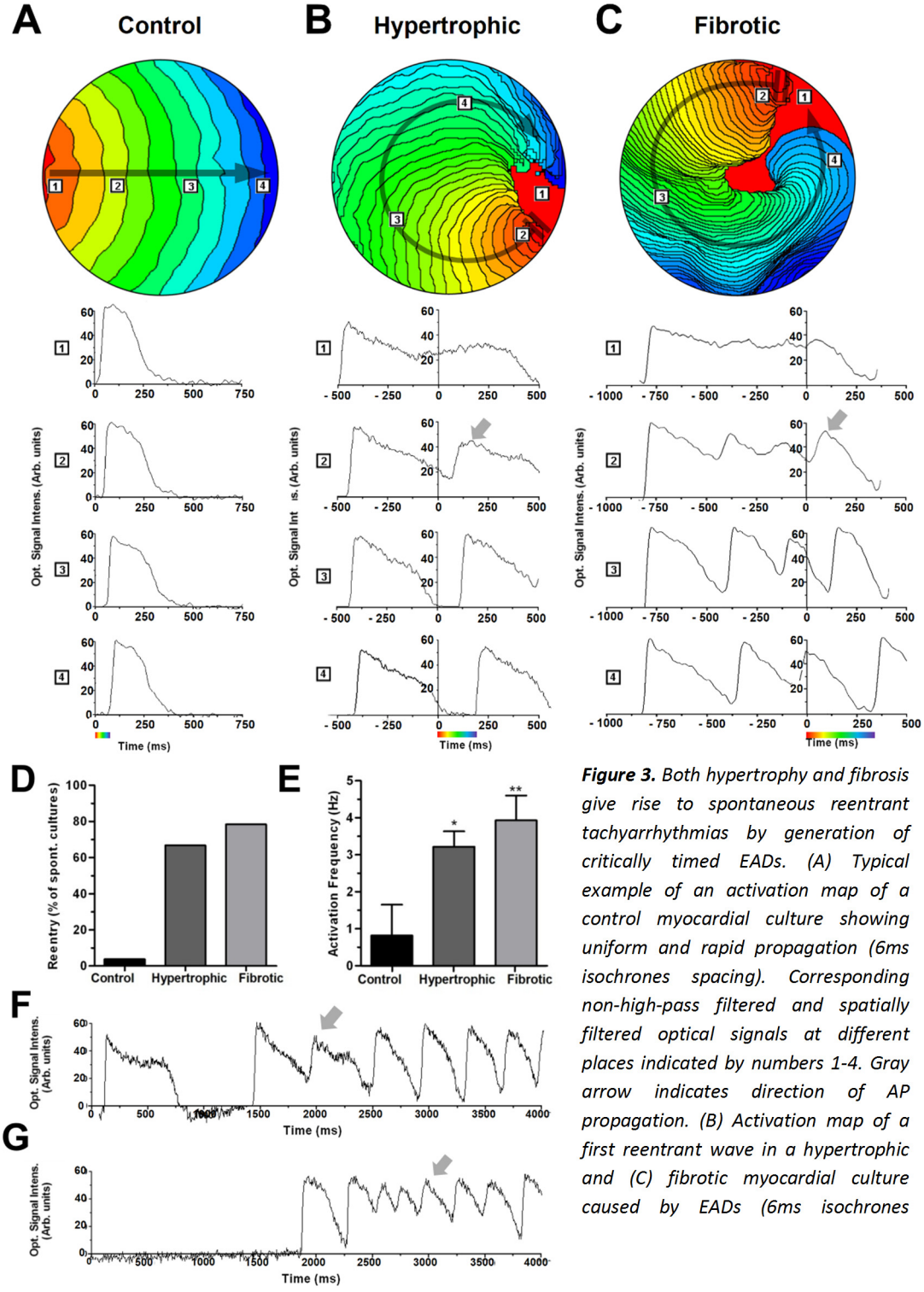

Figure 3. *Both hypertrophy and fibrosis give rise to spontaneous reentrant tachyarrhythmias by generation of critically timed EADs. (A) Typical example of an activation map of a control myocardial culture showing uniform and rapid propagation (6ms isochrones spacing). Corresponding non-high-pass filtered and spatially filtered optical signals at different places indicated by numbers 1-4. Gray arrow indicates direction of AP propagation. (B) Activation map of a first reentrant wave in a hypertrophic and (C) fibrotic myocardial culture caused by EADs (6ms isochrones*

*spacing). Corresponding optical signals at places indicated by numbers 1-4. Gray arrow indicates the critically timed EAD. Double black lines indicate unidirectional block, black arrow indicates direction of AP propagation. (D) Incidence of spontaneous reentrant tachyarrhythmias. (E) Activation frequency in normal, uniformly propagating control cultures compared to hypertrophic or fibrotic cultures showing reentrant conduction. *:P<0.0001 vs. control, **:P<0.0001 vs. control and hypertrophic cultures. (F) Typical example of a full AP trace of a hypertrophic and (G) fibrotic culture, showing a critically timed EAD (gray arrow) followed by a reentrant tachyarrhythmia.*

Substrate-specific effects on electrophysiological properties of CMCs

To investigate substrate-specific effects on CMCs, protein expression of several ion channels and Cx43, as well as action potentials were investigated in all groups. Expression of Kv4.3 was decreased by 29%, in hypertrophic CMCs compared to controls (p=0.015). Expression of Nav1.5, Cav1.2, Kir2.1, and Kv7.1 were not significantly altered in hypertrophic cultures (Figure 4A,B). In contrast to hypertrophic cultures, CMCs in fibrotic cultures exhibited significantly higher expression of Kir2.1 only, compared to CMCs in control cultures (p=0.048 vs. control, Figure 4A, C). However, this difference is most likely not attributable to electrical remodeling, but to Kir2.1 expression in myofibroblasts contributing to the overall Kir2.1 expression when corrected for α-actinin.[10] Expression of intercellular Cx43 between CMCs at the protein level was decreased in hypertrophic cultures, while in fibrotic cultures, intercellular protein expression of Cx43 between CMCs was unaltered (12.2±7.1 arbitrary units in hypertrophy vs. 32.8±10.9 and 33.5±10.2 in control and fibrosis, *P*<0.01) (Figure 4D and 4E). Intracellular membrane potential recordings revealed distinctly different action potential morphologies (Figure 4E); with wide action potentials in hypertrophic CMCs and CMCs in fibrotic cultures and narrow action potentials in control CMCs. Furthermore, CMCs in fibrotic cultures were depolarized as maximal diastolic potentials were -48±7 mV (n=12, *P*<0.0001 vs. control) whereas hypertrophic CMCs showed no such alteration (-62±6 mV, n=8, p=ns) compared with control (-66±7 mV, n=8) (Figure 4F and 4G). Importantly, maximal diastolic potential of CMCs in fibrotic cultures became more negative after gap-junctional uncoupling with 25 µM 2-APB (-59±4 mV (n=5) vs. -48±7 mV (n=12) in untreated fibrotic cultures respectively. In contrast, CMCs in hypertrophic or control cultures showed no significant change after 2-APB in maximal diastolic potential (-62±6 mV without vs. -65±4 mV with 2-APB in hypertrophic cultures, p>0.05 n=4 and -66±7 without vs. -68±5 mV with 2-APB in control cultures, p>0.05, n=4). Moreover, APD_{80} was strongly reduced in CMCs in fibrotic cultures after uncoupling (608±20ms without vs. 286±32ms with 2-APB, *P*<0.05, n=5) while APD_{80} remained largely unchanged after uncoupling CMCs in hypertrophic (732±26ms without vs. 715±23ms with 2-APB, p>0.05, n=4) or CMCs in control cultures (216±11ms without vs. 202±13ms with 2-APB, p>0.05). These data imply intrinsic electrical remodeling that decreases repolarization reserve as a pro-arrhythmic mechanism of

hypertrophy, as opposed to extrinsic MFB-induced depolarization as a pro-arrhythmic mechanism of fibrosis.

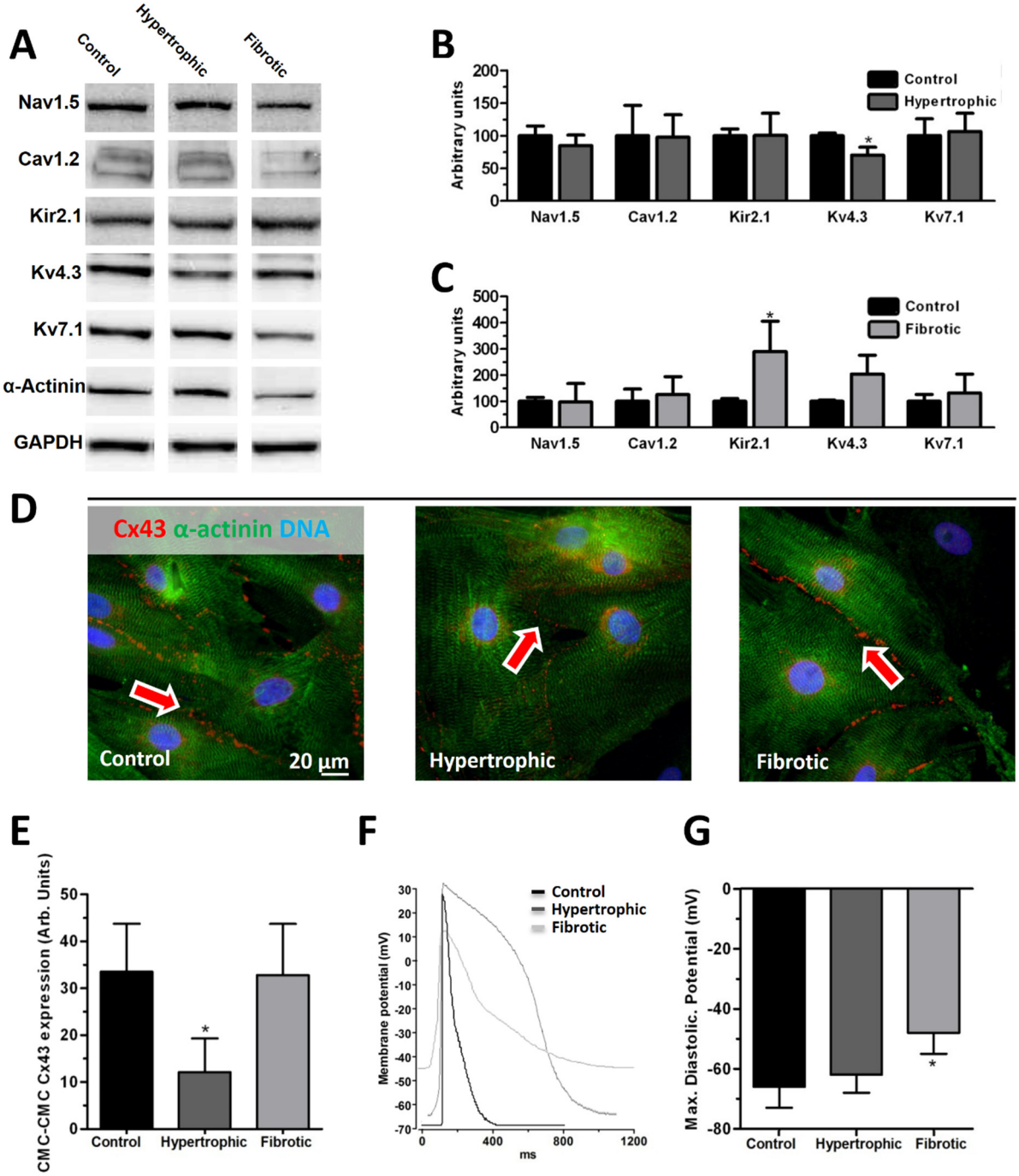

Figure 4. *Conduction slowing and AP triangulation are associated with either ion channel- and gap junctional remodeling or MFB-induced depolarization. (A) Typical examples of protein expression profiles in hypertrophic, fibrotic or control cultures as visualized by Western Blot analysis. (B) Quantification of ion channel protein expression corrected for corresponding GAPDH expression and α-actinin in control and hypertrophic cultures (*:P<0.01) and (C) control and fibrotic cultures. (D) Immunocytological staining of α-actinin (green) and Cx43 (red) in control, hypertrophic or fibrotic cultures. (E) Quantification of intercellular Cx43 signal, *:P<0.01. (F) Current-clamp traces of action potential in control, hypertrophic and fibrotic cultures. (G) Quantification of maximal diastolic potential. *:P<0.001.*

Substrate-specific effects of pharmacological interventions imply differing pro-arrhythmic mechanisms

To further characterize differences between pro-arrhythmic mechanisms of hypertrophy and fibrosis, *in vitro* effects of several drugs on arrhythmogeneity were compared between hypertrophic and fibrotic myocardial cultures. Single point 1Hz stimulation for 10 ms evoked focal or reentrant arrhythmias in hypertrophic and fibrotic cultures (Figure 5A, lower records) with incidences of 75% in hypertrophy, 78% in fibrosis and 3% in control. To study the role of reduced repolarization reserve in arrhythmogeneity, 0.5 mmol/L sotalol was administered to control cultures, prolonging APD_{80} to 118% of initial values. Moreover, cultures showed EADs and reentrant arrhythmias after sotalol, which thereby increased arrhythmic incidence from 0% to 50% (n=16). L-type calcium channels were blocked by 3 µM nitrendipine, which is expected to lower net inward current and thereby reduce APD and arrhythmia incidence. In both hypertrophic and fibrotic cultures, no EADs, focal or reentrant arrhythmias could be evoked after nitrendipine (n=25 and n=15 for hypertrophic and fibrotic cultures) (Figure 5B and 5C). Pacing at 1Hz after nitrendipine administration resulted in electrical capture in all hypertrophic cultures (n=24), and shortening of APD_{80} (57.7±7.2% of untreated cultures, P<0.001) (Figure 5B), while 9 out of 19 fibrotic cultures were rendered unexcitable (Figure 5B and 5C). In line with these results, 10 µM verapamil treatment fully prevented formation of arrhythmias in both groups, but produced conduction block in fibrotic cultures (11 unexcitable cultures out of 15) (Figure 5B and 5C), while all hypertrophic cultures remained excitable (n=14). To investigate the effect of blockade of the fast sodium channel in the different substrates, 20 µM TTX was administered to hypertrophic or fibrotic cultures in another set of experiments. Before TTX administration, arrhythmic incidence was 13 out of 22 hypertrophic cultures and 12 out of 19 fibrotic cultures. In 16 controls, no arrhythmias were detected. Following TTX administration, EAD incidence remained largely unchanged, as incidences were 16 out of 22 hypertrophic cultures and 11 out of 19 fibrotic cultures, making nav1.5-dependent mechanisms of EADs unlikely in the tested cultures. To test the contribution of altered intracellular calcium handling to arrhythmogenesis in these models, all intracellular calcium was buffered by treatment with 10-50 µM BAPTA-AM in an optical mapping experiment.

Interestingly, BAPTA-AM treatment did not decrease arrhythmia incidence in hypertrophic nor fibrotic cultures (90%, n=40 and 76%, n=39, respectively) compared to non-treated cultures. These findings demonstrate that generation of EADs in these substrates is largely independent of intracellular calcium handling.

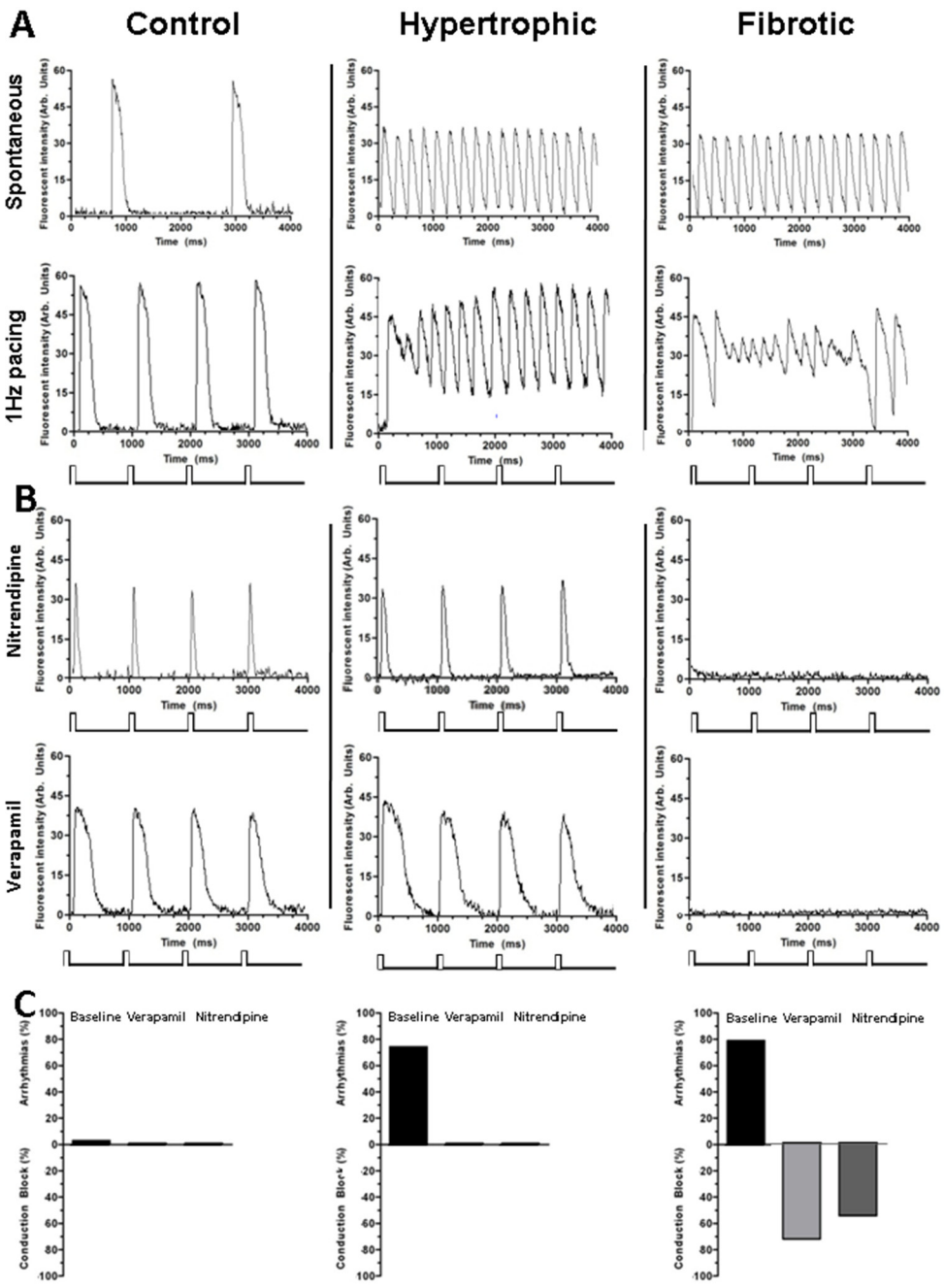

Figure 5. *Substrate-specific effects of L-type calcium channels blockade on arrhythmogeneity. (A) Typical examples of spatially and non-high-pass filtered optical signal traces, occurring spontaneously (above) and during 1Hz pacing (below) in untreated control (left), hypertrophic (middle) and fibrotic (right) cultures. (B) Same traces during 1Hz pacing in control (left), hypertrophic (middle) and fibrotic (right) cultures after treatment with 3 μM nitrendipine (above) and 10 μM verapamil (below). (C) Quantification of the incidence of spontaneous (focal and reentrant) arrhythmias and conduction block in control (left), hypertrophic (middle) and fibrotic (right) cultures after treatment with 10 μM verapamil or 3 μM nitrendipine.*

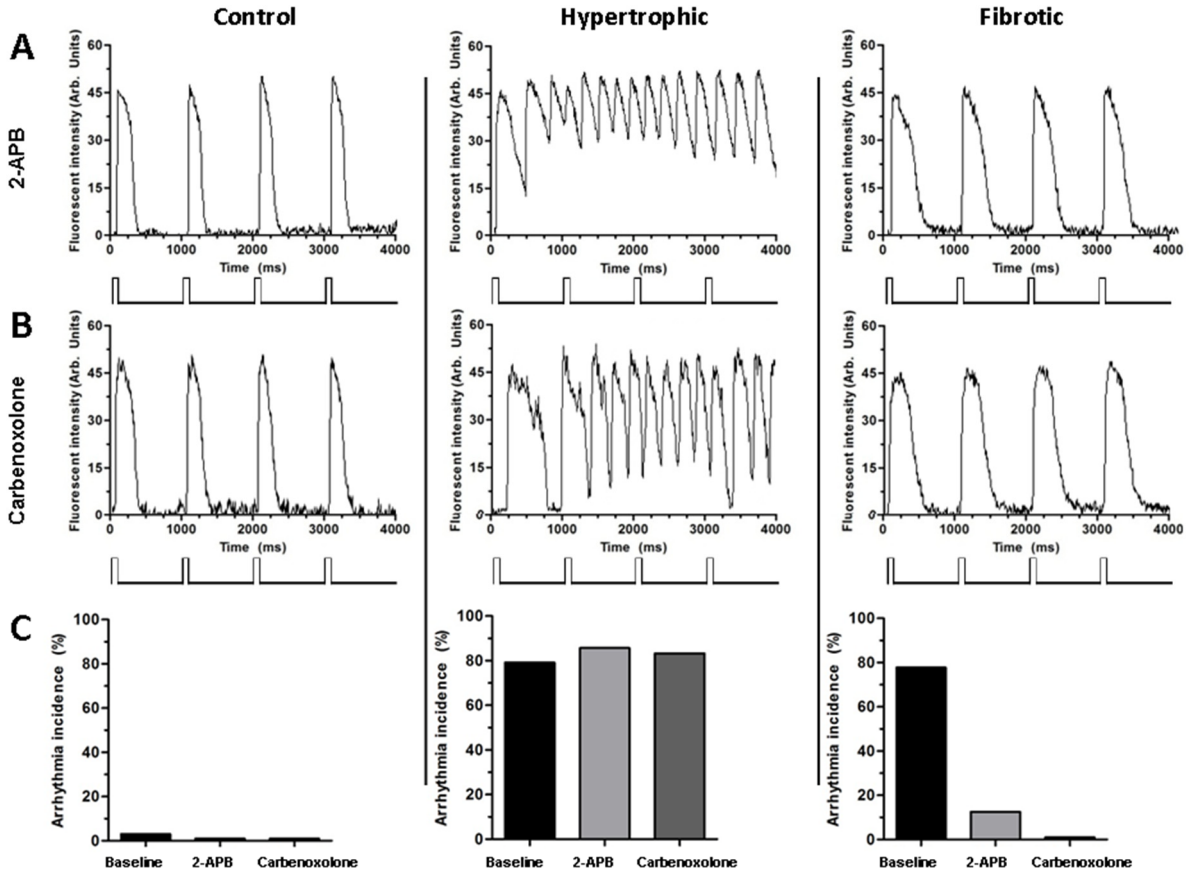

Figure 6. *Effect of gap junctional uncoupling on arrhythmogeneity depends on the arrhythmogenic substrate. (A) Typical examples of spatially filtered and non-high-pass filtered action potential traces during 1Hz pacing in control (left), hypertrophic (middle) and fibrotic (right) cultures after treatment with 5 μM 2-APB or (B) 100 μM carbenoxolone. (C) Quantification of the incidence of spontaneous (focal and reentrant) arrhythmias in control (left), hypertrophic (middle) and fibrotic (right) cultures after treatment with 5 μM 2-APB or 100 μM carbenoxolone.*

As heterocellular coupling is a pro-arrhythmic feature of fibrosis *in vitro*,[11] partial gap junctional uncoupling was performed to further examine differences in arrhythmogeneity of hypertrophic and fibrotic cultures. As MFB-CMC intercellular Cx43 expression is significantly lower than at CMC-CMC junctions (Supplemental Figure 2D), partial uncoupling can lead to inhibition of heterocellular MFB-CMC coupling while preserving sufficient CMC-CMC coupling for propagation. Therefore, cultures were treated with 5 µM 2-APB or 100 µM carbenoxolone. Treatment with 2-APB reduced arrhythmias in fibrotic cultures (12.5%, n=16 vs. 78%, n=18 in untreated fibrotic cultures, $P<0.05$) (Figure 6A and 6C), and decreased APD_{80} (68.7±31.7% of untreated cultures, $P<0.05$). Such anti-arrhythmic effect was absent in hypertrophic cultures (86% arrhythmias n=14, vs. 75% n=12 in untreated hypertrophic cultures) (Figure 6A and 6C). Carbenoxolone also ameliorated arrhythmogeneity in fibrotic cultures, while arrhythmia incidence remained high in hypertrophic cultures (83% arrhythmias, n=12) (Figure 6B and 6C).

Discussion

Key findings of this study are (1) both hypertrophic and fibrotic myocardial cultures give rise to triggered activity causing both focal and reentrant tachyarrhythmias. (2) Underlying pro-arrhythmic mechanisms highly differ between these two pathological conditions; mainly being electrical remodeling of CMCs in hypertrophic cultures or MFB-induced depolarization of CMCs in fibrotic cultures.

Triggered activity, focal and reentrant tachyarrhythmias in experimental models

Cardiac fibrosis and cardiac hypertrophy are both associated with spontaneous tachyarrhythmias.[1-3,12] Traditionally, whole-heart mapping studies suggest either focal or reentrant mechanisms underlying these ventricular tachyarrhythmias.[13,14] However, the complexity of 3-dimensional myocardial tissue hampers complete interpretation of findings and therefore, arrhythmogenesis has also been investigated in experimental 2D and computational models to unequivocally establish the existence of reentrant and focal mechanisms.[15,16] Additionally, despite the spontaneous occurrence of arrhythmias in patients, arrhythmogenesis has been mostly studied by externally applied burst stimulation to force induction of arrhythmias, [17-19] thereby precluding investigation of internal arrhythmic triggers in arrhythmogenesis.

In this study, triggered activity in the form of EADs was found spontaneously and could be evoked by low-frequency stimulation. Moreover, this activity was found to be responsible for the initiation of both focal and reentrant tachyarrhythmias in hypertrophic and fibrotic cultures. It was shown that the onset of focal and reentrant tachyarrhythmias depends on the generation of EADs, which either oscillate during phase 2 or 3 of the AP (focal) or are critically timed to form unidirectional block, slow conduction and thereby facilitate reentry.

The importance of EADs in the onset of ventricular tachycardias is in line with previous *in silico*, *in vitro* and *in vivo* studies.[20,21] Traditionally, this correlation of EADs with arrhythmias was studied by inducing EADs by pharmacological or genetic interventions or, in the case of *in silico* studies, by altering ion channel properties to reduce repolarization reserve. While these studies proved useful to implicate EADs as a principal underlying mechanism of arrhythmogeneity**,** it remained unclear how prevalent acquired cardiac diseases such as hypertrophy or fibrosis may lead to arrhythmias. For hypertrophy, spontaneous EAD generation has been demonstrated in isolated CMCs.[22,23] The current study shows that EADs in hypertrophy also overcome electrotonic load and propagate in 2-dimensional tissue. Additionally, how predicted source-sink mismatching of propagated EADs is overcome is illustrated by the concave waveform (Figure 2B, C) found during focal tachyarrhythmias. This is in accordance with calculations that show that EAD propagation is favored in concave activation as such waveform morphology helps to overcome the source-sink mismatch that determines the threshold of EAD propagation.[24]

As EADs are reactivations of depolarizing current during repolarization, slowed repolarization is a critical facilitating factor for EAD generation. This was demonstrated in the present study by adding sotalol to control cultures, which prolonged APD and caused focal tachyarrhythmias. In addition, dispersion of repolarization causes steep repolarization gradients, which may provide the depolarizing force necessary for reactivation.[25] This reactivation was mainly calcium-dependent, as Nav1.5 blockade had no pronounced anti-arrhythmic effect in either hypertrophic or fibrotic cultures. Additionally, intracellular calcium buffering was ineffective to prevent EADs and arrhythmias while Cav1.2 blockade ameliorated EADs. Findings of prolonged and dispersed repolarization may readily explain the similar pro-arrhythmogenic findings of triggered activity in hypertrophic or fibrotic tissue. However, the similarities between pro-arrhythmogeneity of hypertrophy and fibrosis end at the cellular level of the mechanisms of repolarization prolongation and dispersion.

Substrate-specific pro-arrhythmic mechanisms in cardiac hypertrophy and fibrosis

During cardiac remodeling, hypertrophy and fibrosis may develop to varying degrees. As a result, the resulting pro-arrhythmic features found in cardiac remodeling remain incompletely understood, as concomitance of these substrates precludes distinction between pro-arrhythmic mechanisms of these substrates and therefore, hamper the development of novel anti-arrhythmic treatment modalities. In this study, cellular and ionic mechanisms of arrhythmogeneity substantially differed between cardiac fibrosis and hypertrophy. In fibrosis, fibroblast proliferation and extracellular matrix deposition are known to extrinsically alter cardiac action potential propagation by forming spatial separations between CMCs, which reduces cell-to-cell contact, favors zigzag conduction and provides anatomic obstacles that increase the propensity towards arrhythmias.[26,27] [17].

However, in recent years, focus has shifted towards the MFB in cardiac fibrosis as a possible key factor in the extrinsic pro-arrhythmic mechanisms of fibrosis.[28-31] In culture, MFBs can inactivate voltage-gated potassium channels by depolarizing CMCs and thereby preclude proper repolarization and facilitate EAD generation.[11,12,32] This study confirms these extrinsic effects on CMCs, as high MFB content in cardiac cultures was associated with depolarized membrane potentials in CMCs, prolonged APD_{80} and an increased incidence of EADs that ultimately led to tachyarrhythmias. Other studies showed that paracrine factors secreted from cardiac fibroblasts were also able to induce a certain degree of ion channel remodeling in CMCs, although no EADs were reported in these CMCs.[33] However, no such effects were detected if cardiac fibroblasts were directly co-cultured with CMCs, as was done in the present study. In our study fibrosis led to an increase in Kir2.1 expression when corrected for alpha actinin. However, this is unlikely the result of a functional overexpression of Kir2.1 in cardiomyocytes. In the hypothetical case of functional kir2.1 overexpression in CMCs the MDP in fibrotic cultures would be more negative after uncoupling compared to non-fibrotic controls, while the opposite is true. This means that either the extra kir2.1 is derived from myofibroblasts or does not lead to an increase in inward rectifier current. Furthermore, Findings of strong anti-arrhythmic effects of partial uncoupling confirm dominance of coupling-based pro-arrhythmic mechanisms over paracrine mechanisms in the currently used model. This anti-arrhythmic effect is possibly due to the vast functional reserve capacity of CMC-CMC coupling, which is considerably lower in MFB-CMC coupling and thereby allows for heterocellular uncoupling.[34]

In contrast to fibrosis, partial uncoupling had no anti-arrhythmic effects in hypertrophic tissue indicating differing pro-arrhythmic mechanisms. Reduction of total expression and altered distribution of Cx43 are all features of pathologically hypertrophied myocardium that compromise proper intercellular conduction and thereby lead to conduction slowing.[354] In addition, repolarization reserve is diminished by down regulation of voltage-gated potassium channels, which may increase the propensity towards EADs and ultimately towards arrhythmias.[365] In our study, lowered Cx43 expression, increased ANP and altered ion channel protein expression were confirmed in hypertrophic CMCs, and absent in CMCs in fibrotic and control cultures (Supplemental Figures 1, 2 and Figure 4 C, D). The down regulation of Kv4.3, which contributes to the transient outward current (I_{to}) was in accordance with other studies.[37,387] Hoppe et al showed that a reduction in I_{to} leads to a marked increase in APD by an increase in the plateau potential, thereby altering the early trajectory of repolarization.[398]

Due to differences in pro-arrhythmic mechanisms, L-type calcium channel blockade shortened APD and was anti-arrhythmic in hypertrophic cultures but blocked conduction in fibrotic cultures as propagation in such cultures was largely dependent on calcium channels

due to MFB-induced depolarization and concomitant inactivation of fast sodium channels. Nevertheless, the arrhythmogenic pathways of hypertrophy and fibrosis converge at the point of prolongation of repolarization, APD dispersion and EAD formation. These results suggest that lowering the incidence of spontaneous arrhythmias by preventing EAD generation may require a different approach in hypertrophic or fibrotic-substrates. Alternatively, common pro-arrhythmic factors should be targeted. Future research is needed to elaborate on the implications these findings may have for the *in vivo* setting.

Study Limitations

In our study, fibrosis was mimicked by MFB proliferation in myocardial cultures. However, the deposition of extracellular matrix as another component of fibrosis was not investigated, as *in vitro* deposition of matrix comparable to *in vivo* quality and quantity is difficult to achieve. Although it is well established that MFBs and CMCs functionally couple *in vitro*, strong, undeniable proof of this phenomenon *in vivo* has yet to appear. The implications of changes in expression of Kv4.3 protein found in hypertrophic rat cells cannot be directly extrapolated to human hearts due to differences in expression levels and functions of the associated currents. Consequently, this study establishes an *in vitro* proof-of-principle of cellular pro-arrhythmic mechanisms and recognizes that more *in vivo* research is necessary before this kind of *in vitro* results can be translated to clinical implications.

Conclusions

Hypertrophic and fibrotic myocardial tissues are independent, pro-arrhythmic substrates. Both substrates are characterized by slow conduction, APD prolongation, formation of EADs and subsequent focal and reentrant tachyarrhythmias. However, while pathological hypertrophy is characterized by electrical remodeling of CMCs, fibrosis is mainly characterized by MFB-induced depolarization of CMCs. These differences may stress the importance of a substrate-based approach in the treatment of cardiac arrhythmias.

Acknowledgements

We wish to thank Dr. W.P.M van Meerwijk for helpful discussions, and Huybert J.F. van der Stadt for excellent technical support.

Sources of funding
This work was supported by the Dutch Heart Foundation (2008/B119) and the Netherlands Organisation for Scientific Research (NWO; VENI grant (91611070), D.A.P).

Conflict of Interest
None declared.

Supplemental Material

Materials and Methods

All animal experiments were approved by the Animal Experiments Committee of the Leiden University Medical Center and conform to the Guide for the Care and Use of Laboratory Animals as stated by the US National Institutes of Health.

Experimental protocol

All control cultures were treated with the antiproliferative agent Mitomycin-C (10 µg/ml, Sigma-Aldrich, St. Louis, MO, USA), to prevent proliferation of endogenously present, α-smooth muscle actinin-positive myofibroblasts (MFBs). For this purpose Mitomycin-C dissolved in PBS was diluted in growth medium (Ham's F10 supplemented with 10% fetal bovine serum (FBS, Invitrogen, Carlsbad, CA, USA), 10% horse serum (HS, Invitrogen) and penicillin (100U/ml) and streptomycin (100 µg/ml, P/S; Bio-Whittaker, Carlsbad, CA, USA) and incubated for 2 hours. Subsequently, cultures were rinsed twice in PBS and once in a 1:1 mixture of DMEM/HAMS F10 supplemented with 5% HS and P/S before being kept on this medium throughout the experiment. To induce hypertrophy, Mitomycin-C treated cultures were exposed to 100 µM phenylephrine (PE, Sigma) for 24h at day 3 and day 8[4]. To mimic fibrosis, endogenously present MFBs were allowed to proliferate freely, by treatment with PBS instead of Mitomycin-C. Fibrotic cultures were rinsed identically as control cultures control and hypertrophic cultures after Mitomycin-C/PBS treatment. For reasons of comparability, fibrotic cultures and control cultures received PBS instead of PE.

Immunocytological analyses

Immunocytological stainings were performed as described in earlier studies.[9,40] Cultures were fixed in 1% paraformaldehyde for 20 minutes on ice, after which cultures were rinsed twice with Phosphate Buffered Saline (PBS) and permeabilized with 0.1% Triton X-100. After 2 subsequent wash-steps, cultures were incubated overnight with primary antibodies diluted in PBS with 1% Fetal Bovine Serum. Primary antibodies were directed against α-actinin (Sigma), α-smooth muscle actinin (Sigma), α-skeletal muscle actinin (Abcam, Cambridge, MA, USA), atrial natriuretic peptide (Abcam) or Collagen type I (Abcam) and used at a dilution of 1:200. Double-staining was performed by using primary antibodies that were raised in either mouse or rabbit host species. Corresponding secondary donkey anti-rabbit or donkey anti-mouse Alexa fluor-conjugated antibodies (Invitrogen) were incubated for 2 hours at room temperature at a dilution of 1:400. After rinsing twice, nuclei of these cultures were counterstained for 5 minutes with Hoechst 33321 (Invitrogen). Following 2 wash steps, stained glass coverslips were mounted in Vectashield mounting medium (Vector Laboratories Inc, Burlingame, CA, USA) to minimize photobleaching. Images of cultures were taken and quantified using dedicated software (Image-Pro Plus, version

4.1.0.0, Media Cybernetics, Silver Spring, MD, USA). Quantification of all staining was performed in at least 6 cultures per group with at least 20 photos taken per culture. Quantification of fluorescent signal intensity was performed in at least 15-fold per photo.

To confirm a pathological hypertrophic phenotype in PE-treated CMCs, cultures were characterized at day 9 for protein expression of the hypertrophic markers atrial natriuretic peptide and α-skeletal muscle actin by immunocytological staining. In addition, cell surface area of CMCs was quantified as another measure of hypertrophy. To confirm fibrosis in cardiac cultures, cultures were stained for collagen-I (Abcam) and positive cells were considered to be MFBs and quantified.[9]

Optical mapping

Propagation of action potentials was investigated on a whole-culture scale in hypertrophic, fibrotic or control cultures using voltage-sensitive dye mapping as described earlier.[9] For reasons of standardization and reproducibility, only cultures without structural inhomogeneities as judged by mapping and light microscopy were included for further analyses. Cardiac cultures were plated out in 24-well plates (Corning) at a cell density of $8x10^5$ cells per well. At day 9, cultures were optically mapped. At least 2 hours after the daily refreshing of culture medium, cultures were incubated with culture medium containing 8 µmol/L di-4-ANEPPS for 15±5 minutes at 37º C in a humidified incubator. Subsequently, cultures were refreshed with serum-free, colorless DMEM/HAMS F10 mixed in a 1:1 ratio. Next, electrical propagation patterns were recorded by optical mapping at 37ºC. Mapping experiments typically did not exceed 30 minutes per 24-wells plate. Also, cultures were not exposed to excitation light for longer than 50 s to limit possible phototoxic effects. Excitation light (e_{ex} = 525±25 nm) was delivered by a halogen arc-lamp (MHAB-150W, Moritex Corporation, San Jose, CA, USA) through epi-illumination. Fluorescent emission light passed through a dichroic mirror and a long-pass emission filter (>590 nm) and was focused onto a 100x100 pixels CMOS camera (Ultima-L, SciMedia, Costa Mesa, CA, USA) by a 1.6x converging lens (Leice, Wetzlar, Germany). This resulted in a spatial resolution of 160 µm/pixel and a field of view of 16 by 16 mm. Spontaneous or stimulated electrical activity was recorded for 6-24 seconds at 6ms exposure time per frame. Data analysis was performed with specialized software (Brainvision Analyze 1101, Brainvision Inc, Tokyo, Japan) after pixels signals were averaged with 8 of its nearest neighbors to minimize noise-artifacts. Conduction velocity (CV), maximal optical action potential upstroke (dF/dT_{max}), maximal action potential downstroke velocity (dF/dTmin), action potential duration until 80% repolarization (APD_{80}) were determined at ≤1 Hz at six different locations equally distributed throughout the culture and averaged before inclusion in further analyses. Spatial dispersion of repolarization was defined as the maximal difference in APD_{80} within a culture and was determined at activation frequencies of ≤1 Hz.

Assessment of EADs and focal tachyarrhythmias

As prevalent reentrant conduction precludes assessment of conduction patterns other than reentry, reentry needed to be eliminated to analyze all possible conduction patterns and spontaneous activity in included cultures. To maintain ion channel properties, reentry had to be eliminated in a non-pharmacological manner. For this purpose, we used a custom-made epoxy-coated platinum electrode and performed unipolar stimulation with 6 V for 4 seconds using an electrical stimulus module with corresponding software (Multichannel Systems), which successfully eliminated reentry in >90% of the cultures. After absence of reentry was confirmed by 2s optical mapping, spontaneous activity was detected by mapping of the cultures for 24 seconds following application of the stimulus. This allowed for detection of EADs and spontaneous focal arrhythmias that otherwise would be overruled by reentrant activation. All cultures included in this analysis, regardless of the presence of reentry, underwent equal stimulation for standardization purposes.

Pharmacological anti-arrhythmic interventions

To investigate the antiarrhythmic potential of pharmacological interventions in different substrates, several pharmacological agents were administered to hypertrophic, fibrotic or control cultures under optical mapping conditions. Inhibition of L-type Ca^{2+} inward current was performed by application of a relatively low dose of verapamil (10 μM) (Centrafarm, Etten-Leur, the Netherlands) or nitrendipine (3 μM) (Sigma) directly into the mapping medium. As this instantly abolished all spontaneous activity in all cultures regardless of composition, cultures were stimulated at 2V (1Hz intervals) for 4 seconds to evaluate capture and propagation parameters. For standardization purposes, arrhythmic activity before verapamil and nitrendipine administration was also investigated following 1Hz stimulation.

To reduce heterocellular coupling between CMCs and MFBs in hypertrophic or fibrotic myocardial cultures, a relatively low dose of the 2-APB (5 μM) (Tocris Bioscience, Bristol, United Kingdom) or carbenoxolone (100 μM) (Sigma) was supplied in the mapping medium and incubated for 20 minutes. To investigate effects of Nav1.5 blockade, tetrodotoxin (TTX, 20 μM, Alomone Labs) was pipetted into the medium and incubated for 10s. For investigation of the involvement of intracellular calcium handling in arrhythmogeneity, intracellular calcium was buffered using 10-50 μM BAPTA-AM (Sigma) which incubated for 20 minutes. To investigate the effect of action potential duration (APD) prolongation on arrhythmogeneity, 0.5 mM sotalol (Sigma) was used. For reproducibility and comparability between all pharmacological interventions, all cultures were paced with a 1 Hz supra-threshold stimulation protocol during optical mapping recordings.

Whole-cell patch-clamp

Whole-cell current-clamp measurements were performed in spontaneously active (0.2-1 Hz) hypertrophic, fibrotic or control cultures. For fibrotic cultures, MFBs were labeled with eGFP using the vesicular stomatitis virus G protein-pseudotyped self-inactivating lentivirus vector CMVPRES as described previously.[9] Subsequently, these labeled MFBs were plated out with CMCs in equal quantity and density as fibrotic cultures with freely proliferating MFBs at day 9. To maintain the initially plated ratio, cultures were treated with mitomycin-C. Therefore, CMCs were easily identifiable in these fibrotic cultures. At day 9, after identification of CMCs by fluorescence microscopy, current-clamp experiments were performed in these cells. Whole-cell recordings were performed at 25°C using a L/M-PC patch-clamp amplifier (3kHz filtering) (List-Medical, Darmstadt, Germany). The pipette solution contained (in mmol/L) 10 Na_2ATP, 115 KCl, 1 $MgCl_2$, 5 EGTA, 10 HEPES/KOH (pH 7.4). Tip and seal resistance were 2.0-2.5 MΩ and >1 GΩ, respectively. The bath solution contained (in mmol/L) 137 NaCl, 4 KCl, 1.8 $CaCl_2$, 1 $MgCl_2$, and 10 HEPES (pH 7.4). In a subset of experiments, CMCs were functionally uncoupled by incubation for 20 minutes with 25 µmol/L 2-APB to investigate intrinsic action potential morphology in hypertrophic, fibrotic or control cultures. For data acquisition and analysis, pClamp/Clampex8 software (Axon Instruments, Molecular Devices, Sunnyvale, CA, USA) was used.

Statistical analysis

Statistical analyses were performed using SPSS11.0 for Windows (SPSS Inc., Chicago, IL, USA). Comparison between numerical data of groups was performed using the student-t test or paired t-test where appropriate. Values were expressed as mean±SD. Significance of differences in incidences between groups was determined by the Chi-square statistical test. Differences were considered statistically significant if $p<0.05$.

References

1. Haider AW, Larson MG, Benjamin EJ, Levy D. Increased left ventricular mass and hypertrophy are associated with increased risk for sudden death. *J Am Coll Cardiol*. 1998;32:1454-1459.

2. McLenachan JM. Ventricular arrhythmias in patients with hypertensive left ventricular hypertrophy. 1987.

3. van der Burg AE, Bax JJ, Boersma E, Pauwels EK, van der Wall EE, Schalij MJ. Impact of viability, ischemia, scar tissue, and revascularization on outcome after aborted sudden death. *Circulation*. 2003;108:1954-1959.

4. Kuck KH, Schaumann A, Eckardt L, Willems S, Ventura R, Delacretaz E, Pitschner HF, Kautzner J, Schumacher B, Hansen PS. Catheter ablation of stable ventricular

tachycardia before defibrillator implantation in patients with coronary heart disease (VTACH): a multicentre randomised controlled trial. *Lancet*. 2010;375:31-40.

5. Zeppenfeld K and Stevenson WG. Ablation of ventricular tachycardia in patients with structural heart disease. *Pacing Clin Electrophysiol*. 2008;31:358-374.

6. Borleffs CJ, van EL, Schotman M, Boersma E, Kies P, van der Burg AE, Zeppenfeld K, Bootsma M, van der Wall EE, Bax JJ, Schalij MJ. Recurrence of ventricular arrhythmias in ischaemic secondary prevention implantable cardioverter defibrillator recipients: long-term follow-up of the Leiden out-of-hospital cardiac arrest study (LOHCAT). *Eur Heart J*. 2009;30:1621-1626.

7. Arshad A, Mandava A, Kamath G, Musat D. Sudden cardiac death and the role of medical therapy. *Prog Cardiovasc Dis*. 2008;50:420-438.

8. Pijnappels DA, Schalij MJ, Ramkisoensing AA, van Tuyn J, de Vries AA, van der Laarse A, Ypey DL, Atsma DE. Forced alignment of mesenchymal stem cells undergoing cardiomyogenic differentiation affects functional integration with cardiomyocyte cultures. *Circ Res*. 2008;103:167-176.

9. Askar SF, Ramkisoensing AA, Schalij MJ, Bingen BO, Swildens J, van der Laarse A, Atsma DE, de Vries AA, Ypey DL, Pijnappels DA. Antiproliferative treatment of myofibroblasts prevents arrhythmias in vitro by limiting myofibroblast-induced depolarization. *Cardiovasc Res*. 2011.

10. Walsh KB and Zhang J. Neonatal rat cardiac fibroblasts express three types of voltage-gated K+ channels: regulation of a transient outward current by protein kinase C. *Am J Physiol Heart Circ Physiol*. 2008;294:H1010-H1017.

11. Askar SF, Bingen BO, Swildens J, Ypey DL, van der Laarse A, Atsma DE, Zeppenfeld K, Schalij MJ, de Vries AA, Pijnappels DA. Connexin43 silencing in myofibroblasts prevents arrhythmias in myocardial cultures: Role of maximal diastolic potential. *Cardiovasc Res*. 2011.

12. Kleber AG and Rudy Y. Basic mechanisms of cardiac impulse propagation and associated arrhythmias. *Physiol Rev*. 2004;84:431-488.

13. Pogwizd SM, Hoyt RH, Saffitz JE, Corr PB, Cox JL, Cain ME. Reentrant and focal mechanisms underlying ventricular tachycardia in the human heart. *Circulation*. 1992;86:1872-1887.

14. de Bakker JM, van Capelle FJ, Janse MJ, Wilde AA, Coronel R, Becker AE, Dingemans KP, van Hemel NM, Hauer RN. Reentry as a cause of ventricular tachycardia in

patients with chronic ischemic heart disease: electrophysiologic and anatomic correlation. *Circulation*. 1988;77:589-606.

15. Allessie MA, Bonke FI, Schopman FJ. Circus movement in rabbit atrial muscle as a mechanism of tachycardia. III. The "leading circle" concept: a new model of circus movement in cardiac tissue without the involvement of an anatomical obstacle. *Circ Res*. 1977;41:9-18.

16. Hou L, Deo M, Furspan P, Pandit SV, Mironov S, Auerbach DS, Gong Q, Zhou Z, Berenfeld O, Jalife J. A major role for HERG in determining frequency of reentry in neonatal rat ventricular myocyte monolayer. *Circ Res*. 2010;107:1503-1511.

17. Lim ZY, Maskara B, Aguel F, Emokpae R, Jr., Tung L. Spiral wave attachment to millimeter-sized obstacles. *Circulation*. 2006;114:2113-2121.

18. Baker LC, London B, Choi BR, Koren G, Salama G. Enhanced dispersion of repolarization and refractoriness in transgenic mouse hearts promotes reentrant ventricular tachycardia. *Circ Res*. 2000;86:396-407.

19. Chang MG, Zhang Y, Chang CY, Xu L, Emokpae R, Tung L, Marban E, Abraham MR. Spiral waves and reentry dynamics in an in vitro model of the healed infarct border zone. *Circ Res*. 2009;105:1062-1071.

20. Weiss JN, Garfinkel A, Karagueuzian HS, Chen PS, Qu Z. Early afterdepolarizations and cardiac arrhythmias. *Heart Rhythm*. 2010;7:1891-1899.

21. Sato D, Xie LH, Sovari AA, Tran DX, Morita N, Xie F, Karagueuzian H, Garfinkel A, Weiss JN, Qu Z. Synchronization of chaotic early afterdepolarizations in the genesis of cardiac arrhythmias. *Proc Natl Acad Sci U S A*. 2009;106:2983-2988.

22. Qin D, Zhang ZH, Caref EB, Boutjdir M, Jain P, El-Sherif N. Cellular and ionic basis of arrhythmias in postinfarction remodeled ventricular myocardium. *Circ Res*. 1996;79:461-473.

23. Stengl M, Ramakers C, Donker DW, Nabar A, Rybin AV, Spatjens RL, van der Nagel T, Wodzig WK, Sipido KR, Antoons G, Moorman AF, Vos MA, Volders PG. Temporal patterns of electrical remodeling in canine ventricular hypertrophy: focus on IKs downregulation and blunted beta-adrenergic activation. *Cardiovasc Res*. 2006;72:90-100.

24. Xie Y, Sato D, Garfinkel A, Qu Z, Weiss JN. So little source, so much sink: requirements for afterdepolarizations to propagate in tissue. *Biophys J*. 2010;99:1408-1415.

25. Liu J and Laurita KR. The mechanism of pause-induced torsade de pointes in long QT syndrome. *J Cardiovasc Electrophysiol*. 2005;16:981-987.

26. Spach MS and Dolber PC. Relating extracellular potentials and their derivatives to anisotropic propagation at a microscopic level in human cardiac muscle. Evidence for electrical uncoupling of side-to-side fiber connections with increasing age. *Circ Res*. 1986;58:356-371.

27. de Bakker JM, van Capelle FJ, Janse MJ, Tasseron S, Vermeulen JT, de JN, Lahpor JR. Slow conduction in the infarcted human heart. 'Zigzag' course of activation. *Circulation*. 1993;88:915-926.

28. Vasquez C, Mohandas P, Louie KL, Benamer N, Bapat AC, Morley GE. Enhanced fibroblast-myocyte interactions in response to cardiac injury. *Circ Res*. 2010;107:1011-1020.

29. Miragoli M, Salvarani N, Rohr S. Myofibroblasts induce ectopic activity in cardiac tissue. *Circ Res*. 2007;101:755-758.

30. Miragoli M, Gaudesius G, Rohr S. Electrotonic modulation of cardiac impulse conduction by myofibroblasts. *Circ Res*. 2006;98:801-810.

31. Zlochiver S, Munoz V, Vikstrom KL, Taffet SM, Berenfeld O, Jalife J. Electrotonic myofibroblast-to-myocyte coupling increases propensity to reentrant arrhythmias in two-dimensional cardiac monolayers. *Biophys J*. 2008;95:4469-4480.

32. Askar SF, Bingen BO, Swildens J, Ypey DL, van der Laarse A, Atsma DE, Zeppenfeld K, Schalij MJ, de Vries AA, Pijnappels DA. Connexin43 silencing in myofibroblasts prevents arrhythmias in myocardial cultures: role of maximal diastolic potential. *Cardiovasc Res*. 2012;93:434-444.

33. Pedrotty DM, Klinger RY, Kirkton RD, Bursac N. Cardiac fibroblast paracrine factors alter impulse conduction and ion channel expression of neonatal rat cardiomyocytes. *Cardiovasc Res*. 2009;83:688-697.

34. Danik SB, Liu F, Zhang J, Suk HJ, Morley GE, Fishman GI, Gutstein DE. Modulation of cardiac gap junction expression and arrhythmic susceptibility. *Circ Res*. 2004;95:1035-1041.

35. Peters NS, Green CR, Poole-Wilson PA, Severs NJ. Reduced content of connexin43 gap junctions in ventricular myocardium from hypertrophied and ischemic human hearts. *Circulation*. 1993;88:864-875.

36. Furukawa T and Kurokawa J. Potassium channel remodeling in cardiac hypertrophy. *J Mol Cell Cardiol*. 2006;41:753-761.

37. Zitron E, Gunth M, Scherer D, Kiesecker C, Kulzer M, Bloehs R, Scholz EP, Thomas D, Weidenhammer C, Kathofer S, Bauer A, Katus HA, Karle CA. Kir2.x inward rectifier potassium channels are differentially regulated by adrenergic alpha1A receptors. *J Mol Cell Cardiol*. 2008;44:84-94.

38. Zhang TT, Takimoto K, Stewart AF, Zhu C, Levitan ES. Independent regulation of cardiac Kv4.3 potassium channel expression by angiotensin II and phenylephrine. *Circ Res*. 2001;88:476-482.

39. Hoppe UC, Marban E, Johns DC. Molecular dissection of cardiac repolarization by in vivo Kv4.3 gene transfer. *J Clin Invest*. 2000;105:1077-1084.

40. Pijnappels DA, Schalij MJ, van Tuyn J, Ypey DL, de Vries AA, van der Wall EE, van der Laarse A, Atsma DE. Progressive increase in conduction velocity across human mesenchymal stem cells is mediated by enhanced electrical coupling. *Cardiovasc Res*. 2006;72:282-291.

Cellular and Molecular Mechanisms of Arrhythmias in Cardiac Fibrosis and Beyond:

From Symptoms to Substrates towards Solutions

Chapter V

Prolongation of Minimal Action Potential Duration in Sustained Fibrillation Decreases Complexity by Transient Destabilization

Brian O. Bingen, MD; **Saïd F. A. Askar, MSc**; Martin J. Schalij, MD, PhD; Ivan V. Kazbanov, Msc; Dirk L. Ypey, PhD; Alexander V. Panfilov, PhD; Daniël A. Pijnappels, PhD.

Adapted from Cardiovasc Res 2013;97:161-170

Abstract:

Aims: Sustained ventricular fibrillation (VF) is maintained by multiple stable rotors. Destabilization of sustained VF could be beneficial by affecting VF complexity (defined by the number of rotors). However, underlying mechanisms affecting VF stability are poorly understood. Therefore this study aimed to correlate changes in arrhythmia complexity with changes in specific electrophysiological parameters, allowing to search for novel factors and underlying mechanisms affecting stability of sustained VF.

Methods & Results: Neonatal rat ventricular cardiomyocyte monolayers, and Langendorff-perfused adult rat hearts, were exposed to increasing dosages of the gap junctional uncoupler 2-aminoethoxydiphenyl borate (2-APB) to induce arrhythmias. Ion channel blockers/openers were added to study effects on VF stability. Electrophysiological parameters were assessed by optical-mapping and patch-clamp techniques.

Arrhythmia complexity in cardiomyocyte cultures increased with increasing dosages of 2-APB (n>38), leading to sustained VF: 0.0±0.1 phase singularities/cm^2 in controls vs. 0.0±0.1, 1.0±0.9, 3.3±3.2, 11.0±10.1 and 54.3±21.7 in 5,10,15,20 and 25µmol/L 2-APB, respectively. Arrhythmia complexity inversely correlated with wavelength. Lengthening of wavelength during fibrillation could only be induced by agents ($BaCl_2$/BayK8644) increasing APD at maximal activation frequencies (minimal APD); 123±32%/117±24% of control. Minimal APD prolongation led to transient VF destabilization, shown by critical wave front collision leading to rotor termination, followed by significant decreases in VF complexity and activation frequency (52%/37%). These key findings were reproduced *ex vivo* in rat hearts (n=6 per group).

Conclusions: These results show that stability of sustained fibrillation is regulated by minimal APD. Minimal APD prolongation leads to transient destabilization of fibrillation, ultimately decreasing VF complexity, thereby providing novel insights into anti-fibrillatory mechanisms.

Introduction

Ventricular fibrillation (VF) is the most common cause of sudden cardiac death.[1] Treatment of VF has vastly improved over the past years, mainly through progress in engineering strategies that resulted in defibrillating devices. However, while defibrillators can have a significant effect on survival, the majority of VF victims are not defibrillator candidates and at least 50% have VF as their first symptom of heart problems.[2] This is indicative of an unabated need to expand the current understanding of mechanisms underlying VF stability and termination.

One of the factors which can underpin the initiation of VF is gap junction remodeling. It is widely accepted that gap junctions are redistributed or down regulated following myocardial infarction, in cardiac hypertrophy and other causes of cardiomyopathy.[3] Such reorganization of gap junctions is associated with the onset of malignant ventricular tachyarrhythmias.[3-5]

After initiation, VF progresses through several distinct activation pattern phases, of which the hindmost are characterized by a reduction in the number of new rotor formations, reduced rotor meandering and increased spatiotemporal periodicity,[6-10] leading to a more organized and stable form of fibrillation. Affecting the stability of sustained VF may lead to a lower complexity of VF (estimated by the number of phase singularities per cm^2), but the underlying mechanisms are poorly understood. Traditionally, the fibrillatory aspect of conduction as well as arrhythmia complexity during fast VF is believed to be determined by conduction velocity (CV), action potential duration (APD), APD restitution slope and wavelength (the product of CV and APD).[11-13] However, considering the distinctive VF activation patterns, the importance of these factors could differ significantly during the different phases of VF. Furthermore, while data on the first phases after VF initiation are abundant,[11,14-16] data on sustained VF are scarce.[5] Therefore, a new *in vitro* and *ex vivo* model of sustained VF was developed that enabled to correlate a systematic and controllable increase in arrhythmia complexity with changes in specific electrophysiological parameters. Subsequent pharmacological modification of key parameters was used to search for novel factors affecting the stability of sustained VF and thereby unravel the underlying anti-fibrillatory mechanisms.

Methods

All animal experiments were approved by the Animal Experiments Committee of the Leiden University Medical Center and conform to the Guide for the Care and Use of Laboratory Animals as stated by the US National Institutes of Health. A more detailed description can be found in the Supplemental Material.

Cell isolation and culture

Neonatal rat ventricular myocytes were isolated by collagenase digestion as described previously,[17] Animals were anaesthetized with 4–5% isoflurane inhalation anesthesia. Adequate anesthesia was assured by the absence of reflexes prior to rapid heart excision. Ventricles were minced and digested using collagenase (Worthington, Lakewood, NJ, USA) and DNAse (Sigma-Aldrich, St. Louis, MO, USA). After isolation, cells were plated out isotropically on fibronectin-coated, round glass coverslips (15 mm) at a cell density of 2-8x10^5 cells/well in 24-well plates (Corning Life Sciences, Amsterdam, the Netherlands). To prevent overgrowth of remaining cardiac fibroblasts, proliferation was inhibited by Mitomycin-C (Sigma-Aldrich, St. Louis, MO, USA) treatment at day 1, as described previously.[17] All cultures were refreshed daily with DMEM/HAM's F10 in a 1:1 mixture with 5% HS and cultured in a humidified incubator at 37º C and 5% CO_2.

Immunocytological analyses

Cultures were stained for Connexin40 (Sigma), Connexin43 (Santa Cruz Biotechnologies, Santa Cruz, CA, USA) and Connexin45 (Santa Cruz) to assess presence of gap junctional proteins, and for active caspase-3 (Abcam, Cambridge, MA, USA) to assess the number of apoptotic cells. Images of cultures were taken and quantified using dedicated software (ImageJ, National Institutes of Health, USA).

Optical mapping of myocardial cultures

At day 4 of culture, propagation of action potentials was investigated on a whole-culture scale by optical mapping using di-4-anepps (Sigma) as voltage sensitive dye, as described previously.[17] Cells were incubated with 2-APB in 5 different concentrations (5, 10, 15, 20 and 25 μM) for 20±2 minutes, targeting Connexin43, Connexin45 and Connexin40[18,19] to induce arrhythmias of increasing complexity, while vehicle-treated cultures were used as controls. Data analysis, construction of activation maps and stripe analysis (e.g. plotting of optical signal amplitude against time, at the maximal diameter of a culture or short and long axis of whole heart) were performed with specialized software (Brainvision Analyze 1101, Brainvision Inc, Tokyo, Japan) after pixel signals were averaged with 8 of its nearest neighbors, minimizing noise-artifacts. CV in cultures with uniform or reentrant activation patterns was calculated perpendicular to the activation wave front, between two 3 by 3 pixel grids typically spaced 2-8 mm apart. CV, activation frequency, minimal APD (during

maximal paced activation frequency) and 1Hz APD were determined at 6 different locations equally distributed throughout the culture and averaged before further analysis. APD was determined at 80% of repolarization (APD_{80}) because of the rat action potential shape. Wavelength was calculated by the product of average CV and an APD_{80} (for uniform propagation) or reentrant cycle length[12]. Arrhythmia complexity was defined as the number of phase singularities per cm^2, determined by using the phase space method[20] and correlated with CV, APD_{80} and wavelength in order to identify potential targets that can be modified to affect VF stability and thereby reduce VF complexity. As a result of the outcome of this correlation, appropriate drugs (3 µmol/L nitrendipine (Sigma), 1 mmol/L sotalol (Sigma), 0.5 mmol/L $BaCl_2$ (Merck, Darmstadt, Germany) or 1 µmol/L BayK8644 (Sigma)) were administered to 2-APB treated and control cultures to modify these targets and study the effects on arrhythmia complexity.

Assessment of arrhythmia complexity

Arrhythmia complexity in cardiomyocyte cultures was defined as the number of phase singularities per cm^2. To quantify the number of phase singularities the phase space approach was used.[20] Time series analyses using the empirical mode decomposition method and the Hilbert transform were used to determine the phase.[21] Data was smoothed by Gaussian filtering with a spatial size of 5 pixels (approx. 0.75 mm) and a temporal size of 5 frames (30 ms). Subsequently, a discrete Fourier transform was performed for each pixel over the full time series. By using the Fourier spectra the dominant frequency was determined. After that a band-pass filter was applied to each time series removing low and high frequencies. Next, the local extrema for the time series were found using a half of the inverse dominant frequency as the window size. Local maxima (and local minima) were interconnected by a piece-wise linear curve and their mean curve was subtracted from the corresponding time series. Then by using the Hilbert transform of the resulting time series the phase $\varphi_{ij}(t)$ for every pixel (i, j) at the moment of time t was determined as

$$\varphi_{ij}(t) = \operatorname{atan2}\left(I_{ij}(t), H\left[I_{ij}(t)\right]\right)$$

Where $I_{ij}(t)$ is the filtered and detrended intensity of the optical mapping signal for the pixel (i, j) at the moment t and $H[\cdot]$ denotes the Hilbert transform.

The topological charge of the area Ω is determined by

$$n(\Omega) = \frac{1}{2\pi} \oint_{\partial\Omega} \operatorname{grad} \varphi \mathrm{d}\boldsymbol{l}$$

where the integral is taken along the oriented boundary of Ω. For each pixel (i, j) we defined Ω_{ij} as a square around it with the side of 3 pixels. Thus the integral was approximated by the sum of 9 finite differences.

$$n(\Omega_{ij}) = \frac{1}{2\pi}\left(\left(\varphi_{i-1,j-1} - \varphi_{i-1,j}\right) + \left(\varphi_{i-1,j} - \varphi_{i-1,j+1}\right) + \cdots + \left(\varphi_{i,j-1} - \varphi_{i-1,j-1}\right)\right)$$

The overall algorithm was implemented in the OCaml programming language using the GTK+ toolkit for visualization.
Meandering of the phase singularities was defined as the maximal straight distance covered by the same phase singularity within 6 s of optical mapping.

Whole-cell patch-clamp

Whole-cell measurements were performed in spontaneously active cultures plated out in a density of $4x10^5$ cells/well in 24 well plates as described previously.[17] At day 4 of culture, current-clamp experiments were performed in CMCs at 25°C using an L/M-PC patch-clamp amplifier (3 kHz filtering) (List-Medical, Darmstadt, Germany). To study the effects of 2-APB on electrophysiological properties of CMCs, 25 µM 2-APB (Tocris Bioscience, Bristol, United Kingdom) was incubated for 20 min prior to measurements.

Ex vivo experiments

For *ex vivo* experiments, female adult Wistar rats of 6±3 months were anesthetized through inhalation of 3-5% isoflurane and received 400 IE of heparin intraperitoneally. After confirmation of adequate anesthesia by absence of pain reflexes, beating hearts were rapidly excised and immediately submersed in cold Tyrode solution comprised of (in mM) NaCl 130, $CaCl_2$ 1.8, KCl 4.0, $MgCl_2$ 1.0, NaH_2PO_4 1.2, $NaHCO_3$ 24 and glucose 5.5 at pH 7.4. Subsequently, the aorta was canulated and retrogradely perfused with Tyrode that was freshly oxygenated with carbogen (95% O_2, 5% CO_2) and supplemented with 20mM of 2,3-butanedione monoxime (BDM) to reduce motion artifacts, at a constant flow of 15±2 ml/min at 37° C using a modified Langendorff apparatus (AD instruments, Spechbach, Germany). Hearts were stained with 2 µM di-4-anepps by a 10 ml bolus injection into the bubble trap. The optical mapping camera was positioned facing the ventral surface of the heart, viewing equal portions of the left and the right ventricle during mapping. All hearts exhibited spontaneous sinus rhythm during initial acclimatization. Arrhythmia complexity was defined as the as the number of separate wave fronts present at the epicardial surface of the heart. The targets that were shown to affect arrhythmia complexity *in vitro* were modified by administration of 0.5 mM $BaCl_2$ to the perfusate for 10 minutes prior to measurements to confirm their *ex vivo* effects on arrhythmia complexity.

Statistical analysis

Statistical analyses were performed using SPSS11.0 for Windows (SPSS, Inc., Chicago, IL, USA). Data were compared with one-way ANOVA test with Bonferroni post-hoc correction if appropriate and expressed as mean±SD. Comparison between two groups was performed using a student t-test. Before and after comparisons were performed with a paired t-test. Differences were considered statistically significant if $P<0.05$. Non-linear regression curves were constructed by using a robust exponential two phase decay curve fit. Accuracy of these curves was expressed as the robust standard deviation of the residuals (RSDR).

Results

Cell culture characterization and the effect of gap junctional uncoupling by 2-APB

Immunocytological analysis of cultures by collagen-I and α-actinin double-staining, suitable for distinction between fibroblasts and CMCs,[17] showed that cultures consisted of 17.6±3.1% fibroblasts (n=6) (Supplemental Figure 1A). Fibroblasts were homogeneously spread across the culture. In addition, cultures showed expression of Connexin43 and Connexin45 as well as heterogeneous expression of Connexin40 in between CMCs, which are the targets for 2-APB,[18,19] as judged by immunocytological staining (Supplemental Figure 1B, 1C and 1D).

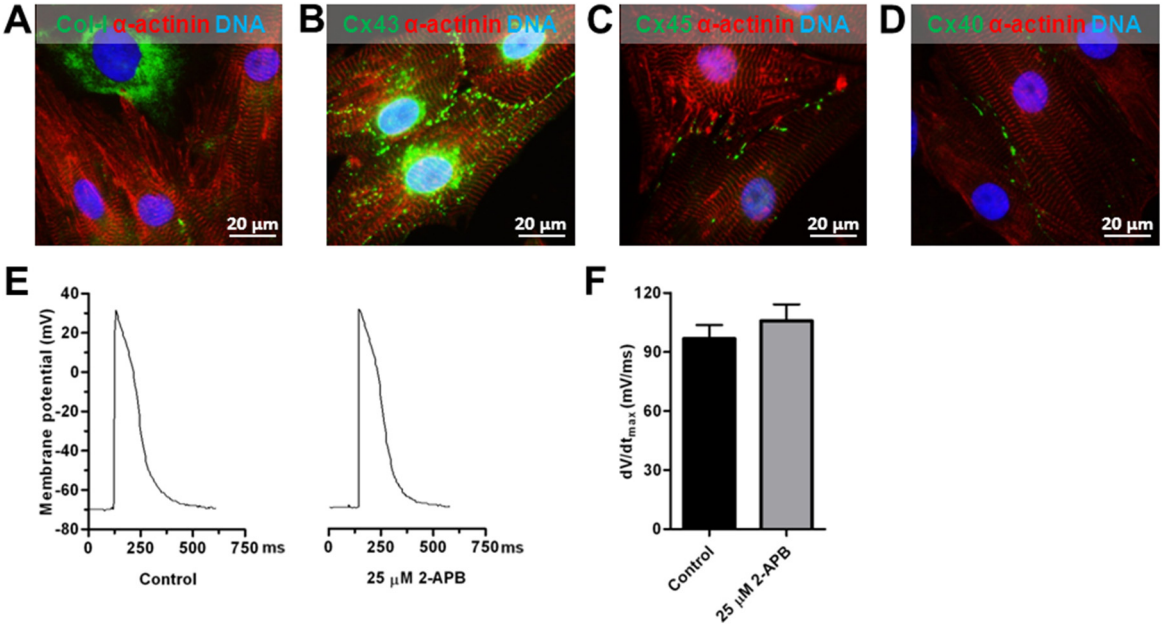

Supplemental Figure 1. *Cell culture characterization, gap junctional protein expression and modulation of gap junctional coupling*. (A) Immunocytological double-staining of α-actinin (red) and collagen-I (green), (B) Connexin43 (green), (C) Connexin45 (green) and (D) Connexin40. (E) Typical examples of membrane potential traces in control cultures and cultures treated with 25 µmol/L 2-APB and (F) Assessment of dV/dTmax.

2-APB causes stable multi-rotor tachyarrhythmias, resembling sustained VF, in a dose-dependent relation

During optical mapping, spontaneously active control cultures typically showed uniform and fast conduction (Figure 1A). However, after incubation with 2-APB, cultures showed a strong increase in the incidence of spontaneous reentrant tachyarrhythmias (Figure 1A and 1B). Furthermore, we observed a significant increase in the complexity of tachyarrhythmias, as

judged by the number of phase singularities per cm^2 with increasing dosages of 2-APB (Figure 1A, 1C and Supplemental movie 1). As a consequence of the increasing incidence of reentry with increasing 2-APB dosages (activation is higher during reentrant activation when compared to spontaneous uniform activation), average activation frequency was significantly increased after incubation with increasing dosages of 2-APB (Figure 1D). CV was dose-dependently decreased by treatment with 2-APB (Figure 1E). The decrease in CV remained apparent even when determined only during reentrant activation (Figure 1E, hatched subsets). Despite the high complexity of the tachyarrhythmias observed, the arrhythmias showed a high degree of stability that resembled sustained VF. In more detail, after initiation of reentry by treatment with 2-APB cultures showed a minimal extent of rotor meandering, which further decreased significantly with increasing 2-APB dosages (Supplemental Figure 3B). In addition, a relatively low number of fibrillating cultures showed new rotor formations, while all cultures showed minimal dispersion in optical signal amplitude as well as reentrant cycle length (Supplemental Figure 3 C-E), exemplified by stripe analysis of optical mapping recordings (Figure 1F).

The effect of gap junctional uncoupling by 2-APB

Treatment by 2-APB did not significantly change the AP morphology (Figure 1E), and dV/dT_{max} (Supplemental Figure 1F). Apoptosis was not increased in 2-APB treated cultures as judged by the expression of active caspase-3 (*P*=ns vs. control) (Supplemental Figure 2). Together these results suggest that the gap junction uncoupling agent 2-APB does not negatively affect cell excitability and viability.

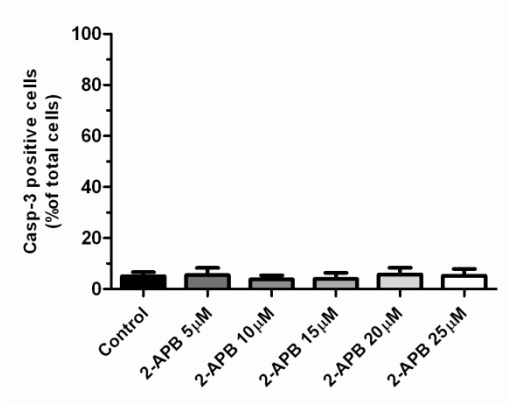

Supplemental Figure 2. *2-APB does not increase apoptosis in myocardial cultures. Quantification of apoptosis as judged by immunocytological staining of caspase-3 positive cells as a percentage of total cells (number of positive nuclei for Hoechst 33342 counterstaining).*

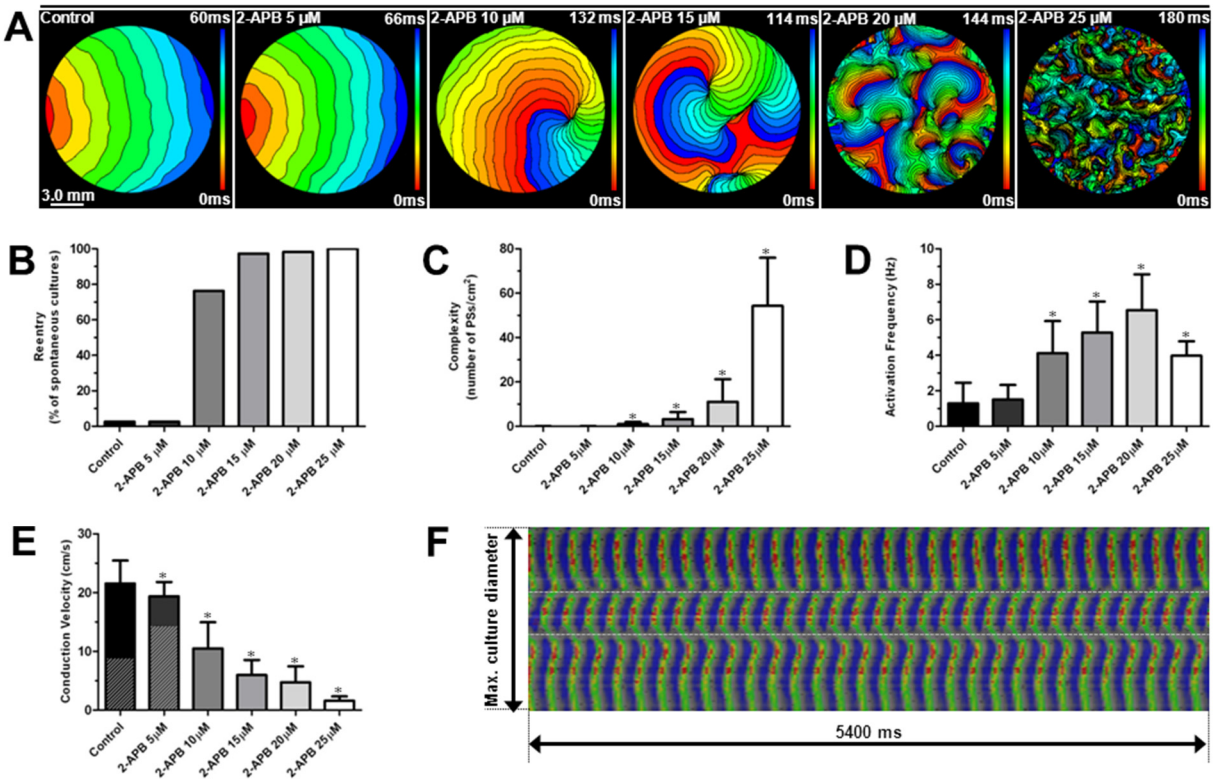

Figure 1. *(A) Activation maps (**6**ms isochronal spacing) of control cultures and 5-25µmol/L 2-APB treated cultures. (B) Quantification of reentry incidence, (C) complexity, (D) average activation frequency (both uniform and reentrant conduction included) and (E) CV in control cultures and 5-25µmol/L 2-APB treated cultures (n=38, n=38, n=39, n=39, n=61 and n=39 respectively). Hatched subsets indicate average CV during reentry in control and 5µmol/L 2-APB treated cultures (n=1 and 1). *: P<0.05 vs. control. (F) Typical line scan analysis across the diameter of a culture treated with 20µmol/L 2-APB (dotted line indicates rotor position).*

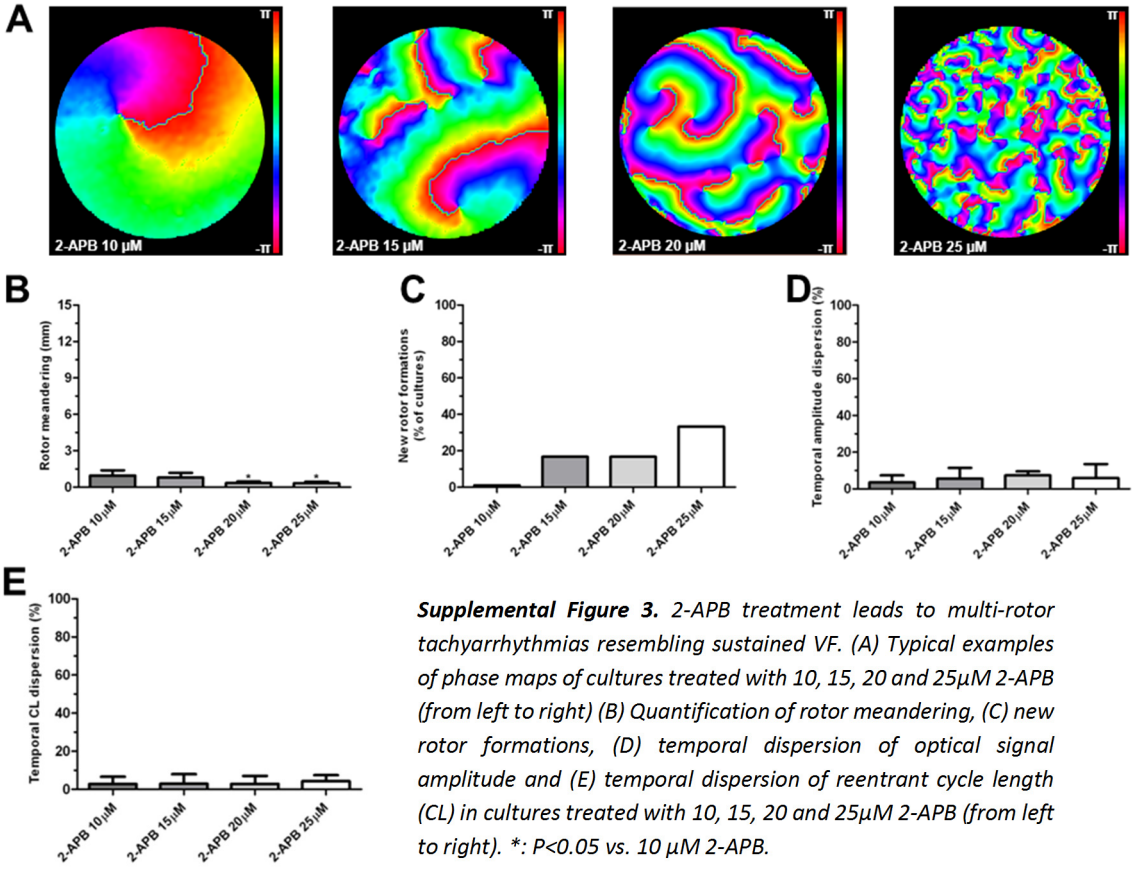

Supplemental Figure 3. *2-APB treatment leads to multi-rotor tachyarrhythmias resembling sustained VF. (A) Typical examples of phase maps of cultures treated with 10, 15, 20 and 25µM 2-APB (from left to right) (B) Quantification of rotor meandering, (C) new rotor formations, (D) temporal dispersion of optical signal amplitude and (E) temporal dispersion of reentrant cycle length (CL) in cultures treated with 10, 15, 20 and 25µM 2-APB (from left to right). *: P<0.05 vs. 10 µM 2-APB.*

Arrhythmia complexity increase is strongly related to wavelength shortening

To identify factors associated with increased arrhythmia complexity, the relationship between several electrophysiological parameters and complexity were investigated at variable 2-APB concentrations. As increasing 2-APB concentrations dose-dependently increased complexity, while at the same time decreasing CV, expectedly CV showed a strong hyperbolic-like relationship with complexity (RSDR=1.9) (Figure 2A). Furthermore, APD_{80} showed a weak inverse correlation with complexity in the low complexity range (Figure 2B). However, as at the highest 2-APB concentration the beating frequency decreases (Figure 1D), APD increases in cultures treated with 25µmol/L 2-APB. This slightly decreased the negative correlation between APD and complexity, while greatly increasing variation in APD. As wavelength is the product of CV and APD, wavelength shortening strongly related to complexity increases (RSDR=0.4) (Figure 2C). Together, these results support that inversely, complexity may be strongly diminished by increasing wavelength.

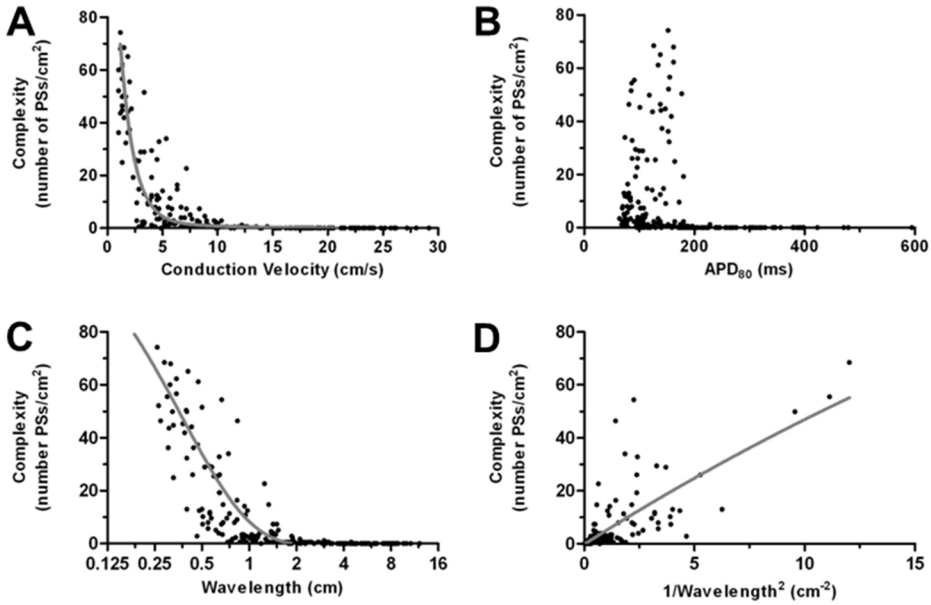

Figure 2. *Relationship between (A) CV and complexity, (B) APD_{80} and complexity, (C) wavelength and complexity (D) 1/[wavelength]^2 and complexity in control and 2-APB treated cultures (5-25µmol/L).*

Effects of pharmacological ion current modulators on 1Hz and minimal APD

To test whether arrhythmia complexity can be diminished by increasing wavelength, several ion channel modulators were selected, which according to their mechanism of action should have an effect on APD and wavelength. However, as fast activation, during fibrillation, can have an effect on activation and inactivation status of targeted ion channels,[22] the effect of the selected ion channel modulators might differ between fibrillation and normal uniform activation. Therefore, we assessed the effect of pharmacological ion channel modulation on APD at 1Hz electrical activation and at the minimal diastolic interval during 1-10Hz pacing (measuring minimal APD) in absence of reentrant circuits. As expected, nitrendipine, which inhibits I_{CaL}, significantly shortened the 1Hz APD by 28% (to 72±12%, P<0.05 vs. control) (Figure 3A and 3I), as well as minimal APD (to 84±14%, P<0.05 vs. control) (Figure 3E and 3J). Treatment with sotalol and $BaCl_2$ slowed repolarization and thus prolonged 1Hz APD (to 117±12% P<0.05 and 162±25% P<0.05 vs. control, respectively) (Figure 3B, 3C and 3I). However, the effect of sotalol on minimal APD was not significant, (Figure 3F and 3J), while $BaCl_2$ still had a significantly prolonging effect on APD during 10Hz pacing (to 145±9%, P<0.05 vs. control) (Figure 3G and 3J). Additionally, activation of I_{CaL} by Bayk8644 increased both 1Hz (to 168±13% P<0.05 vs. control) (Figure 3D and 3I) and minimal APD (to 133.7±9.6% P<0.05 vs. control) (Figure 3H and 3J) significantly.

Different effects of ion channel modulators on 2-APB induced fibrillation

In order to correlate the effects of selected ion channel modulators on minimal APD with their effects on the characteristics of fibrillation (i.e. APD, wavelength, stability, activation frequency and complexity), tachy-arrhythmic cultures induced by 2-APB were treated with nitrendipine, sotalol, $BaCl_2$ and BayK8644 (n>24 per agent).

In line with the previous, electrically stimulated experiments, APD_{80} was significantly decreased by nitrendipine throughout all 2-APB dosages, while APD was increased by both $BaCl_2$ and BayK8644. In contrast, sotalol did not affect APD significantly (Figure 4A, supplemental table 1). Wavelength was decreased significantly by nitrendipine treatment in the lowest concentration of 2-APB, although there was no significant effect in the other 2-APB dosages. In contrast, wavelength was significantly increased after $BaCl_2$ and BayK8644 treatment while sotalol did not significantly affect wavelength (Figure 4B, Supplemental Table 2). Interestingly, decreasing the APD with nitrendipine increased activation frequency of tachyarrhythmias. Conversely, lengthening of APD decreased activation frequency as seen after treatment with $BaCl_2$ and BayK8644 throughout all 2-APB dosages (Figure 4C, Supplemental Table 3). Sotalol induced a small but significant decrease in activation frequency in 15 and 20µmol/L 2-APB treated cultures only.

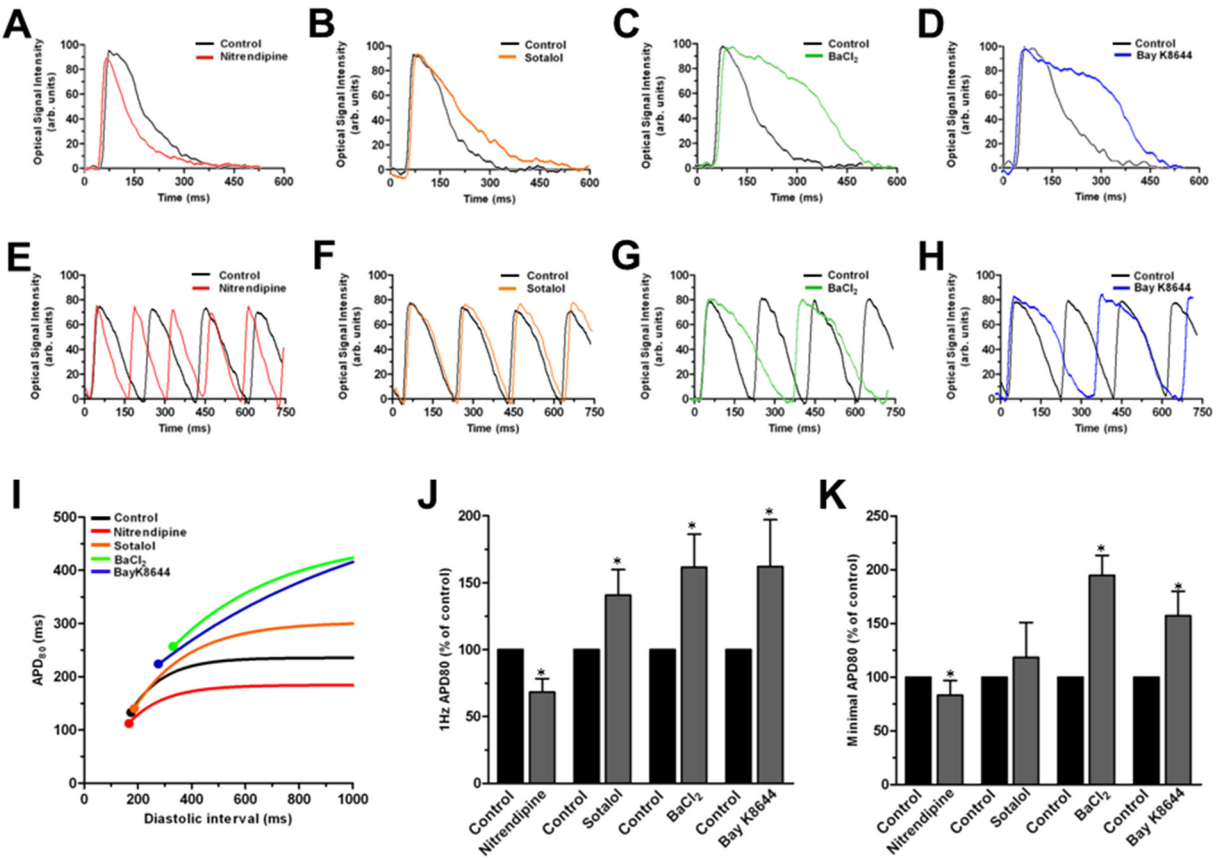

Figure 3. *Typical optical action potential records in control (black) and (A) nitrendipine (red), (B) sotalol (orange), (C) $BaCl_2$ (green) and (D) BayK8644 (blue) treated cultures illustrating treatment effects on 1Hz APD and minimal APD (E-H) and (I) APD restitution. Colored circles indicate the average minimal APD. Quantification of (J) 1Hz APD and (K) minimal APD before and after treatments. *: P<0.05 vs. control.*

The average complexity of conduction did not significantly alter after nitrendipine, while sotalol only had a small but significant effect on complexity in 25µmol/L 2-APB treated cultures. However, in $BaCl_2$ and BayK8644 treated cultures arrhythmia complexity was significantly lowered throughout all 2-APB concentrations except for the less complex arrhythmias after 10µmol/L 2-APB (Figure 4D, Supplemental Table 4). These results are indicative of the importance of minimal APD in decreasing and increasing complexity, through specific ion channel modulation.

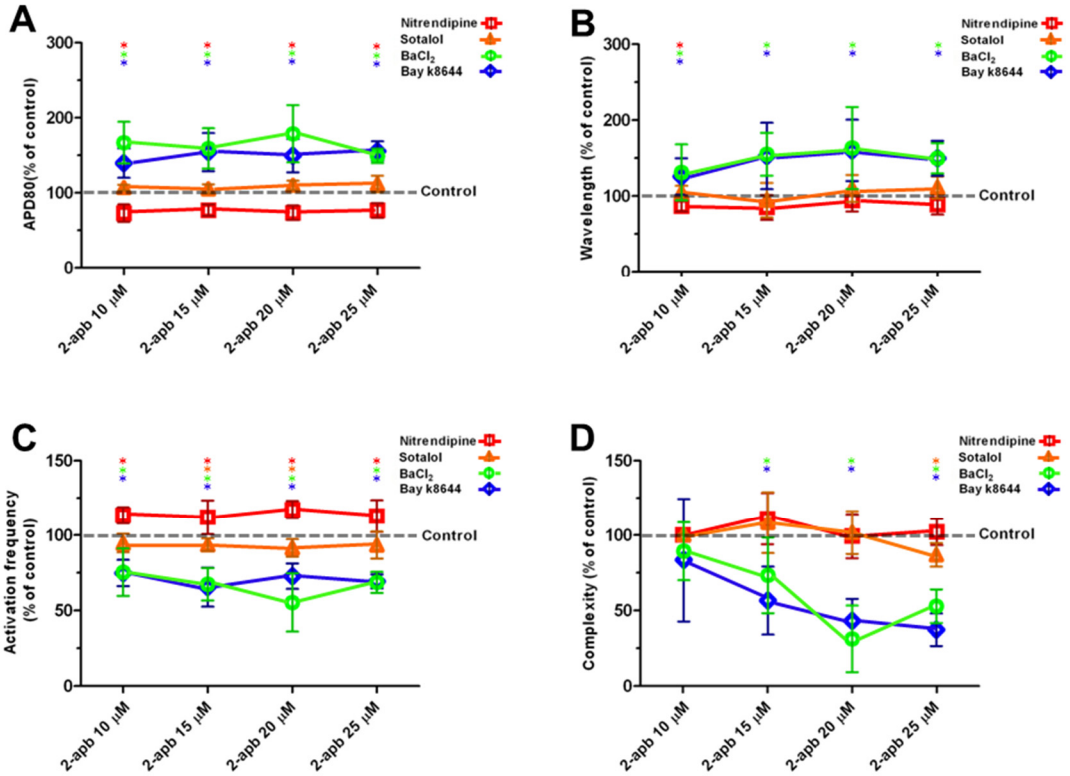

Figure 4. *(A) Quantification of APD, (B) wavelength, (C) activation frequency and (D) complexity after treatment with sotalol (orange), nitrendipine (red), $BaCl_2$ (green) and BayK8644 (blue). Dotted black lines indicate controls (prior to treatment set at 100%). *: P<0.05 vs. control.*

Mechanism of decrease in arrhythmia complexity by increase in minimal APD

Optical mapping through a permeable membrane during minimal APD prolongation by BayK8644 and $BaCl_2$ again showed that both substances decrease the number of rotors *in vitro* (Figure 5A). Prior to the addition of $BaCl_2$ or BayK8644, optical signal amplitude, spatial rotor distribution and rotor cycle lengths were highly stable (Figure 5B, D left). During incubation of $BaCl_2$ or BayK8644 transient instability in optical signal amplitude, spatial rotor distribution and rotor cycle length was induced (Figure 5B, D middle and Supplemental Figure 4A,B). Subsequently, a new equilibrium was formed, with increased optical signal amplitude, decreased number of rotors and stable but increased rotor cycle lengths (Figure 5B, D right and Supplemental Figure 4A,B). During incubation of $BaCl_2$ and BayK8644 this transient instability, which was mediated by an increase in wavelength, led to termination of neighboring rotors. Rotor termination resulted from critical collisions of wave fronts propagated from 2 different rotors, after which activation of that particular tissue is taken over by a separate pre-existing rotor, decreasing the total number of rotors (Figure 5C, 5D).

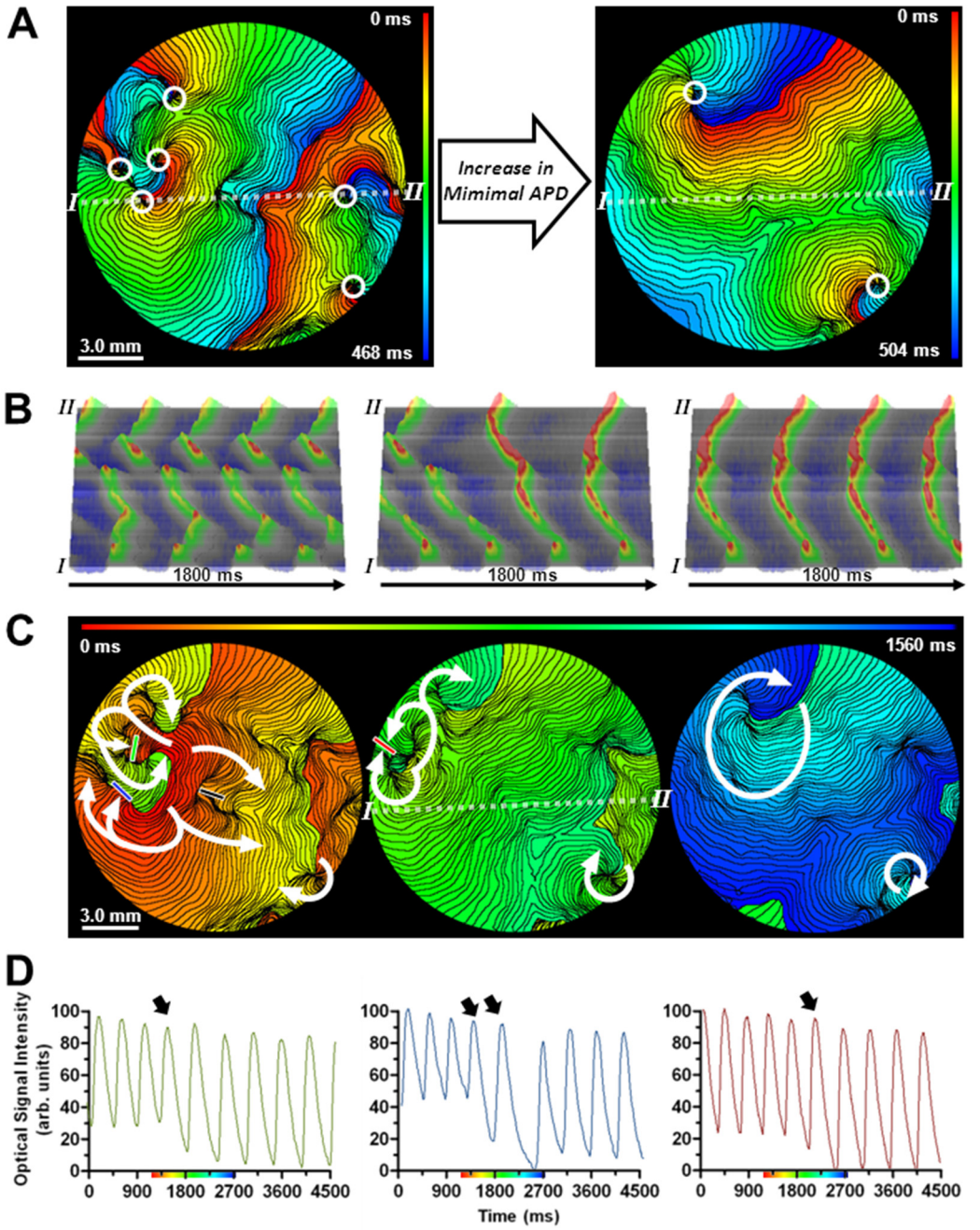

Figure 5. *(A) Activation maps of a culture treated with 20μM 2-APB, before (left) and after (right) minimal APD prolongation. White circles indicate rotor position. (B) Examples of 3 consecutive 3D (rotated 15º) line scan analyses, during 1800 s, from point I to point II in culture shown in A, before (left), during (center) and after (right) minimal APD prolongation. (C) Consecutive activation maps*

during rotor termination by APD prolongation. The green, blue, black and red bars indicate the area of critical wave front collision. (D) Optical action potentials at the areas of critical wave front collision of corresponding colors shown in C. Black arrows mark the moment of critical wave front collision.

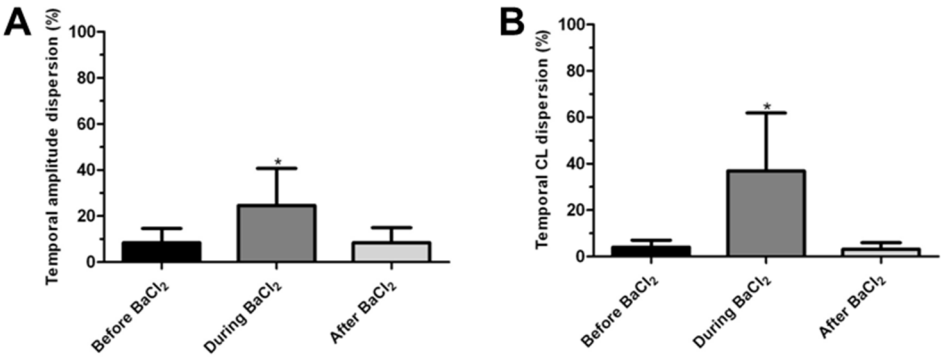

Supplemental Figure 4. *Increasing minimal APD by $BaCl_2$ causes transient instability in optical signal amplitude and rotor cycle length. (A) Quantification of temporal dispersion of optical signal amplitude and (B) temporal dispersion of rotor cycle length, prior to, during and after increasing minimal APD by the incubation with $BaCl_2$. *:P<0.05 vs. before $BaCl_2$.*

2-APB in adult rat heart ventricles

To investigate the functional implications of *in vitro* findings on the intact heart, Langendorff-perfused adult rat hearts were subjected to *ex vivo* optical mapping. Baseline activation frequency before addition of BDM to the oxygenated Tyrode perfusate was 4.50±0.5Hz. After addition of BDM sinus rhythm remained stable for at least 1 hour at an average activation frequency of 2.5±0.4Hz (Supplemental Figure 5A and 5B). Perfusion with oxygenated Tyrode supplemented with 5µmol/L 2-APB for 20 minutes slowed conduction from 54.1±3.2cm/s to 27.8±2.7cm/s (n=6, P<0.05). No arrhythmias developed at this dosage and sinus rhythm was maintained at 2.5±0.5Hz (Supplemental Figure 5A-C, P>0.05 vs. control). Perfusion of hearts with 10 µmol/L 2-APB caused VT in all hearts (2.2±0.2 wave fronts at 5.4±3.3Hz, n=6), whereas complexity of arrhythmias increased to fibrillation with 20µmol/L 2-APB (5.0±1.1 wave fronts at 11.0±0.9Hz, n=6) (Supplemental Figure 5A and 5C). Complexity of arrhythmias stabilized within 10 minutes of incubation with 2-APB.

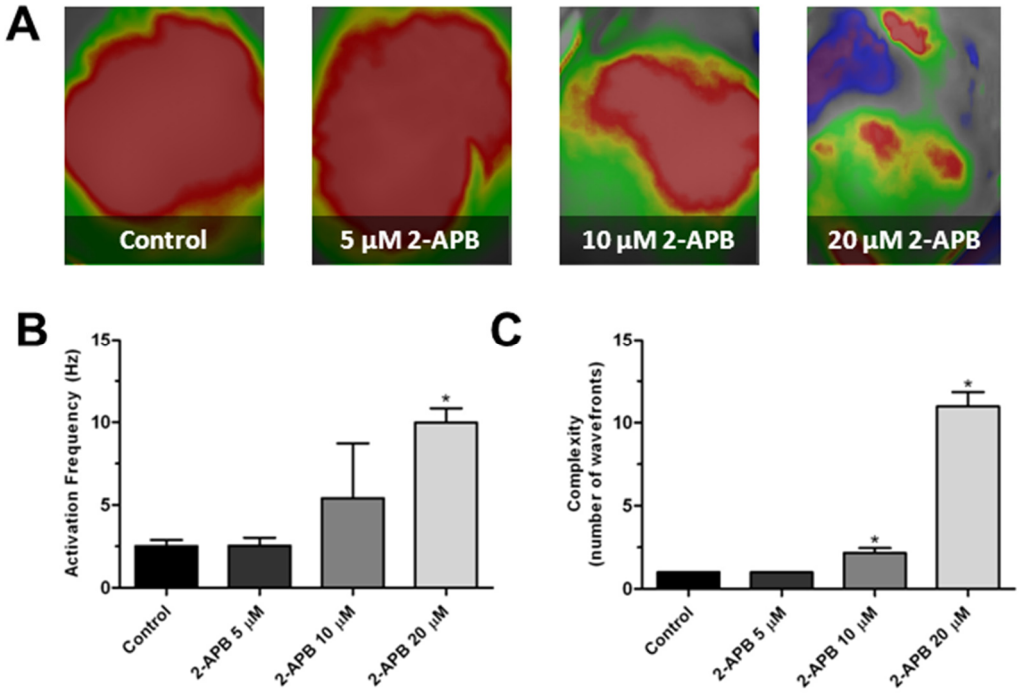

Supplemental Figure 5. *A 2-APB dose-dependent increase in arrhythmia complexity in adult Wistar rat hearts leading to sustained VF. (A) Typical snapshots of ventricular activation during optical mapping of Langendorff-perfused adult rat heart perfused with (from left to right) normal Tyrode solution and tyrode solution supplemented with 5, 10 and 20 µM 2-APB. (B) Quantification of average activation frequency and (C) complexity in control hearts, and hearts treated with 2-APB. *: P<0.05 vs control*

Minimal APD determines arrhythmia complexity in adult rat heart ventricles

To investigate whether $BaCl_2$ lowered arrhythmia complexity ex vivo as in vitro, rat hearts were first perfused with 20mmol/L 2-APB until fibrillation was present and stable for at least 5 min. Then, 500 mmol/L of $BaCl_2$ was added to the perfusate consisting of tyrode with 20mmol/L 2-APB. Typically within 5 min, $BaCl_2$ decreased arrhythmia complexity by 71.4% compared with controls (Figure 6A, C, and D, n = 6). Also, activation frequency decreased from 9.98+0.9 to 2.8+0.3 Hz by $BaCl_2$ (Figure 6A and C). Importantly, $BaCl_2$ treatment significantly increased minimal APD80 to 265.4+35.1% of control hearts (Figure 6B, n = 6). Together these results show that, similar to in vitro experiments, arrhythmia complexity can be decreased by increasing minimal APD ex vivo.

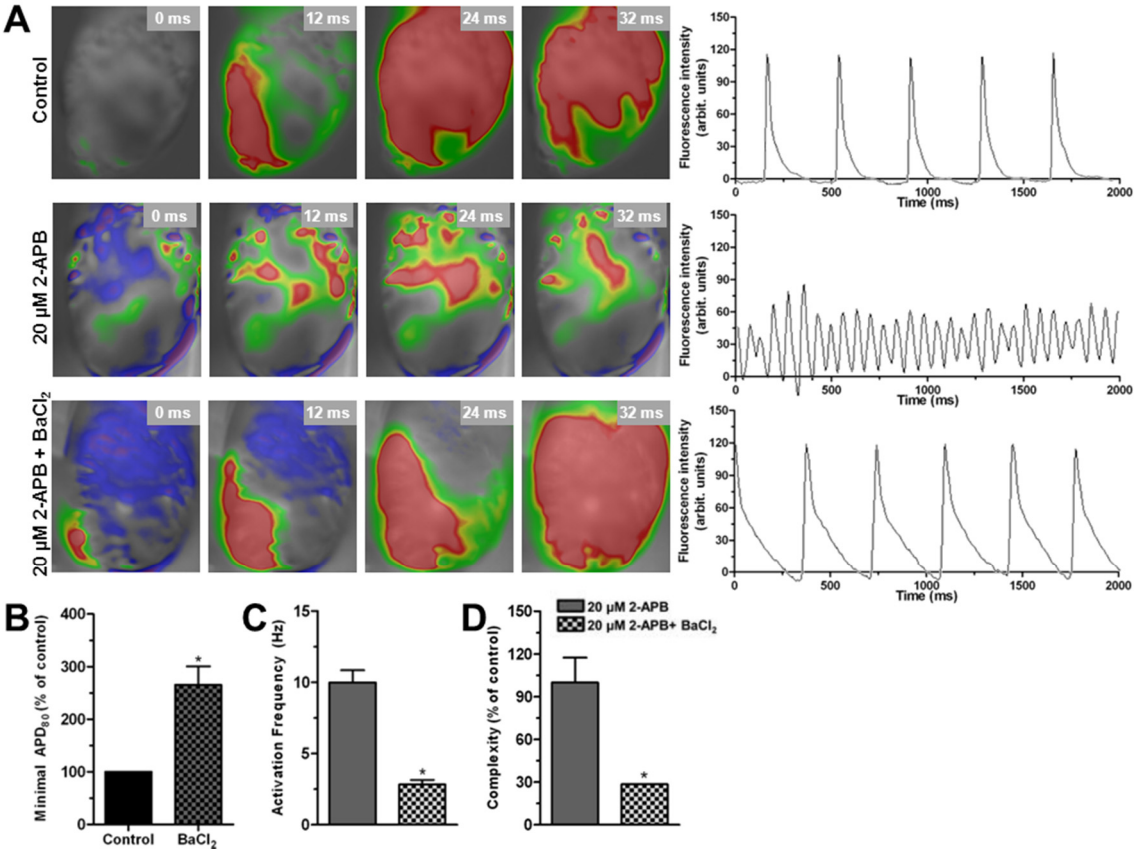

Figure 6. *(A) Typical sequence (12ms between snapshots) of activation in (from top to bottom) Langendorff-perfused control hearts, 20µM 2-APB treated hearts, and 20µM 2-APB treated hearts after introduction of $BaCl_2$ with corresponding optical action potential signals. (B) Quantification of minimal APD in control hearts and hearts perfused with 500µmol/L $BaCl_2$. (C) Assessment of activation frequency and (D) complexity in hearts treated with 20µM 2-APB before and after introduction of $BaCl_2$. *: P<0.05 vs. control.*

Discussion

The key findings of this study are (1) incubation with 2-APB induces reentrant tachyarrhythmias in myocardial cultures and adult rat hearts, which are maintained by multiple stable and co-existing rotors, resembling sustained VF. (2) The complexity of these arrhythmias increases exponentially with increasing dosages of 2-APB, allowing a systematic study of arrhythmia complexity *in vitro* and *ex vivo*. (3) Increasing arrhythmia complexity during fibrillation is associated with a shortening of the average wavelength and APD. (4) Hence, complexity and activation frequency during fibrillation could be decreased pharmacologically by transient destabilization of sustained VF through prolongation of minimal APD *in vitro* and *ex vivo*, regardless of ionic mechanism.

The importance of wavelength in reentrant tachyarrhythmias

Since the introduction of the circus movement reentry theory[23] and the leading circle concept,[24] it has been established that if the wavelength of a given reentrant circuit exceeds the path-length, reentry cannot be sustained as a consequence of a vanishing excitable gap. Hence, wavelength prolongation has traditionally been viewed as an important anti-arrhythmic strategy.[12,13] Elaborating on this theory, we now demonstrated that wavelength prolongation affects co-existence of multiple neighboring rotors, although rotor termination by prolongation of wavelength in single rotor tachyarrhythmias appeared to be more complicated (Figure 4D; 10µmol/L 2-APB). The slope in the relationship between wavelength and complexity is steepest in the low complexity range (<2 rotors) (Figure 2D). This implies that in the lower complexity range a greater wavelength prolongation is necessary to facilitate the same decrease in complexity. Also, the absence of boundaries formed by neighboring rotors diminishes the chance of rotor termination in the lower complexity range. Moreover, we show that the effect of a given agent on arrhythmia complexity depends on the activity of the agent at high frequency activation, which can differ from its effect at low frequencies. Sotalol, for instance had a significant effect on 1Hz APD, but not on minimal APD , which may explain the inability of sotalol to terminate rotors during VF. In contrast, increasing minimal APD by $BaCl_2$ and BayK8644, induced a notable reduction in the number of rotors during VF. However, decreasing minimal APD by nitrendipine treatment did not increase average arrhythmia complexity. This can be explained by the minute tendency for the formation of new wave breaks during sustained VF, despite an increase in effective size of the culture.

Importantly, in earlier *in silico* work by Ten Tusscher *et al*., minimal APD was shown to be predictive of arrhythmia complexity in animal and human hearts.[25,26] We now showed that minimal APD is not only predictive of arrhythmia complexity, but that prolongation of minimal APD also strongly and effectively reduced arrhythmia complexity.

APD and CV restitution in fibrillation

Other theories involving prevention or termination of VF mostly originate from the 'multiple wavelet' and the 'mother rotor' theory.[16,27] In general, both assume flattening of APD restitution or narrowing of CV restitution should prevent wave breaks and consequent disorganization of conduction, which should result in termination of VF.[16,27] Indeed, several studies confirmed that flattening of APD restitution by for instance verapamil or bretylium can convert VF to VT.[10,11,14,28]

However, the anti-fibrillatory effects of aforementioned substances are generally confirmed by mapping or *in silico* models during or resembling the first minute after VF induction. Yet, Wiggers *et al*. showed that the heart goes through several stages during VF,[9] by which organization and periodicity increase after the first 2 min.[6-8,10] Hence, therapies aiming to decrease disorganization of conduction could prove to be effective only in this first phases of fibrillation. The findings in the present study partially explain Wiggers' stages III and IV of fibrillation because as ischemia progresses, gap junctional coupling is reduced which may slow VF into a stable, organized and periodical multi-rotor arrhythmia. Our data on these typical characteristics of sustained VF are consistent with a previous report of sustained (slow) VF in an isolated rabbit heart model of VF.[10] Furthermore, we showed that during these phases of VF, interventions that flatten APD or CV restitution in an attempt to terminate VF may be considered inadequate. This is best exemplified by the effect of the I_{CaL} inhibitor nitrendipine on VF after 2-APB treatment, which according to earlier studies should have flattened APD restitution and terminated VF. However, nitrendipine only caused detrimental effects: increasing activation frequency without affecting complexity. Interestingly, activation of I_{CaL}, by BayK8644 treatment, did decrease complexity during VF, exemplifying the reversal of effects of I_{CaL} targeting in the early phases through the later phases of VF.

I_{K1} blockade and VF termination

Another approach to revert sustained VF to VT or sinus rhythm could be to destabilize the rotors maintaining VF in an effort to achieve termination of these rotors by collision with a preexisting boundary.[15,29] In several studies rotor stability was demonstrated to depend on specific ion channel currents, such as I_{K1}.[14,15,29-31] We showed that blockade of I_{K1} during VF decreased rotor frequency and the complexity of conduction, ultimately reverting VF back to VT.[32] However, rotor stability during VF did not seem to be specifically dependent on the I_{K1} current but on the effect blockade of I_{K1} had on the minimal APD. Therefore, the decrease in complexity could be reproduced with Bayk8644, a substance that increases minimal APD by augmenting I_{CaL}, without affecting I_{K1}.[33] By altering the stability of these rotors, collision of rotors with preexisting boundaries, but also novel critical boundaries formed by wave fronts propagated from adjacent rotors are enforced, significantly reducing the complexity of activation patterns during fibrillation.

Patients suffering from sustained VF are still in a timeframe to be resuscitated without cerebral damage.[34] Therefore, the observation that an increase in minimal APD decreases complexity of sustained VF may have important consequences for the treatment of VF, since VF, when driven by a smaller number of rotors, requires less energy for defibrillation.[35]

Study limitations

In our study, 2-APB treatment was used to induce arrhythmias. This agent is known to block gap junctional communication, but also the IP3 receptor and TRP channels, while causing activation of voltage- independent calcium channels.[18,19,36] Of these effects, gap junctional uncoupling has been shown to be related to arrhythmia induction in CMC cultures as a consequence of wave breaks caused by preexistent heterogeneity in gap junctional coupling.[2,37,38] In addition, voltage-independent calcium influx may also cause pro-arrhythmic features in 2-APB treated hearts.[36] As such, the clinical significance of these mechanisms of VF initiation may be very limited. However, as VF can show the same maintenance properties, regardless of the method of initiation[39], this does not hinder the study of VF maintenance and termination as was performed in the present study.

In the *ex vivo* mapping experiments, complexity was determined by the number of epicardial wave fronts, instead of the number of rotors. However, in line with previous research we found that during sustained VF, the number of epicardial rotors is minimal, attenuating the significance of the epicardial number of rotors.[10]

Moreover, this study makes use of a neonatal rat cardiomyocyte culture model as well as adult rat hearts. Rat hearts differ considerably from human hearts in terms of the ion currents determining the action potential morphology. Hence, the conclusions drawn from this study are only conceptual in relation to the mechanisms of ventricular fibrillation maintenance and cannot be readily extrapolated to the human or clinical setting.

Conclusions

Incubation of neonatal rat myocardial cultures or Langendorff-perfused adult rat hearts with increasing dosage of 2-APB allows for the systematic study of arrhythmia complexity, ultimately resembling sustained VF. Arrhythmia complexity and activation frequency during fibrillation can be decreased pharmacologically by transient VF destabilization through prolongation of minimal APD *in vitro* and *ex vivo*, regardless of ionic mechanism. Accordingly, this study could provide a novel conceptual framework for future anti-arrhythmic drug design as well as an extension in the rationale for treatment options of sustained VF.

Funding
This work was supported by the Netherlands Organisation for Scientific Research (NWO; VENI grant [91611070 to D.A.P], the Dutch Heart Foundation [2008/B119], the Fund for Scientific Research Flanders (FWO grant [G084811N to I.V.K. and A.V.P.]) and Institut des Hautes Etudes Scientifiques, Bures-sur-Yvette, France, and to the James Simons Foundation [I.V.K.].

Acknowledgements
We wish to thank Wilbert P.M van Meerwijk, PhD for helpful discussions, Adriana C. Gittenberger-de Groot, PhD for helpful comments on the manuscript, and Huybert J.F. van der Stadt and Gerry T.M. Wagenaar, PhD for excellent technical and scientific support.

Conflict of interest
None declared.

Supplemental Material

Methods

All animal experiments were approved by the Animal Experiments Committee of the Leiden University Medical Center and conform to the Guide for the Care and Use of Laboratory Animals as stated by the US National Institutes of Health.

Cell Isolation and culture

Neonatal rat ventricular myocytes were isolated by collagenase digestion as described previously.[17] Briefly, animals were anaesthetized with 4–5% isoflurane inhalation anesthesia.

Adequate anesthesia was assured by the absence of reflexes prior to rapid heart excision.

After animal sacrifice by rapid heart excision, ventricles were minced and digested using collagenase (Worthington, Lakewood, NJ, USA) and DNAse (Sigma-Aldrich, St. Louis, MO, USA). Cell suspensions from a 50 minutes and a subsequent 45 minutes dissociation were pooled, centrifuged and resuspended in HAM's F10 medium supplemented with 10% fetal bovine serum and 10% horse serum (HS) (Invitrogen, Carlsbad, CA, USA). Cells were preplated on Primaria coated culture dishes (BD Biosciences, Franklin Lakes, NJ, USA) to allow preferential attachment of cardiac fibroblasts. Subsequently, cell aggregates and debris were removed by filtering non-adherent cells through a 70 µM cell strainer. Following isolation myocardial cells were plated out on fibronectin-coated, round glass coverslips (15 mm) at a cell density of 2-8x10^5 cells/well in 24-well plates (Corning Life Sciences, Amsterdam, the Netherlands) depending on the experiment. To prevent overgrowth of remaining cardiac fibroblasts, proliferation was inhibited by Mitomycin-C (Sigma) treatment at day 1, as described previously.[17] All cultures were refreshed daily with DMEM/HAM's F10 in a 1:1 mixture with 5% HS and cultured in a humidified incubator at 37º C and 5% CO_2.

Immunocytological analyses

Cultures were stained for Connexin40 (Santa Cruz Biotechnologies, Santa Cruz, CA, USA) connexin43 (Sigma), and connexin45 (Santa Cruz) to assess presence of gap junctional proteins, and for active caspase-3 (Abcam, Cambridge, MA, USA) to assess the number of apoptotic cells. For this purpose, cells were fixated in 1% paraformaldehyde in PBS and permeabilized with 0.1% Triton X-100 in PBS. Primary antibodies and corresponding secondary Alexa fluor-conjugated antibodies (Invitrogen) were used at a 1:200 dilution. Counterstaining of nuclei was performed with Hoechst 33342 (Invitrogen). Images of cultures were taken and quantified using dedicated software (ImageJ, National Institutes of Health, USA).

Whole-cell patch-clamp

Whole-cell measurements were performed in spontaneously active cultures plated out in a density of $4x10^5$ cells/well in 24 well plates. At day 4 of culture, current-clamp experiments were performed in CMCs at 25° C using an L/M-PC patch-clamp amplifier (3 kHz filtering) (List-Medical, Darmstadt, Germany). The pipette solution contained (in mmol/L) 10 Na_2ATP, 115 KCl, 1 $MgCl_2$, 5 EGTA, 10 HEPES/KOH (pH 7.4). To study the effects of gap junctional uncoupling by 2-APB on electrophysiological properties of CMCs, 25 µM 2-APB (Tocris Bioscience, Bristol, United Kingdom) was incubated for 20 minutes prior to measurements.[17,40]

Tip and seal resistance were 2.0-2.5 MΩ and >1 GΩ, respectively. The bath solution contained (in mmol/L) 137 NaCl, 4 KCl, 1.8 $CaCl_2$, 1 $MgCl_2$, and 10 HEPES (pH 7.4). For data acquisition and analysis, pClamp/Clampex8 software (Axon Instruments, Molecular Devices, Sunnyvale, CA, USA) was used.

Optical mapping

At day 4 of culture, propagation of action potentials was investigated on a whole-culture scale by optical mapping using di-4-anepps as voltage sensitive dye, as described previously.[17] Structurally inhomogeneous cultures, as judged by light microscopy and mapping, were excluded for reasons of reproducibility and standardization (90 out of every 100 cultures were included). CMC cultures were plated out in 24-well plates (Corning) at a cell density of $8x10^5$ cells per well. Cultures underwent daily refreshing of culture medium and >2 hours prior to mapping, after which cultures were incubated with serum-free DMEM and colorless HAM's F10 in a 1:1 mixture (mapping medium), with 8 µmol/L di-4-anepps (Sigma) for 15±5 minutes at 37º C in a humidified incubator. Subsequently, cultures were refreshed with mapping medium. Cells were incubated with 2-APB dissolved in DMSO in 5 different concentrations (5, 10, 15, 20 and 25 µM) for 20±2 min in mapping medium, targeting Connexin43, Connexin45 and Connexin40 to induce gap junctional uncoupling,[18,19] while vehicle treated cultures were used as controls. Next, electrical propagation patterns were recorded by optical mapping at 37º C. Mapping experiments typically did not exceed 20 minutes per 24-wells plate. Also, cultures were not exposed to excitation light for longer than 40 s to limit possible phototoxic effects. Excitation light (e_{ex}=525±25 nm) was delivered by a halogen arc-lamp (MHAB-150W, Moritex Corporation, San Jose, CA, USA) through epi-illumination. Fluorescent emission light passed through a dichroic mirror and a long-pass emission filter (>590 nm) and was focused onto a 100x100 pixels CMOS camera (Ultima-L, SciMedia, Costa Mesa, CA, USA) by a 1.6x converging lens (Leice, Wetzlar, Germany). This resulted in a spatial resolution of 160 µm/pixel and a field of view of 16 by 16 mm. Spontaneous or stimulated electrical activity was recorded for 6-24 s at 6 ms exposure time per frame. Data analysis, construction of activation maps and stripe analysis (e.g. plotting

of optical signal amplitude against time, at the maximal diameter of a culture or short and long axis of whole heart) were performed with specialized software (Brainvision Analyze 1101, Brainvision Inc, Tokyo, Japan) after pixel signals were averaged with 8 of its nearest neighbors, minimizing noise-artifacts. Conduction velocity (CV), action potential duration until 80% repolarization (APD_{80}) and activation frequency were determined at six different locations equally distributed throughout the culture and averaged before further analysis. Wavelength was calculated by the product of average CV and APD_{80} (for uniform propagation) or reentrant cycle length.[12] Temporal dispersion of optical signal amplitude was defined as the difference between the minimal and the maximal optical signal amplitude (in arbitrary units) within 6 s of mapping, expressed as a percentage of the minimal optical signal amplitude. Temporal dispersion of reentrant cycle length was defined as the difference between the minimal and the maximal reentrant cycle length (in ms) within 6 s of mapping, expressed as a percentage of the minimal reentrant cycle length.

Assessment and modification of 1 Hz and minimal APD

As a result of the outcome of correlating changes in APD and wavelength with arrhythmia complexity, the effect of several ion channel modulators on APD was tested during low and high-frequency activation. This was necessary to study the effect of ion channel activation and inactivation dynamics during normal versus rapid activation on the outcome of pharmacological ion channel modulation on APD. For this purpose, we used a custom-made epoxy-coated platinum electrode and performed supra-threshold, 10 ms duration, square, unipolar stimulation using an electrical stimulus module with corresponding software (Multichannel Systems, Reutlingen, Germany). Using this electrode, cultures were paced at 1-10 Hz with 1 Hz increments. Minimal APD was defined as the APD_{80} determined at the pacing frequency (1-10 Hz) resulting in the shortest possible diastolic interval for that specific culture. Ion channel modulation was performed by administering specific ion channel modulators (which according to their mechanism of action should have an effect on APD) directly into the mapping medium and dispersing them by gentle agitation. To reduce the Ca^{2+} influx, L-type Ca^{2+} inward current (I_{CaL}) was inhibited by administration of nitrendipine (3 µmol/L) (Sigma) to reduce APD. Sotalol (1mM) (Sigma), 0.5mM $BaCl_2$ (Merck, Darmstadt, Germany), inhibiting the inward rectifier the current and BayK8644 (1 µmol/L) (Sigma) increasing the I_{CaL}, were used to increase APD. Cultures were optically mapped prior to and after 10s incubation with these pharmacological agents

During *ex vivo* experiments in adult rat hearts, APD_{80} was measured during 3 s of pacing with a unipolar platinum electrode at 1-10 Hz, to determine minimal APD. To assess the effect of $BaCl_2$ on minimal APD *ex vivo*, 500 µmol/L $BaCl_2$ was added to the perfusate for 5 minutes prior to determination of minimal APD.

Pharmacological interventions during VF

To investigate the effects of APD modifications on VF characteristics, the above mentioned pharmacological agents were also administered to 2-APB treated and control cultures. Cultures were optically mapped before and after 10 s of incubation.

In experiments involving agents that reduced VF complexity, optical signals were recorded through a transparent, permeable membrane (0.4 µm pore size) (Corning) placed in the solution above the culture that allowed for a slow and even distribution of the agents. Using this method the actual process of complexity reduction could be visualized and its underlying mechanisms could be analyzed.

During *ex vivo* experiments, after initiation of VF by 10 minutes perfusion of 20 µmol/L 2-APB, 500 µmol/L $BaCl_2$ was added to the perfusate for 10 minutes prior to measurements to study its effects on arrhythmia complexity. Importantly, the perfusate contained 2-APB prior to and during $BaCl_2$ perfusion to prevent washout of 2-APB.

Supplemental Results

2-APB dosage	APD_{80} (% of control); p value vs control			
	Nitrendipine	**Sotalol**	**$BaCl_2$**	**BayK8644**
10 µM	73±12%; *P*<0.01	107±3%; *P*=ns	167±28%; *P*<0.05	140±19%; *P*<0.05
15 µM	77±8%; *P*<0.001	105±6%; *P*=ns	159±27%; *P*<0.001	154±25%; *P*<0.01
20 µM	73±10%; *P*<0.0001	110±6%; *P*=ns	179±38%; *P*<0.0001	150±20%; *P*<0.001
25 µM	77±10%; *P*<0.01	112±11%; *P*=ns	149±10%; *P*<0.0001	155±13%; *P*<0.0001

Supplemental Table 1. APD_{80} values after pharmacological ion channel modulation by nitrendipine, sotalol, $BaCl_2$ or BayK8644 during 2-APB (10-25 µM) induced fibrillation. Controls are set at 100%. ns: non-significant.

2-APB dosage	Wavelength (% of control); p value vs control			
	Nitrendipine	**Sotalol**	**$BaCl_2$**	**BayK8644**
10 µM	87±7%; *P*<0.01	105±9%; *P*=ns	131±37%; *P*<0.05	126±24%; *P*<0.05
15 µM	85±16%; *P*=ns	95±23%; *P*=ns	155±28%; *P*<0.001	153±44%; *P*<0.05
20 µM	94±14%; *P*=ns	110±18%; *P*=ns	163±54%; *P*<0.001	160±40%; *P*<0.01
25 µM	89±13%; *P*=ns	111±15; *P*=ns	150±20%; *P*<0.01	150±23%; *P*<0.001

Supplemental Table 2. Wavelength values after pharmacological ion channel modulation by nitrendipine, sotalol, $BaCl_2$ or BayK8644 during 2-APB (10-25 µM) induced fibrillation. Controls are set at 100%. ns: non-significant.

2-APB dosage	Activation frequency (% of control); p value vs control			
	Nitrendipine	**Sotalol**	**$BaCl_2$**	**BayK8644**
10 µM	113±6%; *P*<0.01	95±6%; *P*=ns	75±16%; *P*<0.05	75±9%; *P*<0.01
15 µM	112±11%; *P*<0.05	94±4%; *P*<0.05	67±11%; *P*<0.0001	66±13%; *P*<0.001
20 µM	117±6%; *P*<0.0001	92±6%; *P*<0.05	55±19%; *P*<0.0001	73±8%; *P*<0.0001
25 µM	112±11%; *P*<0.05	93±9%; *P*=ns	69±7%; *P*<0.0001	69±5%; *P*<0.0001

Supplemental Table 3. Activation frequency values after pharmacological ion channel modulation by nitrendipine, sotalol, $BaCl_2$ or BayK8644 during 2-APB (10-25 µM) induced fibrillation. Controls are set at 100%. ns: non-significant.

2-APB dosage	Complexity (% of control); p value vs control			
	Nitrendipine	**Sotalol**	**$BaCl_2$**	**BayK8644**
10 µM	100±0%; *P*=ns	100±0%; *P*=ns	89±19%; *P*=ns	83±41%; *P*=ns
15 µM	111±17%; *P*=ns	108±20%; *P*=ns	73±25%; *P*<0.05	56±22%; *P*<0.01
20 µM	99±15%; *P*=ns	102±14; *P*=ns	30±22%; *P*<0.0001	43±15%; *P*<0.0001
25 µM	102±9%; *P*=ns	87±7%; *P*<0.01	52±11%; *P*<0.0001	37±11%; *P*<0.0001

Supplemental Table 4. Complexity values after pharmacological ion channel modulation by nitrendipine, sotalol, $BaCl_2$ or BayK8644 during 2-APB (10-25 µM) induced fibrillation. Controls are set at 100%. ns: non-significant

References

1. Zipes DP and Wellens HJ. Sudden cardiac death. *Circulation*. 1998;98:2334-2351.

2. Huikuri HV, Castellanos A, Myerburg RJ. Sudden death due to cardiac arrhythmias. *N Engl J Med*. 2001;345:1473-1482.

3. Severs NJ, Bruce AF, Dupont E, Rothery S. Remodelling of gap junctions and connexin expression in diseased myocardium. *Cardiovasc Res*. 2008;80:9-19.

4. Weiss JN, Qu Z, Chen PS, Lin SF, Karagueuzian HS, Hayashi H, Garfinkel A, Karma A. The dynamics of cardiac fibrillation. *Circulation*. 2005;112:1232-1240.

5. Gutstein DE, Morley GE, Tamaddon H, Vaidya D, Schneider MD, Chen J, Chien KR, Stuhlmann H, Fishman GI. Conduction slowing and sudden arrhythmic death in mice with cardiac-restricted inactivation of connexin43. *Circ Res*. 2001;88:333-339.

6. Clayton RH, Nash MP, Bradley CP, Panfilov AV, Paterson DJ, Taggart P. Experiment-model interaction for analysis of epicardial activation during human ventricular fibrillation with global myocardial ischaemia. *Prog Biophys Mol Biol*. 2011;107:101-111.

7. Huang J, Rogers JM, Killingsworth CR, Singh KP, Smith WM, Ideker RE. Evolution of activation patterns during long-duration ventricular fibrillation in dogs. *Am J Physiol Heart Circ Physiol*. 2004;286:H1193-H1200.

8. Kleber AG, Riegger CB, Janse MJ. Electrical uncoupling and increase of extracellular resistance after induction of ischemia in isolated, arterially perfused rabbit papillary muscle. *Circ Res*. 1987;61:271-279.

9. Wiggers CJ, Bell JR, Paine M. Studies of ventricular fibrillation caused by electric shock: II. Cinematographic and electrocardiographic observations of the natural process in the dog's heart. Its inhibition by potassium and the revival of coordinated beats by calcium. *Ann Noninvasive Electrocardiol*. 2003;8:252-261.

10. Wu TJ, Lin SF, Weiss JN, Ting CT, Chen PS. Two types of ventricular fibrillation in isolated rabbit hearts: importance of excitability and action potential duration restitution. *Circulation*. 2002;106:1859-1866.

11. Garfinkel A, Kim YH, Voroshilovsky O, Qu Z, Kil JR, Lee MH, Karagueuzian HS, Weiss JN, Chen PS. Preventing ventricular fibrillation by flattening cardiac restitution. *Proc Natl Acad Sci U S A*. 2000;97:6061-6066.

12. Panfilov AV. Is heart size a factor in ventricular fibrillation? Or how close are rabbit and human hearts? *Heart Rhythm*. 2006;3:862-864.

13. Rensma PL, Allessie MA, Lammers WJ, Bonke FI, Schalij MJ. Length of excitation wave and susceptibility to reentrant atrial arrhythmias in normal conscious dogs. *Circ Res*. 1988;62:395-410.

14. Samie FH, Mandapati R, Gray RA, Watanabe Y, Zuur C, Beaumont J, Jalife J. A mechanism of transition from ventricular fibrillation to tachycardia : effect of calcium channel blockade on the dynamics of rotating waves. *Circ Res*. 2000;86:684-691.

15. Warren M, Guha PK, Berenfeld O, Zaitsev A, Anumonwo JM, Dhamoon AS, Bagwe S, Taffet SM, Jalife J. Blockade of the inward rectifying potassium current terminates ventricular fibrillation in the guinea pig heart. *J Cardiovasc Electrophysiol*. 2003;14:621-631.

16. Zaitsev AV, Berenfeld O, Mironov SF, Jalife J, Pertsov AM. Distribution of excitation frequencies on the epicardial and endocardial surfaces of fibrillating ventricular wall of the sheep heart. *Circ Res*. 2000;86:408-417.

17. Askar SF, Ramkisoensing AA, Schalij MJ, Bingen BO, Swildens J, van der Laarse A, Atsma DE, de Vries AA, Ypey DL, Pijnappels DA. Antiproliferative treatment of myofibroblasts prevents arrhythmias in vitro by limiting myofibroblast-induced depolarization. *Cardiovasc Res*. 2011;90:295-304.

18. Bai D, del CC, Srinivas M, Spray DC. Block of specific gap junction channel subtypes by 2-aminoethoxydiphenyl borate (2-APB). *J Pharmacol Exp Ther*. 2006;319:1452-1458.

19. Harks EG, Camina JP, Peters PH, Ypey DL, Scheenen WJ, van Zoelen EJ, Theuvenet AP. Besides affecting intracellular calcium signaling, 2-APB reversibly blocks gap junctional coupling in confluent monolayers, thereby allowing measurement of single-cell membrane currents in undissociated cells. *FASEB J*. 2003;17:941-943.

20. Gray RA, Pertsov AM, Jalife J. Spatial and temporal organization during cardiac fibrillation. *Nature*. 1998;392:75-78.

21. Nash MP, Mourad A, Clayton RH, Sutton PM, Bradley CP, Hayward M, Paterson DJ, Taggart P. Evidence for multiple mechanisms in human ventricular fibrillation. *Circulation*. 2006;114:536-542.

22. Kleber AG and Rudy Y. Basic mechanisms of cardiac impulse propagation and associated arrhythmias. *Physiol Rev*. 2004;84:431-488.

23. Mines GR. On dynamic equilibrium in the heart. *J Physiol*. 1913;46:349-383.

24. Allessie MA, Bonke FI, Schopman FJ. Circus movement in rabbit atrial muscle as a mechanism of trachycardia. *Circ Res*. 1973;33:54-62.

25. ten Tusscher KH, Mourad A, Nash MP, Clayton RH, Bradley CP, Paterson DJ, Hren R, Hayward M, Panfilov AV, Taggart P. Organization of ventricular fibrillation in the human heart: experiments and models. *Exp Physiol*. 2009;94:553-562.

26. ten Tusscher KH, Hren R, Panfilov AV. Organization of ventricular fibrillation in the human heart. *Circ Res*. 2007;100:e87-101.

27. Moe GK and ABILDSKOV JA. Atrial fibrillation as a self-sustaining arrhythmia independent of focal discharge. *Am Heart J*. 1959;58:59-70.

28. Riccio ML, Koller ML, Gilmour RF, Jr. Electrical restitution and spatiotemporal organization during ventricular fibrillation. *Circ Res*. 1999;84:955-963.

29. Sekar RB, Kizana E, Cho HC, Molitoris JM, Hesketh GG, Eaton BP, Marban E, Tung L. IK1 heterogeneity affects genesis and stability of spiral waves in cardiac myocyte monolayers. *Circ Res*. 2009;104:355-364.

30. Jalife J. Inward rectifier potassium channels control rotor frequency in ventricular fibrillation. *Heart Rhythm*. 2009;6:S44-S48.

31. Tsuchihashi K and Curtis MJ. Influence of tedisamil on the initiation and maintenance of ventricular fibrillation: chemical defibrillation by Ito blockade? *J Cardiovasc Pharmacol*. 1991;18:445-456.

32. Rees SA and Curtis MJ. Specific IK1 blockade: a new antiarrhythmic mechanism? Effect of RP58866 on ventricular arrhythmias in rat, rabbit, and primate. *Circulation*. 1993;87:1979-1989.

33. Yatani A, Kunze DL, Brown AM. Effects of dihydropyridine calcium channel modulators on cardiac sodium channels. *Am J Physiol*. 1988;254:H140-H147.

34. Safar P. Cerebral resuscitation after cardiac arrest: research initiatives and future directions. *Ann Emerg Med*. 1993;22:324-349.

35. Hillebrenner MG, Eason JC, Trayanova NA. Mechanistic inquiry into decrease in probability of defibrillation success with increase in complexity of preshock reentrant activity. *Am J Physiol Heart Circ Physiol*. 2004;286:H909-H917.

36. Wang P, Umeda PK, Sharifov OF, Halloran BA, Tabengwa E, Grenett HE, Urthaler F, Wolkowicz PE. Evidence that 2-aminoethoxydiphenyl borate provokes fibrillation in perfused rat hearts via voltage-independent calcium channels. *Eur J Pharmacol*. 2012;681:60-67.

37. Nakagami T, Tanaka H, Dai P, Lin SF, Tanabe T, Mani H, Fujiwara K, Matsubara H, Takamatsu T. Generation of reentrant arrhythmias by dominant-negative inhibition of connexin43 in rat cultured myocyte monolayers. *Cardiovasc Res*. 2008;79:70-79.

38. Bub G, Shrier A, Glass L. Spiral wave generation in heterogeneous excitable media. *Phys Rev Lett*. 2002;88:058101.

39. Curtis MJ and Hearse DJ. Ischaemia-induced and reperfusion-induced arrhythmias differ in their sensitivity to potassium: implications for mechanisms of initiation and maintenance of ventricular fibrillation. *J Mol Cell Cardiol*. 1989;21:21-40.

40. Pijnappels DA, Schalij MJ, Ramkisoensing AA, van Tuyn J, de Vries AA, van der Laarse A, Ypey DL, Atsma DE. Forced alignment of mesenchymal stem cells undergoing cardiomyogenic differentiation affects functional integration with cardiomyocyte cultures. *Circ Res*. 2008;103:167-176.

Cellular and Molecular Mechanisms of Arrhythmias in Cardiac Fibrosis and Beyond:

From Symptoms to Substrates towards Solutions

Chapter VI

Engraftment Patterns of Human Adult Mesenchymal Stem Cells Expose Electrotonic and Paracrine Pro-Arrhythmic Mechanisms in Myocardial Cell Cultures

Mesenchymal Stem Cells and Arrhythmias

Saïd F.A. Askar, MSc*; Arti A. Ramkisoensing, MSc, MD*; Douwe E. Atsma, MD, PhD; Martin J. Schalij, MD, PhD; Antoine A.F. de Vries, PhD*; Daniël A. Pijnappels, PhD*.

*Equal Contribution

Adapted from Circ Arrhythm Electrophysiol 2013;6:380-91

Abstract

Background: After intramyocardial injection, mesenchymal stem cells (MSCs) may engraft and influence host myocardium. However, engraftment rate and pattern of distribution are difficult to control *in vivo*, hampering assessment of potential adverse effects. In this study, the role of MSCs engraftment patterns on arrhythmicity in controllable *in vitro* models is investigated.

Methods & Results: Co-cultures of 4×10^5 neonatal rat cardiomyocytes (nrCMCs) and 7% or 28% adult human (h) MSCs in diffuse or clustered distribution patterns were prepared. Electrophysiological effects were studied by optical mapping and patch-clamping. In diffuse co-cultures, hMSCs dose-dependently decreased nrCMC excitability, slowed conduction and prolonged APD_{90}. Triggered activity (14% vs. 0% in controls) and increased inducibility of reentry (53% vs. 6% in controls) were observed in 28% hMSC co-cultures. MSC clusters increased APD_{90}, slowed conduction locally, and increased reentry inducibility (23%), without increasing triggered activity. Pharmacological heterocellular electrical uncoupling increased excitability and conduction velocity to 133% in 28% hMSC co-cultures, but did not alter APD_{90}. Transwell experiments showed that hMSCs dose-dependently increased APD_{90}, APD dispersion, inducibility of reentry and affected specific ion channel protein levels, while excitability was unaltered. Incubation with hMSC-derived exosomes did not increase APD in nrCMC cultures.

Conclusions: Adult hMSCs affect arrhythmicity of nrCMC cultures by heterocellular coupling leading to depolarization-induced conduction slowing and by direct release of paracrine factors that negatively affect repolarization rate. The extent of these detrimental effects depends on the number and distribution pattern of hMSCs. These results suggest that caution should be urged against potential adverse effects of myocardial hMSC engraftment.

Introduction

Over the past decade, stem cell therapy has been subject of studies aiming to improve function of damaged hearts. Particularly mesenchymal stem cells (MSCs) have been of interest in these efforts.[1,2] In spite of the fact that only low percentages of injected MSCs survive and integrate in damaged myocardium, therapeutic effects have been found in pre-clinical studies.[3,4] Moreover, genetically modified MSCs have also been investigated as vehicles of biological functions such as biological pacemakers.[5] Also, intramyocardial transplantation of bone marrow-derived cells, including human (h) MSCs, into diseased human myocardium has been shown to improve cardiac function.[6] These positive effects on cardiac function are believed to be mainly mediated by paracrine factors released from the transplanted cells.[7] Therefore, increasing engraftment rate to improve the therapeutic effects of transplanted cells seems a logical step and is indeed the focus of current stem cell research.[8,9] However, the risk of adverse effects with higher engraftment rates in largely uncontrolled engraftment patterns is unknown. The number of transplanted cells that actually engrafts and their distribution patterns are difficult to regulate. Only few studies have focused on these aspects. Fukushima *et al.* showed that engraftment patterns of transplanted bone marrow cells may depend on administration route, *i.e.* direct intramyocardial injection resulted in a more clustered distribution than intracoronary infusion.[10] Such clustering may lead to formation of local conduction blocks, potentially facilitating reentrant tachyarrhythmias. Additionally, *in vitro* studies by Chang *et al.* have indicated that administration of hMSCs to myocardial cell cultures may indeed increase pro-arrhythmic risk.[11] However, besides indirect implications that electrotonic coupling of MSCs with host cardiomyocytes may be responsible for their pro-arrhythmic effects, the mechanisms underlying MSC-dependent arrhythmogeneity remain unknown. Also, insights concerning differences between pro-arrhythmic effects of distinct engraftment profiles of MSCs are still limited. As a result, further investigation of potentially pro-arrhythmic actions of hMSCs is required. Such studies are especially important to improve therapeutic efficacy and to contain the hazardous potential of MSC therapy in the heart. Therefore, this study aimed to investigate the effects of engraftment characteristics of MSCs (*i.e.* different numbers and distribution patterns) on arrhythmicity using controllable *in vitro* models. We found that hMSCs can indeed be pro-arrhythmic depending on their number and distribution pattern and that direct contact between neonatal rat ventricular cardiomyocytes (nrCMCs) and hMSCs as well as paracrine effects of hMSCs on nrCMCs are important contributors to the pro-arrhythmic effects of hMSCs. The results of this study suggest that caution is warranted against potential pro-arrhythmic effects of MSC transplantation in cardiac tissue. The acquired knowledge about the mechanisms by which hMSCs can cause arrhythmias may help to develop strategies how to increase the safety and efficacy of intramyocardial hMSC administration.

Materials and Methods

A more detailed description of the materials and methods can be found in the Supplemental Material, which also includes methods of immunocytological stainings, western blot, dye-transfer and patch-clamp experiments.

Isolation, culture and characterization of hMSCs

Human tissue samples were collected after having obtained written informed consent of the donors and with the approval of the medical ethics committee of Leiden University Medical Center (LUMC). The procedures used in this investigation conformed to the Declaration of Helsinki. Human MSCs were purified from leftover bone marrow samples derived from adult ischemic heart disease patients (n=4 donors). hMSCs were characterized by immunophenotyping and by their adipogenic and osteogenic differentiation potential as described in the online supplement.

Isolation and culture of nrCMCs

All animal experiments were approved by LUMC's animal experiments committee and conform to the Guide for the Care and Use of Laboratory Animals, as stated by the US National Institutes of Health (10236).[12] Briefly, hearts were rapidly excised from isoflurane-anesthetized animals, the ventricles were minced into pieces and dissociated by treatment with collagenase type I (450 units/mL; Worthington Biochemical, Lakewood, NJ). The myocardial cells were pre-plated to minimize contamination of the nrCMC cultures with non-cardiomyocytes. Purified myocardial cells were plated on fibronectin (Sigma-Aldrich Chemie, Zwijndrecht, the Netherlands)-coated coverslips in 24-wells plates (Corning Life Sciences, Amsterdam, the Netherlands) at a density of 1-4×10^5 cells/well depending on the experiment. All cultures were treated with 10 µg/mL mitomycin-C (Sigma-Aldrich Chemie) to halt proliferation of endogenous fibroblasts.

Co-culture of nrCMCs and clustered or diffusely spread hMSCs

To investigate the effects on arrhythmicity of myocardial engraftment of hMSCs in different patterns and doses, co-cultures of nrCMCs and hMSCs were prepared. To mimic a diffuse engraftment pattern, 4.0×10^5 nrCMCs were mixed with 2.8×10^4 (7%) or 1.12×10^5 (28%) hMSCs and added onto coverslips in wells of a 24-well cell culture plate. To mimic a clustered engraftment pattern, rings with an outer diameter of 15 mm and a central inner diameter of 3 or 6 mm were lasered in Parafilm M (Bemis Company, Neenah, WI, USA) and attached to the coverslips. Next, hMSCs were applied in these circles (3 mm: 2.8×10^4 cells or 6 mm: 1.12×10^5 cells). After attachment, the Parafilm was removed and the attached hMSCs were overlaid with 4.0×10^5 nrCMCs.

Optical mapping

Electrophysiological parameters were determined by optical mapping as described previously.[13] Cultures were loaded with di-4-ANEPPS (Invitrogen, Breda, the Netherlands) for 10 min at 37°C. Cultures were then given fresh DMEM/F12 (Invitrogen) and optically mapped using the Micam Ultima-L optical mapping system (Scimedia USA, Costa Mesa, CA).

Analysis of the influence of paracrine factors on electrophysiological parameters of nrCMC cultures

Mitomycin-C-treated adult hMSCs were seeded in 24-well plate transwell inserts (Corning Life Sciences). To mimic as much as possible the conditions of the non-transwell experiments, the inserts contained 2.8×10^4 or 1.12×10^5 hMSCs and were placed above 4.0×10^5 mitomycin-C-treated nrCMCs seeded on fibronectin-coated coverslips. Control cultures consisted of nrCMC cultures with no, empty or nrCMC (1.12×10^5 cells)-filled transwell inserts. In addition, exosomes were derived from hMSCs[14,15] and incubated with nrCMCs cultures for 9 days.

Statistics

Experimental data was analyzed by the Mann-Whitney-U test for direct comparisons, or the Wilcoxon signed-rank test for paired observations. For multiple comparisons, the Kruskal-Wallis test with Dunn' s *post-hoc* correction was used. Experimental results were expressed as mean±standard deviation (SD) for a given number (n) of observations. Statistical analysis was performed using SPSS 16.0 for Windows (SPSS, Chicago, IL). Differences were considered statistically significant at $P<0.05$.

Results

Diffusely spread hMSCs dose-dependent decrease conduction velocity (CV) and excitability in myocardial cell cultures

Adult hMSCs used in this study fulfilled established identity criteria, as shown in the Online Supplement (Supplemental Figure 1). The pro-arrhythmic effects of hMSCs were first investigated in co-cultures of hMSCs and nrCMCs in which the hMSCs were evenly distributed throughout the monolayer (Figure 1A). Addition of 7% or 28% hMSCs to nrCMCs dose-dependently slowed conduction from 21.6±1.8 cm/s (0% hMSCs, n=15) to 17.1±3.1 (7% hMSCs, n=20) and 12.6±3.2 cm/s (28% hMSCs, n=64, P<0.05 between experimental groups, Figure 1B). Current-clamping of parallel cultures revealed a decrease in upstroke velocity in 28% hMSC-containing myocardial cell cultures (10±2 [n=5] vs. 94±10 V/s [n=7] in control cultures, P<0.05, Figure 1C-D). Moreover, maximal diastolic potentials (MDPs) were less negative for nrCMCs in co-culture with 28% hMSCs (-44±5 [n=5] vs. -72±5 mV [n=7] in control cultures, P<0.05, Figure 1E-F). To study the effects of diffusely spread hMSCs on excitability of nrCMC cultures, CV after administration of the voltage-gated sodium channel blocker tetrodotoxin (TTX) in increments of 5 µmol/L to 20 µmol/L was measured. In co-cultures containing 0% or 7% hMSCs, a TTX concentration-dependent decrease in CV was observed for the entire dose range (Figure 1G). However, in cultures with 28% added hMSCs, the conduction-slowing effect of TTX was saturated between 15 and 20 µmol/L (P>0.05). Moreover, the magnitude of the drop in CV by increasing TTX doses declined with increasing hMSC numbers, indicating diminished availability of Nav1.5 and thereby confirming the ability of hMSCs to decrease excitability.

hMSCs exert pro-arrhythmic effects through electrical coupling with neighboring nrCMCs

The mechanisms through which hMSCs negatively affect the excitability of nrCMCs were studied by investigating co-cultures for the expression of N-cadherin, α smooth muscle actinin (αSMA) and connexin-43 (Cx43). Adult hMSCs co-cultured with nrCMCs (n=3,000 hMSCs analyzed) stained negative for αSMA (Supplemental Figure 2A). Also, no N-cadherin was present at hMSC-nrCMC junctions (Supplemental Figure 2B). Cx43 was detected at interfaces between hMSCs and nrCMCs (Figure 2A1), but in lower quantities (20.2$\pm$2.2%, P<0.0001) than at nrCMC-nrCMC junctions (Figure 2A2). Functional electrical heterocellular coupling between hMSCs and nrCMCs was investigated by dye-transfer experiments. The enhanced green fluorescent protein (GFP)-labeled hMSCs showed a significantly lower dye intensity (18.7$\pm$3.0%, P<0.001) than adjacent, calcein-loaded nrCMCs (Figure 2B1-B2).

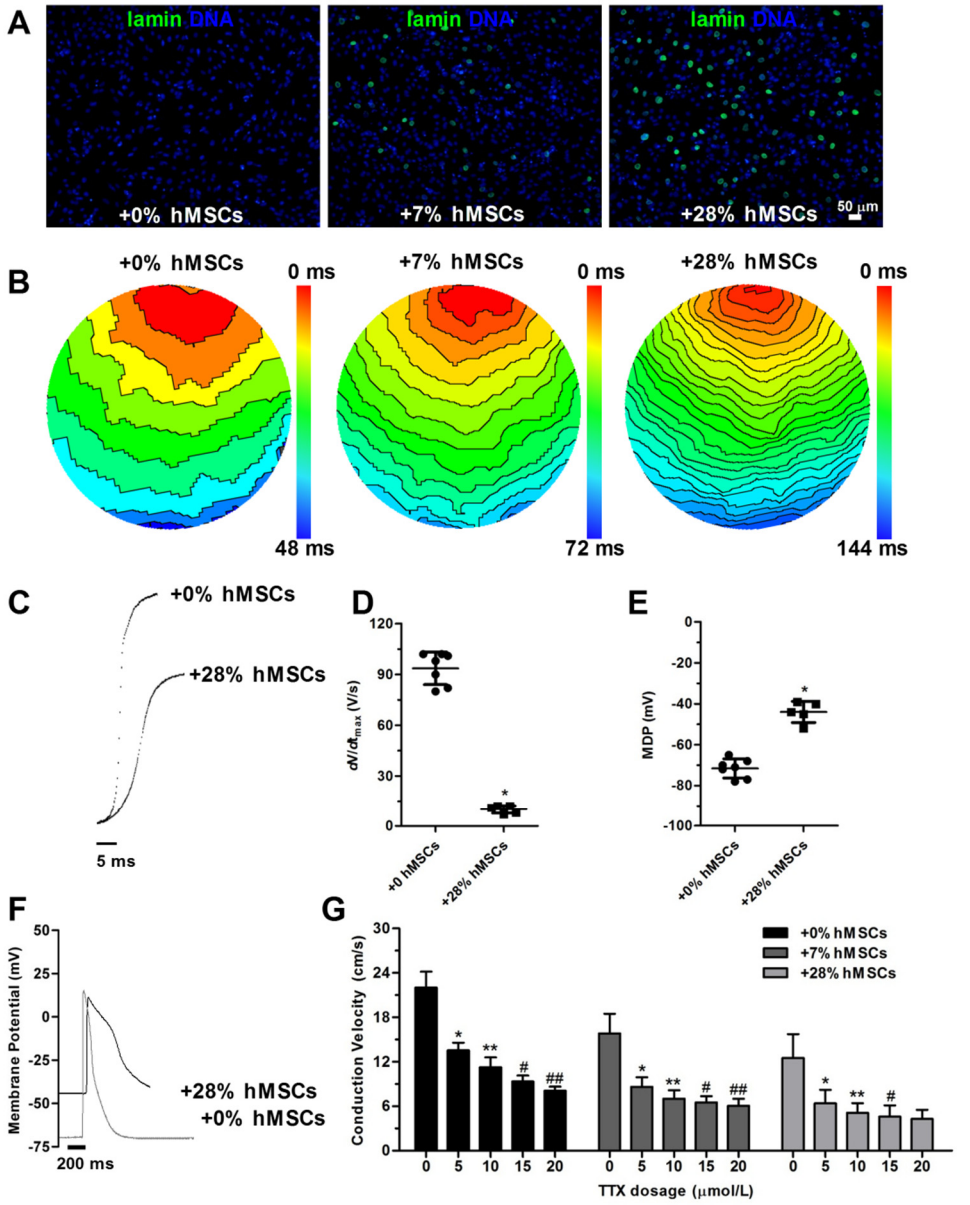

Figure 1. *Conduction slowing and decreased excitability in myocardial cell cultures containing diffusely spread hMSCs. (A) Fluorescent microscopy images of myocardial cell cultures containing 0%, 7% or 28% hMSCs stained for human-specific lamin A/C (green). (B) Activation maps of myocardial cell cultures with 0%, 7% or 28% added hMSCs. Isochrones: 6 ms. (C) Typical action potential upstroke traces recorded with current-clamp in nrCMCs in a control culture or in culture with 28% hMSCs.*

*(D) Quantification of maximum depolarization rate (dV/dt_{max}). *P<0.05 vs. 0% hMSCs. (E) Quantification of MDP recorded in nrCMCs. *P<0.05 vs. 0% hMSCs. (F) Typical voltage traces from nrCMCs in myocardial cell cultures containing 0% or 28% hMSCs. (G) Quantification of the effect of stepwise increasing TTX dose. *P<0.05 vs. 0 µmol/L TTX, **P<0.05 vs. 5 µmol/L TTX, #P<0.05 vs. 10 µmol/L TTX, ##P<0.05 vs. 15 µmol/L TTX.*

Also, although a large fraction of GFP-positive cells had taken up the dye (84.5±4.5%), not all hMSCs were positive for calcein.

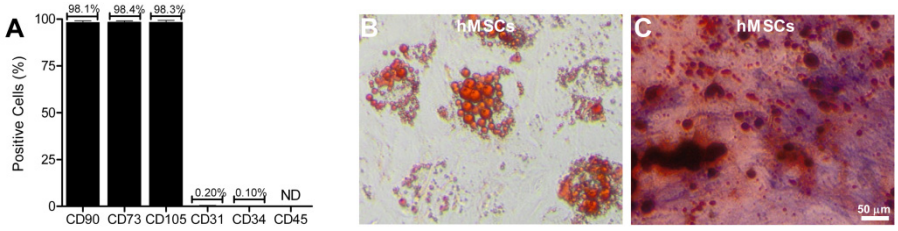

Supplemental figure 1. *Characterization of adult BM hMSCs. (A) Flow cytometric analyses showed abundant surface expression of the MSC markers CD90, CD73 and CD105 and hardly any surface expression of the hematopoietic cell markers CD34 and CD45 or the endothelial cell marker CD31. Percentages are means of ≥4 measurements. ND is not detected. (B) Adipogenic differentiation was visualized by the presence of Oil Red O-stained fat vacuoles. (C) Calcium depositions and alkaline phosphatase activity were present after osteogenic differentiation of the hMSCs.*

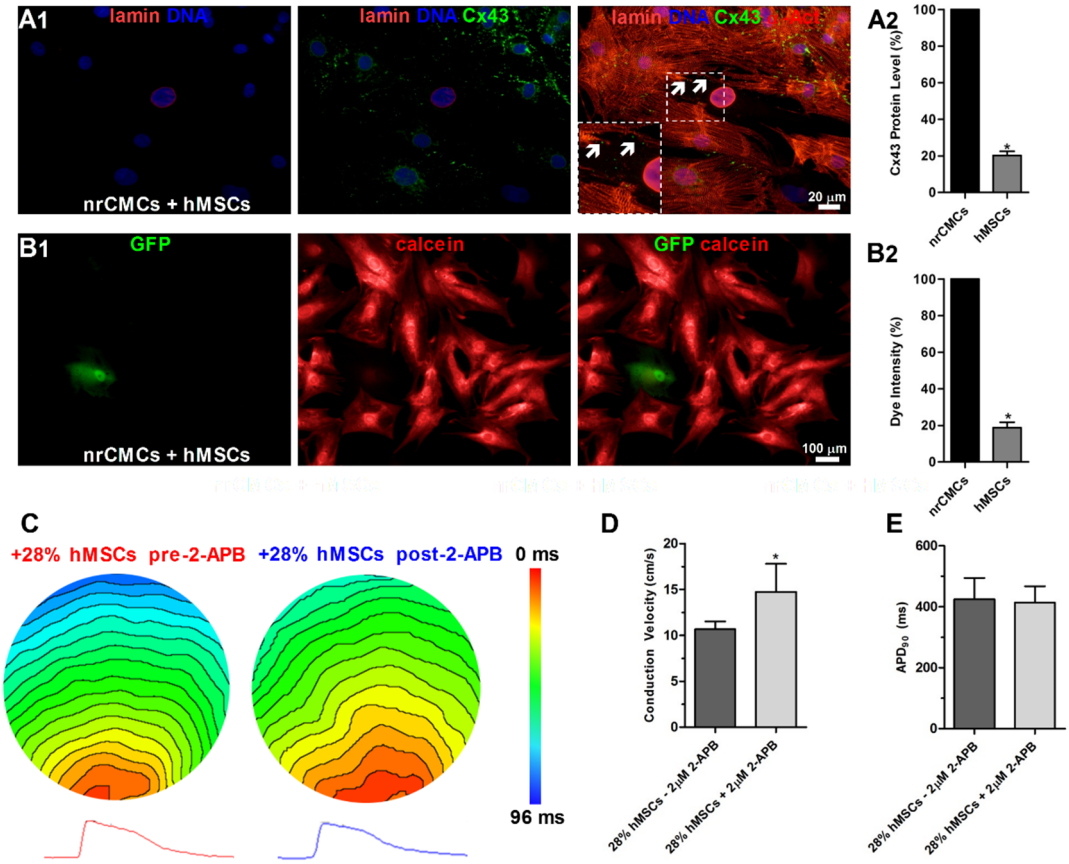

Figure 2. *Diffusively spread hMSCs slow conduction through electrotonic coupling. (A1) Immunocytological analyses reveals lower Cx43 (green) levels at heterocellular interfaces between human lamin A/C-positive hMSCs (red) and α-actinin-positive nrCMCs (red/orange) than at homocellular junctions between nrCMCs. (A2) Quantification of junctional Cx43 levels at hMSC-nrCMC and at nrCMC-nrCMC interfaces. *P<0.001 vs. nrCMCs. (B1) Dye transfer from nrCMCs to GFP-positive hMSCs. (B2) Quantification of dye intensity in GFP-positive hMSCs. *P<0.001 vs. nrCMCs. (C) Activation maps before and after 2-APB administration to a myocardial cell culture containing 28% diffusely spread hMSCs. (D) 2-APB treatment increases CV in myocardial cell cultures with hMSCs. *P<0.05 vs. pre-2-APB. (E) Partial uncoupling by 2-APB does not affect repolarization in myocardial cell cultures containing evenly spread hMSCs.*

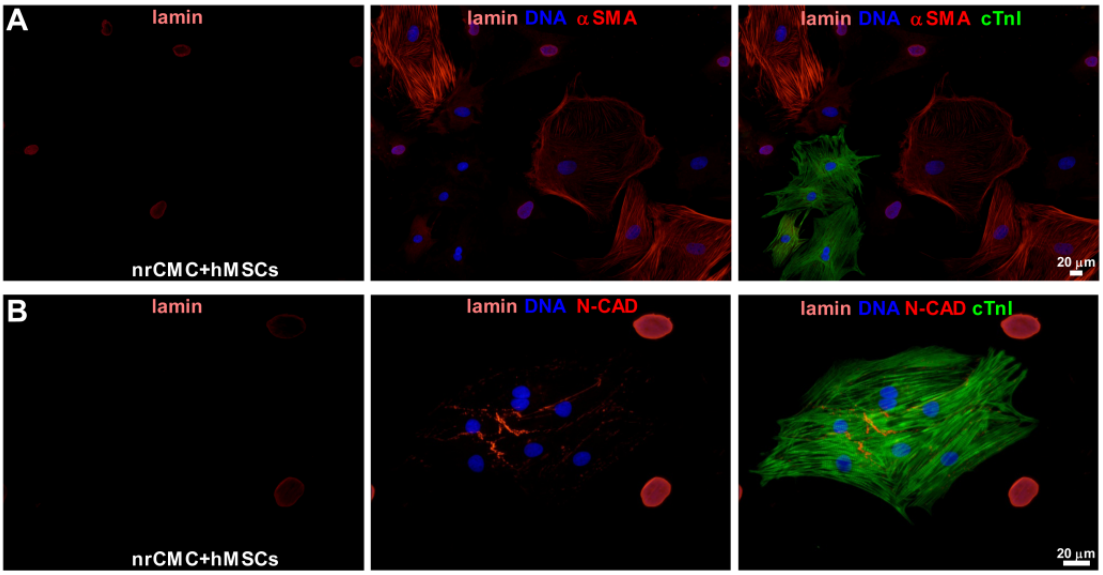

Supplemental figure 2. *Analysis of markers involved in mechanical coupling. (A) Immunocytological staining showed no expression of alpha smooth muscle actin (αSMA; orange/red) by adult BM hMSCs in co-culture with nrCMCs. (B) Also, no N-cadherin (indicated as N-CAD; orange/red), was detected at contact areas between hMSCs and nrCMCs. hMSCs were detected using an antibody directed against human-specific lamin A/C (red), while nrCMCs were identified using an antibody directed against cardiac troponin I (cTnI; green). Nuclei were stained with the DNA-binding fluorochrome Hoechst 33342.*

The lower Cx43 levels at hMSC-nrCMC borders than at nrCMC-nrCMC interfaces were utilized to investigate the effect of heterocellular uncoupling by a low dose of the gap-junctional uncoupler 2-aminoethoxydiphenylborate (2-APB) on conduction in hMSC-nrCMC co-cultures. After administration of 2 µmol/L 2-APB, CV in 19 co-cultures of nrCMCs and 28% hMSCs rose to 133±16% of the values measured before 2-APB addition (Figure 2C-D), whereas vehicle-treated (0.01% DMSO, n=5) cultures showed no significant change (*i.e.* CV post 0.01% DMSO was 104±8% of CV before 0.01% DMSO). 2-APB increased action potential upstroke velocity from 10±3 to 29±7 V/s (n=4, $P<0.05$). Furthermore, negativity of MDP of nrCMCs increased by 33% to -59±4 mV ($P<0.05$ vs. without 2-APB) while action potential duration until 90% repolarization (APD_{90}) remained unaltered by the 2-APB treatment of the co-cultures (Figure 2E). Importantly, treatment with 2 µmol/L 2-APB did not significantly affect any of these parameters in myocardial cell cultures lacking hMSCs (data not shown).

Diffusely spread hMSCs decrease repolarization reserve and increase arrhythmicity in myocardial cell cultures

APD_{90} was 314±61 and 379±60 ms in myocardial cell cultures containing 7% (n=24) and 28% hMSCs (n=86), respectively, compared to 221±43 ms in control cultures (n=16) (Figure 3A-B). This corresponds to an hMSC dose-dependent prolongation of repolarization time of 142% and 171%, respectively (P<0.05 between all groups). These findings were confirmed with patch-clamp experiments (APD_{60} of 186±10 ms for nrCMCs in control cultures and of 300±21 ms in cultures with 28% added hMSCs [n=5, P<0.05]). Optical mapping showed that addition of hMSCs to myocardial cell cultures caused an increase in spatial heterogeneity of repolarization (Figure 3C). In control cultures, the maximal spatial difference between APD_{90} values within the same culture was 65±21 ms (n=18). In cultures with 7% or 28% added hMSCs, APD_{90} dispersion was 103±29 (n=13) and 181±59 ms (n=17), respectively (P<0.05, Figure 3D).

Pro-arrhythmic consequences of these findings were revealed by 1 Hz stimulation, which evoked triggered activity in 14% of cultures with 28% added hMSCs (n=66, Figure 3E). Cultures containing 7% hMSCs showed a lower incidence of triggered activity (2.6%, n=39) and triggered activity was absent in control cultures (n=39, Figure 3F). Next, inducibility of reentrant arrhythmias was investigated by applying a burst stimulation protocol (Figure 3G). Reentry was induced in 6% (n=16), 20% (n=10) and 53% (n=15) of cultures containing 0%, 7% and 28% hMSCs, respectively (Figure 3H).

After confirming reproducibility of triggered activity in the same culture, the ATP-sensitive K^+-channel opener P1075 was administered, which abolished all episodes of triggered activity (n=6, Figure 4A, B). As P1075 strongly shortened APD_{90} (Figure 4C) and reduced APD dispersion (Figure 4D) without affecting CV (Figure 4E), reduced repolarization reserve and steeper spatial APD gradients caused by hMSCs seem to be crucial for inducing triggered activity.

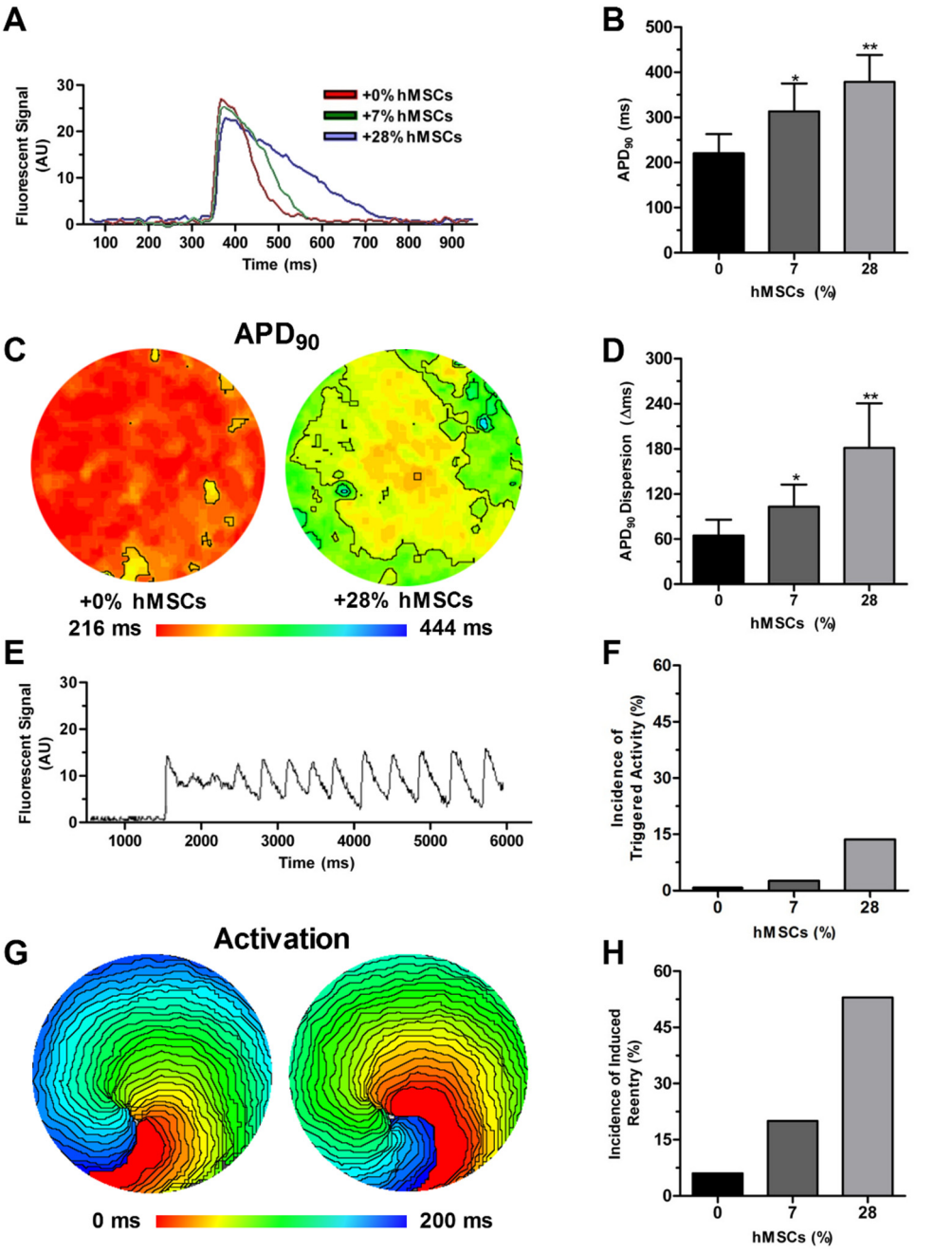

Figure 3. *Slowing and dispersion of repolarization in myocardial cell cultures containing diffusely spread hMSCs. (A) Optical traces of myocardial cell cultures containing 0%, 7% or 28% hMSCs show (B) prolongation of repolarization in an hMSC dose-dependent manner. *P<0.05 vs. 0 and 28% hMSCs,*

***P<0.05 vs. 0% and 7% hMSCs. (C) APD_{90} maps of myocardial cell cultures reveal (D) an hMSC dose-dependent increase in dispersion of repolarization throughout the entire culture. *P<0.05 vs. 0 and 28% hMSCs, **P<0.05 vs. 0% and 7% hMSCs. (E) Optical trace of triggered activity in a myocardial cell culture containing 28% hMSCs. (F) Incidence of triggered activity positively correlates with the number of hMSCs in myocardial cell cultures. (G) Activation map of 2 consecutive reentrant activations during a reentrant tachyarrhythmia in a myocardial cell culture containing 28% hMSCs. (H) Inducibility of reentry increases with the number of hMSCs in myocardial cell cultures.*

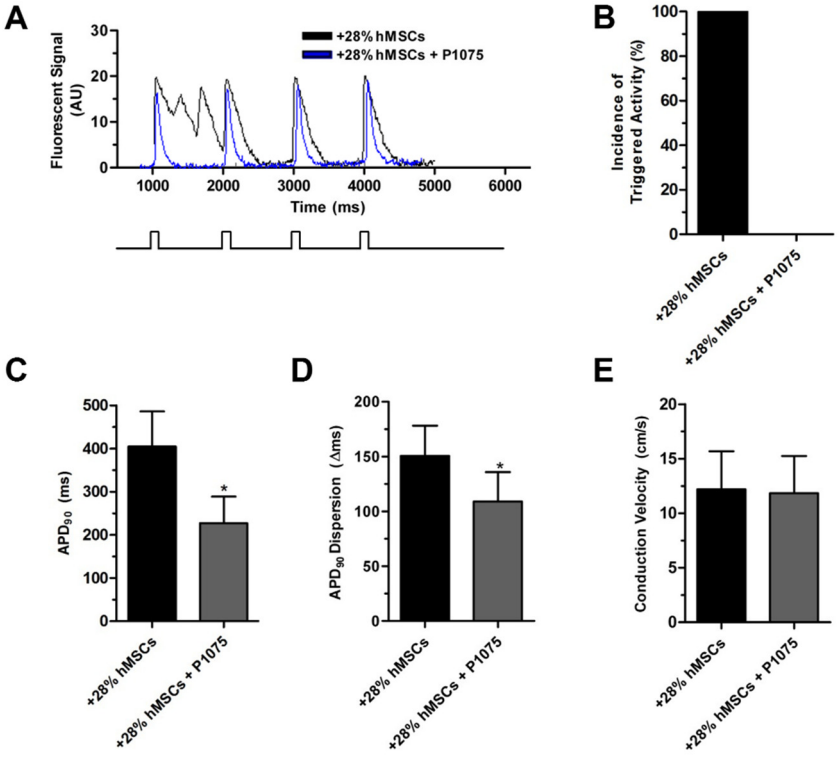

Figure 4. *Increasing repolarization reserve lowers the incidence of triggered activity in nrCMC cultures containing diffusely spread hMSCs. (A) Optical traces of a myocardial cell culture with 28% hMSCs before and after P1075 administration, and corresponding (B) incidences of triggered activity. (C) Quantification of APD_{90}, (D) APD_{90} dispersion and (E) CV before and after P1075 treatment in myocardial cell cultures with 28% hMSCs. *P<0.05 vs. 28% hMSCs.*

Clustered hMSCs provide a substrate for reentry in myocardial cell cultures.

Optical mapping of myocardial cell cultures containing a central cluster of hMSCs revealed local slowing of conduction to 4.7±1.6 and 5.4±1.3 cm/s in hMSC clusters with a diameter of 3 mm (n=21) and of 6 mm (n=20), respectively (*P*=NS), whereas CV outside these clusters remained as high as in control cultures (22.2±1.7 and 22.4±1.8 vs. 22.4±2.3 cm/s, *P*=NS, Figure 5A-C). APD_{90} was prolonged inside the 3-mm hMSC clusters (333±30 vs. 254±58 ms

outside, *P*<0.05) and inside the 6-mm hMSC clusters (343±48ms vs 310±40 ms outside, *P*<0.05, Figure 5D-G). Due to these local effects, APD_{90} dispersion was also increased in cultures with a 3- or 6 mm cluster of hMSCs (Figure 5D). Interestingly, APD_{90} in the ring of nrCMCs around 6-mm hMSC clusters was significantly prolonged (310±40 ms) compared to that in control cultures (245±61 ms) or in the ring of nrCMCs around 3-mm hMSC clusters (254±58 ms, *P*<0.05 vs. all, Figure 5F-G). No triggered activity was observed in any of these cultures. However, burst stimulation induced reentry in 6% of the control cultures (n=16) and in 14% (n=22) and 23% (n=30) of the cultures with 3- and 6-mm central clusters of hMSCs, respectively (Figure 5H-J). Induced reentrant arrhythmias anchored to the hMSC clusters.

hMSCs release free paracrine factors that prolong repolarization but do not affect conduction

To study a possible paracrine contribution[16] to hMSC-induced APD prolongation, transwell experiments were conducted. Transwells with inserts containing 0%, 7% or 28% hMSCs had almost identical CVs of 21.9±0.9, 22.3±1.3 and 22.9±0.7 cm/s (*P*=NS). Additionally, the conduction-slowing effect of TTX was very similar for transwell cultures containing different numbers of hMSCs (*P*>0.05, Figure 6A). However, APD_{90} was dose-dependently affected by hMSCs, as APD_{90} was 227±35 ms for controls (n=38) as compared to 300±91 and 362±88 ms for transwells with inserts containing 7% hMSCs (n=46) and 28% hMSCs (n=45), respectively (*P*<0.05, Figure 6B). Dispersion of repolarization showed a similar positive relation with hMSC numbers, with APD_{90} dispersion values of 78±23, 105±50 and 148±72 ms for transwells whose inserts contained 0%, 7% and 28% hMSCs (Figure 6C). None of the transwell cultures displayed triggered activity. However, inducibility of reentry was slightly increased from 14% (n=29) in controls to 16% (n=44) and 24% (n=38) for transwells with 7% and 28% of hMSCs, respectively (Figure 6D). Patch-clamp experiments also showed a prolonged APD in nrCMCs exposed to the secretome of 28% hMSCs (335±6 ms, n=4) compared to unexposed CMCs (193±7 ms, n=4, *P*<0.05, Figure 7A-B).

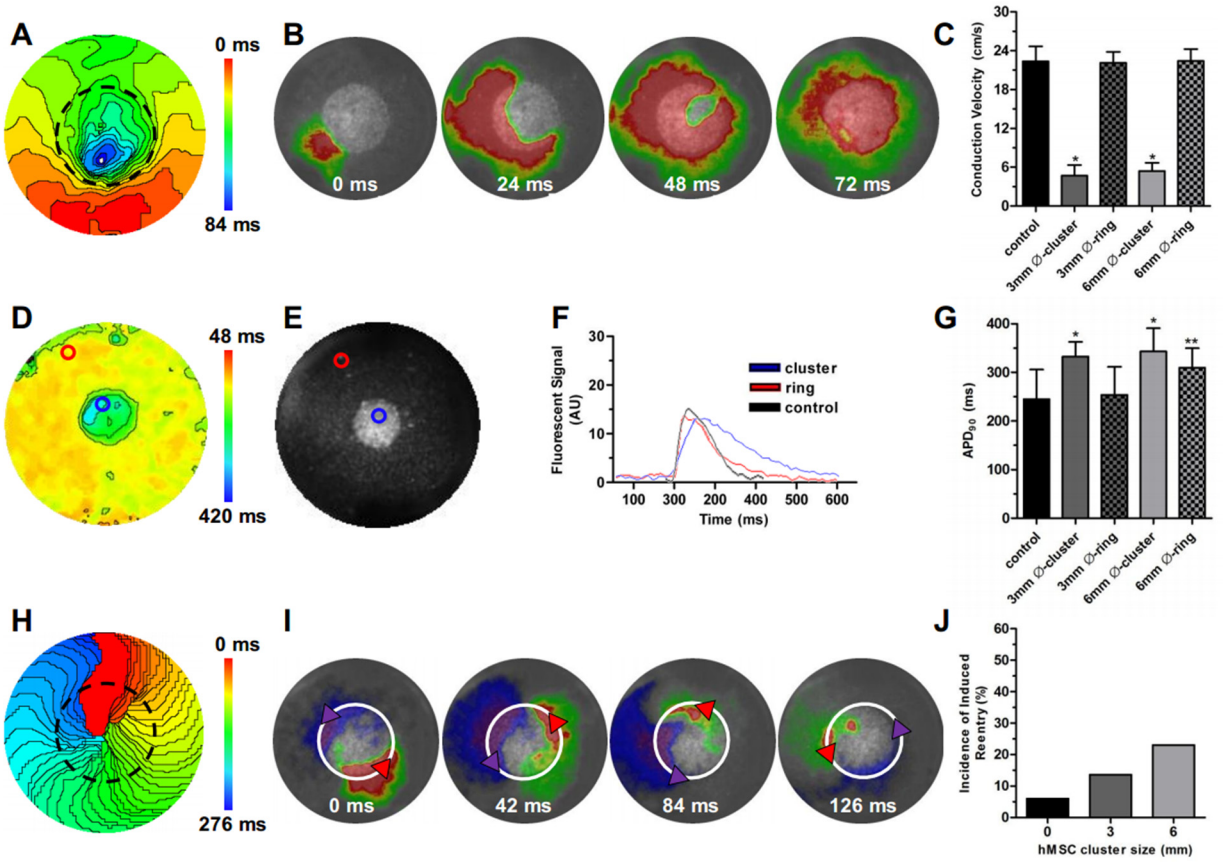

Figure 5. *Myocardial cell cultures containing clustered hMSCs are substrates for reentry. (A) Typical activation map of a myocardial cell culture containing 28% hMSCs in a centrally located cluster with a diameter of 6 mm (black dotted line). (B) Pseudo-voltage map sequence projected over a picture of the same culture containing a 6-mm hMSC cluster shows (C) local conduction slowing inside the cluster. *P<0.05 vs. outer ring. (D) APD_{90} map of a culture with a 3-mm cluster of hMSCs. (E) Micrograph of a myocardial cell culture with a 3-mm hMSC cluster and (F) traces of action potentials inside (blue) and outside (red) of the hMSC cluster. (G) APD_{90} in myocardial cell cultures containing different-sized hMSC clusters. *P<0.05 vs. outer ring, **P<0.05 vs. control and outer, 3-mm ring. (H) Activation map and (I) pseudo-voltage map sequence of a reentrant tachyarrhythmia anchored at a 6-mm hMSC cluster (demarcated by black dotted and white line, respectively). (J) The incidence of induced reentry in myocardial cell cultures increases with the size of the centrally located hMSC cluster.*

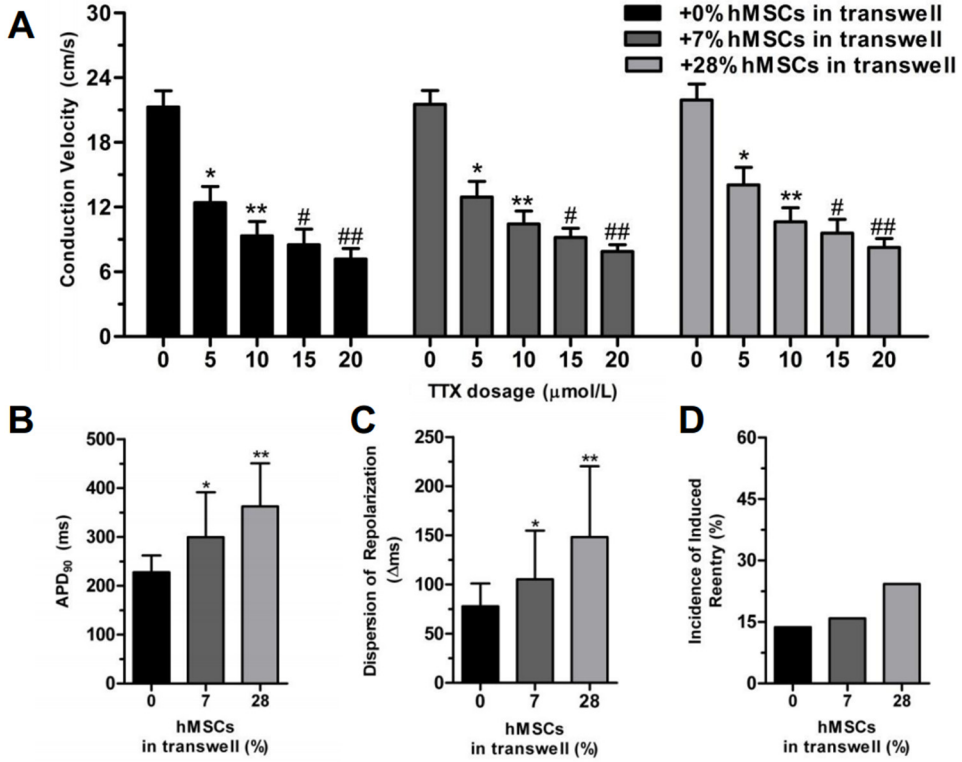

Figure 6. *Paracrine mechanisms are responsible for hMSC-dependent prolongation of repolarization in myocardial cell cultures. (A) Dose-dependent effects of Nav1.5 blockade by TTX do not differ between control cultures and myocardial cell cultures exposed to the secretomes of different numbers of hMSCs. *P<0.05 vs. 0 µmol/L TTX, **P<0.05 vs. 5 µmol/L TTX, #P<0.05 vs. 10 µmol/L TTX, ##P<0.05 vs. 15 µmol/L TTX. (B) Quantification of APD_{90}. *P<0.05 vs. 0% and 28% hMSCs, **P<0.05 vs. 0% and 7%. (C) Quantification of dispersion of repolarization. *P<0.05 vs. 0%. (D) Incidences of induced reentry in myocardial cell cultures exposed to transwells containing 0%, 7% or 28% of added hMSCs.*

However, dV/dt_{max} (104±7 V/s vs. 107±9 V/s in controls, *P*=0.72, Figure 7C) and resting membrane potential (-68±4 mV vs. -67±3 mV in controls, *P*=0.72) were unaffected by the hMSC secretome. Western blot analysis of ion channel protein levels in nrCMCs exposed to the hMSC secretome of 28% hMSCs revealed lower levels of Cav1.2 (0.43±0.01 vs. 0.22±0.04 arbitrary units, *P*<0.05) and Kv4.3 (0.26±0.04 vs. 0.22±0.04 arbitrary units, *P*<0.05), while the Kir2.1 level was not significantly altered (0.30±0.03 vs. 0.27±0.05, *P*>0.05, Figure 7D).

To investigate whether exosomes (*i.e.* microvesicles secreted by mammalian cells containing instructive molecules including cytokines, mRNAs and miRNAs) were responsible for these effects, exosomes from the hMSC secretome (representing 28% hMSCs) were

added to pure nrCMC cultures and refreshed every 2 days (Figure 8A). At day 9, optical mapping did not reveal any changes in APD_{90} (Figure 8B) or CV (Figure 8C) by adding hMSC-derived exosomes to nrCMC cultures, suggesting that the effect of the hMSC secretome on APD prolongation is primarily mediated by directly secreted factors, rather than by secreted microvesicle-associated factors.

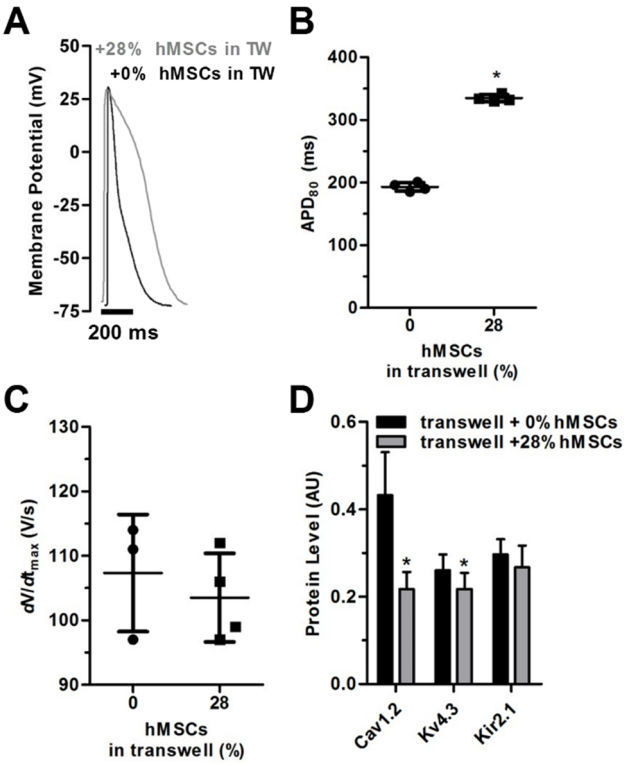

Figure 7. *The hMSC secretome also affects nrCMCs at the cellular level. (A) Typical voltage traces of action potentials recorded in current-clamp experiments on nrCMCs subjected to the hMSC secretome and on control nrCMCs show (B) prolonged APD but (C) normal dV/dt_{max}.*P<0.05 vs. 0% hMSCs in transwells. (D) Quantification of western blot analyses of Cav1.2, Kv4.3 and Kir2.1 levels. Values are corrected for glyceraldehyde 3-phosphate dehydrogenase (GAPDH) levels. *P<0.05 versus transwell + 0% hMSCs. TW: transwell.*

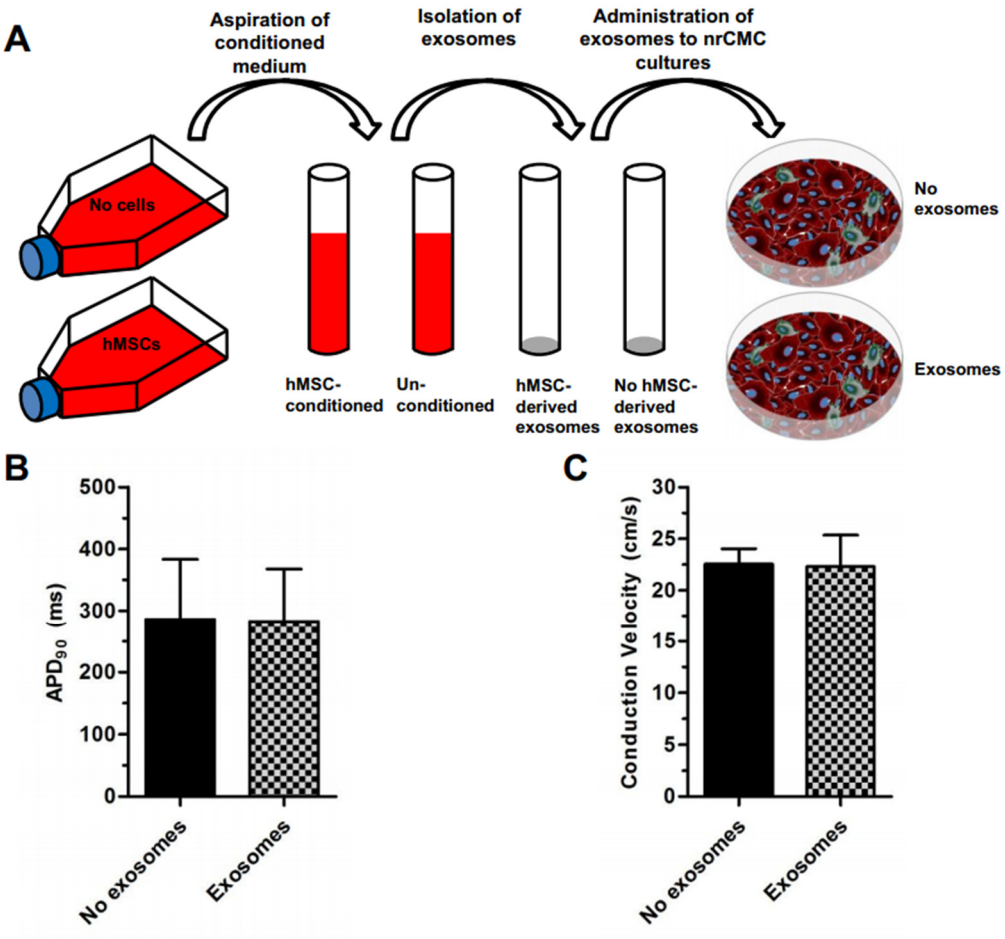

Figure 8. *Human MSC-derived exosomes do not appear to exert pro-arrhythmic effects on nrCMCs. (A) Schematic overview of experiments investigating the pro-arrhythmic effects of hMSC-derived exosomes. (B) Adding exosomes to nrCMC cultures does not affect CV or (C) APD_{90} under optical mapping conditions.*

Discussion

This study has shown that (i) adult bone marrow-derived hMSCs contribute to APD dispersion, triggered activity and reentrant tachyarrhythmias in neonatal rat myocardial cell cultures; (ii) the pro-arrhythmic effects of hMSCs are mediated by two separate mechanisms, *i.e.* functional coupling of hMSCs with adjacent nrCMCs resulting in partial nrCMC depolarization and conduction slowing, and paracrine signaling of hMSCs to neighboring nrCMCs that slows nrCMC repolarization; and (iii) the number and distribution pattern of the MSCs in the myocardial cell cultures determine the type and severity of the arrhythmias.

Effect of hMSC transplantation on cardiac electrophysiology

Whether and how cardiac cell therapy may increase the risk of ventricular arrhythmias remain topics of debate.[17-20] Gap-junctional coupling between transplanted cells and host cardiomyocytes appears to be essential for functional electrical integration, thereby preventing an increase in electrical heterogeneity, leading to arrhythmias.[21] Other studies have emphasized the role of cell alignment in electrical integration of transplanted cells in recipient myocardium and the potential pro-arrhythmic consequences of malalignment.[22] The number and distribution of donor cells in the host myocardium may also affect their arrhythmogenic potential.[11] However, very little is known about cell therapy-associated pro-arrhythmic mechanisms.

The current study demonstrates that both evenly spread and clustered hMSCs can exert pro-arrhythmic effects in myocardial cell cultures in a dose-dependent manner. However, the types of evoked arrhythmias depended on hMSC distribution pattern. By applying the hMSCs in a diffuse pattern, interactions with surrounding nrCMCs are maximized leading to increases in triggered activity and induced reentry incidence, while in myocardial cell cultures containing central clusters of hMSCs only the propensity towards reentry was increased. Triggered activity in diffuse co-cultures was associated with decreased repolarization reserve as APD shortening by opening of ATP-sensitive K^+-channels abolished such episodes, which together with pseudo-electrogram morphology, points to early afterdepolarizations as likely cause of triggered activity. As the P1075-treated cultures did not show any triggered activity, the concomitant APD shortening by P1075 did not lead to increased reentry incidence.[23]

The mechanism of early afterdepolarizations is considered to be reactivation of L-type calcium channels that linger within the window current due to a decreased repolarizing force.[23] As this mechanism is based on a highly complex and delicate balance between depolarizing and repolarizing forces that depends on activation and (de-)inactivation mechanics of ion channels, the absence of triggered activity in myocardial cell cultures containing clustered hMSCs can be explained by hMSC density-dependent skewing of action

potential dynamics beyond the window current. The notion of density-dependent pro-arrhythmic effects of hMSCs is supported by findings of differences in CV and APD inside the 6-mm hMSC clusters in comparison to equal amounts of more diffusely integrated hMSCs. As hMSC clusters formed local zones of conduction delay and refractoriness, the cluster size-dependent increase in inducibility of reentry is most likely attributable to the increased possibility of spiral wave anchoring with increasing obstacle sizes.[24] Higher inducibility of reentry in cultures with diffusely spread hMSCs than in those containing clustered hMSCs indicates stronger pro-arrhythmic effects of widespread than of locally concentrated hMSC-nrCMC interactions.

Role of heterocellular coupling in conduction slowing by hMSCs

Conduction slowing is widely recognized as a pro-arrhythmic feature that increases the probability of wave front collision, partial conduction block and spiral wave formation.[23] In an earlier study, Chang *et al.* revealed that hMSCs slow conduction in myocardial cell cultures, presumably by electrotonic heterocellular interactions.[11] Two other studies showed the ability of hMSCs to overcome local conduction blocks by functional coupling to nrCMCs and passively and slowly conducting action potentials.[25,26] In the present study, we confirmed slowed conduction by hMSCs in myocardial cell cultures without anatomical conduction block. Importantly, hMSCs were shown to reduce nrCMC excitability as dV/dt_{max} and TTX sensitivity were decreased. Treatment of diffuse co-cultures with low doses of the gap-junctional uncoupler 2-ABP indicated that heterocellular coupling was the dominant mechanism responsible for the conduction-slowing effect of hMSCs. Although 2-APB, as most pharmacological agents, has other known effects, [27,28] these effects occur at higher dosages and cannot account for the increase in CV observed in Figure 2D. Partial heterocellular uncoupling increased CV in co-cultures and nrCMCs showed a more negative MDP and a higher action potential upstroke velocity, which are all indicative of partially restored excitability.[29] Heterocellular mechanical coupling was also investigated in the current study. Myofibroblasts were recently shown to exert pro-arrhythmic effects by providing a non-compliant mechanical resistance through their rigid cytoskeleton, which contains large amounts of αSMA and may thereby activate stretch-activated ion channels in nrCMCs.[30,31] However, the adult hMSCs used in this study did not express αSMA or N-cadherin in co-cultures with nrCMCs, which makes it unlikely that mechanical coupling plays a major role in hMSC-associated conduction slowing and arrhythmicity.

Role of paracrine signaling in repolarization slowing and dispersion by hMSCs

In cardiac arrhythmogenesis, prolonged repolarization times and dispersion of repolarization are considered crucial pro-arrhythmic factors for triggered activity and reentrant tachyarrhythmias.[23] Interestingly, while experiments with commercially obtained hMSCs reported no effect of these cells on repolarization or the incidence of triggered

activity,[11] the present study provides evidence that clinically used hMSCs from ischemic heart disease patients in co-culture with nrCMCs can prolong repolarization time, increase repolarization dispersion and promote triggered activity, which is likely to be caused by spatial repolarization gradient steepening.[23] The mechanism of decreased repolarization reserve was elusive at first. In contrast to the effects of heterocellular uncoupling between nrCMCs and myofibroblasts,[32] decreasing heterocellular coupling between hMSCs and nrCMCs did not affect APD. However, it is becoming increasingly evident that the hMSC is a cell type with high paracrine activity that secretes a wide variety of directly secreted and exosome/microvesicle-associated factors associated with reverse remodeling and anti-inflammatory and pro-angiogenic activity.[33-35] These findings combined with the APD prolongation at the periphery of co-cultures containing clustered hMSCs, where there is no physical contact between hMSCs and nrCMCs raised the possibility that paracrine rather than electrotonic mechanisms are responsible for the decreased repolarization reserve. Indeed, experiments with hMSCs in transwell inserts to allow passage of the hMSC secretome without physical contact between hMSCs and nrCMCs, revealed hMSC dose-dependent increases in APD, dispersion of repolarization and inducibility of reentry in the nrCMCs seeded on the bottom of the transwell. As hMSC-derived exosomes did not significantly affect nrCMC APD, it is likely that APD prolongation in our model was based on directly secreted paracrine factors. Loss of biological activity of exosomes is unlikely, since they were purified using established procedures.[14,15] The current study has not provided any indication of pro-arrhythmic effects of exosomes purified from hMSC cultures. As exosomes may have a significant contribution to the therapeutic effects caused by the paracrine activity of MSCs, they might therefore represent a safer alternative to cell therapy for improving heart function.[16,36]

Paracrine activity of hMSCs has been associated with beneficial effects in *in vivo* models of cardiac remodeling.[33] A common feature of these models was the low engraftment rate of the hMSCs. As suggested in this study, higher hMSC engraftment rates might lead to increased production of paracrine factors tipping the balance from beneficial to adverse effects. Interestingly, paracrine signaling did not alter conduction or excitability, as the sensitivity of CV to Nav1.5 blockade by TTX remained the same between myocardial cell cultures exposed to the secretome of 0%, 7% or 28% hMSCs. It did, however, change the ion channel levels as revealed by western blot analyses. In particular, Cav1.2 and Kv4.3 levels were significantly lowered by exposure to the hMSC secretome. While decreased Cav1.2 expression would theoretically shorten APD, lowered Kv4.3 expression prolongs APD by decreasing I_{to}.[37] Since APD prolongation was found both in optical mapping and patch-clamp experiments, the effect of lowered Kv4.3 expression appeared to be dominant in our cultures. The Kir2.1 level was not significantly altered in nrCMCs cultured below hMSC-containing transwell inserts, which is consistent with findings of intact excitability of nrCMCs exposed to the hMSC secretome. Although functional effects of

altered ion channel expression are likely, more research is needed to be certain, since paracrine factors may also modulate the activity of proteins involved in cardiac impulse propagation by direct binding to these proteins or by inducing their post-translational modification. For example, a recent study by Desantiago showed that MSCs are able to increase I_{CaL} through the PI3K/Akt pathway.[38] Pinpointing the paracrine factors that are responsible for the pro-arrhythmic effects observed in our study and unraveling their mechanisms of action are subjects of future studies. The findings of the current study may raise cautionary concerns regarding the use of genetically-modified MSCs as biological pacemakers. [5] Such an approach relies on the premise that MSCs are electrically inert, other than their ability to couple to surrounding cells and achieve automaticity by electrotonic interactions. If MSCs modulate electrical behavior via secreted factors, using MSCs as pacemakers may have unintended APD prolonging effects and may increase the pro-arrhythmic risk.

Study Limitations

Due to ethical and technical limitations, cardiomyocytes of human adults could not be not investigated in this study. As an alternative, nrCMCs were used as these cells are available in large amounts and can be maintained in culture as contractile monolayers for the time period needed for mechanistic studies on stem cell engraftment. However, their ion channel expression profile and distribution of gap junctions differs from those of human adult CMCs. Therefore, the comparability of neonatal rat CMCs to adult and clinical situations may be limited. Nevertheless, 2-dimensional *in vitro* models of rat myocardial tissue have shown to be relevant for studying cardiac electrophysiology, by mimicking key electrophysiological processes in the intact heart.[39]

As the current model utilized healthy nrCMCs, the implications of current findings for disease models for stem cell therapy need to be investigated in future studies. To assess the consequences of this study for hMSC transplantation in the heart, our findings should be considered in the context of 3-dimensional, anisotropic myocardium.

Conclusion

In myocardial cell cultures, adult hMSCs slow conduction, prolong repolarization, increase spatial dispersion of repolarization and cause triggered activity and reentrant arrhythmias by different mechanisms. Electrotonic coupling of hMSCs to nrCMCs reduces excitability and thereby CV, while the paracrine factors that are directly secreted by hMSCs slows nrCMC repolarization. Thus, caution is warranted against potential pro-arrhythmic effects of MSC transplantation in cardiac tissue. The observation that the pro-arrhythmic activity of hMSCs in co-cultures with nrCMCs is strongly influenced by their number and distribution suggests that by controlling MSC engraftment rate and patterns the critical balance between

therapeutic potential and hazardous risk of MSC therapy for cardiac diseases may be tipped in the right direction.

Funding
The financial contribution of the Netherlands Organisation for Scientific Research (NWO, Veni grant 91611070, D.A.P.), Dutch Heart Foundation (NHS, 2008/B119) and SMARTCARE of the BioMedical Materials program (project-P1.04) is gratefully acknowledged.

Disclosure
None.

Acknowledgements
We thank H.J.F. van der Stadt, J.N. Schalij, A. van ’t Hof, R. van Leeuwen and the technicians of the stem cell laboratory for their excellent technical support.

Supplemental Material

Isolation, culture and characterization of human mesenchymal stem cells (hMSCs)
Human tissue samples were collected after having obtained written informed consent of the donors and with the approval of the medical ethics committee of Leiden University Medical Center (LUMC), where all investigations were performed. Investigations with human tissues conformed to the Declaration of Helsinki. Adult hMSCs were purified from leftover bone marrow (BM) samples derived from ischemic heart disease patients (n=4 donors). Briefly, the mononuclear cell fraction of the BM was isolated by Ficoll density gradient centrifugation, transferred to a 75-cm^2 cell culture flask (Becton Dickinson, Franklin Lakes, NJ) in standard hMSC culture medium (*i.e.* Dulbecco's modified Eagle's medium [DMEM; Invitrogen, Breda, the Netherlands] containing 10% fetal bovine serum [FBS; Invitrogen and incubated at 37ºC in humidified 95% air/5%CO_2. Twenty-four h after seeding, the non-adherent cells were removed and the remaining hMSCs were expanded by serial passage using standard methods.[40] The hMSCs were characterized according to generally accepted criteria using flow cytometry for the detection of surface antigens and adipogenic and osteogenic differentiation assays to establish multipotency. Surface marker expression was examined after culturing the cells for at least 3 passages. Thereafter, the hMSCs were detached using a buffered 0.05% trypsin-0.02% EDTA solution (TE; Lonza, Vervier, Belgium), suspended in phosphate-buffered saline (PBS) containing 1% bovine serum albumin fraction V (BSA; Sigma-Aldrich Chemie, Zwijndrecht, the Netherlands) and divided in aliquots of 10^5 cells. Cells were then incubated for 30 min at 4°C with fluorescein isothiocyanate- or phycoerythrin-conjugated monoclonal antibodies (MAbs) directed against human CD105 (Ancell, Bayport, MN), CD90, CD73, CD45, CD34 or CD31 (all from Becton Dickinson). Labeled cells were washed three times with PBS containing 1% BSA and analyzed using a BD LSR II flow cytometer (Becton Dickinson). Isotype-matched control MAbs (Becton Dickinson) were used to determine background fluorescence. At least 10^4 cells per sample were acquired and data were processed using FACSDiva software (Becton Dickinson). Established differentiation assays were used to determine the adipogenic and osteogenic differentiation ability of the cells. Briefly, 5×10^4 hMSCs per well were plated in a 12-well cell culture plate (Corning Life Sciences, Amsterdam, the Netherlands) and exposed to adipogenic or osteogenic differentiation medium. Adipogenic differentiation medium consisted of MEM-plus (*i.e.* α-minimum essential medium [Invitrogen] containing 10% FBS, supplemented with insulin, dexamethason, indomethacin and 3-isobutyl-1-methylxanthine (all from Sigma-Aldrich Chemie) to final concentrations of 5 µg/mL, 1 µmol/L, 50 µmol/L and 0.5 µmol/L, respectively, and was refreshed every 3-4 days for a period of 3 weeks. Lipid accumulation was assessed by Oil Red O (Sigma-Aldrich Chemie) staining of the cultures (15 mg of Oil Red O per mL of 60% 2-propanol). Osteogenic differentiation medium consisted of MEM-plus containing 10 mmol/L β-glycerophosphate, 50 µg/mL ascorbic acid and 10

nmol/L dexamethason (all from Sigma-Aldrich Chemie) and was refreshed every 3-4 days for a period of 3 weeks. Osteogenic differentiation was evaluated by histochemical detection of alkaline phosphatase activity and calcium deposition. To measure alkaline phosphatase activity, cells were washed with PBS and subsequently incubated for 5 min with substrate solution (0.2 mg/mL α-naphthyl-1-phosphate [Sigma-Aldrich Chemie] 0.1 mol/L Tris-HCl [pH 8.9], 0.1 mg/mL magnesium sulfate and 0.6 mg/mL Fast Blue RR [Sigma-Aldrich Chemie]). Thereafter, calcium deposits were visualized by staining of the cells for 5 min with 2% Alizarin Red S (Sigma-Aldrich Chemie) in 0.5% NH_4OH (pH 5.5).

Neonatal rat ventricular cardiomyocyte (nrCMC) isolation and culture

All animal experiments were approved by LUMC's animal experiments committee and conformed to the Guide for the Care and Use of Laboratory Animals, as stated by the US National Institutes of Health[12] (permit number: 10236). Isolation of nrCMCs from two-day-old neonatal Wistar rats was done essentially as described previously.[26] In brief, hearts were rapidly excised from isoflurane-anesthetized animals and minced into small pieces. After two sequential digestion steps with collagenase type I (450 units/mL; Worthington, Lakewood, NJ), a 75-min pre-plating step was performed to minimize the number of non-cardiomyocytes in the myocardial cell suspension. Next, the resulting cell suspension was passed through a nylon cell strainer with a mesh pore size of 70 µm (Becton Dickinson) to remove cell aggregates and, after counting, the cells were plated on fibronectin (Sigma-Aldrich Chemie)-coated round glass coverslips in 24-well cell culture plates (Corning Life Sciences, Amsterdam, the Netherlands) at a density of 1-4×10^5 cells/well depending on the experiment. To stop cell proliferation and to maintain the initial established ratios between cell types, cultures were incubated for 2 h with 10 µg/mL mitomycin-C (Sigma-Aldrich Chemie) at day 1 of culture. Culture medium was refreshed daily, except in experiments investigating paracrine effects. In these experiments, cells received fresh medium every 2 days to allow for sufficient exposure to paracrine factors. Cultures were refreshed with DMEM/Ham's F10 culture medium (1:1, v/v; both from Invitrogen) supplemented with 5% horse serum (HS; Invitrogen) and cultured in a humidified incubator at 37ºC and 5% CO_2.

Preparation of co-cultures between nrCMCs and clustered or diffusely spread hMSCs

To investigate in an *ex vivo* model system the effects of myocardial engraftment of hMSCs in different patterns and doses on arrhythmogeneity, co-cultures of nrCMCs and hMSCs were prepared. To mimic a diffuse engraftment pattern, 4.0×10^5 nrCMCs with mixed with 2.8×10^4 (7%) or 1.12×10^5 (28%) hMSCs and added onto a fibronectin-coated glass coverslip in a well of a 24-well cell culture plate. To mimic a clustered engraftment pattern, the hMSCs were applied to the center of a glass coverslip in a circle with a diameter of 3 mm (2.8×10^4 cells) or of 6 mm (1.12×10^5 cells). To keep the hMSCs centered, rings with an outer diameter

of 15 mm and an inner diameter of 3 or 6 mm were lasered in Parafilm M (Bemis Flexible Packaging, Neenah, WI, USA) using a PLS3.60 laser (Universal Lasersystems. Scottsdale, AZ). Next, these rings were sterilized with 70% ethanol and attached to fibronectin-coated coverslips. A drop of hMSC suspension was then applied to the center of each ring and the cells were allowed to adhere for at least 2 h. Finally, the rings of Parafilm M were removed and 4.0×10^5 nrCMCs were plated out on top of the hMSC cluster.

Electrophysiological measurements in co-cultures of nrCMCs and hMSCs

To facilitate the identification of hMSCs in co-cultures with nrCMCs, these cells were labeled with enhanced green fluorescent protein (GFP) using the vesicular stomatitis virus G protein-pseudotyped, self-inactivating human immunodeficiency virus type 1 vector CMVPRES,[41] essentially as described by van Tuyn *et al*.[42] At day 9 of culture, co-cultures of nrCMCs and GFP-labeled hMSCs in a diffuse or clustered pattern were subjected to whole-cell patch-clamp experiments in parallel to optical mapping experiments. Whole-cell current-clamp recordings were performed at 25ºC using an L/M-PC patch-clamp amplifier (List Medical, Darmstadt, Germany) with 3 kHz filtering. Pipette solution contained (in mmol/L) 10 Na_2ATP, 115 KCl, 1 $MgCl_2$, 5 EGTA, 10 HEPES/KOH (pH 7.4). Tip resistance was 2.0 – 2.5 MΩ, and seal resistance >1 GΩ. The bath solution contained (in mmol/L) 137 NaCl, 4 KCl, 1.8 $CaCl_2$, 1 $MgCl_2$, 10 HEPES/KOH (pH 7.4). For data acquisition and analysis pClamp/Clampex8 software (Axon Instruments, Molecular Devices, Sunnyvale, CA) was used. Current-clamp recordings were performed in unlabeled nrCMCs adjacent to GFP-labeled hMSCs. For partial uncoupling experiments, nrCMCs were studied after 20 min of incubation with 2-aminoethoxydiphenyl borate (2-APB; Tocris, Ballwin, MO).

Optical mapping

Electrophysiological parameters were determined by optical mapping as described previously.[13] In brief, nrCMC-hMSC co-cultures were loaded with 6 µmol/L of the voltage-sensitive dye di-4-ANEPPS (Invitrogen) diluted in DMEM/Ham's F12 culture medium (Invitrogen) for 10 min at 37ºC in humidified 95% air/5%CO_2. Subsequently, the culture medium was replaced by fresh DMEM/Ham's F12 and the cultures were optically mapped using the Micam Ultima-L optical mapping system (SciMedia USA, Costa Mesa, CA). Optical signals were recorded and analyzed using Brainvision Analyze 1108 (Brainvision, Tokyo, Japan). Cultures were electrically stimulated with a 10 ms pulse at ≥1.5× diastolic threshold and paced at 1 Hz (Multichannel systems, Reutlingen, Germany) to determine conduction velocity **(CV)** and action potential duration at 90% of full repolarization (APD_{90}), as well as dispersion of repolarization. Dispersion of repolarization was calculated as the maximal spatial difference in APD_{90} within the same culture. Areas of dispersion analysis were at least 4×4 pixels. Inducibility of reentry was tested by applying a bipolar, 14-Hz burst stimulation protocol. Reentry was defined as >2 consecutive circular activations. For partial

uncoupling experiments, cultures were mapped before and after 20 min of incubation with 2-APB. The principle of partial uncoupling was based on the low connexin 43 (Cx43) plaque density at heterocellular hMSC-nrCMC junctions as compared to that at homocellular nrCMC-nrCMC junctions. This renders the gap junctional communication between nrCMCs and hMSCs more sensitive to uncoupling by 2 µmol/L of 2-APB than that between nrCMCs and nrCMCs. Thus, treatment of the co-cultures with 2-APB could effectively uncouple hMSCs from nrCMCs while preserving nrCMC reserves of Cx43 necessary for conduction. Although 2-APB may have other known effects, these are not expected to be active at the used dosages[27,28] and are not expected to increase conduction velocity. To study the effects of fast sodium channel blockade, cultures were successively exposed to 5, 10, 15 and 20 µmol/L tetrodotoxin (TTX; Alomone Labs, Jerusalem, Israel) by stepwise increasing the drug concentration. The influence of APD on arrhythmicity was studied using the ATP-sensitive potassium channel opener P1075 (10 µmol/L; Tocris).

Analysis of markers involved in mechanical and electrical coupling

Alpha smooth muscle actin (αSMA) and N-cadherin, proteins involved in mechanical coupling, were visualized by immunostaining as described previously.[40] In short, on day 9 after culture initiation, the co-cultures of nrCMCs and adult BM hMSCs were fixed on ice with 4% formaldehyde in PBS for 30 min, washed with PBS, permeabilized with 0.1% Triton X-100 in PBS for 5 min at 4°C and rinsed again with PBS. To decrease non-specific antibody binding, the cells were next incubated at room temperature with 0.1% donkey serum (Sigma-Aldrich Chemie) in PBS for 30 min. Thereafter, the co-cultures were incubated overnight at 4°C with an αSMA-specific mouse MAb (clone 1A4; A2547; Sigma-Aldrich Chemie) or with an N-cadherin-specific mouse MAb (clone ID-7.2.3; C3825; Sigma-Aldrich Chemie) diluted 1:400 and 1:100, respectively, in PBS containing 0.1% donkey serum. To distinguish nrCMCs from hMSCs, co-cultures were stained with a rabbit polyclonal antibody (PAb) recognizing the striated muscle-specific protein troponin I (H-170; Santa Cruz Biotechnology, Santa Cruz, CA; dilution 1:100). Binding of the primary antibodies to their target antigen was visualized using Alexa Fluor 568-conjugated donkey anti-mouse IgG and Alexa Fluor 488-conjugated donkey anti-rabbit IgG (both from Invitrogen) at dilutions of 1:200. hMSCs in the co-cultures were identified by labeling with a human lamin A/C-specific murine MAb (clone 636; Vector Laboratories, Burlingame, CA; dilution 1:200). Lamin A/C staining was visualized with Qdot 655-streptavidin conjugates (Invitrogen; dilution 1:200) after incubation of the cells with biotinylated goat anti-mouse IgG2b secondary antibodies (Santa Cruz Biotechnology; dilution 1:200). Nuclei were stained by incubating the cells for 10 min at room temperature with 10 µg/mL Hoechst 33342 (Invitrogen) in PBS.

The expression of the gap junctional protein Cx43, which plays an important role in the electrical coupling of nrCMCs, was also studied by immunocytological stainings. Co-cultures

of nrCMCs and hMSCs were stained with a Cx43-specific rabbit PAb (C6219; Sigma-Aldrich Chemie) and with a mouse MAb recognizing sarcomeric α-actinin (clone EA53; Sigma-Aldrich Chemie; dilution 1:200). The primary antibodies were visualized using Alexa Fluor 568-coupled donkey anti-mouse IgG and Alexa Fluor 488-linked donkey anti-rabbit IgG secondary antibodies at dilutions of 1:200 (both Invitrogen). Again, the hMSCs in the co-cultures were identified by labeling with a human lamin A/C-specific murine MAb as described above. Nuclei were stained using a 10 µg/mL solution of Hoechst 33342 in PBS. Cells that went through the entire staining procedure but were not exposed to primary antibodies served as negative controls. A fluorescence microscope equipped with a digital color camera (Nikon Eclipse 80i; Nikon Instruments Europe, Amstelveen, the Netherlands) and dedicated software (NIS Elements [Nikon Instruments Europe] together with ImageJ [version 1.43; National Institutes of Health, Bethesda, MD]) were used for data analysis. ImageJ was used to determine the intensity of the Cx43-associated fluorescence in several randomly chosen, equally-sized border regions between hMSCs and nrCMCs and between adjoining nrCMCs. Fluorescent images of cells stained with the same antibody were always recorded with the same exposure time.

Analysis of functional coupling

Dye transfer assays were used to directly determine functional heterocellular coupling between nrCMCs and GFP-positive hMSCs. Four days after cell isolation, nrCMC cultures with a density of 2×10^5 cells per well in a 12-well cell culture plate (Corning Life Sciences) were loaded with dye by incubation for 15 min with 4 µmol/L calcein red-orange AM (calcein; Invitrogen) in Hank's balanced salt solution (Invitrogen). Thereafter, the cells were rinsed three times with PBS and were kept in the incubator in nrCMC culture medium supplemented with 2.5 mmol/L Probenecid (Invitrogen) for ≥30 min before 2×10^4 GFP-positive hMSCs (n=3 cultures for each of the 4 hMSC isolates) were added. Probenecid blocks organic anion transporters located in the plasma membrane thus preventing calcein efflux from the dye-loaded nrCMCs. Fluorescent images (≥30 per group) were captured after 8 h and evaluated in a blinded manner. In all experimental groups, GFP-positive hMSCs surrounded by the same number of nrCMCs were analyzed. ImageJ was used to determine the intensity of the calcein-associated fluorescence in several randomly chosen, equally-sized subcellular regions for both the GFP-positive hMSCs and the adjoining nrCMCs. To correct for possible variations in calcein loading efficiency, the dye intensity in the GFP-positive hMSCs was expressed as a percentage of that in the surrounding nrCMCs. The percentage of calcein-positive cells among the GFP-labeled hMSCs was also determined by counting these cells in ≥60 fields of view per experimental group.

Analysis of the influence of paracrine factors on nrCMC cultures

To investigate the influence of hMSC paracrine factors on the electrophysiological properties of nrCMC cultures, transwell experiments were conducted. Mitomycin-C-treated adult hMSCs were seeded in 24-well plate transwell inserts (membrane diameter: 6.5 mm, surface area: 0.33 cm^2, membrane pore size: 0.4 µm; Corning Life Sciences). To allow direct comparison with the previously described co-culture experiments, the transwell inserts contained 2.8×10^4 or 1.12×10^5 hMSCs, which were placed above 4.0×10^5 mitomycin-C-treated nrCMCs seeded on fibronectin-coated coverslips. Control cultures consisted of nrCMC cultures with empty transwells, nrCMC cultures without transwells and nrCMC cultures with transwells containing 1.12×10^5 nrCMCs. All cultures included in these experiments were refreshed with standard nrCMC culture medium every 2 days. To confirm optical mapping results, patch-clamp experiments were also performed on nrCMCs exposed to the hMSC secretome using the transwell cell culture system and on nrCMCs of control cultures.

Western blot analyses

To investigate Cav1.2, Kir2.1 and Kv4.3 levels, western blot analyses were performed on whole-cell protein extracts obtained from nrCMC layers cultured under transwell inserts containing hMSCs or no cells. Proteins were extracted by homogenization using RIPA buffer (150 mM NaCl, 1% Nonidet P-40, 0.5% sodium deoxycholate, 0.1% SDS, 50 mM Tris-HCl [pH 8.0] supplemented with protease inhibitors [cOmplete, Mini Protease Inhibitor Cocktail Tablets from Roche Diagnostics Nederland, Almere, the Netherlands]). At least 5 samples comprised of ≥2 cultures per group were used. Total protein (10 µg/lane) was loaded onto NuPage 10% Bis-Tris gels (Invitrogen) and electrophoresis was performed for 2 h at 150 V, after which proteins were transferred to Hybond-P polyvinylidene difluoride membranes (GE healthcare, Diegem, Belgium) overnight using a wet blotting system. After blocking for 1 h at room temperature with 10 mmol/L Tris-HCl (pH7.6), 0.05% Tween-20 and 150 mmol/L NaCl (TBST) containing 5% BSA, the membranes were incubated for 1 h at room temperature with primary antibodies diluted in TBST-5% BSA. The primary antibodies were affinity-purified rabbit anti-mouse Cav1.2 (ACC-003; Alomone labs; dilution: 1/500), rabbit anti-human Kir2.1 (APC-026; Alomone labs; dilution: 1/1,000) and rabbit anti-rat Kv4.3 (P0358; Sigma-Aldrich Chemie; dilution: 1/1,000). For normalization purposes, a mouse MAb recognizing the housekeeping protein glyceraldehyde-3-phosphate dehydrogenase (GAPDH; clone 6C5; MAB374; Merck Millipore, Billerica, MA; dilution 1:50,000) was used. Following three 15-min washing steps with TBST, the membranes were incubated with appropriate horseradish peroxidase (HRP)-conjugated rabbit or mouse IgG-specific goat secondary antibodies (sc-3837 and sc-2005 from Santa Cruz Biotechnology, Santa Cruz, CA) diluted 15,000-fold in TBST-5% BSA. Following additional washing steps, blots were developed using SuperSignal West Femto Maximum Sensitivity Substrate (Thermo

Scientific, Rockford, IL). The chemiluminescence signals were captured using a ChemiDoc XRS imaging system (Bio-Rad Laboratories, Veenendaal, the Netherlands).

Exosome experiments

To investigate their pro-arrhythmic effects, exosomes from the hMSC secretome were isolated under sterile conditions using previously established procedures.[14,15] Human MSCs were seeded into porcine skin gelatin type A (Sigma-Aldrich Chemie)-coated cell culture flasks with a surface area of 75 cm^2 (1.8 million cells per flask). As control, equal-sized gelatin-coated flasks without cells were used. Every 2 days, culture medium was collected from the flasks and spun for 10 minutes at 303 × *g* to remove cellular debris. The supernatant was transferred to clean tubes and stored shortly at 4°C. Subsequently, supernatants were centrifuged for 30 min at 4°C and 10,000 × *g* in a precooled Optima L-70K ultracentrifuge (Beckman Coulter Nederland, Woerden, the Netherlands) for another debris removal step. Next, supernatants were filtered through Millex 0.45-µm pore size polyethersulfone syringe filters (Merck Millipore) and spun for 60 min at 4°C and 100,000 × *g* to pellet the exosomes. Exosomes were resuspended in ice-cold PBS by gentle agitation for 2 h at 4°C. Exosomes were stored at -80°C until later use.

To study the effects of the hMSC-derived exosomes on the electrical properties of nrCMCs, 4×10^5 of these cells were added to single wells of a 24-well cell culture plate onto a fibronectin-coated glass coverslip. The resulting nrCMC cultures were given fresh medium with or without exosomes every 2 days. Exosomes were added to the medium in a quantity calculated to approximate the amount of exosomes in the hMSC secretome during the transwell experiments (Amount of hMSCs per flask / amount of hMSCs in transwells (*i.e.* 1.12 $x10^5$ cells) = dilution of exosome stock needed per nrCMC culture). After 9 days of culture, nrCMC cultures were subjected to optical mapping for electrophysiological investigation by a blinded researcher.

References

1. Gerson SL. Mesenchymal stem cells: no longer second class marrow citizens. *Nat Med*. 1999;5:262-264.

2. Prockop DJ. Marrow stromal cells as stem cells for nonhematopoietic tissues. *Science*. 1997;276:71-74.

3. Grauss RW, Winter EM, van Tuyn J, Pijnappels DA, Steijn RV, Hogers B, van der Geest RJ, de Vries AA, Steendijk P, van der Laarse A, Gittenberger-de Groot AC, Schalij MJ, Atsma DE. Mesenchymal stem cells from ischemic heart disease

patients improve left ventricular function after acute myocardial infarction. *Am J Physiol Heart Circ Physiol*. 2007;293:H2438-H2447.

4. Pijnappels DA, Gregoire S, Wu SM. The integrative aspects of cardiac physiology and their implications for cell-based therapy. *Ann N Y Acad Sci*. 2010;1188:7-14.

5. Plotnikov AN, Shlapakova I, Szabolcs MJ, Danilo P, Jr., Lorell BH, Potapova IA, Lu Z, Rosen AB, Mathias RT, Brink PR, Robinson RB, Cohen IS, Rosen MR. Xenografted adult human mesenchymal stem cells provide a platform for sustained biological pacemaker function in canine heart. *Circulation*. 2007;116:706-713.

6. van Ramshorst J, Bax JJ, Beeres SL, Dibbets-Schneider P, Roes SD, Stokkel MP, de Roos A, Fibbe WE, Zwaginga JJ, Boersma E, Schalij MJ, Atsma DE. Intramyocardial bone marrow cell injection for chronic myocardial ischemia: a randomized controlled trial. *JAMA*. 2009;301:1997-2004.

7. Segers VF and Lee RT. Stem-cell therapy for cardiac disease. *Nature*. 2008;451:937-942.

8. Cheng K, Li TS, Malliaras K, Davis DR, Zhang Y, Marban E. Magnetic targeting enhances engraftment and functional benefit of iron-labeled cardiosphere-derived cells in myocardial infarction. *Circ Res*. 2010;106:1570-1581.

9. Segers VF and Lee RT. Biomaterials to enhance stem cell function in the heart. *Circ Res*. 2011;109:910-922.

10. Fukushima S, Varela-Carver A, Coppen SR, Yamahara K, Felkin LE, Lee J, Barton PJ, Terracciano CM, Yacoub MH, Suzuki K. Direct intramyocardial but not intracoronary injection of bone marrow cells induces ventricular arrhythmias in a rat chronic ischemic heart failure model. *Circulation*. 2007;115:2254-2261.

11. Chang MG, Tung L, Sekar RB, Chang CY, Cysyk J, Dong P, Marban E, Abraham MR. Proarrhythmic potential of mesenchymal stem cell transplantation revealed in an in vitro coculture model. *Circulation*. 2006;113:1832-1841.

12. National Institutes of Health. Guide for the Care and Use of Laboratory Animals. 1-1-2002. Ref Type: Statute

13. Askar SF, Ramkisoensing AA, Schalij MJ, Bingen BO, Swildens J, van der Laarse A, Atsma DE, de Vries AA, Ypey DL, Pijnappels DA. Antiproliferative treatment of

myofibroblasts prevents arrhythmias in vitro by limiting myofibroblast-induced depolarization. *Cardiovasc Res*. 2011;90:295-304.

14. Lasser C, Eldh M, Lotvall J. Isolation and characterization of RNA-containing exosomes. *J Vis Exp*. 2012;e3037.

15. Thery C, Amigorena S, Raposo G, Clayton A. Isolation and characterization of exosomes from cell culture supernatants and biological fluids. *Curr Protoc Cell Biol*. 2006;Chapter 3:Unit.

16. Ranganath SH, Levy O, Inamdar MS, Karp JM. Harnessing the mesenchymal stem cell secretome for the treatment of cardiovascular disease. *Cell Stem Cell*. 2012;10:244-258.

17. Gepstein L. Electrophysiologic implications of myocardial stem cell therapies. *Heart Rhythm*. 2008;5:S48-S52.

18. Ly HQ and Nattel S. Stem cells are not proarrhythmic: letting the genie out of the bottle. *Circulation*. 2009;119:1824-1831.

19. Macia E and Boyden PA. Stem cell therapy is proarrhythmic. *Circulation*. 2009;119:1814-1823.

20. Smith RR, Barile L, Messina E, Marban E. Stem cells in the heart: what's the buzz all about? Part 2: Arrhythmic risks and clinical studies. *Heart Rhythm*. 2008;5:880-887.

21. Abraham MR, Henrikson CA, Tung L, Chang MG, Aon M, Xue T, Li RA, O' Rourke B, Marban E. Antiarrhythmic engineering of skeletal myoblasts for cardiac transplantation. *Circ Res*. 2005;97:159-167.

22. Pijnappels DA, Schalij MJ, Ramkisoensing AA, van Tuyn J, de Vries AA, van der Laarse A, Ypey DL, Atsma DE. Forced alignment of mesenchymal stem cells undergoing cardiomyogenic differentiation affects functional integration with cardiomyocyte cultures. *Circ Res*. 2008;103:167-176.

23. Kleber AG and Rudy Y. Basic mechanisms of cardiac impulse propagation and associated arrhythmias. *Physiol Rev*. 2004;84:431-488.

24. Lim ZY, Maskara B, Aguel F, Emokpae R, Jr., Tung L. Spiral wave attachment to millimeter-sized obstacles. *Circulation*. 2006;114:2113-2121.

25. Beeres SL, Atsma DE, van der Laarse A, Pijnappels DA, van Tuyn J, Fibbe WE, de Vries AA, Ypey DL, van der Wall EE, Schalij MJ. Human adult bone marrow mesenchymal stem cells repair experimental conduction block in rat cardiomyocyte cultures. *J Am Coll Cardiol*. 2005;46:1943-1952.

26. Pijnappels DA, Schalij MJ, van Tuyn J, Ypey DL, de Vries AA, van der Wall EE, van der Laarse A, Atsma DE. Progressive increase in conduction velocity across human mesenchymal stem cells is mediated by enhanced electrical coupling. *Cardiovasc Res*. 2006;72:282-291.

27. Maruyama T, Kanaji T, Nakade S, Kanno T, Mikoshiba K. 2APB, 2-aminoethoxydiphenyl borate, a membrane-penetrable modulator of Ins(1,4,5)P3-induced Ca2+ release. *J Biochem*. 1997;122:498-505.

28. Harks EG, Camina JP, Peters PH, Ypey DL, Scheenen WJ, van Zoelen EJ, Theuvenet AP. Besides affecting intracellular calcium signaling, 2-APB reversibly blocks gap junctional coupling in confluent monolayers, thereby allowing measurement of single-cell membrane currents in undissociated cells. *FASEB J*. 2003;17:941-943.

29. Kizana E, Chang CY, Cingolani E, Ramirez-Correa GA, Sekar RB, Abraham MR, Ginn SL, Tung L, Alexander IE, Marban E. Gene transfer of connexin43 mutants attenuates coupling in cardiomyocytes: novel basis for modulation of cardiac conduction by gene therapy. *Circ Res*. 2007;100:1597-1604.

30. Rosker C, Salvarani N, Schmutz S, Grand T, Rohr S. Abolishing myofibroblast arrhythmogeneicity by pharmacological ablation of alpha-smooth muscle actin containing stress fibers. *Circ Res*. 2011;109:1120-1131.

31. Thompson SA, Copeland CR, Reich DH, Tung L. Mechanical coupling between myofibroblasts and cardiomyocytes slows electric conduction in fibrotic cell monolayers. *Circulation*. 2011;123:2083-2093.

32. Askar SF, Bingen BO, Swildens J, Ypey DL, van der Laarse A, Atsma DE, Zeppenfeld K, Schalij MJ, de Vries AA, Pijnappels DA. Connexin43 silencing in myofibroblasts prevents arrhythmias in myocardial cultures: role of maximal diastolic potential. *Cardiovasc Res*. 2012;93:434-444.

33. Timmers L, Lim SK, Arslan F, Armstrong JS, Hoefer IE, Doevendans PA, Piek JJ, El Oakley RM, Choo A, Lee CN, Pasterkamp G, de Kleijn DP. Reduction of myocardial

infarct size by human mesenchymal stem cell conditioned medium. *Stem Cell Res*. 2007;1:129-137.

34. Williams AR and Hare JM. Mesenchymal stem cells: biology, pathophysiology, translational findings, and therapeutic implications for cardiac disease. *Circ Res*. 2011;109:923-940.

35. Lai RC, Chen TS, Lim SK. Mesenchymal stem cell exosome: a novel stem cell-based therapy for cardiovascular disease. *Regen Med*. 2011;6:481-492.

36. Lai RC, Arslan F, Lee MM, Sze NS, Choo A, Chen TS, Salto-Tellez M, Timmers L, Lee CN, El Oakley RM, Pasterkamp G, de Kleijn DP, Lim SK. Exosome secreted by MSC reduces myocardial ischemia/reperfusion injury. *Stem Cell Res*. 2010;4:214-222.

37. Hoppe UC, Marban E, Johns DC. Molecular dissection of cardiac repolarization by in vivo Kv4.3 gene transfer. *J Clin Invest*. 2000;105:1077-1084.

38. Desantiago J, Bare DJ, Semenov I, Minshall RD, Geenen DL, Wolska BM, Banach K. Excitation-contraction coupling in ventricular myocytes is enhanced by paracrine signaling from mesenchymal stem cells. *J Mol Cell Cardiol*. 2012;52:1249-1256.

39. Tung L and Zhang Y. Optical imaging of arrhythmias in tissue culture. *J Electrocardiol*. 2006;39:S2-S6.

Cellular and Molecular Mechanisms of Arrhythmias in Cardiac Fibrosis and Beyond:

From Symptoms to Substrates towards Solutions

Chapter VII

Forced Cellular Fusion of Human Ventricular Scar Cells with Neonatal Rat Cardiomyocytes Ameliorates Their Arrhythmicity

Saïd F. A. Askar, MSc; Brian O. Bingen, MD; Martin J. Schalij, MD, PhD; Zeinab Neshati, MSc; Michel I.M. Versteegh, MD; Robert J.M. Klautz, MD, PhD; Jerry Braun, MD, PhD; Antoine A. F. de Vries, PhD*; Daniël A. Pijnappels, PhD*.

*Equal contribution

Abstract

Aims: Fibroblasts can be pro-arrhythmic due to their detrimental effects on cardiomyocyte electrophysiology through several mechanisms that rely on suboptimal integration into the cardiac syncytium. To force full integration of fibroblasts into the cardiac syncytium, the feasibility of heterocellular fusion between fibroblasts and cardiomyocytes as a novel anti-arrhythmic strategy was investigated.

Methods & Results: Human ventricular scar cells (hVSC) were isolated from human ventricular post-myocardial infarction scars. Co-cultures of eGFP- or Vesicular-Stomatitis-G-protein- and eGFP-expressing hVSCs and neonatal rat cardiomyocytes (nrCMCs) were prepared in a 1:4 ratio. Fusion was induced by brief exposure to acidic buffer (pH6.0) at day 3 and electrophysiological effects of fusion were evaluated at day 5 by optical mapping. Simultaneous expression of fibroblast-specific collagen-I and nrCMC-specific α-actinin was observed in multinucleated cells that contained both human and rat nuclei, without increased apoptosis as judged by annexin V staining. These nrCMC-hVSC heterokaryons retained sarcomeric α-actinin expression and remained contractile, while vimentin expression in nrCMC-hVSC heterokaryons was lower than in non-fused hVSCs. Moreover, Cx43 and Cav1.2 protein levels were increased in heterokaryons compared to unfused hVSCs. Fused cultures showed faster conduction (16.8±1.6 vs. 10.3±2.6 cm/s, $P<0.05$) and shorter action potential duration (328±56 vs. 480±79ms, $P<0.05$). Triggered activity and reentry were ameliorated by heterocellular fusion (incidences of 63%, n=8 vs. 0%, n=23 in fused co-cultures).

Conclusion: Heterocellular fusion between hVSCs and nrCMCs is feasible and well-tolerated as it forms contractile heterokaryons. Importantly, heterocellular fusion had strong anti-arrhythmic effects. As the nrCMC phenotype appeared to be dominant within the heterokaryon, these results may provide novel insights in anti-arrhythmic reprogramming of fibroblasts.

Introduction

Despite the well-established pro-arrhythmic role of cardiac fibrosis, its mechanisms remain incompletely understood. Although the extracellular matrix-synthesizing fibroblasts have long been known to be key effectors of fibrosis, it has only relatively recently become apparent that fibroblasts themselves can contribute to arrhythmogeneity through several mechanisms.[1-3] These unexcitable cells are abundantly present after pro-fibrotic myocardial injury such as myocardial infarction. Such fibroblastic ventricular scar cells (VSCs) form clusters and intersperse between cardiomyocytes, which due to their inexcitability and poor gap-junctional coupling to cardiomyocytes, anatomically obstructs conduction and contributes to pro-arrhythmogeneity. Moreover, their membrane is more depolarized compared to cardiomyocytes, which leads to pro-arrhythmic effects by heterocellular gap-junctional coupling.[2] Therefore, targeting fibroblast integration may be too complex to be broadly applicable as an anti-arrhythmic strategy if fibroblast inexcitability is not overcome.[4] Moreover, pro-arrhythmic mechanisms of fibroblasts based on paracrine factors and mechanical coupling are unlikely to be affected by such an approach.[1,3] Therefore, alternative strategies of modifying electrical fibroblast integration need to be explored that may offer a radically different, but effective approach.

In regenerative medicine, cellular fusion has been studied mostly as an infrequently occurring spontaneous phenomenon between stem cells and cardiomyocytes in the context of cellular (de-)differentiation.[5,6] However, its effects have never been experimentally studied in the context of fibrosis-associated arrhythmias. Heterocellular fusion between fibroblasts and cardiomyocytes may not only promote full electrical integration of fibroblasts with cardiomyocytes, but also may limit all of their pro-arrhythmic mechanisms as cellular properties can be altered by cellular fusion.[7] Thereby, cellular fusion may provide a novel strategy to target the pro-arrhythmic effects of fibroblasts. In the current study, we therefore investigated the effects of cellular fusion between human ventricular scar cells (hVSCs) and neonatal rat cardiomyocytes to explore the concept of heterocellular fusion as a strategy to limit pro-arrhythmic effects exhibited by hVSCs *in vitro*.

Methods

All animal experiments were approved by the Animal Experiments Committee of the Leiden University Medical Center and conform to the Guide for the Care and Use of Laboratory Animals as stated by the US National Institutes of Health.

Cardiomyocyte isolation and culture

All animal experiments were approved by the Animal Experiments Committee of the Leiden University Medical Center (LUMC) and conform to the Guide for the Care and Use of Laboratory Animals, as stated by the US National Institutes of Health[7] (permit number 10236). Ventricular cardiomyocytes (nrCMCs) were isolated from neonatal Wistar rats and cultured as described previously.[8] In brief, hearts were rapidly excised from animals after confirmation of adequate anesthesia with 4-5% isoflurane and subsequently minced into small pieces. After two sequential digestion steps with collagenase I (450 units/mL; Worthington, Lakewood, NJ, USA), a pre-plating step was performed to minimize neonatal rat fibroblast contamination of the myocardial cell suspension. Myocardial cells were plated on fibronectin-coated cover slips in 24-wells plates (Corning Life Sciences, Amsterdam, the Netherlands) at a density of $5x10^5$ cells/well. To stop proliferation and maintain initially plated cell population ratios, cultures were treated with 10 µg/mL mitomycin-C (Sigma-Aldrich, St. Louis, MO, USA) at day 1 of culture for 2 h.

Human Ventricular Scar Fibroblast isolation

All human-derived tissues were collected in accordance to guidelines posed by the Medical Ethics committee of the LUMC and adhered to the principles described in the Declaration of Helsinki. Human Ventricular Scar Cells (hVSCs) were isolated from human myocardial scar tissue of 6 different post-myocardial infarction patients that was excised during the surgical Dor procedure. After dissection into small pieces, the tissue was placed in 0.1% gelatin coated six-wells plates (Corning) and covered by glass cover slips to prevent floating of the tissue. Culture plates were refreshed twice a week with culture medium consisting of Dulbecco's modified Eagle's medium (DMEM, Invitrogen, Breda, the Netherlands) supplemented with 10% fetal bovine serum (FBS, Invitrogen), 100 µg/mL penicillin and 100 µg/mL streptomycin (Bio-Whittaker, Carlsbad, CA, USA). Cells grew out for 2-4 weeks, and were trypsinized and passaged 3-6 times before use in experiments. During cell culture, hVSCs were refreshed twice a week.

Co-cultures of hVSCs and cardiomyocytes were prepared by counting and mixing the cell suspensions in ratios of 1:4 and plated out in a cell density of $2\text{-}5.0x10^5$ cells per well depending on the experiment.

Lentiviral Viral Vector production

Self-inactivating human immunodeficiency virus type I vectors were produced in 293T cells as described previously.[2] In brief, these cells were transfected with a lentiviral vector shuttle plasmid together with psPAX2 (Addgene, Cambridge, MA, USA) and pLP/VSVG (Invitrogen) using 25-kDa linear polyethyleneimine (Polysciences, Warrington, PA, USA) as transfection agent. After 16 hours, transfection medium was replaced by culture medium and after 64 hours, the culture fluid was collected by centrifugation and freed of cellular debris by filtration. Concentration of lentiviral vector particles was performed by ultracentrifugation through a 20% (w/V) sucrose cushion. Pellets containing vector particles were suspended in phosphate-buffered saline with 1% bovine serum albumin fraction V (Sigma-Aldrich).

Viral Transduction

One day prior to transduction, hVSCs were trypsinized and plated onto a 0.1% gelatin-coated six-well plate at a density of 4×10^5 cells per well. Cells from different patients were pooled for standardization and reproducibility. Cells were subsequently exposed overnight to an inoculum of 800 µL culture medium containing 10 µg/ml DEAE dextran and lentiviral particles of either LV.hCMV-IE.VSV-G.IRES.eGFP.hHBVPRE or LV.IRES.eGFP.hHBVPRE as control. Following transduction, cultures were rinsed three times with PBS and kept on culture medium until usage in experiments.

Induction and assessment of fusion

To induce fusion, a recently developed technique termed V-fusion was utilized.[10] This technique uses transgenic expression of the Vesicular Stomatitis Virus – G (VSV-G) protein which normally is involved in viral entry into mammalian cells. Fusogenic potency of this protein is increased by exposure to acidic solutions. Therefore, VSV-G expressing hVSCs in confluent co-culture with nrCMCs were exposed to CMC culture medium adjusted to pH 6.0 using 0.5 mol/L 2-(N-Morpholino)ethanesulfonic acid sodium salt (MES, Sigma-Aldrich) during 3-5 minutes at 37^{o}C at day 3 of culture. All cultures, including cultures containing control hVSCs that solely expressed eGFP and control cultures without hVSCs were identically treated with acidic buffer.

Fusion was assessed using immunocytological staining for co-expression of the normally mutually exclusive cytoplasmic expression of collagen-I (hVSC-specific) and α-actinin (nrCMC specific) as well as the presence of multiple nuclei, positive (of human origin) or negative (of rat origin) for human-specific Lamin A/C. Fused cells were defined as multinucleated cells as judged by cytoplasmic collagen-I expression with nuclear lacunae, whereas heterokaryons were defined as multinucleated cells that also contained at least 1 human nucleus and 1 rat nucleus.

Immunocytological characterization

Co-cultures were fixed in 4% formaldehyde, permeabilized with 0.1% Triton X-100 for 20 min, and stained with primary antibodies. Permabilization for >15 min resulted in loss of eGFP signal. Primary antibodies specific for human lamin A/C (Vector laboratories, Burlingame, CA, USA), cardiac α-actinin, (all Sigma-Aldrich Chemie, Zwijndrecht, the Netherlands) and collagen type I (Abcam, Cambridge, MA, USA) were used to distinguish between hVSCs and CMCs. Antibodies specific for Connexin43 (Cx43) or α-smooth muscle actin (αSMA) and N-cadherin were used to investigate expression of proteins involved in electrical or mechanical coupling, respectively. Primary antibodies were visualized with Alexa fluor-conjugated antibodies (Invitrogen), or with biotin-labeled secondary antibodies (Santa Cruz Biotechnology, Santa Cruz, CA, USA), and Qdot 655-streptavidin conjugates (Invitrogen). Nuclei were stained using Hoechst 33342 (Invitrogen). A fluorescence microscope equipped with a digital camera (Nikon Eclipse, Nikon Europe, Badhoevedorp, The Netherlands) and dedicated software (NIS Elements, Nikon and Image J, version 1.43; Institutes of Health, Bethesda, MD) were used to analyze the data. All cultures were treated equally using the same antibody dilutions and exposure times. Quantification of average pixel intensity from pictures of fluorescent staining was performed in areas of interest of a fixed size per cell that showed maximal fluorescent intensity to compare the uppers limit of expression potential of the cells in question. Quantification was performed on cells within fused co-cultures, as these cultures contained unfused hVSCs, unfused nrCMCs and heterokaryons and therefore facilitate the highest degree of comparability. In addition, quantifications in unfused co-cultures showed that the expression values of unfused hVSCs and unfused nrCMCs in these cultures was not significantly different from the expression levels found in the same cell types in fused co-cultures (data not shown).

Optical mapping

Investigation of electrophysiological parameters at the tissue level were performed with optical mapping as described previously.[11] In brief, cultures were loaded with 6 μmol/L of the voltage-sensitive dye di-4-ANEPPS (Invitrogen) diluted in DMEM/HAMS F12 (Invitrogen) for 10 min in a humidified incubator at 37°C. Cultures were refreshed with DMEM/HAMS F12 and optically mapped using the Micam Ultima-L optical mapping system (Scimedia, Costa Mesa, CA, USA). Optical signals were recorded and subsequently analyzed using Brainvision Analyze 1108 (Brainvision Inc, Tokyo, Japan). Cultures were electrically stimulated with a 10 ms pulse at ≥1.5x diastolic threshold and paced at 1-2Hz (Multichannel systems, Reutlingen, Germany) to determine conduction velocity (CV) and action potential duration (APD_{90}), as well as dispersion of repolarization. Arrhythmic episodes of reentrant tachyarrhythmias and early-afterdepolarizations were quantified during spontaneous activity or following 1Hz pacing. Dispersion of repolarization was

calculated as the maximal spatial difference in APD_{90} within the same culture during the same activation wave. The size of areas of dispersion was at least 4x4 pixels.

Statistical Analyses

Experimental results were expressed as mean±standard deviation (SD) for a given number (n) of observations. Data was analyzed by Student's t-test for direct comparisons. Analysis of variance followed by the appropriate *post-hoc* analysis was performed for multiple comparisons. Statistical analysis was performed using SPSS 16.0 for Windows (SPSS, Chicago, IL). Differences were considered statistically significant at $P<0.05$.

Results

hVSCs are highly pro-arrhythmic in co-culture with nrCMCs

CMCs and hVSCs were characterized with immunocytological staining. Human VSCs were all positive for collagen-I (n=506 cells) and vimentin (n=713 cells), but were negative for α-actinin. Cardiomyocytes were defined as α-actinin positive, and were negative for collagen-I (n=645 cells). Purified neonatal rat ventricular monolayers consisted of 12.6±3.9% neonatal rat fibroblasts and 87.4±3.9% CMCs as determined by collagen I/α-actinin staining as described previously.[12] Fibrotic co-cultures of nrCMCs and hVSCs contained 24.4±5.8% hVSCs as determined by human-specific Lamin A/C staining. At day 5 of culture, optical mapping revealed that CV was severely decreased by the presence of hVSCs (11.1±2.7 cm/s vs. 23.4±0.6 cm/s in control ($P<0.05$, Figure 1 A-C). In addition, pseudo-voltage traces showed a distinctly different action potential morphology (Figure 1D), signified by an increase in APD_{80} (349±52 ms vs. 259±25 ms in controls, $P<0.05$, Figure 1E). In addition, spatial dispersion of APD_{90} was increased by hVSCs (103±33 ms vs. 38±19 ms, $P<0.05$, Figure 1F).

Importantly, hVSCs were found to be highly pro-arrhythmic. Arrhythmic episodes, defined as early afterdepolarizations and reentrant arrhythmias could be observed frequently in the hVSC group (22 out of 25 cultures) but were rarely observed in the control group (1 out of 25 cultures, Figure 1G).

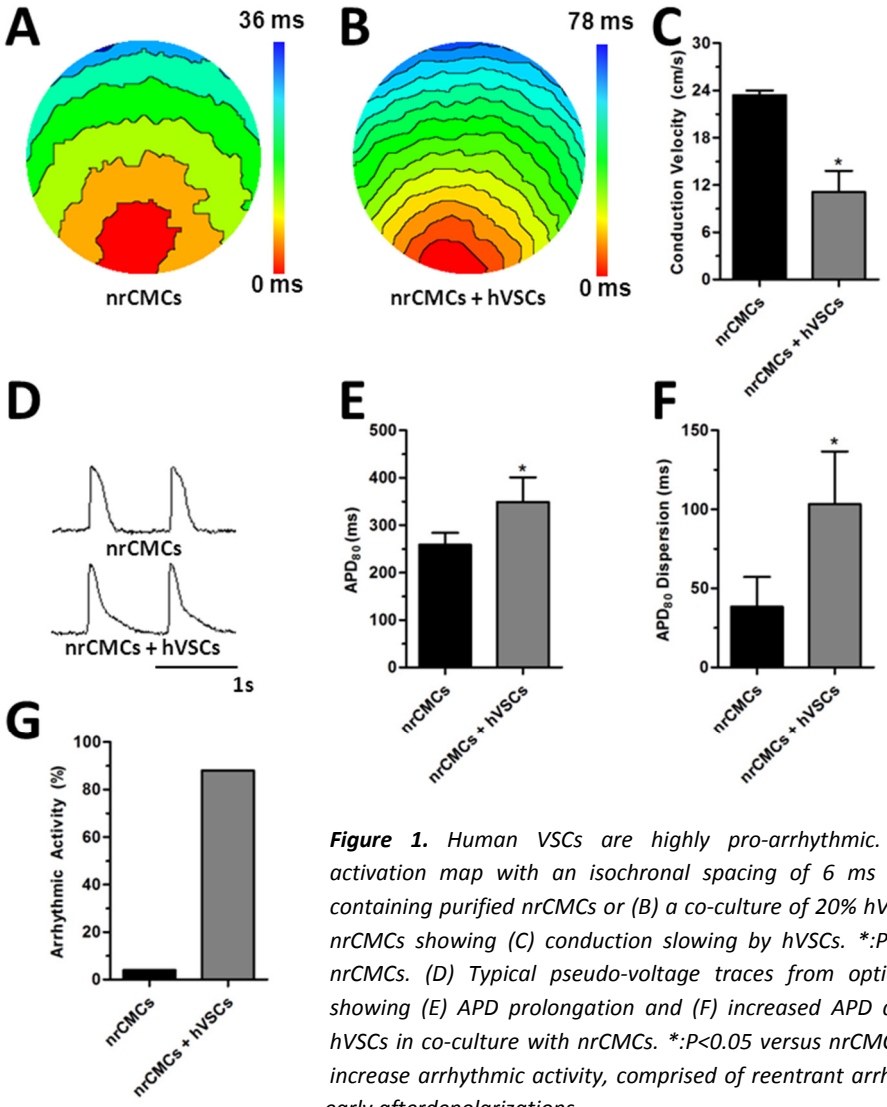

Figure 1. *Human VSCs are highly pro-arrhythmic. (A) Typical activation map with an isochronal spacing of 6 ms of a culture containing purified nrCMCs or (B) a co-culture of 20% hVSCs and 80% nrCMCs showing (C) conduction slowing by hVSCs. *:P<0.05 versus nrCMCs. (D) Typical pseudo-voltage traces from optical mapping showing (E) APD prolongation and (F) increased APD dispersion by hVSCs in co-culture with nrCMCs. *:P<0.05 versus nrCMCs. (G) hVSCs increase arrhythmic activity, comprised of reentrant arrhythmias and early afterdepolarizations.*

The V-fusion protocol leads to well-tolerated heterocellular fusion between hVSCs and nrCMCs

To induce cellular fusion without affecting intracellular membranes, a technique named V-fusion was utilized that was mediated by lentiviral VSV-G overexpression and subsequent fusion induction by brief exposure to acidic (pH=6.0) buffer. Overexpression of VSV-G was confirmed by immunocytological staining, and absence of VSV-G was confirmed in control hVSCs expressing eGFP (Figure 2A). Exposure to acidic buffer induced cellular fusion in VSV-G expressing hVSCs (Figure 2B).

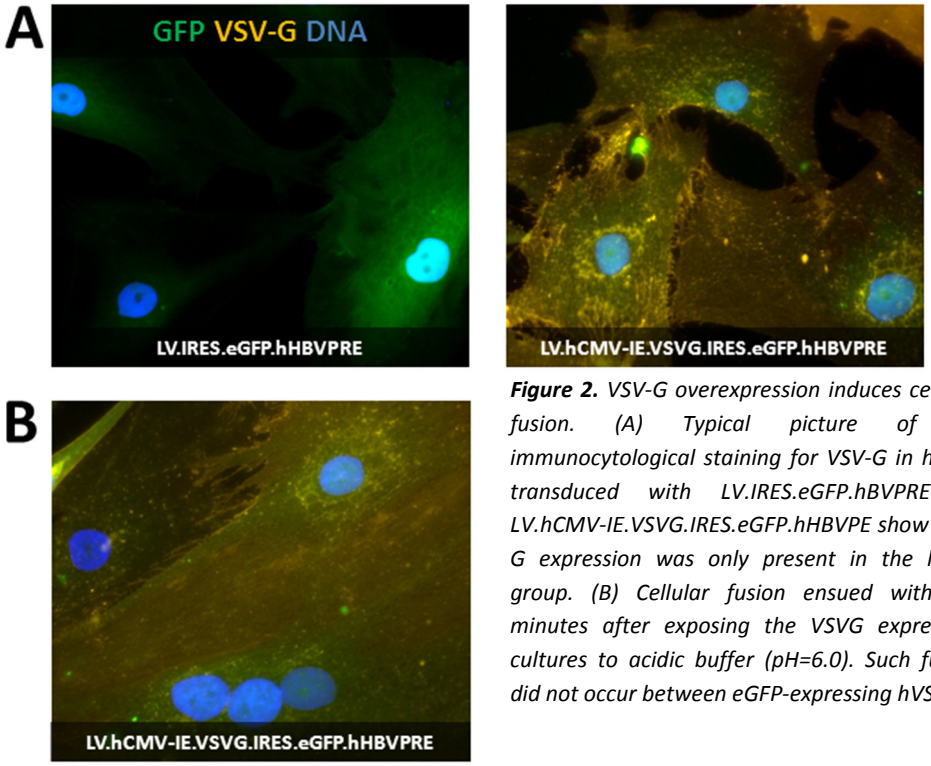

Figure 2. *VSV-G overexpression induces cellular fusion. (A) Typical picture of an immunocytological staining for VSV-G in hVSCs transduced with LV.IRES.eGFP.hBVPRE or LV.hCMV-IE.VSVG.IRES.eGFP.hHBVPE show VSV-G expression was only present in the latter group. (B) Cellular fusion ensued within 5 minutes after exposing the VSVG expressing cultures to acidic buffer (pH=6.0). Such fusion did not occur between eGFP-expressing hVSCs.*

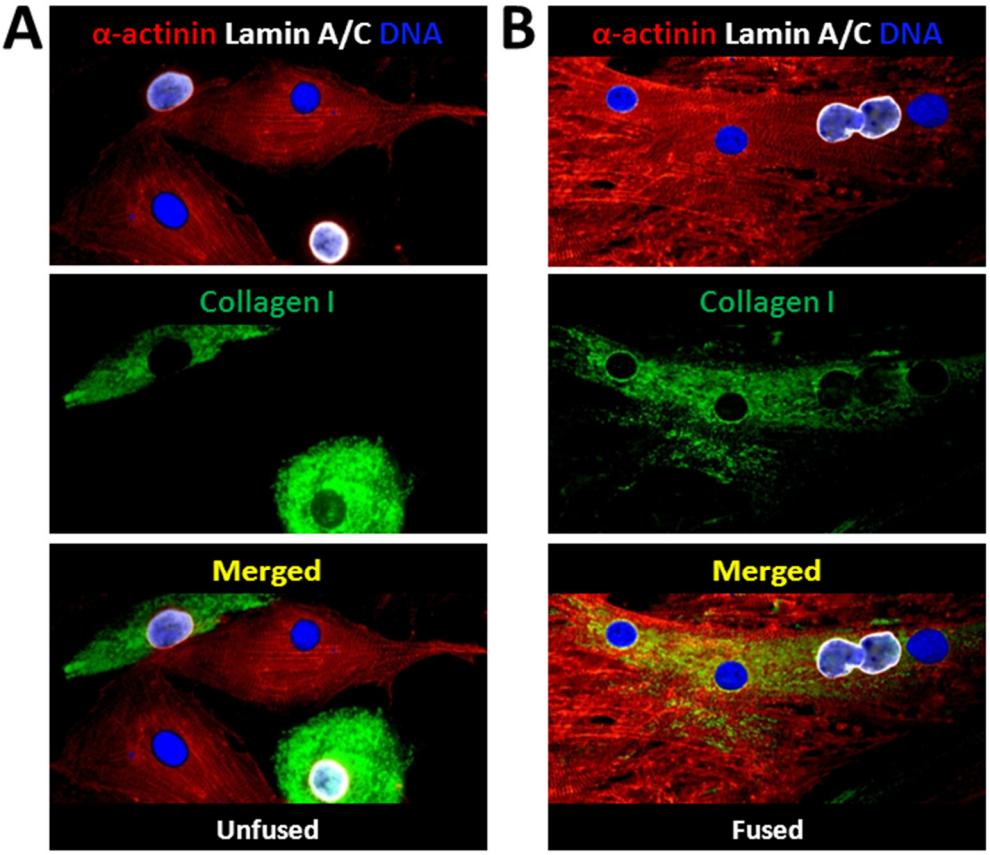

Figure 3. *Forced heterocellular fusion of nrCMCs and hVSCs leads to formation of hybrid heterokaryotic cells. (A) Typical picture of an immunocytological staining for α-actinin, lamin A/C and DNA of an unfused co-culture. For unfused cells, collagen-I expression is normally specific to hVSCs and not found in nrCMCs, while α-actinin is specific to nrCMCs and never found in hVSCs. (B) By forced heterocellular fusion, both of these markers were co-expressed within the same cell. Moreover, human nuclei (Lamin A/C positive) and rat nuclei (Lamin A/C negative) were shown to be present within the same cytoplasm as evidenced by the nuclear cavities seen in cytoplasmic collagen I expression.*

Next, co-cultures containing VSV-G expressing hVSCs and nrCMCs (from here on referred to as “fused co-cultures”) or solely eGFP expressing hVSCs and CMCs in a 1:4 ratio (henceforth referred to as unfused co-cultures) were prepared. Effects of heterocellular fusion were characterized at day 5 by immunocytological staining for human-specific Lamin A/C, Collagen-I, α-actinin and DNA. In unfused co-cultures, hVSCs expressed collagen-I and did not show positive staining for α-actinin (Figure 3A). Moreover, there were no human-specific Lamin A/C-expressing nuclei observed in α-actinin expressing

cells. However, fused co-cultures did contain heterokaryons, which were defined as cells that contained at least 2 nuclei of different species within the same cytoplasm.

Such heterokaryons co-expressed collagen-I and α-actinin and contained multiple nuclei of human and rat origin (Figure 3B). In fused co-cultures, 70±9% of human nuclei were present inside multinucleated cells, while 1±2% of human nuclei in unfused co-cultures were present within multinucleated cells. The collagen-I staining also stains cytoplasmic pro-collagen I, which produces nuclear cavities in the staining profile and, when combined with human-specific lamin A/C and Hoechst staining, allowed to identify nuclei from different species within the same cytoplasm (Figure 3). On average, heterokaryons consisted of 6±3 nuclei per cell (range of 2-17). Of these nuclei, 46±18% was positive for lamin A/C and therefore originated from hVSCs (range of 13-83%). In unfused co-cultures, 7 multinucleated cells were found, of which 6 contained only human nuclei. Moreover, all these cells contained 2 nuclei. Analysis of nuclear composition of heterokaryons (n=45) showed that 13 heterokaryons contained more than 50% human nuclei, while 10 heterokaryons contained exactly 50% human nuclei. Concomitantly, 22 heterokaryons contained more nrCMC nuclei than human nuclei. There were 3 fused cells (of 48 fused cells) that were comprised of only human nuclei. Annexin-V staining revealed no increases in apoptosis by forced cellular fusion (1.3±1.3% in eGFP controls versus 0.9±1.3% in VSV-G co-cultures, $P>0.05$), indicating that heterocellular fusion was well-tolerated.

Cytoskeletal reorganization after heterocellular fusion

To investigate cytoskeletal composition after heterocellular fusion, vimentin expression was quantified by immunocytological staining. In unfused nrCMCs, vimentin expression was low whereas vimentin expression was high in unfused hVSCs (Figure 4A, B). Interestingly, heterokaryons showed a substantial decrease in vimentin expression compared to unfused hVSCs (Figure 4B). Moreover, vimentin expression did not correlate ($r^2=0.05$) to the percentage of nuclei of human origin within the heterokaryon (Figure 4C). The contribution of nrCMC-specific cytoskeletal protein to the cytoskeleton of the heterokaryon appeared more dominant, as quantification of α-actinin staining revealed that sarcomeres remained intact in the majority of heterokaryons. More specifically, 89% of 46 heterokaryons expressed sarcomeric α-actinin, while none out of 8 fused cells comprised of only hVSCs expressed sarcomeric α-actinin. Moreover, hybrid cells remained contractile as observed under phase-contrast light microscopy.

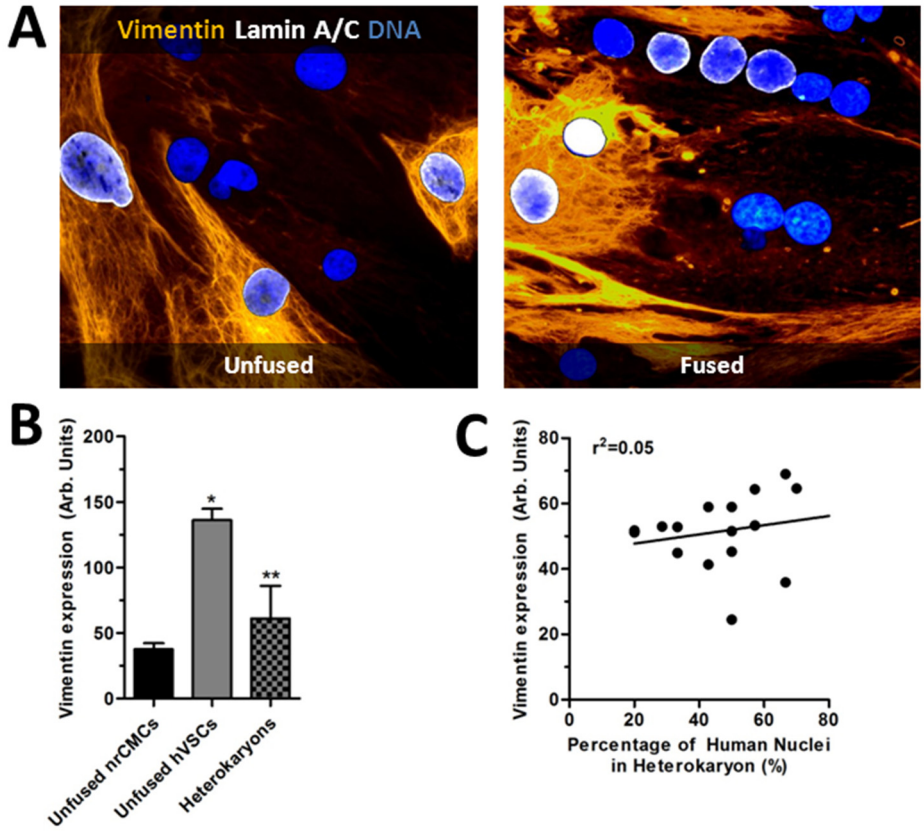

Figure 4. *Cytoskeletal rearrangement after cellular fusion. (A) Typical example of a vimentin staining showing Lamin A/C positive unfused hVSCs that are strongly positive, whereas unfused nrCMCs express lower amounts of vimentin. (B) Quantification of vimentin expression levels based on immunocytological staining. *:P<0.05 vs. fused cells and nrCMCs. **:P<0.05 vs. unfused hVSCs and nrCMCs. (C) Vimentin expression levels weakly correlated with the percentage of human nuclei within the heterokaryon.*

Effects of forced heterocellular fusion on gap-junctional protein and ion channel expression levels

To investigate whether expression of proteins involved in electrophysiology were affected by heterocellular fusion, fused and unfused cultures were stained for Cx43, the dominant cardiac gap-junctional protein. This staining revealed that while unfused hVSCs expressed low amounts of intercellular Cx43, unfused nrCMCs expressed high amounts of Cx43 at intercellular junctions (Figure 5A, B). Moreover, heterokaryons expressed Cx43 at levels higher than hVSCs and similar to nrCMCs (Figure 5B). Interestingly, Cx43 expression levels did not linearly correlate in the slightest to the amount of human nuclei present within the heterokaryon (r^2=0.05, Figure 5C). To investigate ion channel expression in heterokaryons, staining were performed for Cav1.2, the pore-forming unit of the L-type calcium channel, which was strongly expressed in unfused nrCMCs but barely detectable in unfused hVSCs (Figure 6A). Interestingly, Cav1.2 was also expressed in fused heterokaryons (Figure 6B), and in higher quantities than in unfused hVSCs (Figure 6C). Expression levels of Cav1.2 did not linearly correlate (r^2=0.02) to the amount of human nuclei present within heterokaryons, showing positive staining even when human nuclei outnumbered rat nuclei 1:4 (Figure 6D).

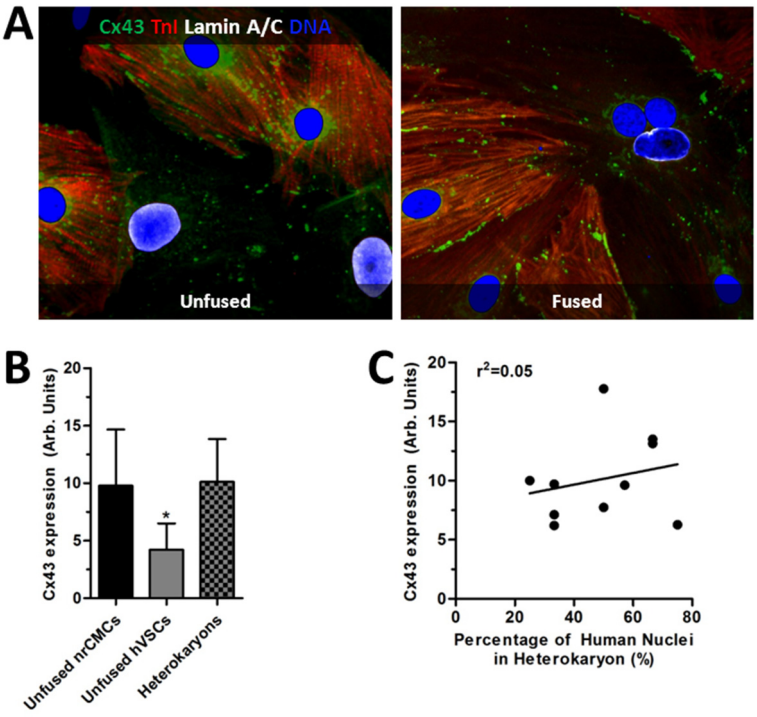

Figure 5. *Cx43 expression in heterokaryons. (A) Typical examples of Cx43 staining on unfused and fused cells showing (B) cx43 expression levels in heterokaryons was equal to those of CMCs. *:P<0.05 vs. all. (C) Cx43 expression levels in heterokaryons does not linearly depend on the amount of human nuclei present within heterokaryons.*

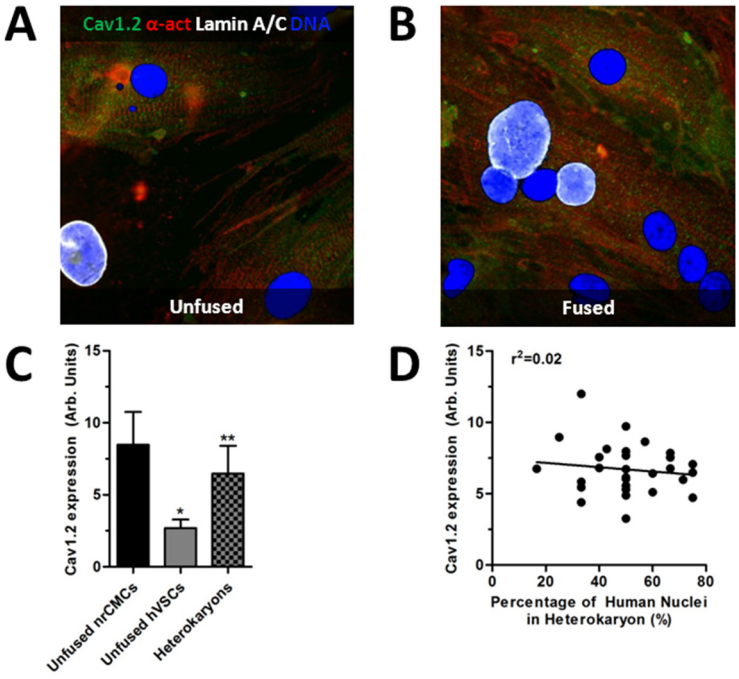

Figure 6. *Heterocellular fusion leads to Cav1.2 expression in heterokaryons. (A) Typical examples of immunocytological staining for Cav1.2 in unfused and (B) fused hVSCs showing (C) increased Cav1.2 expression levels in heterokaryons compared to hVSCs.*:P<0.05 vs. nrCMCs and fused cells. **:P<0.05 vs. CMC and No-fusion. (D) Cav1.2 expression levels did not linearly depend on the amount of human nuclei present within the heterokaryon.*

Forced cellular fusion of hVSCs and CMCs is anti-arrhythmic

Electrophysiological effects of heterocellular fusion were evaluated at day 5, 2 days after induction of fusion with the acidic buffer. Importantly, this buffer did not affect CV or APD_{90} within 4 hours after exposure or 2 days after exposure in purified CMC cultures (data not shown). By induction of heterocellular fusion, CV was significantly higher than in unfused co-cultures (16.8±1.6 cm/s vs. 10.3±2.6 cm/s, $P<0.05$, Figure 7A, B), while the amount of hVSC nuclei were confirmed to be equal in both groups (19.6±6.0% of nuclei in non-fused co-cultures [n=30 pictures with 74±21 nuclei per picture] vs. 21.2±7.0% of nuclei in fused co-cultures [n=42 pictures with 72±23 nuclei per picture, $P>0.05$], $P>0.05$).

Additionally, APD_{90} was significantly shorter and optical action potential morphology was distinctly different by heterocellular fusion (328±56ms vs. 480±79 ms, $P<0.05$, Figure 7C,D). Spatial dispersion of repolarization was also significantly lowered by heterocellular fusion (86±45 ms vs. 156±40 ms in unfused co-cultures, $P<0.05$, Figure 7C, E). Early afterdepolarizations and reentrant arrhythmias were not observed in fused cultures (n = 23), whereas 63% of non-fused cultures (n=8) showed such arrhythmic activity (Figure 7F).

Next, culture excitability was tested by programmed electrical stimulation. Lowest bipolar stimulus voltage to result in 2Hz capture was found to be 2.6±1.4V in fused co-cultures, as opposed to 5.1±2.2V in unfused co-cultures without VSV-G expression (P<0.05, Figure 7G), indicating increased excitability of these cultures by heterocellular fusion. In addition, the maximal capture rate was increased by heterocellular fusion (2.9±0.3 vs. 2.2±0.4 Hz in control cultures, P<0.05, Figure 7H).

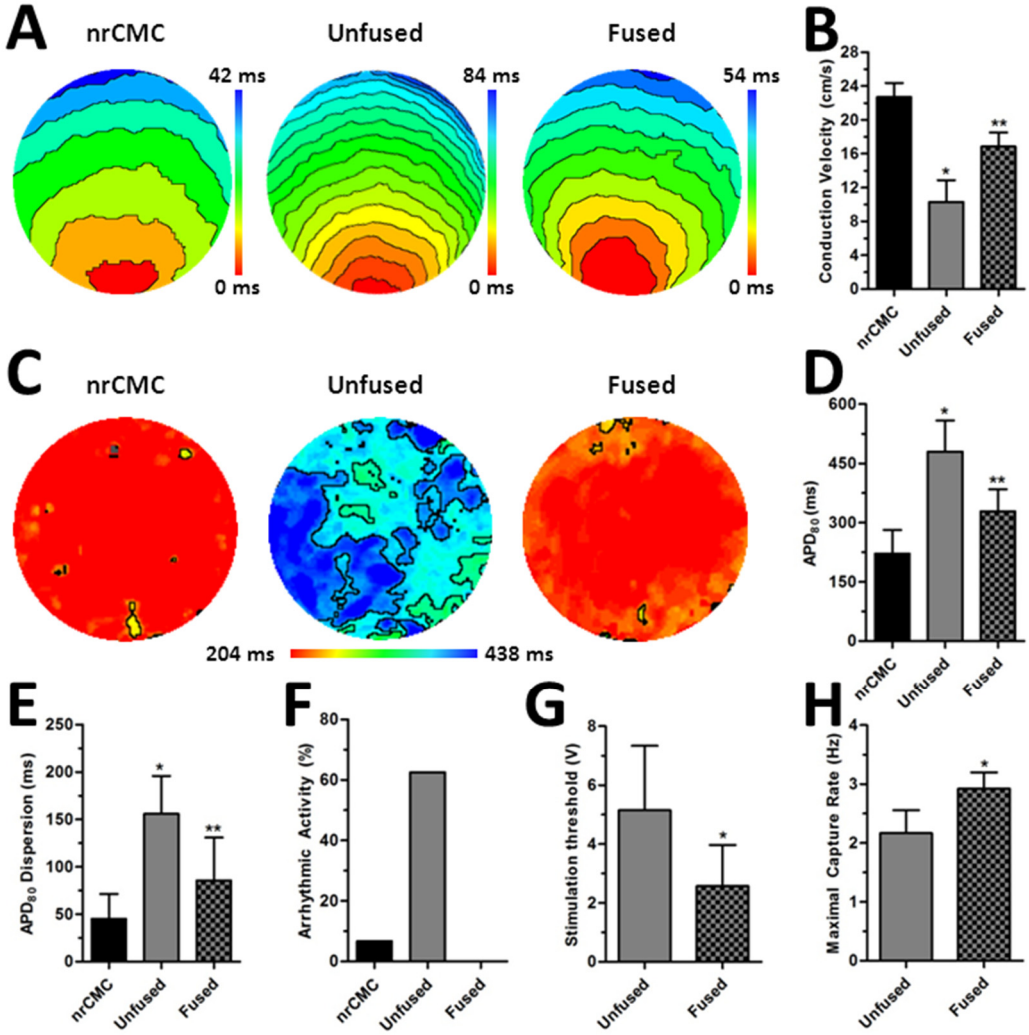

Figure 7. *Forced heterocellular fusion is anti-arrhythmic. (A) Typical activation maps with 6ms isochronal spacing showing (B) increased CV by heterocellular fusion. *:P<0.05 vs. nrCMC and fused co-cultures. **:P<0.05 vs. unfused co-cultures and nrCMCs. (C) Typical APD maps of nrCMC cultures, unfused co-cultures and fused co-cultures. (D) APD was shortened in cultures with heterocellular*

*fusion. *:P<0.05 vs. nrCMC and fused co-cultures. **:P<0.05 vs. unfused co-cultures and nrCMC cultures. (E) APD dispersion was decreased by heterocellular fusion. *:P<0.05 vs. nrCMC cultures and fused co-cultures. **:P<0.05 vs. unfused co-cultures and nrCMC cultures. (F) Arrhythmic activity was ameliorated by heterocellular fusion. (G) The threshold of electrical stimulation to evoke electrical activation was lower in fused co-cultures. *:P<0.05 vs. unfused co-cultures. (H) Maximal capture rate is increased in fused co-cultures. *:P<0.05 vs. unfused co-cultures.*

Discussion

Key findings of this study are (1) heterocellular fusion of hVSCs and nrCMCs is feasible, well-tolerated and preserves cellular structural integrity and (2) can be anti-arrhythmic (3) Moreover, the nrCMC phenotype appears to be dominant in heterokaryons, suggesting heterocellular fusion may serve as a strategy to reprogram fibroblasts towards cardiomyocytes.

Pro-arrhythmic aspects of fibroblasts

Fibrosis, an increase in extracellular matrix deposition and number of fibroblasts in response to cardiac injury, can cause conduction slowing and block, which predispose to potentially lethal cardiac arrhythmias.[13] Apart from the anatomical obstructions provided by the ECM, recent evidence suggests that fibroblasts themselves may be pro-arrhythmic through several mechanisms. Due to the poor gap-junctional coupling capacity of fibroblasts, these cells act as current-sinks with a high intercellular resistance.[14,15] Conduction is hindered even further by their inexcitability, which is paramount for fast conduction and therefore leads to slow, electrotonic conduction.[14] Moreover, fibroblasts can intersperse between CMCs and may therefore obstruct conduction by reducing the gap-junctional communication between CMCs due to physical separation. Therefore, conduction slowing and block by fibroblast interspersion may play an important role in fibrosis-associated arrhythmias. By increasing gap-junctional coupling of fibroblasts, conduction block could be overcome *in vitro*, implying a potentially anti-arrhythmic effect of such an intervention.[16] However, modulating electrical fibroblast integration as an anti-arrhythmic strategy may proof to be more challenging, as fibroblast inexcitability and their depolarized membrane can negatively affect CMC electrophysiology through gap-junctional coupling.[2,15,17,18] Overcoming the inexcitability, depolarized membrane and poor intercellular coupling of fibroblast may represent a robust anti-arrhythmic strategy that is becoming increasingly successful.[19-21] In the current study, a novel alternative solution which consisted of forced cellular fusion of hVSCs with nrCMCs in an attempt to fully electrically integrate these fibroblastic cells into the cardiac syncytium was investigated. By heterocellular fusion, the amount of interspersed fibroblastic cells that were taken from human post-myocardial infarction scars was decreased while the amount of nuclei

remained the same. Thereby, electrical integration of hVSCs would be expected to be maximized as per definition, intercellular resistance is non-existent if cells have been fused together into one hybrid cell. Such forced heterocellular fusion decreases the amount of interspersed, high resistance current-sinks and forced the incorporation of inexcitable cellular membrane of a fibroblast into an excitable membrane of the CMC. Overall, these changes translated to an increased CV in fused co-cultures, indicating that maximizing fibroblast integration by incorporating them within an excitable membrane may represent a novel anti-arrhythmic strategy. Although cellular fusion has been previously used to induce ion channel expression in cells,[22] the current study is, to our knowledge, the first to use such a strategy as an anti-arrhythmic intervention.

Electrophysiological effects of cellular fusion

Although cellular fusion is an established phenomenon in biology, its implications for cardiology have mostly been studied in the context of regenerative medicine and stem cell differentiation while little research has focused on its implications for electrophysiological concepts.[5] In the current study, a recently developed protocol of inducing cellular fusion was utilized, which is termed V-fusion.[10] By overexpressing the Vesicular Stomatitis Virus G-protein in a cell and subsequently lowering the extracellular pH to 6.0 for a brief period, fusion was easily induced in a more efficient manner than older methods of cellular fusion.[10] In addition, V-fusion only causes cellular membrane fusion without causing fusion of intracellular membranes as seen with other types of cellular fusion induction and thereby appears to be a solid, well-tolerated technique to investigate the effects of cellular fusion on electrophysiology.[23] Theoretically, by cellular fusion, intercellular resistance becomes void while cellular capacitance increases as the cellular volume increases with the amount of fused cells. While the increased cellular capacitance may delay phase 0 of the action potential and thereby slow conduction, the decreased intracellular resistance increase CV.[13] Moreover, the altered source-sink relationships caused by increased capacitance through heterocellular fusion may lower the ease by which EADs are propagated. [24] In the current study, cultures with heterocellular fusion showed no EADs, while unfused hVSCs did cause EADs. Apart from altered source-sink relations, the APD shortening that was accomplished by heterocellular fusion may also contribute to the lack of observed EADs. Moreover, overall culture excitability was increased, as electrical stimulus threshold was significantly lowered by heterocellular fusion. Considering the importance of excitability for fast conduction, CV may have been increased by increased excitability in fused co-cultures. Besides the anti-arrhythmic implications of increased excitability, the lower electrical stimulus threshold to evoke electrical activation may therefore also be relevant to cardiac resynchronization therapy, of which the efficacy is hindered by the presence of scar tissue. [25]

Phenotypical dominance of nrCMCs within heterokaryons

Increased excitability of fused co-cultures was likely to be a result of the expression of cardiac ion channels from the nrCMC part of the heterokaryon, as cav1.2 was found to be expressed within the membrane of heterokaryons. Indeed, cellular fusion leads to merging of cellular membranes, and thereby their integrins and ion channels are expressed and functional in the resultant hybrid membrane. [22] In addition, connexin expression was also increased for heterokaryons compared to unfused hVSCs and was equal to connexin expression levels of nrCMCs. This suggests that the degree of electrical integration of heterokaryons into the cardiac syncytium was higher compared to unfused hVSCs. However, if heterokaryons were just a sum of their parts, their expression levels of Cx43 would not be expected to be equal to nrCMC expression levels and therefore, dominance of the nrCMC phenotype is likely. In line with these findings were the findings that expression levels of Cx43, vimentin or Cav1.2 did not linearly correlate with the nuclear composition of the heterokaryon. Phenotypical dominance of nrCMCs within heterokaryons in our study was further supported by the observation that most heterokaryons retained sarcomeric α-actinin expression and were contractile, which is consistent with current literature.[26] Since our purified nrCMC cultures contained a small amount of endogenous fibroblasts, it is likely that the low numbers of heterokaryons that did not express α-actinin contained neonatal rat fibroblasts instead of nrCMCs. Inversely, as vimentin is more dominantly expressed in fibroblasts, the steep decrease in vimentin expression in fused cells compared to non-fused hVSCs is also consistent with dominance of the nrCMC phenotype within heterokaryons. The mechanism of nrCMC dominance is unlikely to be based on a simple “majority-rules” principle, as heterokaryons were often composed of more hVSCs than nrCMCs while retaining cardiac-specific protein expression at levels higher than to be expected for such a principle. Rather, the mechanism of nrCMC dominance within heterokaryons may be more complex. By forcing multiple nuclei inside the same cytoplasm, exposure to normally separated intracellular environments that are rich in celltype specific gene, mRNA, miRNA and protein expression profiles may occur. Such pancellular cross-talk can influence all present nuclei to alter their gene expression profiles[27,28]. Since CMCs can increase their size and protein expression profiles in response to mechanical[29] and humoral stimuli[30] and even changes in ionic currents,[31] the dominance of the nrCMC phenotype may lie in increased transcriptional and translational activity in response to the strong alterations in cellular configuration after heterocellular fusion.

Although hVSCs were outnumbered by nrCMCs (in a 1:4 ratio) in the current study, the average number of human nuclei within a heterokaryon exceeded the more predictable value of 20%, indicating that homocellular hVSC-fusion is favored. This is likely due to VSV-G expression in both cells that allows for easier fusion than in heterocellular fusion.

Despite the relatively high amount of human nuclei within heterokaryons, the apparent phenotypical dominance of CMCs within heterokaryons suggests that heterocellular fusion may even have anti-arrhythmic effects in circumstances where CMCs are outnumbered by fibroblasts. As modifying fibroblasts to resemble or even mimic CMCs is a key focus in current anti-arrhythmic research, heterocellular fusion may represent a novel and promising candidate for more in-depth exploration.

Future Perspectives

Cardiac architecture and intercellular contacts are highly regulated *in vivo* through intercalated discs and anisotropic fiber direction to optimize conduction and contraction. Cellular fusion may interfere with these important aspects of cardiac physiology and may be undesirable as a widespread anti-arrhythmic solution in the 3-dimensional heart. Therefore, heterocellular fusion would be most suited for sites with a high degree of CMC-Fibroblast interactions that are prone to arrhythmias, such as the infarct border zone of which selective genetic modification can yield anti-arrhythmic effects.[32] *In vivo*, extracellular matrix deposition may limit physical contact between CMCs and fibroblasts and thereby limit the potential for fusion to occur. However, such deposition of matrix occurs in later healing phases and adequate timing of fusogenic interventions may circumvent such hindrances. In addition, should the dominance of the CMC phenotype prevail *in vivo* as well, reduced extracellular matrix deposition may occur by heterocellular fusion. By increasing tissue excitability, heterocellular fusion may have implications for cardiac resynchronization therapy as lower voltages could be used for electrical stimulation. Although such perspectives must remain speculative for the time being, the strong anti-arrhythmic effects of heterocellular fusion demonstrated in this proof-of-concept study provide strong incentive to explore the feasibility of forced heterocellular fusion as an anti-arrhythmic intervention.

Conclusion

Forced heterocellular fusion of hVSCs with nrCMCs is feasible and well-tolerated and produces a hybrid, contractile cell type. Moreover, forcing cellular fusion in hVSC-nrCMC co-cultures is anti-arrhythmic. Moreover, nrCMCs appear to be dominant within the heterokaryon which indicates that heterocellular fusion may represent a novel concept of anti-arrhythmic reprogramming of fibroblasts.

Study limitations

In the current study, neonatal rat cardiomyocytes were utilized due to their availability and ability to remain in culture for extended periods of time, although use of human adult cardiomyocytes would bear more clinical relevance. Nevertheless, using a 2d-model with these cells has proven to be relevant for studying key electrophysiological processes in the

heart. The use of 2 species in our fusion experiments was necessary to distinguish between human and rat nuclei and determine heterokaryon compositions. Despite the similarities between rat and human cells, interspecies differences and effects that depend on these differences are unlikely but possible. Although staining showed that ion channel and connexin expression did not linearly depend on nuclear composition of the heterokaryon, a technique to correct functional ion channel measurements for the heterokaryon nuclear composition is currently unknown due to technical limitations. As a result, despite the implied likelihood of non-linear functional effects of heterocellular fusion on ionic currents, such “dose-dependent” effects cannot be determined at a functional level in the current study, and need to be investigated in a dedicated future study with novel technical refinements.

Acknowledgements
We would like to thank H. van der Stadt and R. van Leeuwen for excellent technical support.

References

1. Pedrotty DM, Klinger RY, Kirkton RD, Bursac N. Cardiac fibroblast paracrine factors alter impulse conduction and ion channel expression of neonatal rat cardiomyocytes. *Cardiovasc Res*. 2009;83:688-697.

2. Askar SF, Bingen BO, Swildens J, Ypey DL, van der Laarse A, Atsma DE, Zeppenfeld K, Schalij MJ, de Vries AA, Pijnappels DA. Connexin43 silencing in myofibroblasts prevents arrhythmias in myocardial cultures: role of maximal diastolic potential. *Cardiovasc Res*. 2012;93:434-444.

3. Thompson SA, Copeland CR, Reich DH, Tung L. Mechanical coupling between myofibroblasts and cardiomyocytes slows electric conduction in fibrotic cell monolayers. *Circulation*. 2011;123:2083-2093.

4. Kirkton RD and Bursac N. Engineering biosynthetic excitable tissues from unexcitable cells for electrophysiological and cell therapy studies. *Nat Commun*. 2011;2:300.

5. Avitabile D, Crespi A, Brioschi C, Parente V, Toietta G, Devanna P, Baruscotti M, Truffa S, Scavone A, Rusconi F, Biondi A, D'Alessandra Y, Vigna E, Difrancesco D, Pesce M, Capogrossi MC, Barbuti A. Human cord blood CD34+ progenitor cells acquire functional cardiac properties through a cell fusion process. *Am J Physiol Heart Circ Physiol*. 2011;300:H1875-H1884.

6. Acquistapace A, Bru T, Lesault PF, Figeac F, Coudert AE, Le CO, Christov C, Baudin X, Auber F, Yiou R, Dubois-Rande JL, Rodriguez AM. Human mesenchymal stem cells reprogram adult cardiomyocytes toward a progenitor-like state through partial cell fusion and mitochondria transfer. *Stem Cells*. 2011;29:812-824.

7. Metzele R, Alt C, Bai X, Yan Y, Zhang Z, Pan Z, Coleman M, Vykoukal J, Song YH, Alt E. Human adipose tissue-derived stem cells exhibit proliferation potential and spontaneous rhythmic contraction after fusion with neonatal rat cardiomyocytes. *FASEB J*. 2011;25:830-839.

8. National Institutes of Health. Guide for the Care and Use of Laboratory Animals. 1-1-2002. Ref Type: Statute

9. Pijnappels DA. Progressive increase in conduction velocity across human mesenchymal stem cells is mediated by enhanced electrical coupling. 2006.

10. Gottesman A, Milazzo J, Lazebnik Y. V-fusion: a convenient, nontoxic method for cell fusion. *Biotechniques*. 2010;49:747-750.

11. Askar SF, Ramkisoensing AA, Schalij MJ, Bingen BO, Swildens J, van der Laarse A, Atsma DE, de Vries AA, Ypey DL, Pijnappels DA. Antiproliferative treatment of myofibroblasts prevents arrhythmias in vitro by limiting myofibroblast-induced depolarization. *Cardiovasc Res*. 2011;90:295-304.

12. Askar SF, Ramkisoensing AA, Schalij MJ, Bingen BO, Swildens J, van der Laarse A, Atsma DE, de Vries AA, Ypey DL, Pijnappels DA. Antiproliferative treatment of myofibroblasts prevents arrhythmias in vitro by limiting myofibroblast-induced depolarization. *Cardiovasc Res*. 2011;90:295-304.

13. Kleber AG and Rudy Y. Basic mechanisms of cardiac impulse propagation and associated arrhythmias. *Physiol Rev*. 2004;84:431-488.

14. Gaudesius G, Miragoli M, Thomas SP, Rohr S. Coupling of cardiac electrical activity over extended distances by fibroblasts of cardiac origin. *Circ Res*. 2003;93:421-428.

15. Miragoli M, Gaudesius G, Rohr S. Electrotonic modulation of cardiac impulse conduction by myofibroblasts. *Circ Res*. 2006;98:801-810.

16. Pijnappels DA, van Tuyn J, de Vries AA, Grauss RW, van der Laarse A, Ypey DL, Atsma DE, Schalij MJ. Resynchronization of separated rat cardiomyocyte fields with genetically modified human ventricular scar fibroblasts. *Circulation*. 2007;116:2018-2028.

17. Miragoli M, Salvarani N, Rohr S. Myofibroblasts induce ectopic activity in cardiac tissue. *Circ Res*. 2007;101:755-758.

18. Zlochiver S, Munoz V, Vikstrom KL, Taffet SM, Berenfeld O, Jalife J. Electrotonic myofibroblast-to-myocyte coupling increases propensity to reentrant arrhythmias in two-dimensional cardiac monolayers. *Biophys J*. 2008;95:4469-4480.

19. Chen JX, Krane M, Deutsch MA, Wang L, Rav-Acha M, Gregoire S, Engels MC, Rajarajan K, Karra R, Abel ED, Wu JC, Milan D, Wu SM. Inefficient reprogramming of fibroblasts into cardiomyocytes using Gata4, Mef2c, and Tbx5. *Circ Res*. 2012;111:50-55.

20. Ieda M, Fu JD, Delgado-Olguin P, Vedantham V, Hayashi Y, Bruneau BG, Srivastava D. Direct reprogramming of fibroblasts into functional cardiomyocytes by defined factors. *Cell*. 2010;142:375-386.

21. Qian L, Huang Y, Spencer CI, Foley A, Vedantham V, Liu L, Conway SJ, Fu JD, Srivastava D. In vivo reprogramming of murine cardiac fibroblasts into induced cardiomyocytes. *Nature*. 2012;485:593-598.

22. Hoppe UC, Johns DC, Marban E, O'Rourke B. Manipulation of cellular excitability by cell fusion: effects of rapid introduction of transient outward K+ current on the guinea pig action potential. *Circ Res*. 1999;84:964-972.

23. Kerkis AY and Zhdanova NS. Formation and ultrastructure of somatic cell hybrids. *Electron Microsc Rev*. 1992;5:1-24.

24. Xie Y, Sato D, Garfinkel A, Qu Z, Weiss JN. So little source, so much sink: requirements for afterdepolarizations to propagate in tissue. *Biophys J*. 2010;99:1408-1415.

25. Bleeker GB, Schalij MJ, van der Wall EE, Bax JJ. Postero-lateral scar tissue resulting in non-response to cardiac resynchronization therapy. *J Cardiovasc Electrophysiol*. 2006;17:899-901.

26. Matsuyama D and Kawahara K. Maintenance and characterization of spontaneous contraction rhythm in cultured cardiac myocytes fused with cardiac fibroblasts. *Biosystems*. 2008;92:226-232.

27. Cowan CA, Atienza J, Melton DA, Eggan K. Nuclear reprogramming of somatic cells after fusion with human embryonic stem cells. *Science*. 2005;309:1369-1373.

28. Bonde S, Pedram M, Stultz R, Zavazava N. Cell fusion of bone marrow cells and somatic cell reprogramming by embryonic stem cells. *FASEB J*. 2010;24:364-373.

29. Bupha-Intr T, Holmes JW, Janssen PM. Induction of hypertrophy in vitro by mechanical loading in adult rabbit myocardium. *Am J Physiol Heart Circ Physiol*. 2007;293:H3759-H3767.

30. Long CS, Ordahl CP, Simpson PC. Alpha 1-adrenergic receptor stimulation of sarcomeric actin isogene transcription in hypertrophy of cultured rat heart muscle cells. *J Clin Invest*. 1989;83:1078-1082.

31. Kassiri Z, Zobel C, Nguyen TT, Molkentin JD, Backx PH. Reduction of I(to) causes hypertrophy in neonatal rat ventricular myocytes. *Circ Res*. 2002;90:578-585.

32. Lau DH, Clausen C, Sosunov EA, Shlapakova IN, Anyukhovsky EP, Danilo P, Jr., Rosen TS, Kelly C, Duffy HS, Szabolcs MJ, Chen M, Robinson RB, Lu J, Kumari S, Cohen IS, Rosen MR. Epicardial border zone overexpression of skeletal muscle sodium channel SkM1 normalizes activation, preserves conduction, and suppresses ventricular arrhythmia: an in silico, in vivo, in vitro study. *Circulation*. 2009;119:19-27.

Cellular and Molecular Mechanisms of Arrhythmias in Cardiac Fibrosis and Beyond:

From Symptoms to Substrates towards Solutions

Chapter VIII

Development of adeno-associated virus vectors for the transduction of myocardial fibroblasts

J. Swildens, PhD; **S.F.A. Askar, MSc;** J. van Tuyn, PhD; M.J. Schalij, MD, PhD; A. van der Laarse, PhD; D.E. Atsma, MD, PhD; A.A.F. de Vries, PhD

In preparation

Abstract

Introduction: Scar formation after myocardial infarction is an important cause of cardiac dysfunction. This makes myocardial scar fibroblasts (MSFs) interesting targets for therapeutic intervention. One way of modulating the properties of MSFs is by genetic modification with viral vectors. Among the currently used viral gene delivery vehicles, adeno-associated virus (AAV) vectors stand out for their *in vivo* safety and ability to spread easily through tissues. The aim of this study was to compare the transduction of neonatal rat cardiomyocytes (nrCMCs) and of human, mouse and rat MSFs by AAV vectors with different capsids and with transgenes driven by different promoters.

Methods & Results: AAV vector shuttle plasmids containing a *LacZ* gene driven by 9 different promoters including the human, mouse and rat cytomegalovirus *immediate early* gene (CMV-IE) promoter were constructed. The AAV vector genomes specified by these plasmids were packaged in AAV serotype 2 (AAV2) capsids. β-galactosidase assays revealed that of all CMV-IE promoters, the human CMV-IE promoter outperformed the rodent CMV-IE promoters in human MSFs while the rodent CMV-IE promoters were more active in murine and rat MSFs. Furthermore, of all nine promoters tested the human *eukaryotic translation elongation factor 1 alpha 1* gene (hEF1α) promoter was most active in rodent MSFs while the Rous sarcoma virus (RSV) promoter gave the highest transgene expression in nrCMCs. A comparison of the transduction efficiency of rat MSFs and nrCMCs with AAV2 vectors carrying capsids of AAV serotypes 2, 5, 6, 8 and 9 showed that transduction of rat MSFs was most efficient with AAV2/2 vectors whereas AAV2/9 best transduced the nrCMCs. Substitution of the surface-exposed tyrosine residues at amino acid positions 444, 500 and 730 in the AAV2 VP1 protein resulted in a 6-fold increase in the transduction efficiency of rMSFs by AAV2/2 vectors but also quadrupled their ability to transduce nrCMCs.

Conclusion: The highest transgene expression in rat MSFs is obtained by transduction with an AAV2/2 vector containing an hEF1α promoter-driven transgene while transgene expression in nrCMC is highest after transduction with an AAV2/9 vector in which foreign gene expression is controlled by the RSV promoter.

Introduction

After myocardial infarction (MI), cardiomyocytes in the affected region die and are replaced by scar tissue consisting of fibroblasts and dense extracellular matrix (ECM). The scar tissue contributes to the stiffening of the myocardium, reducing the overall contractile performance of the heart.[1] Furthermore, the scar tissue prevents proper action potential propagation due to (i) poor electrical coupling of scar fibroblasts with each other and with adjacent cardiomyocytes and (ii) high electrical resistance of the ECM.[2]

To overcome the adverse mechanical and electrical effects of scar tissue on cardiac performance, several approaches have been tested. First of all, transplantation of unmodified autologous bone marrow-derived stem cells (BMSCs) has been attempted to regenerate the damaged myocardium.[3] Some minor improvement of cardiac function was observed in some studies,[4-6] with the therapeutic effect being predominantly attributable to paracrine factors released by the donor cells rather than to the differentiation of the injected BMSCs into cardiomyocytes.[7] To increase their therapeutic effect, it has been proposed to endow BMSCs with genes that can induce their cardiomyogenic differentiation before injecting them into the heart.[8] However, numerous issues remain with cardiac cell therapy, including the inefficient retention of the donor cells at the site of injection, the poor survival of the injected cells, and the low propensity of the surviving BMSCs to differentiate into cardiomyocytes.

A possible strategy to bypass at least some of the limitations associated with cell therapy is to directly target the resident myocardial scar fibroblasts (MSFs) using *in vivo* gene therapy with the aim to endow them with more favorable biosynthetic, contractile and/or electric properties. Via this approach, the number of cells available for therapeutic intervention would be much higher than by the injection of stem cells, provided that the MSFs can be efficiently transduced *in vivo* with the gene construct of choice. Of the various gene delivery vehicles available for cardiac gene therapy, adeno-associated virus (AAV) vectors constitute an attractive option due to their excellent *in vivo* safety record and small size (≈20 nm in diameter) allowing them to penetrate dense tissues better than other commonly used viral vectors. Other advantages of AAV vectors are their low immunogenicity and the long-term persistence of their genomes in target cells mainly as episomes leading to prolonged transgene expression with a low chance of insertional mutagenesis.[9] Vectors based on recombinant AAV serotype 2 (AAV2) genomes packaged in capsids of AAV serotypes 1 through 9 (i.e. AAV2/1 through AAV2/9 vectors) have been tested in healthy rodent hearts. [10-13] Unfortunately, in none of these *in vivo* experiments the identity of the transduced cardiac cells was investigated making it impossible to determine the contribution of the four major cell types in the non-diseased heart (i.e. cardiac fibroblasts, cardiomyocytes, vascular smooth muscle cells and endothelial cells) to the observed transgene expression. However, Qi et al. did test the ability of AAV2/2, AAV2/5, AAV2/7, AAV2/8 and AAV2/9 vectors to transduce cardiac fibroblasts and

cardiomyocytes of neonatal rats in culture[13] but thus far the transduction of MSFs by different AAV vector pseudotypes has not been investigated.

Depending on the therapeutic strategy that is being pursued to treat infarcted hearts by gene therapy, it may be important to develop AAV vectors that efficiently transduce MSFs and induce high-level therapeutic expression in these cells but do not cause appreciable transgene expression in cardiomyocytes. In an attempt to generate an AAV vector meeting these requirements, five different AAV vector pseudotypes were tested for the efficiency by which they transduce MSFs as compared to cardiomyocytes. These experiments revealed that AAV2/6 and AAV2/2 vectors best transduce neonatal rat cardiomyocytes (nrCMCs) and rat MSFs (rMSFs), respectively. In addition, MSFs of man, mouse and rat and nrCMCs were exposed to AAV vectors carrying nine different promoters, to determine which of these promoters is most specific for either of these cell types. Of all promoters tested, the human *eukaryotic translation elongation factor 1 alpha 1* gene (hEF1α) promoter was the most active in rodent MSFs while the human cytomegalovirus *immediate early* gene (hCMV-IE) promoter and Rous sarcoma virus (RSV) promoter performed best in human MSFs (hMSFs) and nrCMCs, respectively. We also generated two new helper plasmids based on the widely used AAV packaging construct pDG[14] for the production of AAV2/8 and AAV2/9 vectors in a two-plasmid system. Use of these new helper plasmids resulted in AAV vector yields similar to those obtained with commonly applied AAV2/8 and AAV2/9 vector production systems based on the transfection of host cells with three different plasmids.

Materials and Methods

Primary cell cultures

All animals were treated in accordance with national guidelines and with permission of the Animal Experiments Committee of the Leiden University Medical Center.

rMSFs were obtained from myocardial scar tissue of 16-week-old Wistar Kyoto rats 2 weeks after MI induction by ligation of the left anterior descending artery (LAD). The white scar tissue was dissected from the heart and cut into small pieces. Each of these pieces was then placed in a gelatin-coated 10-cm^2 cell culture dish (Greiner Bio-One, Alphen a/d Rijn, the Netherlands) containing Dulbecco's modified Eagle's medium (DMEM) supplemented with 20% fetal bovine serum (FBS), 100 U/mL penicillin and 100 µg/mL streptomycin (all from Invitrogen, Breda, the Netherlands) and covered with a glass coverslip. After 7 days, the scar tissue was removed and the adherent fibroblasts that had grown out from the tissue were passaged. rMSFs were further propagated in DMEM supplemented with 20% FBS, 100 U/mL penicillin and 100 µg/mL streptomycin.

mMSFs were obtained from myocardial scar tissue of 10 week old NOD/Scid mice 6 days after MI induction by ligation of the LAD. The white scar tissue was dissected from the heart and used to obtain mMSFs following the same protocol as for the isolation of the rMSFs.

Cultures of nrCMCs and neonatal rat cardiac fibroblasts (nrCFBs) were prepared from 2-day-old rats as described before.[15] nrCMCs were cultured in a 1:1 mixture of DMEM and Ham's F10 (Invitrogen) supplemented with 5% HS, (Invitrogen) 100 U/mL penicillin and 100 µg/mL streptomycin. In order to determine the fraction of nrCFBs present in purified nrCMC cultures, these cultures were immunostained for the cardiomyocyte marker sarcomeric α-actinin and for the fibroblast marker collagen type I. To this end, the cells were incubated overnight at 4°C with mouse IgG1-anti-sarcomeric α-actinin antibody (clone EA-53; Sigma-Aldrich, St. Louis, MO) and with collagen type I-specific rabbit IgG (ab292; Abcam, Cambridge, MA) which were diluted 1:400 in phosphate-buffered saline (PBS) + 5% FBS. The next day, the cells were washed once with PBS and then incubated for 1 hour at 4°C with Alexa Fluor 568-conjugated goat-anti-mouse IgG and Alexa Fluor 488-conjugated goat-anti-rabbit IgG antibodies (both from Invitrogen) diluted 1:400 in PBS + 5% FBS. The percentage of nrCFBs in purified nrCMC cultures ranged from 5 to 10% of the total cell number. nrCFBs were cultured in DMEM supplemented with 10% FBS, 100 U/mL penicillin and 100 µg/mL streptomycin.

hMSFs were obtained and cultured as described before.[16] All primary cells were cultured at 37°C in an atmosphere of 10% CO_2 in air saturated with water vapour.

Cell lines

293T cells[17] were cultured in DMEM supplemented with 10% FBS at 37°C and 10% CO_2. 911E4 cells[18] were grown in DMEM supplemented with 10% FBS, 0.4 mg/mL geneticin (Invitrogen) and 0.1 mg/mL hygromycin B (Invitrogen) at 37°C and 10% CO_2. Upon seeding the 911E4 cells for end-point titration of AAV vector stocks, the cells were cultured in DMEM supplemented with 10% FBS, 0.4 mg/mL geneticin, 0.1 mg/mL hygromycin B and 100 ng/mL of doxycyclin (Sigma-Aldrich).

Plasmid constructs

The various AAV vector shuttle plasmids encoding *Escherichia coli* β-galactosidase were constructed as follows. The AAV vector shuttle constructs pDD1, pDD2 and pDD345 containing RSV, hCMV-IE and the hybrid, chicken *β-actin* gene-based CAG promoter, a multiple cloning site and the simian virus 40 (SV40) polyadenylation signal (pA) flanked by the AAV2 inverted terminal repeats (ITRs) were a gift of Dongsheng Duan.[19] First, the 3.1-kb XhoI×XbaI fragment from pCMVβ.LacZnls12co (Marker Gene Technologies, Eugene, OR) containing a *Lac*Z gene that is codon-optimised for expression in mammalian cells and encodes a nuclear-targeted version of β-galactosidase (LacZnls12co) was ligated to the vector backbone of XhoI- and XbaI-digested pDD345 using T4 DNA ligase to create pDD.CAG.nlsLacZco.SV40pA. Next, a 46-bp synthetic polyadenylation (synpA) signal[20] flanked by BamHI and NotI restriction enzyme recognition sequences was created by hybridizing two oligonucleotides (sense strand: 5'-GGCCGCAATAAAATATCTTTATTTTCATTACATCTGTGTGTTGGTTTTTTGTGTG-3'; antisense strand: 5'-GATCCACACAAAAAACCAACACACAGATGTAATGAAAATAAAGATATTTTATTGC-3'). The synpA site was subsequently cloned into BamHI- and NotI-digested pDD.CAG.nlsLacZco.SV40pA to make pDD.CAG.nlsLacZco.synpA. The latter construct was incubated with BamHI and HindIII and the 3.2-kb fragment containing the *Lac*Z gene and synpA was combined with the 4.7-kb fragment of BamHI- and HindIII-digested pDD2 to produce pDD.hCMV-IE.nlsLacZco.synpA.

The hybrid, SV40 *early* gene-based SRα promoter was excised from plasmid pMX1 (R&D Systems, Abingdon, UK) using XbaI and BglII and inserted in XbaI- and BamHI-digested pBluescriptSK(-) (Stratagene, Palo Alto, CA) to generate pBluescriptSK(-).SRα. The SRα promoter was subsequently excised from pBluescriptSK(-).SRα using EcoRV and inserted in reverse orientation in EcoRV-digested pBluescriptSK(-) to generate pBluescriptSK(-).SRα(-). The latter construct was treated with BcuI and HindIII and the resulting 0.7-kb fragment containing the SRα promoter was combined with the 7.2-kb BcuI×HindIII fragment of pDD.CAG.nlsLacZco.synpA using T4 DNA ligase. This led to the construction of AAV vector shuttle plasmid pDD.SRα.nlsLacZco.synpA.

The RSV promoter was obtained by digestion of pDD1 with XhoI and HincII and cloned into EcoRV- and SalI-digested pBluescriptSK(-) yielding pBluescriptSK(-).RSV. Next, the 0.7-kb BcuI×HindIII fragment from pBluescriptSK(-).RSV containing the RSV promoter was

combined with the 7.2-kb BcuI×HindIII fragment of pDD.CAG.nlsLacZco.synpA yielding pDD.RSV.nlsLacZco.synpA.

The mouse *S100 calcium binding protein A4* gene (mFSP1) promoter[21], rat *lysyl oxidase* (rLOX) promoter, hEF1α promoter, mouse *CMV-IE* gene (mCMV-IE) promoter and rat *CMV-IE* gene (rCMV-IE) promoter sequences were obtained by polymerase chain reaction (PCR). The mFSP1 and rLOX promoters were amplified from chromosomal DNA, whereas the hEF1α, rCMV-IE and mCMV-IE promoters were amplified from pLVET-KRAB[22], pSSHK3[23] and pMH5 (Microbix Biosystems, Mississauga, Ontario, Canada), respectively. The PCRs were performed in a total volume of 50 µL using 200 ng (for genomic DNA) or 10 ng (for plasmid DNA) template, 0.5 µmol/L of both forward and reverse primer (mFSP1: 5'-GCTGATATCGAAGCCTGGTTCCCAGAC-3' and 5'-CTGGATATCACCTTTCTGTGCCTCTCA-3'; rLOX: 5'-GCCGATATCCTGGGGTTTATTCGCTG-3' and 5'-GAAGATATCGATGATCTCCCGGCTCGTC-3'; hEF1α: 5'-GCTGATATCGGCTCCGGTGCCCGTCAG-3' and 5'-CTGGATATCTCACGACACCTGAAATGG-3'; mCMV-IE: 5'-CTAACTAGTGGGGTGGTGACTCAATGGCC-3' and 5'-GATAAGCTTAGTACCGACGCTGGTCGCGC-3'; rCMV-IE: 5'-GTACTAGTTCCCATATTAAGAATGAGTTATAG-3' and 5'-GTAAAGCTTCCGATCCGAAGACTGTGACTG-3'), 200 µmol/L of each dNTP, 1× Phusion HF buffer (Finnzymes, Espoo, Finland) and 1 U Phusion high-fidelity DNA polymerase (Finnzymes). The PCRs were performed according to the protocol provided with the DNA polymerase using an annealing temperature of 60°C and 35 amplification cycles. The 1.1-kb PCR fragment containing the mFSP1 promoter, the rLOX promoter PCR fragment of 0.8 kb and the 1.2-kb PCR fragment containing the hEF1α promoter were digested with EcoRV, purified from agarose gel using the JETSORB gel extraction kit (GENOMED, Löhne, Germany) and cloned into EcoRV-digested pBluescriptSK(-) to produce pBluescriptSK(-).mFSP1, pBluescriptSK(-).rLOX and pBluescriptSK(-).hEF1α, respectively. The mFSP1 promoter was released from pBluescriptSK(-).mFSP1 using EcoRV and combined with the 7.2-kb EcoRV fragment of pDD.SRα.nlsLacZco.synpA to generate pDD.mFSP1.nlsLacZco.synpA. The rLOX and hEF1α promoters were excised from pBluescriptSK(-).rLOX and pBluescriptSK(-).hEF1α, respectively, using BcuI and HindIII and combined with the 7.2-kb BcuI×HindIII fragment of pDD.CAG.nlsLacZco.synpA to produce pDD.rLOX.nlsLacZco.synpA and pDD.hEF1α.nlsLacZco.synpA. The 1.1-kb PCR fragments containing the mCMV-IE and rCMV-IE promoter were digested with BcuI and HindIII, purified from agarose gel and ligated to the 7.2-kb BcuI×HindIII fragment of pDD.CAG.nlsLacZco.synpA yielding pDD.mCMV-IE.nlsLacZco.synpA and pDD.rCMV-IE.nlsLacZco.synpA, respectively. The correctness of the cloned PCR fragments was verified by nucleotide sequence analysis using the BigDyeTerminator v3.1 cycle sequencing kit, the BigDye XTerminator purification kit and the 3730xl DNA analyzer (all from Applied Biosystems Life Technologies, Carlsbad, CA).

To create an AAV vector containing an hEF1α promoter-driven *Aequorea victoria enhanced green fluorescent protein* (eGFP) gene, the AAV vector shuttle plasmid

pTR.hCMV-IE.eGFP.WHVPRE.bGHpA, a derivative of pTR-CMVgfp containing the woodchuck hepatitis virus posttranscriptional regulatory element (WHVPRE)[24] was digested with BamHI and KpnI. Next, the 5'- and 3'-recessed ends were blunted using T4 DNA polymerase and the 1.6-kb fragment containing the *eGFP* gene and the WHVPRE was ligated to the 5.2-kb Klenow DNA polymerase-treated HincII×HindIII fragment of pDD.hEF1α.nlsLacZco.synpA to create pDD.hEF1α.eGFP.WHVPRE.synpA. The latter AAV shuttle plasmid was incubated with MunI and XhoI and the resulting 5.8-kb digestion product was combined with the 0.5-kb RSV promoter-containing MunI×XhoI fragment of pDD1 to produce pDD.RSV.eGFP.WHVPRE.synpA.

Helper plasmids for making AAV2/8 and AAV2/9 vectors in a two-plasmid production system were generated by replacing the AAV2 cap gene in pDG by the cap gene of AAV serotype 8 (AAV8) and AAV serotype 9 (AAV9), respectively. To this end, pDG (obtained from Jürgen Kleinschmidt; [14]) was digested with Bsu15I, treated with the Klenow fragment of DNA polymerase I and subsequently digested with SalI. The AAV8 and AAV9 cap genes were released from pAAV2/8 or pAAV2/9 (both obtained from James Wilson; Penn Vector Core, Philadelphia, PA), respectively, by digesting these plasmids with MssI and SalI. The resulting 3.1-kb fragments containing the cap gene of either AAV8 or AAV9 were combined with the 18.7-kb Bsu15I×SalI fragment of pDG to create pDP8 and pDP9, respectively.

To make, in a three-plasmid production system, wild-type AAV2 vectors and AAV2 vectors in which the surface-exposed tyrosine residues at positions 444, 500 and 730 of the VP1 protein are replaced by phenylalanines, we first generated plasmid pUCBM21.SmaI.Cap2 by combining the 2.6-kb HindIII×Klenow polymerase-blunted Bsu15I fragment from pDG (Grimm et al., 2002) with the 2.7-kb HindIII×SmaI fragment of pUCBM21PSXSP. pUCBM21PSXSP is a derivative of pUCBM21 (Boehringer Mannheim) containing extra non-spaced MssI, SmiI and XhoI restriction enzyme recognition sites (adaptor molecule contained HindIII overhang, MssI, SmiI and XhoI site, complete NcoI site and Eco32I half-end) in between the HindIII and NcoI target sequences and extra non-spaced SmiI and MssI recognition sites (adaptor molecule contained BamHI overhang, complete SmaI site, SmiI and MssI sites and EcoRI overhang) in between the SmaI and EcoRI target sequences. Plasmid pUCBM21.SmaI.Cap2 was used as template for site-directed mutagenesis of the codons corresponding AAV2 VP1 amino acid residues 444, 500 and 730 essentially as described by Liu and Naismith (2008) (reference: Liu H, Naismith JH. An efficient one-step site-directed deletion, insertion, single and multiple-site plasmid mutagenesis protocol. BMC Biotechnol 2008;8:91) except for the use of VELOCITY DNA polymerase (Bioline) instead of Pfu DNA polymerase. The oligodeoxyribonucleotide pairs for introducing the tyrosine-to-phenylalanine substitutions were 5' CTGTATTTCTTGAGCAGAACAAACACTCCAAGTGGAAC 3' and 5' CTGCTCAAGAAATACAGGTACTGGTCGATGAGAGGATTC 3' for Tyr^{444} 5' GTGAATTCTCGTGGACTGGAGCTACCAAGTACCACC 3' and 5' GTCCACGAGAATTCACTGTTGTTGTTATCCGCAGATG

3' for Tyr^{500} and 5' ACCAGATTCCTGACTCGTAATCTGTAATTGCTTGTTAATCAA 3' and 5' of AGTCAGGAATCTGGTGCCAATGGGGCGAG 3' for Tyr^{730}. The plasmid encoding a version of AAV2 VP1 carrying all three tyrosine-to-phenylalanine mutations was designated pUCBM21.SmaI.Cap2Y444500730F. After having confirmed the correctness of the AAV2 sequences in pUCBM21.SmaI.Cap2 and in pUCBM21.SmaI.Cap2Y444500730F by dideoxy nucleotide sequence analysis, both plasmids were incubated with SmiI and the resulting 2.3-kb digestion products were combined with the 4.9-kb SmiI×Eco32I fragment of pAAV2/8 to generate pAAV2/2 and pAAV2/2Y444500730F, respectively.
All restriction and DNA modifying enzymes as well as the dNTPs were purchased from Fermentas (St. Leon-Rot, Germany) and the oligodeoxyribonucleotides were provided by Eurofins MWG Operon (Ebersberg, Germany).

AAV vector production, purification and quantification
AAV vector particles were produced in 293T cells. Per AAV vector production, 10^6 (small scale) or 7×10^7 (intermediate scale) cells were seeded at a density of 10^5 cells/cm^2 and cultured in DMEM supplemented with 10% FBS 1 day before transfection. Two hours prior to transfection, the cell culture medium was refreshed with DMEM + 10% FBS. The cells were transfected with 71 ng AAV vector shuttle plasmid and 214 pDG[14], pDF5, pDG6[25], pDP8 or pDP9 per cm^2 of cells (two-plasmids production system) or 71 ng AAV vector shuttle plasmid, 71 ng pAAV2/2, pAAV2/2Y444500730Y, pAAV2/8 or AAV2/9 and 143 ng pAd.ΔF6 (provided by James Wilson; Penn Vector Core)[26] per cm^2 of cells (three-plasmids production system) using 3 ng linear 25-kDa polyethylenimine (Polysciences Europe, Eppelheim, Germany) per ng DNA as transfection agent. After 16 hours, the medium was replaced by DMEM + 5% FBS. Sixty-four hours after transfection, the 293T cells from four 175 cm^2 flasks were collected in 10 mL PBS + 1 mM $CaCl_2$ + 1 mM $MgCl_2$. The cells were then subjected to 3 cycles of snap freezing in liquid nitrogen and thawing in a water bath of 37°C to release the AAV vector particles from the cells. The AAV vector preparation was then treated for 30 min with 100 U of OmniCleave Endonuclease (EPICENTRE Biotechnologies, Madison, WI) per mL sample at 37°C. Next, the cell debris was pelleted at 250 × *g* and the supernatant was collected.
The AAV vector particles were purified using an iodixanol block gradient. To this end, 17.5 mL of the cleared vector suspension was loaded into a 39-mL polyallomer tube (Quick-Seal, 25 × 89 mm; Beckman Coulter, Fullerton, CA, USA). Next, 9 mL of 15%, 5 mL of 25%, 5 mL of 40% and 3 mL of 60% iodixanol solution (OptiPrep, Sigma-Aldrich) in 1 mM $MgCl_2$, 2.5 mM KCl was sequentially layered under the AAV vector preparation, which was then centrifuged for 70 min at 69,000 revolutions per min in a 70 Ti rotor (Beckman Coulter). Thereafter, the bottom of the centrifuge tube was punctured and the AAV vector particles at the 40-60% iodixanol interface were collected.

Finally, the AAV vector particles were washed with PBS + 5% sucrose and concentrated in three steps to approximately 200 µL per AAV vector in an Amicon Ultra-15 filter unit with a nominal molecular weight limit of 100 kDa (Millipore, Amsterdam, the Netherlands) following the instructions of the filter supplier. AAV vector stocks were stored in 50 µL aliquots at -80°C.

Titration of AAV vector stocks

The titers of AAV vector stocks were determined by dot-blot assay and are based on DNase-resistant AAV genome copies (GC). Two µL of each AAV vector stock was treated for 30 min at 37°C with 10 U OmniCleave in 30 µL 50 mM Tris-HCl (pH 8.0), 1 mM $MgCl_2$ to digest any unpackaged DNA. Then, 10 µL proteinase K solution (50 mM Tris-HCl [pH 8.0], 8 M urea, 4 mM $CaCl_2$ and 1 µg/µl proteinase K [Fermentas]) was added and the sample was incubated at 37°C for 1 hour to release the AAV vector genomes. Next, the samples was boiled for 5 min in a water bath and immediately chilled on ice to denature the vector DNA. The sample was subsequently diluted 1:1 with 20× SSC buffer (3 M NaCl, 300 mM trisodium citrate [pH 7-8]) and blotted onto a Hybond-N+ nylon membrane (GE Healthcare, Diegem, Belgium) using a Bio-Dot microfiltration apparatus (Bio-Rad Laboratories, Veenendaal, the Netherlands). The vector DNA was then fixed to the membrane by incubation for 2 hours at 80°C. The AlkPhos direct labelling and detection system with CDP-*Star* (GE Healthcare) was used to quantify the DNA. As a probe either a 501-bp fragment specific for *nlsLacZco* (primers: 5'-CGTGACCGTGTCCCTGTGGC-3' and 5-'GGCACCATGCCGTGGGTCTC-3') or a 438-bp fragment binding to the WHVPRE (primers: 5'-TCAGGCAACGTGGCGTGGTGTG-3' and 5'-AAGACCAAGCAACACGGACCGG-3' was obtained by PCR and isolated from agarose gel. The membrane was prehybridized for 30 min at 55°C after which 150 ng of the thermostable alkaline phosphatase-labelled probe was added to hybridize overnight at 55°C. Stringency washes and signal detection were performed following the recommendations of GE Healthcare. The ChemiDoc XRS+ system and Quantity One software (both from Bio-Rad Laboratories) were used to quantify the DNA. The titers typically ranged from 10^{11} to 10^{12} GC/mL.

To compare the amount of pTR.hCMV-IE.eGFP.WHVPRE.bGHpA-based AAV vectors produced with the two- and three-plasmid AAV2/8 and AAV 2/9 vector production systems, unconcentrated vector preparations were subjected to end-point titration in 911E4 cells using flow cytometric analysis of *eGFP* expression at 6 days post transduction as readout. Vector yields were expressed in transducing units (TU)/producer cell.

AAV transductions

To test the ability of different AAV vector pseudotypes to transduce MSFs and nrCMCs and to compare the activity of the different promoters in MSFs and nrCMCs, cells were seeded in fibronectin (Sigma-Aldrich)-coated cell culture dishes at a density of 6.25×10^4 cells/cm^2.

For measuring β-galactosidase activity by chemiluminescence assay, cells were cultured in 96-well plates (Corning Life Sciences, Amsterdam, the Netherlands). Chromogenic detection of β-galactosidase activity was done with cells maintained in 24-well plates (Greiner Bio-One). To test the ability of the AAV vectors AAV2/2.hEF1α.eGFP.WHVPRE.synpA, AAV2/2Y444500730Y.hEF1α.eGFP.WHVPRE.synpA (hereinafter referred to as AAV2/2mt.hEF1α.eGFP.WHVPRE.synpA) and AAV2/9.RSV.eGFP.WHVPRE.synpA to achieve cell type-specific transgene expression in rMSFs and nrCMCs, cells were seeded on fibronectin-coated round glass coverslips (14 mm Ø) in 24-well cell culture plates.

All nrCMC cultures were treated with the anti-proliferative agent mitomycin C (10 µg/mL; Sigma-Aldrich) at day 1 of culture for 2 hours to inhibit the proliferation of the remaining nrCFBs in these cultures. The next day, the cells were transduced with 100,000 GC of AAV vector per cell in 500 µL (2-cm^2 well) or 100 µL (0.32-cm^2 well) of a 1:1 mixture of DMEM and Ham's F10 without FBS. After 2 hours, an equal volume of 1:1 mixture of DMEM and Ham's F10 supplemented with 10% HS, 200 U/mL penicillin and 200 µg/mL streptomycin was added to the cells. The MSFs were transduced at day 1 of culture with 100,000 GC of AAV vector per cell in 500 µL (2-cm^2 well) or 100 µL (0.32-cm^2 well) DMEM without FBS. After 2 hours, an equal volume of DMEM + 20% FBS, 200 U/mL penicillin and 200 µg/mL streptomycin was added to the cells.

At 7 days post transduction, the cultures were either lysed and the lysates stored at -80°C for future β-galactosidase activity measurements using a chemiluminescence assay or the cells were fixed for subsequent cytochemical visualisation of β-galactosidase activity.

β-galactosidase activity assays

To quantify β-galactosidase levels in whole cell cultures, cells in a single well of a 96-well plate were lysed in 50 µL lysis buffer (25 mM Tris-HCl [pH 7.8], 2 mM 1,2-diaminocyclohexanetetraacetic acid, 2 mM dithiothreitol, 10% glycerol and 1% Triton X-100). The Galacto-Light β-galactosidase reporter gene assay system (Applied Biosystems Life Technologies) was used to quantify β-galactosidase activity using a Wallac 1420 VICTOR 3 multilabel plate reader (Perkin Elmer Nederland, Groningen, the Netherlands). These experiments were performed in triplicate to allow for statistical analysis.

To visualize β-galactosidase in individual cells, cell cultures were incubated for 10 min with 0.25% (v/v) glutaraldehyde (grade II; Sigma-Aldrich) in PBS. The cells were then washed twice with PBS to remove the fixative and incubated overnight with 5-bromo-4-chloro-3-indolyl-β-D-galactopyranoside (X-gal) solution (1 mg/mL X-gal [Sigma-Aldrich], 100 mM Na_2HPO_4/NaH_2PO_4 [pH 7.0], 2 mM $MgCl_2$, 5 mM $K_3Fe(CN)_6$, 5 mM $K_4Fe(CN)_6$) at 37°C. After two 5-min washes with PBS to remove the X-gal solution, the cells were viewed using an inverse microscope (IX51; Olympus, Zoeterwoude, the Netherlands) equipped with a

Peltier-cooled digital camera (XC30) and CellF software (both from Olympus) for image capture and processing/analysis, respectively.

Immunofluorescent staining

Cell cultures exposed to 10^5 GCs of AAV2/2.hEF1α.eGFP.WHVPRE.synpA, AAV2/2mt.hEF1α.eGFP.WHVPRE.synpA or AAV2/2.RSV.eGFP.WHVPRE.synpA per cell were fixed 7 days after transduction by a 20-min incubation on ice with phosphate-buffered 4% formaldehyde (Mallinckrodt Baker, Phillipsburg, NJ). After fixation, the cells were washed 3 times with PBS containing 10 mM glycine (PBSG) and permeabilized by incubation for 5 min on ice with PBS containing 0.1% Triton X-100. After 3 more washes with PBSG, the cells were incubated for 1 hour with 5% 0.22-µm filter-sterilized FBS in PBS to block potential aspecific antibody binding sites. To distinguish nrCMCs from nrCFBs, the nrCMC cultures were stained for the cardiomyocyte marker sarcomeric α-actinin or for the fibroblast marker collagen type I as described above except for the use of 400-fold diluted Alexa Fluor 568-conjugated donkey-anti-mouse IgG or Alexa Fluor 568-conjugated donkey-anti-rabbit IgG antibodies (both from Invitrogen) as secondary antibodies. Next, the cells were incubated for 10 min at room temperature with 10 µg/ml Hoechst 33342 in PBS. After washing the cells 4 times for 5 min with PBS, staining results were analyzed with the aid of the aforementioned Olympus IX51 inverse fluorescence microscope. The intensity of the fluorescent signals was determined using ImageJ software (http://rsb.info.nih.gov/ij/index.html). Image analysis was performed by a blinded investigator using pictures with a resolution of 1280x1024 pixels and of equal exposure time. Quantification of green fluorescent signal was performed in a fixed area or interest (AOI) of 52 by 47 pixels once per cell and expressed in arbitrary units of the mean grey value. Placement of the AOI in the cytoplasm was at a distance between 0 and 2 AOIs from the nucleus. Picture background was determined at sites without apparent fluorescence, averaged and subtracted from the fluorescent signal of cells in that picture. For quantifications performed on nrCMC cultures that contain endogenous nrCFBs, mean fluorescence of all cells was divided by the average fluorescent signal of nrCFBs to derive the fold difference in transgene expression between cell types per viral vector. Quantification was performed in ≥5 pictures per group and an average of 177 cells.

Western blot analyis

Western blot analysis of eGFP levels was performed on whole-cell protein extracts of purified nrCMC, nrCFB or rMSF cultures exposed to 10^5 GCs of AAV2/2.hEF1α.eGFP.WHVPRE.synpA, AAV2/2mt.hEF1α.eGFP.WHVPRE.synpA or AAV2/9.RSV.eGFP.WHVPRE.synpA per cell. At 7 days post transduction, cells were lysed in RIPA buffer (150 mM NaCl, 1% Nonidet P-40, 0.5% sodium deoxycholate, 0.1% SDS, 50

mM Tris-HCl [pH 8.0] supplemented with protease inhibitors [cOmplete, Mini Protease Inhibitor Cocktail Tablets from Roche Diagnostics Nederland, Almere, the Netherlands]). After clearance of the cell lysates by centrifugation for 20 min at 4°C and 21.130 × *g*, the protein concentration in each sample was determined using the Pierce BCA Protein Assay Kit Total (Thermo Scientific, Rockford, IL). Next, per sample, 4 µg total protein was applied to individual lanes of NuPage 12% Bis-Tris gels (Invitrogen) and electrophoresis was performed for 2 h at 150 V, after which proteins were transferred to Hybond-P polyvinylidene difluoride membranes (GE Healthcare) overnight using a wet blotting system. After blocking for 1 h at room temperature with 10 mmol/L Tris-HCl (pH7.6), 0.05% Tween-20 and 150 mmol/L NaCl (TBST) containing 2% ECL Advance blocking agent (BA; GE Healthcare), the membranes were incubated for 1 h at room temperature with primary antibodies diluted in TBST-2% BA. Primary antibodies were rabbit anti-eGFP (ab290; Abcam; 1:1,000), mouse anti-cardiac troponin I (clone 19C7; 4T21; Hytest, Turku, Finland; 1:1,000), mouse anti-vimentin (clone V9; V6630; Sigma-Aldrich; 1:200). After washing the blots for 4 times 5 min with TBST, membranes were incubated with corresponding horseradish peroxidase (HRP)-conjugated rabbit or mouse IgG-specific goat secondary antibodies (sc-3837 and sc-2005 from Santa Cruz Biotechnology, Santa Cruz, CA) diluted 15,000-fold in TBST-2% BA. Following 4 additional washing steps, blots were developed using ECL Prime Western Detection Reagent (GE Heathcare). The chemiluminescence signals were captured using a ChemiDoc XRS imaging system (Bio-Rad Laboratories, Veenendaal, the Netherlands). Chemiluminescence signals were quantified using ImageJ.

Statistics

The significance of differences between means was calculated by one-way analysis of variance followed by the Bonferroni's *post hoc* test whenever appropriate using Graph Pad Prism 4 (Graph Pad Software, La Jolla, CA). Comparison between two groups was performed using Student's t-test. Differences were considered significant if $p<0.05$. Results are expressed as mean ± standard deviation.

Results

Comparison of two- and three-plasmid AAV vector production systems

AAV vector production protocols that do not require infection of the producer cells with a helper virus have improved the safety of AAV vectors for *in vivo* use. In addition, the development of the AAV helper plasmids pDG, pSH3 and pSH5 encoding not only the AAV Rep and Cap proteins but also adenoviral helper functions has reduced efforts and costs to produce AAV2 vector particles compared to three- or four-plasmid based production systems.[14,27] Two-plasmid-based systems for the production of AAV2 vectors pseudotyped with capsids from AAV serotypes 1, 3, 4, 5 and 6 have also been generated[25] but are not yet available for generating other AAV vector pseudotypes. Since AAV vectors carrying capsids of AAV8 or AAV9 have been shown to efficiently transduce the hearts of rodents [10,11,13,28], we set out to generate pDG-based helper plasmids for the production of AAV2/8 and AAV2/9 vectors. To this end, the *AAV*2 *cap* gene in pDG was replaced by the *cap* gene of AAV8 or of AAV9, resulting in construction of pDP8 and pDP9, respectively.

To compare the AAV vector yields obtained with these new helper plasmids to those achieved with conventional three-plasmid-based AAV2/8 and AAV2/9 vector production methods, crude AAV2/8.hCMV-IE.eGFP.WHVPRE.bGHpA and AAV2/9.hCMV-IE.eGFP.WHVPRE.bGHpA vector preparations were made using both production systems. Limiting dilution assays in 911E4 cells revealed that the amounts of functional AAV vector particles generated with pDP8 and pDP9 did not differ significantly from those obtained with a combination of pAd.ΔF6 and either pAAV2/8 or pAAV2/9 (8.60±3.28 TU/cell vs. 11.75±3.81 TU/cell, $p>0.05$, and 20.70±3.72 TU/cell vs. 24.18±2.68 TU/cell, $p>0.05$, respectively; n=6; Figure 1). These results show that the new helper plasmids pDP8 and pDP9 can be used to produce high-titered stocks of functional AAV2/8 and AAV2/9 vector particles.

Comparison of promoter activity in MSFs and nrCMCs

To compare the efficiency by which MSFs of man, mouse and rat can be transduced by AAV2/2 vectors, cultures of these cells were exposed to equal doses of AAV2/2.hCMV-IE.nlsLacZco.synpA, AAV2/2.mCMV-IE.nlsLacZco.synpA or AAV2/2.rCMV-IE.nlsLacZco.synpA. X-gal staining at 7 days post infection revealed that hMSFs were transduced with a higher efficiency than mMSFs and rMSFs (Figure 2). Furthermore, in hMSFs *LacZ* expression was highest when driven by the hCMV-IE promoter, while in mMSFs and rMSFs the *immediate early* gene promoters of the rodent cytomegaloviruses were more active. These results show that there is some level of species specificity in the activity of CMV-IE promoters.

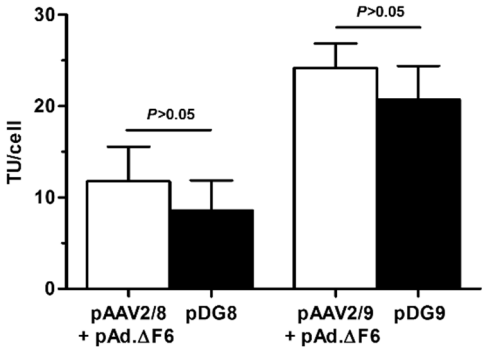

Figure 1. *Titers of small-scale AAV2/8 and AAV2/9 vector stocks generated with the aid of two- or three-plasmid AAV vector production systems. AAV vectors were produced using the eGFP-encoding AAV vector shuttle plasmid pTR.hCMV-IE.eGFP.WHVPRE.bGHpA and titered by serial dilution in 911E4 cells. Titers are based on the number of eGFP-positive cells as assessed by flow cytometry at 6 days post infection and given as the number of TU obtained per producer cell. The titers of AAV vector stocks made with the two-plasmid method (pDG8 or pDG9) did not differ significantly from those produced with the corresponding three-plasmid approach (pAd.ΔF6 and pAAV2/8 or pAAV2/9). Pseudotransduction did not contribute to the observed gene transfer activities as eGFP-positive 911E4 cells were undetectable when the AAV vector productions were carried out with helper plasmids lacking the AAV cap gene (data not shown).*

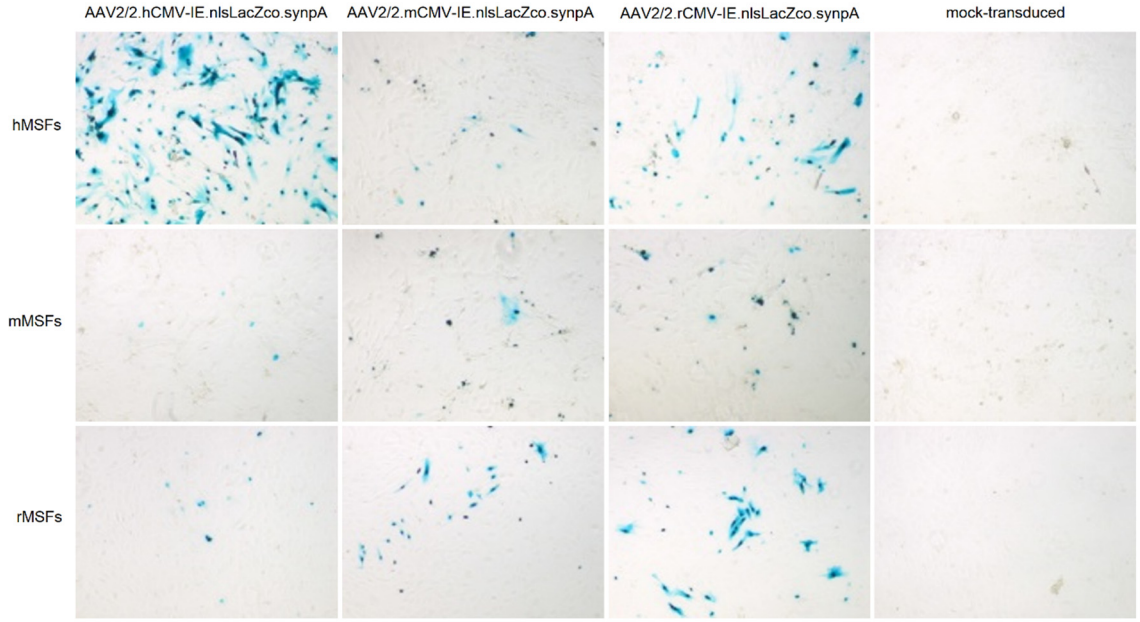

Figure 2. *β-galactosidase staining of AAV2/2 vector- or mock-transduced MSFs. The hCMV-IE promoter induces high-level transgene expression in hMSFs but is hardly active in mMSFs or rMSFs. The mCMV-IE and rCMV-IE promoters are more active in mMSFs and rMSFs than the hCMV-IE promoter and give similar low levels of LacZ expression in hMSFs.*

Next, the activity of the three CMV-IE promoters in MSFs was compared with that of other ubiquitous promoters and of two fibroblast-specific promoters (Table 1). For this purpose, MSF cultures were transduced in quadruplicate by AAV2/2 vectors carrying the *nlsLacZco* gene driven by one of nine different promoters. After 7 days, the cells were lysed and the β-galactosidase activity in the cell lysates was measured to assess the transcription rate of each promoter. The results showed that in hMSFs the hCMV-IE promoter displays the highest transcriptional activity, resulting in significantly higher β-galactosidase levels compared to those found with the other promoters ($p<0.001$; Figure 3A). Furthermore, in mMSFs, rMSFs and nrCFBs the hEF1α promoter showed the highest transcription rate, which resulted in significantly higher β-galactosidase levels than were obtained with the other promoters ($p<0.001$; Figure 3B, C and D).

To achieve the selective transduction of myocardial scar tissue, a promoter should ideally not only direct high levels of transgene expression in MSFs, but also be show low or no activity in cardiomyocytes. Thus, the activity of the nine promoters was also determined in purified nrCMC cultures. Quantification of β-galactosidase levels in each cell culture showed that the RSV promoter had a significantly higher transcriptional activity in nrCMCs than the other promoters ($p<0.001$), whereas the hEF1α promoter was only weakly active in these cells (3E). Together, these results indicate that of the promoters tested, the hEF1α promoter is preferred when targeting myocardial scar tissue in mouse or rat models, since it causes high-level transgene expression in MSFs but is relatively weakly active in nrCMCs.

promoter	promoter length (in nts)	AAV genome length (in nts)
Rous sarcoma virus long terminal repeat (RSV)	715	4503
Simian virus 40 early + R-U5 from human T cell leukemia virus I long terminal repeat (SRα)	741	4368
Human cytomegalovirus immediate-early (hCMV-IE)	1099	4711
Mouse cytomegalovirus immediate-early (mCMV-IE)	1126	4733
Rat cytomegalovirus immediate-early (rCMV-IE)	1177	4824
hCMV-IE enhancer + chicken β-actin core promoter + rabbit β-globin intron (CAG)	1110	4774
Human elongation factor 1α (hEF1α)	803	4484
Mouse fibroblast-specific protein 1 (mFSP1)	522	4284
Rat lysyl oxidase (rLO)	616	4354

Table 1.*Overview of the promoters used to drive LacZ expression in the AAV vectors.*

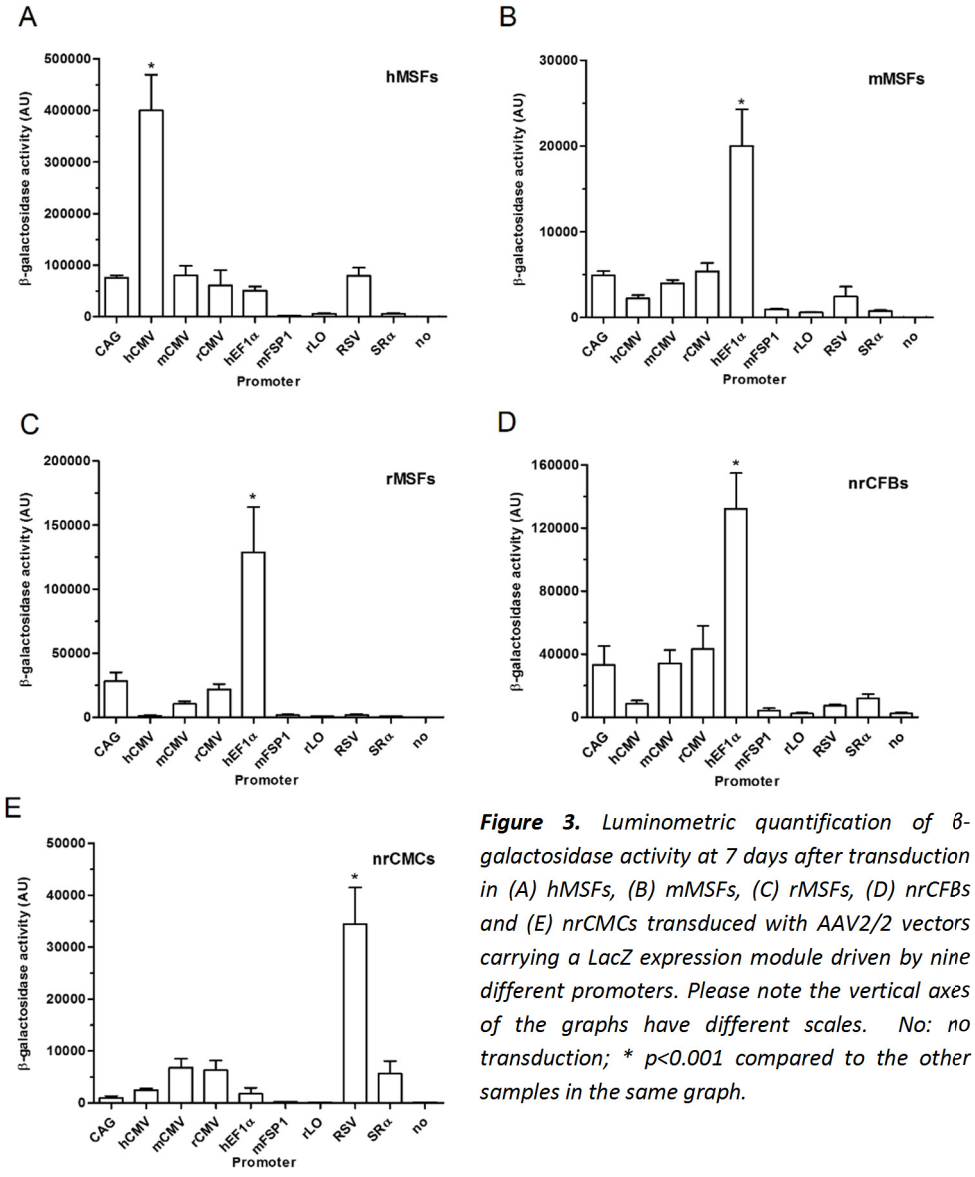

Figure 3. *Luminometric quantification of β-galactosidase activity at 7 days after transduction in (A) hMSFs, (B) mMSFs, (C) rMSFs, (D) nrCFBs and (E) nrCMCs transduced with AAV2/2 vectors carrying a LacZ expression module driven by nine different promoters. Please note the vertical axes of the graphs have different scales. No: no transduction; * p<0.001 compared to the other samples in the same graph.*

Comparison of the gene transfer activity of five different AAV vector pseudotypes in rMSFs and nrCMCs

Beside through transcriptional targeting, cell type-specific transgene expression in MSFs may also be accomplished by transductional targeting. To determine which AAV vector pseudotype transduces MSFs most specifically, rMSF and purified nrCMC cultures were exposed to AAV2 vectors with capsids of AAV serotypes 2, 5, 6, 8 or 9. To achieve the highest possible transgene expression levels, MSFs were transduced with vectors carrying an hEF1α promoter-driven *nlsLacZco* expression unit, whereas the cardiomyocytes received vectors in which the β-galactosidase-coding sequence was preceded by the RSV promoter.

In rMSFs, transduction with AAV2/2 vectors resulted in higher β-galactosidase levels than those obtained with the other AAV vector pseudotypes ($p<0.001$; n=6; Figure 4A). In addition, AAV2/6 vectors showed superior transduction of rMSFs compared to AAV2 vectors with capsids of AAV serotypes 5, 8 and 9 ($p<0.001$ vs. AAV2/8 and AAV2/9 vectors, $p<0.01$ vs. AAV2/5 vectors). In contrast, nrCMCs were most efficiently transduced by AAV2/6 vectors ($p<0.001$ vs. the other AAV vector pseudotypes), followed by AAV2/2 and AAV2/9 vectors ($p<0.001$ vs. AAV2/5 and AAV2/8; Figure 4A).

Based on these results, rMSFs are best transduced with AAV2/2 vectors while AAV2/9 vectors are a good candidate for the selective transduction of nrCMCs since they induce high-level transgene expression in these cells and poorly transduce MSFs, in contrast to AAV2/2 and AAV2/6 vectors (Figure 4B).

Although AAV2/2 vectors better transduced rMSFs than the other AAV vector pseudotypes tested, AAV2/2-mediated gene transfer to these cells was still rather inefficient. Recently, Li et al. (2010) reported that transduction of murine embryonic fibroblasts by AAV2/2 could be greatly improved by substituting the surface-exposed tyrosine residues at positions 444, 500 and 730 of the AAV2 VP1 protein for phenylalanines. To investigate whether the same would hold true for rat cardiac (myo)fibroblasts, AAV2 genomes carrying a recombinant *eGFP* gene under control of the hEF1α promoter were packaged in wild-type AAV2 capsids or AAV2 capsids carrying each of the three aforementioned amino acid substitutions. Next, nrCFBs were exposed to 10^5 GCs/cell of both vectors. As is evident from Figure 5A, the nrCFBs were more efficiently transduced by the vectors with the tyrosine-mutated AAV2 capsids.

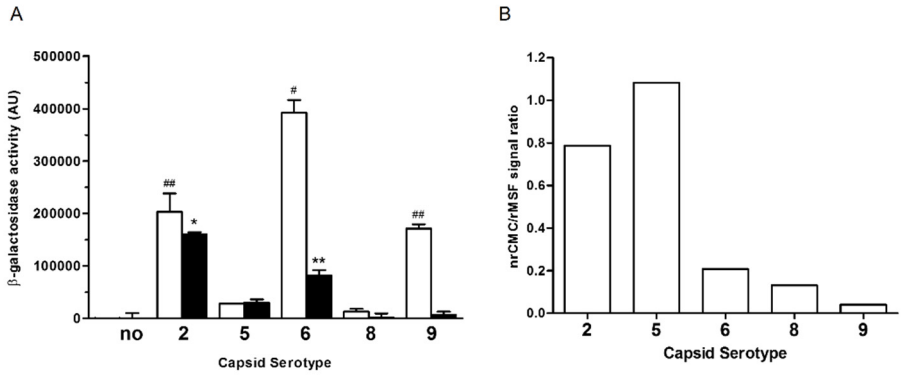

Figure 4. *(A) Comparison of the ability of five different AAV vector pseudotypes to transduce nrCMCs (white bars) or rMSFs (black bars). Transduction efficiencies were determined by luminometric quantification of β-galactosidase levels in lysates of each sample prepared at 7 days after infection (n=6 samples per cell type and per AAV vector pseudotype). The nrCMCs were transduced with AAV vectors carrying LacZ driven by the RSV promoter while the rMSFs were transduced by AAV vectors in which the β-galactosidase-coding sequence was preceded by the hEF1α promoter. No: no transduction; # p<0.001 vs. all other AAV vector pseudotypes in nrCMCs; ## p<0.001 vs. AAV2/5 and AAV2/8 vectors in nrCMCs; * p<0.001 vs. all other AAV vector pseudotypes in rMSFs; ** p<0.001 vs. AAV2/8 and AAV2/9 vector pseudotypes, p<0.01 vs. AAV2/5 vector pseudotypes in rMSFs. (B) Ratio between the β-galactosidase activity in rMSFs and in nrCMCs for AAV2.hCMV-IE.nlsLacZco.synpA vectors packaged in AAV2, AAV5, AAV6, AAV8 or AAV9 capsids.*

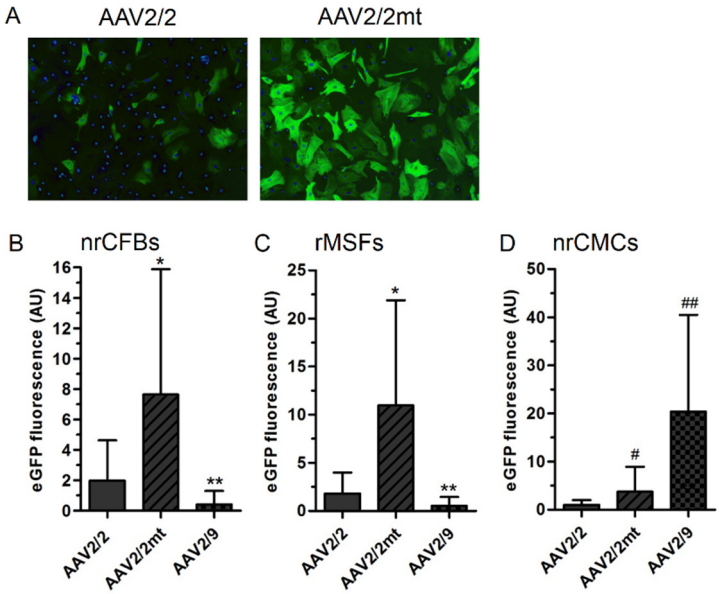

Figure 5. *Representative fluoromicrographs of nrCFB cultures taken at 7 days after transduction with 10^5 GCs/cell of AAV2/2.hEF1α.eGFP.WHVPRE.synpA (AAV2/2) or AAV2/2mt.hEF1α.eGFP.WHVPRE.synpA (AAV2/2mt). (B-D) Quantification of eGFP signals from fluoromicrographs of (B) nrCFB, (C) rMSF, and (D) nrCMC cultures transduced with 10^5 GCs/cell of AAV2/2.hEF1α.eGFP.WHVPRE.synpA (AAV2/2), AAV2/2mt.hEF1α.eGFP.WHVPRE.synpA (AAV2/2mt) or AAV2/9.RSV.eGFP.WHVPRE.synpA (AAV2/9). *:P<0.05 vs. AAV2/2 and AAV2/9. **:P<0.05 vs. AAV2/2 and AAV2/2mt.*

Transduction of nrCMCs and rat cardiac (myo)fibroblasts with optimized AAV vectors

Based on the previous results, we generated an AAV2/9 vector in which *eGFP* expression is driven by the RSV promoter and compared its ability to transduce nrCMCs, nrCFBs and rMSFs with that of AAV2/2.hEF1α.eGFP.WHVPRE.synpA and of AAV2/2mt.hEF1α.eGFP.WHVPRE.synpA. Both nrCFBs and rMSFs were poorly transduced by AAV2/9.RSV.eGFP.WHVPRE.synpA (Figure 5B, C) while this vector greatly outperformed the wild-type and tyrosine-mutant AAV2/2 vector in purified nrCMC cultures (Figure 5D). Substitution of the surface-exposed tyrosine residues at amino acid positions 444, 500 and 730 in the VP1 protein of AAV2/2.hEF1α.eGFP.WHVPRE.synpA yielded 3.9-, 6.1- and 3.6-fold higher transduction levels (in terms of mean eGFP signals) in nrCFBs, rMSFs and nrCMCs (Figure 5B, C and D). The presence in purified nrCMC cultures of 5-10% nrCFBs allowed us to compare in single cultures the efficiency with which both cell types could be transduced by AAV2/2.hEF1α.eGFP.WHVPRE.synpA, AAV2/2mt.hEF1α.eGFP.WHVPRE.synpA or AAV2/9.RSV.eGFP.WHVPRE.synpA through immunostaining for the cardiomyocyte marker α-actinin together with direct eGFP

fluorescence recordings. This experiment confirmed the preferential transduction of cardiac fibroblasts by the AAV2/2 vectors (Figure 6A, B, D and E) and of cardiomyocytes by AAV2/9.RSV.eGFP.WHVPRE.synpA (Figure 6C, F). It also illustrates the increased gene transfer activity of the AAV vectors with the tyrosine mutant AAV2 capsids in comparison to those possessing the wild-type AAV2 capsids (compare the green fluorescence intensity of the α-actinin-negative cell in Figure 6A with that of the α-actinin-negative cell in Figure 6B). Moreover, selectivity for nrCFBs was higher for the AAV2/2 vector with the mutant capsid (Figure 6D, E). These data were supported by western blot analyses (data not shown). Collectively, our results demonstrate that through rational design it is possible to make AAV vectors for the preferential transduction of cardiac (myo)fibroblasts or cardiomyocytes and provide a basis for determining the transduction profiles of AAV2/2(mt).hEF1α.eGFP.WHVPRE.synpA and AAV2/9.RSV.FP650.WHVPRE.synpA in infarcted rat hearts.

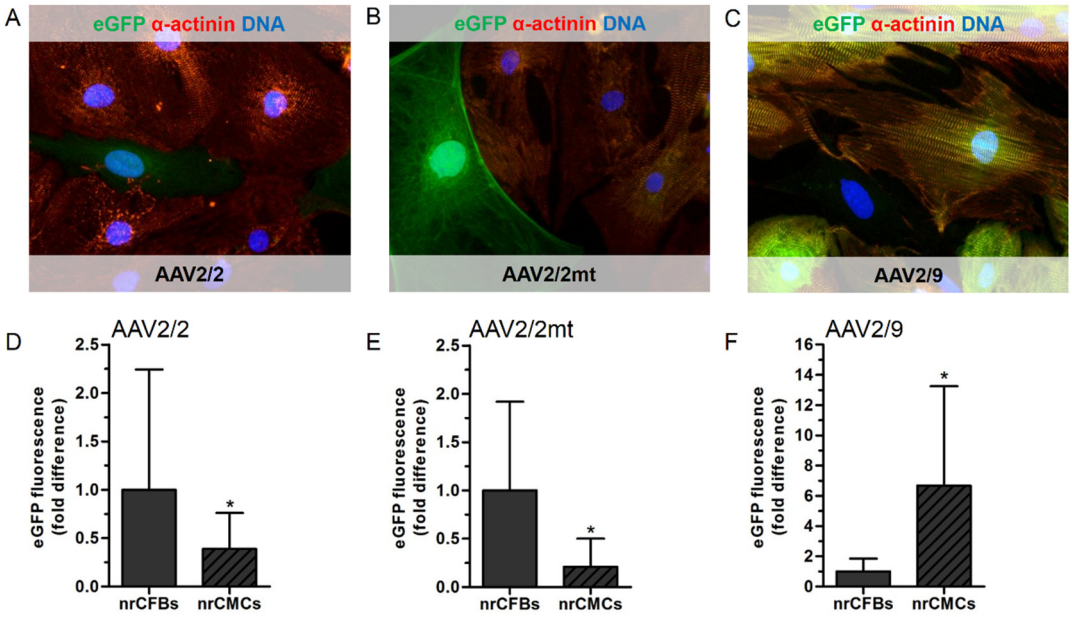

Figure 6. *(A-C) Representative fluoromicrographs of (A) AAV2/2.hEF1α.eGFP.WHVPRE.synpA (AAV2/2)-, (B) AAV2/2mt.hEF1α.eGFP.WHVPRE.synpA (AAV2/2mt)- and (C) AAV2/9.RSV.eGFP.WHVPRE.synpA (AAV2/9)-transduced cultures of nrCMCs containing endogenous nrCFBs. The cells were fixed at 7 days post transduction and stained for α-actinin to discriminate nrCMCs from nrCFBs and with Hoechst 33342 to visualize cell nuclei. (D-F) Quantification of the eGFP signal per cell type in nrCMCs containing endogenous nrCFBs following their transduction with 10^5 GCs/cell of (D) AAV2/2.hEF1α.eGFP.WHVPRE.synpA (AAV2/2), (E) AAV2/2mt.hEF1α.eGFP.WHVPRE.synpA (AAV2/2mt) or (F) AAV2/9.RSV.eGFP.WHVPRE.synpA (AAV2/9). The mean eGFP signal in nrCFBs was set to 1. *:P<0.05 vs. nrCFB.*

Discussion

The aim of this study was to develop AAV vectors conferring MSF-specific transgene expression. To this purpose, nine different promoters were tested for their activity in MSFs and cardiomyocytes. Furthermore, five distinct AAV vector pseudotypes were assessed for the efficiency with which they transduce MSFs and cardiomyocytes. Of the AAV vectors showing sufficiently high absolute transduction levels the ones with capsids of AAV2 and a transgene driven by the hEF1α promoter resulted in most specific transgene expression in rMSFs compared to nrCMCs. In addition, we found that among the effective AAV vectors the one with AAV9 capsids and the RSV promoter was least specific for rMSFs and would therefore be ideal to use when nrCMCs but not rat cardiac (myo)fibroblasts are the preferential target.

Although recombinant baculovirus-based AAV vector production systems are rapidly gaining popularity[29], co-transfection of 293 cells or derivatives of these cells with an AAV vector shuttle plasmid containing the AAV ITRs, a construct encoding AAV Rep and Cap proteins and a plasmid providing adenovirus helper functions (e.g. pAd.ΔF6 or pAd Helper 4.1)[30,31] still represents the most common means of producing AAV vectors. The production of AAV vectors by plasmid transfections has been simplified by the development of packaging constructs such as pDG and later pDP1 and pDP3 to pDP6, in which the AAV *rep* and *cap* genes are combined with the *E2A*, *E4orf6* and *VAI* and *VAII* genes of adenovirus to provide in one plasmid all *trans*-acting functions that are required for efficient AAV vector production and that are not encoded by the producer cells. Similar packaging plasmids have thus far not been reported for the production of AAV vectors with capsids of more recently discovered serotypes. Since several studies comparing different AAV vector pseudotypes for their capability to transduce rodent hearts have shown that AAV2/8 and AAV2/9 vectors are superior compared to the other AAV vector pseudotypes that were tested[10,11,13,28], we constructed two pDG-based helper plasmids for the production of AAV2 vectors with capsids of AAV8 or AAV9. The yields of AAV vectors produced with these new helper plasmids are similar to those of AAV vectors produced using pDG or one of its previously constructed derivatives.[25] pDG8 and pDG9 may thus be useful to facilitate the production of AAV2/8 and AAV2/9 vectors in quantities sufficient for animal experiments.

Cardiac fibrosis or scar formation after MI negatively affect cardiac function and predispose the heart to the development of arrhythmias.[32] To treat the effects of cardiac fibrosis, the electrical properties of the MSFs may be genetically altered to either improve the conduction through these cells or to functionally uncouple them from the surrounding cardiomyocytes thus reducing the risk of early afterdepolarizations. Since coupling between cardiac (myo)fibroblasts and cardiomyocytes results in the partial depolarization

of the latter cells, it may also be beneficial to increase the resting membrane potential of the former cells. Alternatively, it may be possible to endow the MSFs with properties of cardiomyocytes by their genetic reprogramming with cardiac transcription factor genes. However, cardiac (myo)fibroblast-directed gene therapy may have a detrimental effect on the function of neighboring healthy cardiomyocytes when these cells become transduced in parallel. The gene delivery vectors to be used for this purpose should therefore ideally transduce cardiac (myo)fibroblasts with high specificity. Thus far, in papers about the transduction of the heart by AAV vectors, no distinction was made between cardiomyocytes and cardiac (myo)fibroblasts. In this study, we aimed to generate an AAV vector for the preferential transduction of MSFs in comparison to cardiomyocytes. Five distinct AAV vector pseudotypes were compared to determine which of them is most suited for the selective transduction of MSFs. Also, nine different promoters were tested for their transcriptional activity in MSFs versus nrCMCs. In rMSFs and mMSFs, the hEF1α promoter was superior to the other promoters tested, whereas in hMSFs the hCMV-IE promoter was most active. The high transcriptional activity of the hEF1α promoter in the rodent cells is in concurrence with a study by Smolenski et al., who showed by serial analysis of gene expression in mouse cardiac fibroblasts that the *hEF1α* transcript was the most abundant of all RNA polymerase II transcripts. It is conceivable that the rat or mouse EF1α promoter may even be more active in the rodent MSFs than the hEF1α promoter. This will, however, only be beneficial if these rodent promoters not also display an undesirable increase in transgene expression in the nrCMCs. The high and low activity of the RSV promoter in nrCMCs and rat cardiac (myo)fibroblasts, respectively, is consistent with previous findings[33] and suggests that this promoter is very useful to induce high-level transgene expression in cardiomyocytes but not in cardiac (myo)fibroblasts. The fibroblast-specific promoters that were tested displayed only very low activity in the rodent MSFs. Possibly, crucial cis-acting signals and enhancer sequences are missing from these promoters, which had to be kept short due to the limiting packaging capacity of the AAV capsid. A challenge for future research would therefore be to construct a small but strong fibroblast-specific promoter.

Comparison of five different AAV vector pseudotypes showed that only AAV2/2 vectors transduce rMSFs efficiently, whereas cardiomyocytes are best transduced by AAV2/2, AAV2/6 and AAV2/9 vectors. The only other study that investigated the transduction by AAV vectors of cardiac fibroblasts and cardiomyocytes separately yielded similar results, although AAV2/6 vectors were not tested in that study[13]. Since the goal of the aforementioned study was to identify an AAV vector pseudotype that displayed a preferential tropism for cardiomyocytes, they did not investigate other ways to achieve cardiomyocyte-specific transgene expression. However, our findings and those of Qi et al. show that AAV2/2 vectors, whilst being the only option to efficiently transduce MSFs, also targets nrCMCs. Thus, in order to obtain specific transgene expression in MSFs multiple

targeting strategies need to be combined. The combination of transductional and transcriptional targeting to preferentially transduce either rMSFs or nrCMCs was tested with AAV2/2 vectors expressing *eGFP* under control of the hEF1α promoter and with AAV2/9 vectors expressing *eGFP* under control of the RSV promoter. The results indeed show some degree of specificity for rMSF of the AAV2/2.hEF1α.eGFP.WHVPRE.synpA vector that can be attributed to the differential promoter activity. The vector AAV2/9.RSV.eGFP.WHVPRE.synpA, which was designed for the selective transduction of cardiomyocytes, showed a more pronounced difference in transgene expression between rMSFs and nrCMCs, which is due to the combination of both transductional and transcriptional targeting. Ideally, we would like to target the rMSFs with the same level of specificity as the nrCMCs. This may be achieved by incorporating cardiomyocyte-specific microRNA target sites into the untranslated region(s) of the transcripts encoded by the transgene whose expression should occur in cardiac (myo)fibroblasts but not in cardiomyocytes.[34] This method exploits the naturally occurring microRNA-based gene regulatory mechanisms of cells to posttranscriptionally silence expression of genes that contain the target sequence of such a microRNA in their mRNAs. Selective suppression of transgene expression in cardiac muscle cells depends on the identification of cardiomyocyte-specific microRNAs. MicroRNA-1, -133, -206 and -208 may all qualify for this purpose as they have been shown to be (cardiac) muscle cell-specific.[35,36]

Another interesting finding of this study is the difference in the capability of AAV vectors to transduce MSFs from different species. This may be caused by many factors including differences in receptor availability or amino acid sequence or differences in the fate of the vector particles after cellular uptake. In a recent study, Bhrigu and Trempe showed that nuclear entry of AAV2 particles is impaired in murine fibroblasts as compared to that in human cervical carcinoma cells.[37] Furthermore, it was shown that tyrosine-mediated ubiquitination and subsequent proteasomal degradation of internalized AAV particles limits the transduction of cells by AAV2 vectors.[38] Mutation of three tyrosines in the AAV2 capsid into phenylalanines greatly reduced the susceptibility of AAV2/2 vectors to proteasomal degradation and caused a 130-fold increase in transgene expression in mouse fibroblasts transduced with these vectors.[39] These results indicate that it might be beneficial to equip the MSF-specific AAV2/2 vectors with AAV2 capsids containing the three tyrosine-to-phenylalanine substitutions. In addition to increasing gene transfer to both nrCMCs and nrCFBs, our study shows that these capsid mutations also improved the specificity of transduction of cardiac fibroblasts, as the difference in transduction level between nrCMCs and nrCFBs was bigger for the tyrosine mutant AAV2/2 vector than for the wild type AAV2/2 vector. Such selectivity may be beneficial for situations where genetic modification of just one cardiac cell type is desirable.

In conclusion, this study showed that in order to efficiently transduce cardiac (myo)fibroblasts with AAV vectors, an AAV2/2 vector containing a transgene driven by the hEF1α promoter should be used. In addition, in nrCMCs the highest transgene levels are obtained using an AAV2/9 vector that has the RSV promoter to drive the transgene. In the absence of a strong, small-sized fibroblast-specific promoter, some level of specificity for MSFs can be obtained by a combination of transductional and transcriptional targeting, but other (e.g. microRNA-based) targeting principles should be added to achieve truly MSF-specific transgene expression in rMSFs. Our optimized AAV vectors should next be tested *in vivo* to confirm our *in vitro* findings.

Acknowledgments
We thank Joost Verhaagen and Erich Ehlert for sharing their knowledge on the production of AAV vectors.

References

1. Chaturvedi RR, Herron T, Simmons R, Shore D, Kumar P, Sethia B, Chua F, Vassiliadis E, Kentish JC. Passive stiffness of myocardium from congenital heart disease and implications for diastole. *Circulation*. 2010;121:979-988.

2. Spach MS and Boineau JP. Microfibrosis produces electrical load variations due to loss of side-to-side cell connections: a major mechanism of structural heart disease arrhythmias. *Pacing Clin Electrophysiol*. 1997;20:397-413.

3. Abdel-Latif A, Bolli R, Tleyjeh IM, Montori VM, Perin EC, Hornung CA, Zuba-Surma EK, Al-Mallah M, Dawn B. Adult bone marrow-derived cells for cardiac repair: a systematic review and meta-analysis. *Arch Intern Med*. 2007;167:989-997.

4. Gyongyosi M, Lang I, Dettke M, Beran G, Graf S, Sochor H, Nyolczas N, Charwat S, Hemetsberger R, Christ G, Edes I, Balogh L, Krause KT, Jaquet K, Kuck KH, Benedek I, Hintea T, Kiss R, Preda I, Kotevski V, Pejkov H, Zamini S, Khorsand A, Sodeck G, Kaider A, Maurer G, Glogar D. Combined delivery approach of bone marrow mononuclear stem cells early and late after myocardial infarction: the MYSTAR prospective, randomized study. *Nat Clin Pract Cardiovasc Med*. 2009;6:70-81.

5. Krause K, Jaquet K, Schneider C, Haupt S, Lioznov MV, Otte KM, Kuck KH. Percutaneous intramyocardial stem cell injection in patients with acute myocardial infarction: first-in-man study. *Heart*. 2009;95:1145-1152.

6. Assmus B, Rolf A, Erbs S, Elsasser A, Haberbosch W, Hambrecht R, Tillmanns H, Yu J, Corti R, Mathey DG, Hamm CW, Suselbeck T, Tonn T, Dimmeler S, Dill T, Zeiher AM, Schachinger V. Clinical outcome 2 years after intracoronary administration of bone

marrow-derived progenitor cells in acute myocardial infarction. *Circ Heart Fail*. 2010;3:89-96.

7. Gnecchi M, Zhang Z, Ni A, Dzau VJ. Paracrine mechanisms in adult stem cell signaling and therapy. *Circ Res*. 2008;103:1204-1219.

8. van Tuyn J, Knaan-Shanzer S, van de Watering MJ, de GM, van der Laarse A, Schalij MJ, van der Wall EE, de Vries AA, Atsma DE. Activation of cardiac and smooth muscle-specific genes in primary human cells after forced expression of human myocardin. *Cardiovasc Res*. 2005;67:245-255.

9. Chu D, Sullivan CC, Weitzman MD, Du L, Wolf PL, Jamieson SW, Thistlethwaite PA. Direct comparison of efficiency and stability of gene transfer into the mammalian heart using adeno-associated virus versus adenovirus vectors. *J Thorac Cardiovasc Surg*. 2003;126:671-679.

10. Palomeque J, Chemaly ER, Colosi P, Wellman JA, Zhou S, Del MF, Hajjar RJ. Efficiency of eight different AAV serotypes in transducing rat myocardium in vivo. *Gene Ther*. 2007;14:989-997.

11. Bish LT, Morine K, Sleeper MM, Sanmiguel J, Wu D, Gao G, Wilson JM, Sweeney HL. Adeno-associated virus (AAV) serotype 9 provides global cardiac gene transfer superior to AAV1, AAV6, AAV7, and AAV8 in the mouse and rat. *Hum Gene Ther*. 2008;19:1359-1368.

12. Zincarelli C, Soltys S, Rengo G, Koch WJ, Rabinowitz JE. Comparative cardiac gene delivery of adeno-associated virus serotypes 1-9 reveals that AAV6 mediates the most efficient transduction in mouse heart. *Clin Transl Sci*. 2010;3:81-89.

13. Qi Y, Liu X, Li H, Shenoy V, Li Q, Hauswirth WW, Sumners C, Katovich MJ. Selective tropism of the recombinant adeno-associated virus 9 serotype for rat cardiac tissue. *J Gene Med*. 2010;12:22-34.

14. Grimm D, Kern A, Rittner K, Kleinschmidt JA. Novel tools for production and purification of recombinant adenoassociated virus vectors. *Hum Gene Ther*. 1998;9:2745-2760.

15. Li L, Hessel M, van d, V, Bax M, van dL, I, van der Laarse A. Partial and delayed release of troponin-I compared with the release of lactate dehydrogenase from necrotic cardiomyocytes. *Pflugers Arch*. 2004;448:146-152.

16. van Tuyn J, Pijnappels DA, de Vries AA, de V, I, van der Velde-van Dijke, Knaan-Shanzer S, van der Laarse A, Schalij MJ, Atsma DE. Fibroblasts from human

postmyocardial infarction scars acquire properties of cardiomyocytes after transduction with a recombinant myocardin gene. *FASEB J*. 2007;21:3369-3379.

17. DuBridge RB, Tang P, Hsia HC, Leong PM, Miller JH, Calos MP. Analysis of mutation in human cells by using an Epstein-Barr virus shuttle system. *Mol Cell Biol*. 1987;7:379-387.

18. He TC, Zhou S, da Costa LT, Yu J, Kinzler KW, Vogelstein B. A simplified system for generating recombinant adenoviruses. *Proc Natl Acad Sci U S A*. 1998;95:2509-2514.

19. Yue Y and Dongsheng D. Development of multiple cloning site cis-vectors for recombinant adeno-associated virus production. *Biotechniques*. 2002;33:672, 674, 676-672, 674, 678.

20. Levitt N, Briggs D, Gil A, Proudfoot NJ. Definition of an efficient synthetic poly(A) site. *Genes Dev*. 1989;3:1019-1025.

21. Okada H, Danoff TM, Fischer A, Lopez-Guisa JM, Strutz F, Neilson EG. Identification of a novel cis-acting element for fibroblast-specific transcription of the FSP1 gene. *Am J Physiol*. 1998;275:F306-F314.

22. Szulc J, Wiznerowicz M, Sauvain MO, Trono D, Aebischer P. A versatile tool for conditional gene expression and knockdown. *Nat Methods*. 2006;3:109-116.

23. Sandford GR and Burns WH. Rat cytomegalovirus has a unique immediate early gene enhancer. *Virology*. 1996;222:310-317.

24. Ruitenberg MJ, Eggers R, Boer GJ, Verhaagen J. Adeno-associated viral vectors as agents for gene delivery: application in disorders and trauma of the central nervous system. *Methods*. 2002;28:182-194.

25. Grimm D, Kay MA, Kleinschmidt JA. Helper virus-free, optically controllable, and two-plasmid-based production of adeno-associated virus vectors of serotypes 1 to 6. *Mol Ther*. 2003;7:839-850.

26. Auricchio A, Hildinger M, O'Connor E, Gao GP, Wilson JM. Isolation of highly infectious and pure adeno-associated virus type 2 vectors with a single-step gravity-flow column. *Hum Gene Ther*. 2001;12:71-76.

27. Collaco RF, Cao X, Trempe JP. A helper virus-free packaging system for recombinant adeno-associated virus vectors. *Gene*. 1999;238:397-405.

28. Wang Z, Zhu T, Qiao C, Zhou L, Wang B, Zhang J, Chen C, Li J, Xiao X. Adeno-associated virus serotype 8 efficiently delivers genes to muscle and heart. *Nat Biotechnol*. 2005;23:321-328.

29. Galibert L and Merten OW. Latest developments in the large-scale production of adeno-associated virus vectors in insect cells toward the treatment of neuromuscular diseases. *J Invertebr Pathol*. 2011;107 Suppl:S80-S93.

30. Gao GP, Alvira MR, Wang L, Calcedo R, Johnston J, Wilson JM. Novel adeno-associated viruses from rhesus monkeys as vectors for human gene therapy. *Proc Natl Acad Sci U S A*. 2002;99:11854-11859.

31. Sandalon Z, Bruckheimer EM, Lustig KH, Rogers LC, Peluso RW, Burstein H. Secretion of a TNFR:Fc fusion protein following pulmonary administration of pseudotyped adeno-associated virus vectors. *J Virol*. 2004;78:12355-12365.

32. van der Burg AE, Bax JJ, Boersma E, Pauwels EK, van der Wall EE, Schalij MJ. Impact of viability, ischemia, scar tissue, and revascularization on outcome after aborted sudden death. *Circulation*. 2003;108:1954-1959.

33. Maass A, Langer SJ, Oberdorf-Maass S, Bauer S, Neyses L, Leinwand LA. Rational promoter selection for gene transfer into cardiac cells. *J Mol Cell Cardiol*. 2003;35:823-831.

34. Brown BD and Naldini L. Exploiting and antagonizing microRNA regulation for therapeutic and experimental applications. *Nat Rev Genet*. 2009;10:578-585.

35. Callis TE, Chen JF, Wang DZ. MicroRNAs in skeletal and cardiac muscle development. *DNA Cell Biol*. 2007;26:219-225.

36. van RE, Sutherland LB, Qi X, Richardson JA, Hill J, Olson EN. Control of stress-dependent cardiac growth and gene expression by a microRNA. *Science*. 2007;316:575-579.

37. Bhrigu V and Trempe JP. Adeno-associated virus infection of murine fibroblasts with help provided by mouse adenovirus. *Virology*. 2009;390:22-30.

38. Zhong L, Li B, Mah CS, Govindasamy L, Agbandje-McKenna M, Cooper M, Herzog RW, Zolotukhin I, Warrington KH, Jr., Weigel-Van Aken KA, Hobbs JA, Zolotukhin S, Muzyczka N, Srivastava A. Next generation of adeno-associated virus 2 vectors: point mutations in tyrosines lead to high-efficiency transduction at lower doses. *Proc Natl Acad Sci U S A*. 2008;105:7827-7832.

39. Li M, Jayandharan GR, Li B, Ling C, Ma W, Srivastava A, Zhong L. High-efficiency transduction of fibroblasts and mesenchymal stem cells by tyrosine-mutant AAV2 vectors for their potential use in cellular therapy. *Hum Gene Ther*. 2010;21:1527-1543.

Cellular and Molecular Mechanisms of Arrhythmias in Cardiac Fibrosis and Beyond:
From Symptoms to Substrates towards Solutions

Chapter IX

Summary, Conclusions, Discussion and Future Perspectives

Summary

The general introduction of this thesis described the basic mechanisms of cardiac electrophysiology and how these relate to arrhythmias. Furthermore, the current anti-arrhythmic treatments were discussed and while these strategies are effective, it can be concluded that the efficacy of these strategies may be optimized. This suboptimal efficacy may be due to our incomplete understanding of pro-arrhythmic mechanisms, which are often due to structural heart disease that forms pro-arrhythmic substrates. Due to the complexity of such substrates, its components need to be dissected and studied in detail using *in vitro* and *in vivo* models. The aim of this thesis was therefore to investigate cellular and molecular pro-arrhythmic mechanisms in *in vitro* models of pro-arrhythmic substrates such as fibrosis and hypertrophy and provide and expand a mechanistic basis for future, substrate-oriented anti-arrhythmic strategies.

Chapter II investigated the anti-arrhythmic effects of anti-proliferative treatment of myofibroblasts (MFBs) in cardiac cultures. MFB proliferation is a prominent feature of cardiac fibrosis. As cardiac fibrosis is strongly associated with arrhythmias, this study tested the hypothesis that anti-proliferative treatment of MFBs may yield anti-arrhythmic effects. For this purpose, neonatal rat myocardial cultures were treated with mitomycin-C or paclitaxel at day 1 of culture to inhibit proliferation of endogenously present MFBs. Cardiac cell cultures were kept in culture for 9 days, and electrophysiologically evaluated at day 4 and 9 using optical mapping and patch-clamp. Antiproliferative agents did not significantly increase apoptosis at the used dosages and kept MFB content stable throughout the culturing period by limiting their proliferative capacity. While free MFB proliferation progressively slowed conduction between day 4 and 9 (from 15.3±3.5 cm/s to 8.8±0.3 cm/s, $P<0.05$), conduction velocity (CV) was higher and stable throughout the culturing period in cultures that received anti-proliferative treatment. Of fibrotic cultures with high amounts of fibroblasts, 81% showed spontaneous reentrant arrhythmias, whereas 3% of mitomycin-C treated and 5% of paclitaxel-treated cultures showed arrhythmias. Importantly, culture arrhythmogeneity was found to depend on drug-dose and was thereby dependent on the quantity of MFBs. Investigation by patch-clamp experiments revealed that by anti-proliferative treatment of MFBs, cardiomyocytes (CMCs) were less depolarized and more excitable. This study may therefore provide a rationale for future preventive anti-arrhythmic strategies for fibrosis-associated arrhythmias.

In Chapter III, the anti-arrhythmic effect of down regulating heterocellular coupling between CMCs and MFBs was evaluated. For this purpose, shRNA's directed against Cx43 were expressed in MFBs using a lentiviral vector. In MFB-CMC co-cultures with Cx43 knockdown, conduction was faster (16.0±3.2 cm/s vs. 10.6±4.6, $P<0.05$) and action potential duration was shorter. Moreover, the incidence of ectopic activity and spontaneous reentry was significantly lowered by reducing heterocellular coupling. In line with these findings, CMCs were less depolarized in fibrotic co-cultures by reducing heterocellular coupling (-61.4±5.7 mV vs. 51.6±4.0 mV). This depolarization was identified as a key pro-arrhythmic factor, as reintroducing depolarization of the membrane by I_{k1} inhibition with $BaCl_2$ or by increasing extracellular $[K^+]$ rendered the anti-arrhythmic potential of heterocellular uncoupling ineffective. In conclusion, this study showed that MFB-induced depolarization is highly pro-arrhythmic, and that MFB-CMC coupling is a major mechanism of such depolarization.

Chapter IV evaluated differences between pro-arrhythmic mechanisms of fibrosis and hypertrophy *in vitro*, because while arrhythmias are often found in remodeled hearts, discerning between hypertrophy- or fibrosis-associated mechanisms is virtually impossible *in vivo*, although differences in pro-arrhythmic mechanisms may hold relevance for the anti-arrhythmic potential of interventions. Therefore, neonatal rat myocardial cultures were exposed to phenylephrine to induce hypertrophy, or exhibited free MFB proliferation to mimic fibrosis. Interestingly, arrhythmic findings were highly similar, with similar slowing of conduction and repolarization in both groups. Also, incidences of focal arrhythmias (based on early afterdepolarizations) and reentrant arrhythmias were similarly increased in hypertrophic and in fibrotic cultures. However, further investigation revealed differences in their pro-arrhythmic mechanisms. Protein expression levels of Kv4.3 and Cx43 were decreased in hypertrophy but unaffected in fibrosis. Targeting heterocellular coupling by administration of low doses of gap-junctional uncoupling agents was only anti-arrhythmic in fibrotic cultures, whereas l-type calcium channel blockade prevented arrhythmias in hypertrophy, but caused conduction block in fibrosis. These findings provide novel insight into how distinct substrate-specific pro-arrhythmic mechanisms may give rise to similar phenotypical arrhythmicity, and how this might affect therapeutic efficacy.

Chapter V investigated mechanisms that underlie sustained ventricular fibrillation, which is maintained by multiple stable rotors that are difficult to terminate. The aim of this study was to correlate changes in arrhythmia complexity with changes in

specific electrophysiological parameters. This approach would allow for the identification of novel factors and underlying mechanisms that affect the stability of sustained fibrillation and thereby the efficacy of anti-fibrillatory interventions. For this purpose, a novel *in vitro* model of fibrillation was developed that allowed a dose-dependent increase in fibrillatory complexity using the gap-junctional uncoupler 2-aminoethoxydiphenyl borate (2-APB). Arrhythmia complexity in cardiomyocyte cultures increased with increasing dosages of 2-APB (n > 38), leading to sustained VF: 0.0 ± 0.1 phase singularities/cm^2 in controls vs. 0.0 ± 0.1, 1.0 ± 0.9, 3.3 ± 3.2, 11.0 ± 10.1, and 54.3 ± 21.7 in 5, 10, 15, 20, and 25 µmol/L 2-APB, respectively. Arrhythmia complexity inversely correlated with wavelength. Lengthening of wavelength during fibrillation could only be induced by agents ($BaCl_2$/BayK8644) increasing the action potential duration (APD) at maximal activation frequencies (minimal APD); 123 ± 32%/117 ± 24% of control. Minimal APD prolongation led to transient VF destabilization, shown by critical wave front collision leading to rotor termination, followed by significant decreases in VF complexity and activation frequency (52%/37%). Interestingly, these key findings were reproduced *ex vivo* in adult rat hearts (n=6 per group). These results show that stability of sustained fibrillation is highly regulated by the minimal APD. Minimal APD prolongation leads to transient destabilization of fibrillation, ultimately decreasing VF complexity and thereby provides novel insights into anti-fibrillatory mechanisms.

Chapter VI explored the effects of stem cell engraftment on pro-arrhythmic risk. Due to low engraftment rates, the current paradigm for stem cell therapy is to increase engraftment rate to increase its therapeutic effects. However, it is unknown whether increasing the stem cell engraftment rate also increases the risk of pro-arrhythmic effects of stem cell therapy. Moreover, stem cell engraftment patterns are difficult to regulate *in vivo*. To investigate the pro-arrhythmic mechanisms of stem cell therapy, human mesenchymal stem cells (hMSCs) were seeded in co-culture with neonatal rat cardiomyocytes in a quantity of 7% or 28% in a diffuse or clustered pattern, after which electrophysiology was evaluated by optical mapping and patch-clamp experiments at day 9 of culture. Interestingly, in diffuse co-cultures, hMSCs dose-dependently slowed conduction and increased APD. Conduction slowing was shown to be dependent on heterocellular gap-junctional coupling, as partial uncoupling increased CV, but did not affect APD. As hMSCs did not express α-smooth muscle actinin or n-cadherin, mechanical heterocellular coupling did not appear to play a significant pro-arrhythmic role. Triggered activity and inducibility of reentry were dose-dependently increased by diffuse hMSC engraftment. For clustered hMSC engraftment, conduction slowing and APD prolongation were locally observed.

Moreover, only reentry inducibility was dose-dependently increased while triggered activity was not observed with clustered engraftment. Transwell experiments revealed that the hMSC secretome dose-dependently increased APD, APD dispersion and inducibility of reentry, while CV was unaffected. Interestingly, hMSC-derived exosomes did not yield any detectable effects on culture electrophysiology. These findings not only strongly illustrate the pro-arrhythmic potential of higher engraftment rates of hMSCs, but also show that the specific pro-arrhythmic effects are due to gap-junctional coupling and paracrine mechanisms. Thereby, this study provides cautionary data that may aid to prevent future adverse pro-arrhythmic effects of stem cell therapy when engraftment rate is increased beyond the therapeutic window.

Chapter VII investigated a novel method to counteract fibroblast arrhythmicity, as fibroblasts can be pro-arrhythmic due to their detrimental effects on cardiomyocyte electrophysiology through several mechanisms that rely on suboptimal integration into the cardiac syncytium. Therefore, the feasibility of forced cellular fusion between human ventricular scar cells (hVSCs) and nrCMCs as a potentially anti-arrhythmic strategy was explored. For this purpose, hVSC were isolated from human ventricular scars and co-cultured with nrCMCs in a 1:4 ratio. Prior to co-culture, these hVSCs were genetically modified with a lentiviral vector to express Vesicular-Stomatitis-G-protein- and eGFP that produces fusogenic hVSCs or solely eGFP (control hVSCs). Fusion was induced by brief exposure to acidic buffer (pH=6.0) at day 3 and electrophysiological effects of fusion were evaluated at day 5 by optical mapping. Co-expression of fibroblast-specific collagen-I and nrCMC-specific α-actinin was observed in multinucleated cells that contained both human and rat nuclei, without increased apoptosis as judged by annexin V staining. These nrCMC-hVSC hybrids retained sarcomeric α-actinin expression and remained contractile, while vimentin expression in nrCMC-hVSC hybrids was lower than in non-fused hVSCs. Moreover, Cx43 and Cav1.2 protein expression levels were increased in heterokaryons compared to unfused hVSCs. Importantly, the expression levels did not linearly correlate to the percentage of human nuclei in the heterokaryons. Fused cultures showed faster conduction (16.8±1.6 vs. 10.3±2.6 cm/s, $P<0.05$) and shorter action potential duration (328±56 vs. 480±70ms, $P<0.05$). Triggered activity and reentry were ameliorated by heterocellular fusion (incidences of 58%, n=12 vs. 0%, n=23 in fused co-cultures). The results of this study showed that heterocellular fusion between hVSCs and nrCMCs is feasible and well-tolerated as it forms excitable and contractile heterokaryons. Moreover, heterocellular fusion had a strong anti-arrhythmic effect in hVSC-nrCMC co-cultures. As the nrCMC phenotype appeared to

be relatively dominant within the heterokaryon, these results may provide novel insights in anti-arrhythmic reprogramming of fibroblasts.

Chapter VIII investigates viral vectors capable of selectively transducing myocardial scar fibroblasts (MSFs), as these cells may represent therapeutic targets due to their potentially detrimental effects on conduction. One way of modulating the properties of MSFs is by genetic modification with viral vectors. Among the currently used viral gene delivery vehicles, adeno-associated virus (AAV) vectors stand out for their *in vivo* safety and ability to spread easily through tissues. The aim of this study was to compare the transduction of nrCMCs and of human, mouse and rat MSFs by AAV vectors with different capsids and with transgenes driven by different promoters. For this purpose, vector shuttle plasmids containing a *LacZ* gene driven by 9 different promoters including the human, mouse and rat cytomegalovirus *immediate early* gene (CMV-IE) promoter were constructed. The AAV vector genomes specified by these plasmids were packaged in AAV serotype 2 (AAV2) capsids. β-galactosidase assays revealed that of all CMV-IE promoters, the human CMV-IE promoter outperformed the rodent CMV-IE promoters in human MSFs while the rodent CMV-IE promoters were more active in murine and rat MSFs. Furthermore, of all nine promoters tested the human *eukaryotic translation elongation factor 1 alpha 1* gene (hEF1α) promoter was most active in rodent MSFs while the Rous sarcoma virus (RSV) promoter gave the highest transgene expression in nrCMCs. A comparison of the transduction efficiency of rat MSFs and nrCMCs with AAV2 vectors carrying capsids of AAV serotypes 2, 5, 6, 8 and 9 showed that transduction of rat MSFs was most efficient with AAV2/2 vectors whereas AAV2/9 best transduced the nrCMCs. In conclusion, the highest transgene expression in rat MSFs is obtained by transduction with an AAV2/2 vector containing an hEF1α promoter-driven transgene while transgene expression in nrCMC is highest after transduction with an AAV2/9 vector in which foreign gene expression is controlled by the RSV promoter.

In conclusion, MFBs may represent a target for several anti-arrhythmic interventions in the context of cardiac fibrosis. By decreasing the proliferative capacity of MFBs, their numbers and thereby their dose-dependent pro-arrhythmic effects can be limited *in vitro*. However, as anti-proliferative treatment has the potential for serious systemic adverse side-effects, more specific targeting of MFB-induced depolarization can be considered preferable. One such approach was also investigated in this thesis, by limiting heterocellular coupling through genetic connexin43 knockdown in only

MFBs or pharmacological heterocellular uncoupling, which yielded significant anti-arrhythmic effects based on the pro-arrhythmic mechanism. Alternatively, it was shown that through heterocellular fusion, fibrotic co-cultures showed faster conduction, shorter action potential duration (APD) and lower arrhythmic incidence compared to unfused fibrotic co-cultures. Additionally, this thesis emphasizes the importance of targeting such substrate-specific mechanisms in its specific substrate by demonstrating that hypertrophic cultures do not benefit from the same anti-arrhythmic interventions as fibrotic cultures, despite their highly similar arrhythmicity. Instead, these cultures suffered from intrinsic electrical remodeling and benefited from other interventions. By targeting the key parameters of arrhythmias that are formed by the substrate, substantial anti-arrhythmic effects could be achieved in these models. This concept was expanded upon by showing that the minimal APD is the key parameter that determines arrhythmic complexity in an *in vitro* and *ex vivo* model of ventricular fibrillation. In addition, this thesis provides evidence for dose-dependent pro-arrhythmic mechanisms of MSC transplantation. Taken together, this thesis demonstrates multiple cellular and molecular arrhythmic mechanisms in several pro-arrhythmic substrates, and how these mechanisms may be targeted as an anti-arrhythmic intervention.

Discussion and Future Perspectives

In vitro *disease modeling and optimization of anti-arrhythmic treatment*

Although current anti-arrhythmic treatments are beneficial to the patient, the suboptimal efficacy of these strategies may be attributed to an incomplete understanding of the underlying pro-arrhythmic substrate (see the general introduction of this thesis). In clinical cardiology, this realization was responded upon with the Sicilian Gambit, a statement that recognizes the complexity of arrhythmias and the infeasibility of adequately treating different arrhythmias with the same drugs without understanding the arrhythmic mechanisms.[1] The Sicilian Gambit proposed the concept of the vulnerable parameter, which is the critical parameter to alter for optimal anti-arrhythmic effects.[2] To be able to investigate such parameters, basic research using *in vitro* and *in vivo* models to identify and modify pro-arrhythmic substrates is essential to improve upon our current knowledge and therapeutic efficacy of anti-arrhythmic drugs.[3] Such disease models are generally developed to allow for more standardized interpretation of results. For this purpose, most computer simulations and *in vitro* studies using monolayers simplify the 3-

dimensional cardiac structure into a 2-dimensional structure in which pro-arrhythmic mechanisms and features can be studied in greater detail. Due to the complexity of arrhythmias in 3-dimensional context, simplification by such 2-dimensional models facilitates the interpretation of data. Also, *in vitro* models typically facilitate a high degree of control over the experimental environment that allows isolating and investigating key components. By starting with a simplified disease model and then gradually increasing its complexity, not only can novel pro-arrhythmic mechanisms be uncovered that are difficult to investigate *in vivo*, but can these models also be extrapolated eventually to more relevant *in vivo* situations. An example of such a concept of a vulnerable parameter studied in a simplified model in this thesis is the minimal action potential duration (**Chapter V**), which determines the refractory state of tissue during fibrillation. In our 2-dimensional *in vitro* model of ventricular fibrillation that was induced by gap-junctional uncoupling, prolongation of the minimal APD showed a reduction of arrhythmic complexity, which was predicted by *in silico* studies. The mechanism of reducing the complexity of arrhythmias relied on transient destabilization of the arrhythmia, which could only be studied in detail in this model due to its relative simplicity. Moreover, by replicating the same model using adult rat hearts *ex vivo*, it was shown that the *in silico* and *in vitro* concept of prolonging the minimal APD remained relevant to the adult 3-dimensional situation. By increasing the complexity of the *in vivo* models to larger animals, these findings obtained in simplified models may ultimately prove to be relevant to the treatment of human ventricular fibrillation in the future.

In addition to the simplification of pro-arrhythmic substrates, *in vitro* models can also provide a platform that allows the study of substrates that normally coincide *in vivo* independently of each other to be able to distinguish between and elucidate their individual pro-arrhythmic mechanisms. An example of such an approach in this thesis was in the case of hypertrophy and fibrosis which often co-exist during cardiac remodeling.[4] Interestingly, it was found that the arrhythmogeneity of both substrates in separate conditions was highly similar. However, the underlying pro-arrhythmic mechanisms were distinct. These differences could implicate that each substrate may need different pro-arrhythmic treatment. However, regardless of the mechanistic insights such studies offer, it is important to stay vigilant of overstating the implications of *in vitro* models for *in vivo* situations as oversimplification of the *in vivo* situation can be a potential hazard of *in vitro* research. Therefore, it needs to be taken into account what the model represents and how this is achieved. In the current example, fibrosis was mimicked by extensive myofibroblast (MFB) proliferation, which is an established feature of fibrosis *in vivo* that even in the

absence of extensive extracellular matrix deposition produced a highly pro-arrhythmic model. Hypertrophy *in vitro* was achieved by treatment of CMCs with phenylephrine, an α1-agonist that is known to be involved in the induction of hypertrophy *in vivo*. However, hypertrophy may also be induced by other agents and *in vivo* is often a result of altered pressure and volume load in addition to hormonal changes. It is therefore difficult to determine where the *in vitro* hypertrophy fits in the scale of progressive hypertrophy and heart failure that is seen during cardiac remodeling *in vivo*. Due to the strong pro-arrhythmogeneity in this model of hypertrophy, it is likely that it represents an end-stage of hypertrophy, and may therefore hold relevance for the treatment of arrhythmias in the stage of heart failure. Ironically, at that stage of cardiac remodeling, fibrosis which can function as a pro-arrhythmic substrate independently of hypertrophy, is often also present as both hypertrophy and fibrosis are compensatory mechanisms against pressure overload. Furthermore, the extent of fibrosis and hypertrophy may differ between patients, and therefore the extent of the involvement of individual substrate-specific pro-arrhythmic mechanisms may play different roles for different patients in different stages of their structural heart disease. Besides the notion that the concomitance of these two substrates was the motivation behind the investigation of their individual pro-arrhythmic mechanisms, it may also be responsible for the choice of largely symptomatic anti-arrhythmic treatment due to the complexity it proposes. As both substrates were discovered to be equally pro-arrhythmic, treatment of one substrate may yield insufficient anti-arrhythmic effects due to the co-existence of another pro-arrhythmic substrate. Moreover, rather than attempting the complicated task of treating different pro-arrhythmic substrates in proportion to its presence in a heart at a given time, it may be more feasible to target common pro-arrhythmic features in the presence of multiple pro-arrhythmic substrates. In the example of our models of hypertrophy and fibrosis, pharmacologically targeting the common APD prolongation in such substrates may yield beneficial results. However, the complexity of combined arrhythmic substrates also emphasizes the need for more in-depth investigation of pro-arrhythmic substrates for the optimization of anti-arrhythmic drug regimes.

The concept of substrate-specific intervention fits within the surfacing paradigm of tailor-made patient care throughout the field of medicine, in which the complexity of disease is increasingly recognized and responded upon by the investigation and use of mechanism-specific interventions. For example, the realization of the complexity of not only arrhythmias but all human disease has motivated researchers to investigate to possibility of patient-specific drug screening using induced

pluripotent stem cells (iPS cells).[5] By genetically modifying somatic cells with several transcription factors, these cells dedifferentiate to an embryonic stem cell-like phenotype, and can subsequently be differentiated towards different patient-specific cell lineages including cardiomyocytes. Although the maturity and purity of iPS-derived cardiomyocytes remain an issue that needs to be overcome for its clinical relevance, this approach is promising throughout the field of biology.[6] Alternatively, efforts are being made to directly reprogram easily obtainable somatic cells towards CMCs.[7] Using such techniques, patient-derived cell types that are otherwise difficult to obtain such as CMCs can be cultured and tested for their response to specific drugs.[8] Thereby, optimal drug selection can be realized in a patient-specific manner, which may optimize therapeutic effects of pharmacological treatment. By combining this technique with already available *in vitro* models of different pro-arrhythmic substrates, our understanding of arrhythmias may one day be sufficient to pharmacologically treat all patients optimally through tailor-made patient-specific anti-arrhythmic drug regimes.

Targeting of the MFB in vivo *as an anti-arrhythmic strategy*

While drugs are often administered to treat arrhythmias, their efficacy is largely based on symptomatic alleviation. As a result, underlying pro-arrhythmic substrates such as structural heart disease are not modified despite the fact that they are a prominent cause of arrhythmias. Therefore, intrinsically changing the underlying pro-arrhythmic substrates by disease modifying drugs, genetic modification or cell therapy may lead to more optimal and longer lasting results than pharmacological treatment. In the case of fibrosis, myofibroblasts (MFBs) have been gaining interest in recent years as potential key players in fibrosis-associated arrhythmias. Initially thought to be a rather quiescent cell type that maintained the extracellular matrix, the discovery of MFBs functionally coupling to CMCs has implicated these cells in the context of fibrosis-associated arrhythmias.[9] Since then, heterocellular coupling between CMCs and MFBs has been shown to dose-dependently slow conduction,[10] increase ectopic activity[11] and increase the propensity towards reentrant arrhythmias.[12] While these *in vitro* results provide promising concepts that further improve our understanding of arrhythmias and are supported by *in silico* simulations,[13] translation to *in vivo* experiments is expectedly more difficult. As a result, the clinical relevance of such findings is a predictable subject of debate. An example of such a discussion is about the clinical relevance of heterocellular coupling between MFBs and CMCs, which has not been clearly demonstrated *in vivo* yet.[14-16] Functional coupling between administered cells that have been genetically labeled

and native myocardium has been demonstrated *in vivo*,[17] but to unequivocally establish functional coupling between natively present and therefore unlabeled cell types is more difficult to realize from a technical standpoint. Furthermore, although proving functional coupling *in vivo* is technically challenging, it is per definition more challenging to provide compelling evidence that disproves the existence of such mechanisms. Further complicating the matter of MFB-induced arrhythmogeneity is the notion that MFBs may also exert pro-arrhythmic effects through mechanical coupling and paracrine mechanisms.[18,19] As this is in line with the only partial recovery of electrophysiological health after reducing heterocellular coupling *in vitro* (**Chapter III**), this suggests that perhaps the entire phenotype of the MFB itself needs to be targeted instead of targeting all of its individual pro-arrhythmic mechanisms to alleviate fibrosis-associated arrhythmias *in vivo*. Moreover, an intervention that targets MFBs as a whole may also affect extracellular matrix deposition, a feature that is still considered of paramount importance in the pro-arrhythmogeneity of fibrosis *in vivo*, but remains difficult to properly investigate *in vitro*.[20] A potentially feasible approach of targeting the whole of MFB arrhythmogeneity was demonstrated in Chapter II, in which inhibition of MFB proliferation yielded strong anti-arrhythmic effects. Since MFBs can be expected to exert their pro-arrhythmic effects in a dose-dependent manner, decreasing their numbers indirectly lowers the effects of all their combined pro-arrhythmic mechanisms. Limiting proliferative capacity of MFBs has been shown to prevent excessive scar formation in non-cardiac tissue by also limiting extracellular matrix deposition.[21] Expectedly, evidence is surfacing that such a strategy may also yield anti-arrhythmic effects *in vivo*. [22,23] However, pharmacologic agents that inhibit proliferation are notorious for side-effects due to their often systemic administration and unwanted binding affinity to off-target molecules. The technical advantages that genetic modification can offer over pharmacological treatment are important, such as longer-lasting effects and reduced side-effects by selectively targeting specific cell and tissue types using cell type specific promoters and viruses with tissue-specific tropisms. As a result, interventions that alter the behavior of MFBs may be preferentially delivered through genetic modification. For instance, by reducing expression of myocardin-related transcription factor-a, myofibroblast activation is limited and as a result, the pro-fibrotic response of these cells is strongly diminished *in vivo*.[24]

A similar anti-arrhythmic approach that targets the entire MFB is cellular reprogramming, that aims to force MFBs to act like a cell type that is less detrimental to cardiac function, such as stem cells or even CMCs. Initially realized by nuclear reprogramming,[25] cellular reprogramming of MFBs into stem cells or cardiomyocytes

can now be realized by genetic modifications with a few transcription factors, although this approach is still considered rather inefficient.[7] In this context, forced heterocellular fusion as investigated in this thesis may provide a future alternative route of anti-arrhythmic MFB reprogramming, as fusion can effectively be used to genetically reprogram cells.[25] Alternatively, MFBs can be genetically modified to electrically resemble a CMC by forcing expression of the gap-junctional protein connexin43 and the ion channels kir2.1 and nav1.5, which also yields expectable anti-arrhythmic effects.[26,27] A novel and refined method of genetic modification is found in the field of optogenetics, which allows for the regulation of transgene activity by exposure to light. Recently, optical control of even protein activity was demonstrated.[28] Such delicate approaches allow precise direction and timing of the genetic intervention of choice, which due to the complexity of arrhythmic substrates, may be a powerful tool to investigate and targeting pro-arrhythmic mechanisms. Based on the light-sensitive rhodopsins, optogenetics has already been shown to be a powerful technique in the field of neurology and may be used to modify the electrical behavior of cardiomyocytes or fibroblasts as a future anti-arrhythmic strategy.[29] Regardless of the way in which MFBs will be targeted in future *in vivo* studies, the advances in our understanding of their detrimental effects and advances in biological technology are likely to provide novel mechanistic insights into new anti-arrhythmic strategies for the foreseeable future, which may ultimately result in optimal substrate-oriented treatment of fibrosis-associated arrhythmias.

Modifying a substrate beyond its pro-arrhythmic mechanisms as the ultimate anti-arrhythmic strategy

The idea of looking more closely at certain phenomena as the best way to uncover their mechanisms, has been widely incorporated into science since the invention of the microscope. As stated above, targeting of pro-arrhythmic mechanisms is considered necessary to more adequately treat arrhythmias in the future. Therefore, more profound experiments that investigate deeper underlying pro-arrhythmic experiments remain necessary to understand arrhythmias to their finest details. However, the vastly expanding knowledge of different pro-arrhythmic mechanisms may indicate that the complexity of treating pro-arrhythmic mechanisms in all substrates may be too high to realize optimal anti-arrhythmic treatments in the near future. Due to the currently expanding epidemic of atrial fibrillation and structural cardiac disease, there is a need for timely action against pro-arrhythmic substrates. In addition, while targeting of pro-arrhythmic mechanisms of individual substrates

such as fibrosis and hypertrophy may ultimately lead to the optimized treatment of arrhythmias, these pro-arrhythmic substrates are often also associated with decreased mechanical cardiac functionality which in turn may lead to systemic co-morbidity such as emboli and fatigue. While cardiac hypertrophy is a (mal)adaptive response aimed to increase cardiac output, cardiac fibrosis is a response to pressure overload to maintain structural integrity of the heart. As a result, both contractility and myocardial compliance or stiffness are affected. Importantly, cardiac stiffness itself can have pro-arrhythmic consequences. Therefore, targeting of the entire structural substrate may be necessary to alleviate all arrhythmogeneity it is associated with. Regenerative medicine with the use of stem cell therapy is such a strategy that is considered to positively modify and even reverse multiple aspects of structural heart disease and may therefore yield anti-arrhythmic effects at a level upstream of pro-arrhythmic mechanisms. Initially, the rationale behind cardiac stem cell therapy initially was to administer cells capable of cardiomyogenic differentiation to fibrotic myocardium to replenish the loss of excitable cells to counteract arrhythmias. However, the differentiation potential of such cells remains disappointingly low.[30] In recent years, the basis of the small but significant therapeutic effect of stem cell therapy is considered to be mostly based on its paracrine effects that modify structural heart disease.[31] Due to low engraftment rates, the current aim in stem cell research is to increase the therapeutic efficacy by increasing engraftment rates by a variety of strategies that involve tissue engineering and genetically or magnetically modifying cells.[32-34] However, as demonstrated in this thesis, such strategies may invoke its own pro-arrhythmic consequences, as heterocellular coupling and non-exosomal paracrine pro-arrhythmic mechanisms are exhibited by mesenchymal stem cells in a dose-dependent manner in healthy *in vitro* cardiac monolayers. In this context, it needs to be elucidated if the beneficial effects on the modification of the pro-arrhythmic substrates electrophysiologically outweigh the pro-arrhythmic effects of heterocellular coupling and paracrine signaling of MSCs. Interestingly, a large portion of the beneficial effects of stem cell therapy may be attributed to the release of exosomes, which are small lipid vesicles that contain mRNA, miRNAs and proteins that reside in the MSC secretome. [35,36] As exosomes did not show significant pro-arrhythmic effects in our study, these components of the MSC secretome may be a future, safe alternative to cell therapy that may be able to modify the substrate positively without concomitant pro-arrhythmic effects. Besides stem cell therapy, methods such as angiotensin-II blockade counteract fibrosis as a whole and therefore act upstream of its pro-arrhythmic mechanisms, which may yield indirect anti-arrhythmic effects.[37] Alternatively, anti-fibrotic reprogramming by knockdown of transcription factors in

MFBs could be feasible as an anti-arrhythmic strategy that also improves mechanical cardiac function.[24] Such approaches benefit from advances in selective genetic modification targeting specific cell types using adeno-associated-viral vector (AAV) technology as demonstrated in this thesis. Moreover, AAVs may be incorporated into clinical practice sooner rather than later, as phase-I and phase-II clinical trials that demonstrate the success of such strategies are beginning to surface.[38,39] Taken together, all the options and tools that are or soon will be available to investigate and target pro-arrhythmic mechanisms demand more effort, dedication and investigation by the scientific community that may ultimately lead to the best anti-arrhythmic option that can be achieved: curing the pro-arrhythmic substrate instead of treating it.

Dutch Summary - Nederlandse Samenvatting

De algemene introductie van dit proefschrift beschreef de basale mechanismen van cardiale elektrofysiologie en hoe deze zich verhouden tot aritmiën. Tevens werden de huidige anti-aritmische strategiën besproken, waarvan de efficiëntie, ondanks de bewezen werkzaamheid van dergelijke behandelingen, nog geoptimaliseerd kan worden. De suboptimale efficiëntie van deze strategiën is mogelijk te wijten aan het incomplete begrip van pro-aritmische mechanismen, die vaak zijn gerelateerd aan structureel hartlijden en de bijbehorende formatie van pro-aritmische substraten. Wegens de complexiteit van zulke substraten moeten de individuele componenten worden onderscheiden en in detail worden bestudeerd met behulp van *in vitro* en *in vivo* modellen. Het doel van dit proefschrift was daarom om cellulaire en moleculaire pro-aritmische mechanismen in *in vitro* modellen van pro-aritmische substraten zoals fibrose en hypertrofie te bestuderen om zo een mechanistische basis voor toekomstige, substraat-gerichte therapiëen te vormen en uit te breiden.

Hoofdstuk II onderzocht de anti-aritmische effecten van anti-proliferatieve behandeling van myofibroblasten (MFBs) in hartcel-kweken. MFB proliferatie is een prominente eigenschap van cardiale fibrose. Aangezien cardiale fibrose sterk is geassocieerd met aritmiën, testte deze studie de hypothese dat anti-proliferatieve behandeling van MFBs anti-aritmische effecten zou kunnen hebben. Hiertoe werden myocardiale kweken van neonatale rattencellen behandeld met mitomycine-C of paclitaxel op de eerste dag van kweek om proliferatie te remmen van de endogeen aanwezige MFBs. Gedurende de kweekperiode van 9 dagen werd de elektrofysiologie van deze kweken op dag 4 en dag 9 in kaart werd gebracht middels optical mapping en patch-clamp experimenten. Apoptose werd niet significant verhoogd door de antiproliferatieve reagentia en deze hielden de hoeveelheid MFBS constant gedurende de kweekperiode door het remmen van de proliferatieve capaciteit van deze cellen. Hoewel vrije MFB proliferatie de geleidingssnelheid progressief liet afnemen tussen dag 4 en 9 (van 15.3±3.5 cm/s tot 8.8±0.3 cm/s, $P<0.05$), was de geleidingssnelheid hoger en stabiel gedurende de kweekperiode in kweken die anti-proliferatieve behandeling hadden ontvangen. Van de fibrotische kweken met veel fibroblasten had 81% spontane reentry aritmiëen, terwijl slechts 3% van mitomycin-C en 5% van paclitaxel behandelde kweken dergelijke aritmiën liet zien. Aritmogeniteit van de kweken was afhankelijk van de dosering van de anti-proliferatieve drugs en was daarmee afhankelijk van de hoeveelheid MFBs. Patch-clamp experimenten onthulden dat cardiomyocyten (CMCs) minder gedepolariseerd en meer exciteerbaar waren na antiproliferatieve behandeling. Deze studie kan een

rationale verschaffen voor toekomstige preventieve anti-aritmische strategiën voor fibrose-gerelateerde aritmiën.

In hoofdstuk III werd het anti-aritmische effect geëvalueerd van het verminderen van heterocellulaire koppeling tussen CMCs en MFBs. Dit werd bewerkstelligd met shRNA's die waren gericht tegen Cx43, die tot expressie werden gebracht in MFBs met behulp van een lentivirale vector. In MFB-CMC co-culturen met Cx43 knockdown was de geleiding sneller (16.0±3.2 cm/s vs. 10.6±4.6, $P<0.05$) en de actiepotentiaal duur korter. Bovendien was de incidentie van ectopische activiteit en spontane reentry significant lager door de reductie in heterocellulaire koppeling. Eveneens waren CMCs minder gedepolariseerd in fibrotische co-culturen (-61.4±5.7 mV vs. 51.6±4.0 mV). Deze depolarisatie werd geïdentificeerd als een belangrijke pro-aritmische factor, aangezien de herintroductie van depolarisatie van het membraan middels I_{k1} inhibitie met $BaCl_2$ of door het verhogen van extracellulair $[K^+]$ het anti-aritmische effect van heterocellulaire ontkoppeling teniet deed. Deze studie demonstreert dat MFB-geïnduceerde depolarisatie zeer pro-aritmisch is, en dat MFB-CMC koppeling een belangrijk mechanisme is van dergelijke depolarisatie.

Hoofdstuk IV onderzocht verschillen tussen pro-aritmische mechanismen van fibrose en hypertrofie *in vitro*. Ondanks dat aritmiën vaak voorkomen in geremodelleerde harten, is het uitermate lastig onderscheid te maken tussen hypertrofie- of fibrose-geassocieerde mechanismen, hoewel verschillen in pro-aritmische mechanismen mogelijk relevant kunnen zijn voor het anti-aritmische potentiëel van interventies. Myocardiale kweken van neonatale rattenharten werden blootgesteld aan phenylephrine om hypertrofie te induceren, of hadden vrijelijk proliferende MFBs als model voor fibrose. De aritmische bevindingen waren gelijksoortig in beide groepen, die trage geleiding en repolarisatie lieten zien. Incidenties van focale aritmiën (gebaseerd op early afterdepolarizations) en reentry aritmiën waren eveneens gelijksoortig verhoogd in hypertrofische en in fibrotische kweken. Verder onderzoek liet echter zien dat er verschillen waren in hoe deze aritmische uitingen tot stand kwamen. Eiwitexpressie niveaus van Kv4.3 en Cx43 werden verlaagd in hypertrofie maar waren niet aangedaan in fibrose. Gedeeltelijke ontkoppeling door toediening van een lage dosering van gap-junction ontkoppelende stoffen was alleen anti-aritmisch in fibrotische kweken, terwijl L-type calcium kanaal blokkade aritmiën tegenging in hypertrofische kweken maar geleidingsblokkade veroorzaakte in fibrotische kweken. Deze bevindingen verschaffen nieuwe inzichten in hoe sterk verschillende substraat-specifieke pro-

aritmische mechanismen kunnen leiden tot gelijksoortige aritmiciteit en hoe dit mogelijk therapeutische werkzaamheid kan beïnvloeden.

Hoofdstuk V onderzocht de mechanismen van stabiele ventriculaire fibrillatie, dat onderhouden wordt door meerdere stabiele rotors die moeilijk te termineren zijn. Het doel van deze studie was het correleren van veranderingen in aritmie complexiteit met veranderingen in specifieke elektrofysiologische parameters. Middels deze aanpak kunnen nieuwe factoren die de stabiliteit van ventriculaire fibrillatie veranderen worden geïdentificeerd, om uiteindelijk de werkzaamheid van anti-fibrillatoire interventies te verbeteren. Hiervoor werd een nieuw *in vitro* model van fibrillatie ontwikkeld, waarin een dosis-afhankelijke toename in fibrillatoire complexiteit mogelijk werd gemaakt door het gap-junction ontkoppelende farmacon 2-aminoethoxydiphenyl boraat (2-APB). De complexiteit van aritmiën in neonatale rattenhart kweken nam toe met toenemende doseringen van 2-APB (n > 38) en leidde tot stabiele VF: 0.0 ± 0.1 phase singularities/cm^2 in controles versus 0.0 ± 0.1, 1.0 ± 0.9, 3.3 ± 3.2, 11.0 ± 10.1, en 54.3 ± 21.7 in respectievelijk 5, 10, 15, 20, en 25 µmol/L 2-APB. De complexiteit van aritmiën was omgekeerd evenredig met de golflengte van aritmieën. Verlengen van de golflengte gedurende fibrillatie kon slechts worden geïnduceerd met reagentia ($BaCl_2$/BayK8644) die de actiepotentiaal duur verlengen bij maximale activatie frequenties (de zogeheten minimale APD); 123 ± 32%/117 ± 24% van controles. Verlenging van de minimale APD leidde tot tijdelijke destabilisatie van fibrillatie, middels de botsing van activatie-fronten die daarmee tot rotor terminatie leidde, gevolgd door een significante vermindering in de complexiteit en activatiefrequentie van VF (52%/37%). Deze bevindingen werden *ex vivo* gereproduceerd in adulte rattenharten (n=6 per groep). Deze resultaten laten zien dat de stabiliteit van fibrillatie sterk afhankelijk is van de minimale APD. Verlenging van de minimale APD leidt tot tijdelijke destabilisatie van fibrillatie en verlaging van de complexiteit en verschaft daarmee nieuw inzicht in anti-fibrillatoire mechanismen.

Hoofdstuk VI verkende de pro-aritmische effecten van stamceltherapie op myocardiale kweken. Omdat weinig stamcellen na transplantatie in hart achter blijven, is het huidige streven binnen de stamceltherapie om meer stamcellen te laten hechten in het myocard. Het is echter onbekend of dergelijke veranderingen tevens het pro-aritmische risico van stamceltherapie vergroten. Bovendien is het integratie patroon van stamcellen moeilijk te reguleren *in vivo*. Om de pro-aritmische mechanismen van stamcel therapie te onderzoeken werden humane mesenchymale stamcellen (hMSCs) uitgeplaat in co-cultuur met neonatale ratten cardiomyocyten

in hoeveelheden van 7% of 28% in een diffuus of geclusterd patroon, waarna elektrofysiologische eigenschappen middels optical mapping en patch-clamp experimenten in kaart werden gebracht op dag 9 van de kweek. In diffuse co-kweken vertraagden de hMSCs de geleiding op een dosis-afhankelijke wijze, terwijl de APD werd verlengd. Het vertragen van de geleiding was afhankelijk van heterocellulaire koppeling middels gap-junctions, aangezien gedeeltelijke ontkoppeling de CV verhoogde, maar de APD niet veranderde. Omdat hMSCS geen α-smooth muscle actinin of n-cadherine tot expressie brengen was het onwaarschijnlijk dat mechanische heterocellulaire koppeling een significante pro-aritmische rol speelt. Triggered activity en de induceerbaarheid van reentry werden verhoogd op een dosis-afhankelijke manier door diffuus verspreide hMSCs. Voor co-culturen met geclusterde hMSCs werden ter plaatse van het cluster geleidingsvertraging en APD verlenging waargenomen. Bovendien werd alleen de induceerbaarheid van reentry verhoogd op dosisafhankelijke wijze, terwijl triggered activity niet werd geobserveerd. Experimenten met transwells onthulden dat het secretoom van hMSCs op dosisafhankelijke wijze de APD, dispersie van APD en de induceerbaarheid van reentry verhogen, terwijl de geleidingssnelheid niet was aangedaan. Exosomen afkomstig uit dit secretoom hadden geen detecteerbare elektrofysiologische effecten. Deze bevindingen illustreren niet alleen het pro-aritmische potentiëel van het verhogen van het aantal getransplanteerde hMSCs, maar ook dat de specifieke effecten worden gemedieerd door koppeling middels gap-junctions en paracriene mechanismen. Deze studie biedt data die mogelijk helpt eventuele toekomstige pro-aritmische effecten van stamcel therapie te voorkomen wanneer de hoeveelheid gehechte stamcellen toeneemt voorbij de therapeutische index.

Hoofdstuk VII onderzocht een nieuwe methode om fibroblast-geassocieerde aritmiciteit tegen te gaan, aangezien MFBs pro-aritmisch kunnen zijn middels meerdere mechanismen die berusten op suboptimale integratie in het cardiale syncytium. Daarom werd de toepasbaarheid van geforceerde cellulaire fusie tussen humane ventriculaire litteken cellen (hVSCs) en nrCMCs als potentiëel anti-aritmische strategie verkend. Hiertoe werden hVSCs geïsoleerd van humane ventriculaire littekens en in co-cultuur gebracht met nrCMCs in een ratio van 1:4. Voor de co-cultuur werden deze hVSCs genetisch gemodificeerd middels een lentivirale vector om zo Vesiculair-Stomatitis-G-Protein en eGFP tot expressie te brengen en fusogene cellen te produceren, of werd slechts eGFP tot expressie gebracht ter controle. Fusie werd geïnduceerd door korte blootstelling aan zure buffer (pH=6.0) op dag 3 van de kweek en de elektrofysiologische effecten van fusie werden geëvalueerd op dag 5 middels optical mapping. Co-expressie van fibroblast-

specifiek collageen-I en nrCMC-specifiek α-actinine werd geobserveerd in meerkernige cellen die zowel humane als van ratten afkomstige celkernen bevatten, terwijl een annexin-V kleuring niet wees op verhoogde apoptose door cellulaire fusie. Deze nrCMC-hVSC hybriden behielden sarcomerische α-actinine expressie en contractiliteit, terwijl vimentine expressie in nrCMC-hVSC hybriden lager was dan in niet gefuseerde hVSCs. Bovendien waren Cx43 en Cav1.2 eiwitexpressie niveaus hoger in heterokaryons ten opzichte van ongefuseerde hVSCs. De expressie niveaus waren niet recht evenredig met het percentage van humane kernen in heterokaryons. Gefuseerde culturen lieten snellere geleiding (16.8±1.6 vs. 10.3±2.6 cm/s, $P<0.05$) en kortere actiepotentiaal duraties zien (328±56 vs. 480±70ms, $P<0.05$). Heterocellulaire fusie was sterk anti-aritmisch, aangezien triggered activity en reentry niet werden gezien (incidenties van 58%, n=12 in controles vs. 0% n=23 in gefuseerde co-culturen). De resultaten van deze studie lieten zien dat heterocellulaire fusie tussen hVSCs en nrCMCs haalbaar is en goed wordt getolereerd gezien de behouden exciteerbaarheid en contractiliteit van heterokaryons. Bovendien has heterocellulaire fusie een sterk anti-aritmisch effect in hVSC-nrCMC co-culturen. Aangezien het nrCMC fenotype relatief dominant leek te zijn binnen het heterokaryon, kunnen deze resultaten mogelijk nieuwe inzichten verschaffen in anti-aritmische herprogrammering van fibroblasten.

In **hoofdstuk VIII** wordt een studie beschreven waarin virale vectoren worden onderzocht die myocardiale litteken fibroblasten (MSFs) selectief kunnen transduceren, omdat deze cellen therapeutische doelen kunnen zijn wegens de pro-aritmische effecten van deze cellen. Van de huidige vehikels voor genetische modificatie, zijn de adeno-associated viruses (AAV) vectoren het beste hiervoor geschikt wegens de *in vivo* veiligheid en het verpsreidingsgemak door weefsels. Het doel van deze studie was het vergelijken van de transductie van nrCMC en humane, muis en rat MSFs door AAVs met verschillende capsiden en met transgenen die werden gedreven door verschillende promotors. Voor dit doel werden vector shuttle plasmiden met een *LacZ* gen gedreven door 9 verschillende promotors waaronder de humane, muis en rat cytomegalovirus immediate early gene (CMV-IE) geconstrueerd. De AAV vector genomen die werden gespecificeerd door deze plasmiden werden verpakt in AAV serotype 2 (AAV2) capsiden. B-galactosidase assays onthulden dat van alle CMV-IE promotors, de humane CMV-IE promotor beter presteerde dan de murine of rat CMV-IE promotors in humane MSFs, terwijl de murine of rat CMV-IE promotors actiever waren in murine en rat MSFs. Van alle 9 promoters die werden getest was de human eukaryotic translation elongation factor 1 alpha 1 (hEF1α) promotor het meest actief in murine en rat MSFs terwijl de Rous

sarcoma virus (RSV) promotor de hoogste transgen expressie genereerde in nrCMCs. Een vergelijking van de transductie efficiëntie van rat MSFs en nrCMCs met AAV2 vectoren met capsiden van AAV serotypes 2, 5, 6, 8 en 9 liet zien dat transductie van rat MSFs het meest efficiënt is met AAV2/2 vectoren terwijl AAV2/9 de nrCMCs het beste transduceerde. In conclusie werd de hoogste transgen expressie in ratten MSFs verkregen door transductie met een hEF1α promotor in een AAV2/2 vector, terwijl transgen expressie in nrCMCs het hoogste was na transductie met een AAV2/9 vector waarvan de transgen expressie wordt gecontroleerd door de RSV promoter.

Concluderend zijn MFBs een mogelijk aangrijpingspunt voor verschillende anti-aritmische interventies in de context van cardiale fibrose. Door het verlagen van de proliferatieve capaciteit van MFBs kunnen de hoeveelheden en daarmee de dosis-afhankelijke effecten van MFBs worden beperkt *in vitro*. Echter, wegens de kans op ernstige systemische bijwerkingen van anti-proliferatieve behandeling is het wenselijk om MFB-geïnduceerde depolarisatie op specifiekere wijze aan te pakken. Een dergelijke aanpak werd eveneens onderzocht in dit proefschrift, waarbij heterocellulaire ontkoppeling middels farmaca of genetische Cx43 downregulatie in MFBs werd bewerkstelligd en significante anti-aritmische effecten had op basis van het pro-aritmische mechanisme. Een alternatieve aanpak was heterocellulaire fusie, waardoor fibrotische co-culturen sneller geleidden, repolariseerden en minder aritmiën vormden in vergelijking met ongefuseerde co-culturen. Dit proefschrift benadrukt het belang van het aanpakken van dergelijke substraat-specifieke mechanismen met de demonstratie dat hypertrofische kweken niet gebaat zijn bij dezelfde anti-aritmische interventies als fibrotische kweken ondanks de nagenoeg identieke aritmische bevindingen. Hypertrofische kweken leden echter aan intrinsieke elektrische remodelering en behoefden andere interventies ter voorkoming van aritmiëen. Via het aanpakken van belangrijke aritmische parameters, die worden bepaald door het onderliggende substraat, konden substantiële anti-aritmische effecten worden bereikt in deze modellen. Dit concept werd verder verkend door te demonstreren dat de minimale APD de sleutel parameter is die de aritmische complexiteit bepaald in een *in vitro* en *ex vivo* model van ventriculaire fibrillatie. Dit proefschrift verschaft eveneens bewijs voor dosis-afhankelijke pro-aritmische mechanismen van MSC transplantatie. Ter samenvatting, demonstreert dit proefschrift meerdere cellulaire en moleculaire aritmische mechanismen in meerdere pro-aritmische substraten, en hoe deze mechanismen kunnen worden aangepakt middels nieuwe anti-aritmische interventies.

Discussie en toekomst perspectieven

In vitro *ziekte-modellen en de optimalisatie van anti-aritmische behandeling*
Hoewel huidige anti-aritmische behandelingen de patiënt ten goede komen, kan de suboptimale werkzaamheid van deze strategiën mogelijk worden toegeschreven aan een incompleet begrip van het onderliggende pro-aritmische substraat (zie de algemene inleiding van dit proefschrift). In de klinische cardiologie werd gereageerd op deze realisatie met het opstellen van de Sicilian Gambit, een stelling die de complexiteit van aritmiën en de onhaalbaarheid van adequate behandeling van verschillende aritmiën met dezelfde middelen zonder begrip van de onderliggende mechanismen erkende.[1] De Sicillian Gambit stelde het concept van de kwetsbare parameter voor, hetgeen de kritische parameter is om te veranderen voor optimale anti-aritmische effecten.[2] Om zulke parameters te kunnen onderzoeken is basaal onderzoek dat gebruik maakt van *in vitro* en *in vivo* modellen om pro-aritmische substraten te identificeren en modificeren essentiëel om huidige kennis en therapeutische werkzaamheid van anti-aritmische drugs te verbeteren.[3] Dergelijke ziektemodellen worden over het algemeen ontwikkeld wegens de mogelijkheid tot gestandaardiseerde interpretatie van onderzoeksresultaten. Voor dit doeleinde versimpelen de meeste simulatie- en *in vitro* studies die gebruik maken van zogeheten monolayers de 3-dimensionale cardiale structuur tot een 2-dimensionale structuur waarin pro-aritmische mechanismen en kenmerken in groter detail kunnen worden onderzocht. Bovendien faciliteert de 2-dimensionale simplificatie de interpretatie van data, die in de 3-dimensionale context van aritmiën uiterst complex kunnen zijn. Tevens is er typisch een hoge mate van controle over de experimentele omgeving bij *in vitro* modellen, waardoor het mogelijk is sleutelcomponenten te isoleren en te onderzoeken. Door te starten met een versimpeld ziekte model en vervolgens geleidelijk de complexiteit van het model te verhogen, kunnen niet alleen nieuwe pro-aritmische mechanismen worden verkend die *in vivo* moeilijk te onderzoeken zijn, maar is het eveneens mogelijk de bevindingen uit deze modellen te extrapoleren naar klinisch meer relevante *in vivo* situaties. Een voorbeeld van een dergelijk concept van een kwetsbare parameter onderzocht in een versimpeld model binnen dit proefschrift is de minimale actiepotentiaal duratie (Hoofdstuk V), hetgeen de refractaire status bepaalt van weefsel gedurende fibrillatie. In het gepresenteerde 2-dimensionale *in vitro* model van ventriculaire fibrillatie dat werd geïnduceerd middels ontkoppeling van gap-junctions, veroorzaakte verlenging van de minimale APD een reductie in de aritmische complexiteit, hetgeen eerder werd voorspeld door *in silico* studies. Het mechanisme van complexiteit reductie berustte op tijdelijke destabilisatie van de aritmie, hetgeen alleen in dit model bestudeerd

kon worden gezien de relatieve simpliciteit. Bovendien werd middels replicatie van hetzelfde model in adulte ratten harten *ex vivo* gedemonstreerd dat het *in silico* en *in vitro* concept van minimale APD verlenging relevant bleef in de adulte 3-dimensionele situatie. Door de complexiteit van de *in vivo* modellen verder te vergroten richting grotere dieren kunnen de bevindingen uit versimpelde modellen uiteindelijk relevant blijken in de behandeling van humaan ventrikelfibrilleren.

Behalve de simplificatie van pro-aritmische substraten, kunnen *in vitro* modellen tevens een platform bieden waarin gewoonlijk tegelijk voorkomende substraten afzonderlijk kunnen worden onderzocht, zodat er onderscheid tussen pro-aritmische mechanismen kan worden gemaakt en deze uitvoeriger kunnen worden onderzocht. Een voorbeeld van een dergelijke aanpak in dit proefschrift is in het geval van hypertrofie en fibrose welke vaak samen voorkomen bij cardiale remodelering.[4] Een interessante bevinding was dat aritmische bevindingen in elk van deze afzonderlijke substraten nagenoeg gelijk waren *in vitro*. De onderliggende pro-aritmische mechanismen verschilden echter significant. Deze verschillen impliceren dat ieder substraat mogelijk een specifieke pro-aritmische behandeling behoeft. Ongeacht het mechanistische inzicht dat dergelijke studies kunnen verschaffen is het belangrijk om waakzaam te blijven tegen het overdrijven van de implicaties van *in vitro* modellen voor *in vivo* situaties aangezien het overmatig versimpelen van de in vivo situatie een potentieel gevaar is van *in vitro* onderzoek. Daarom moet in acht worden genomen wat het model tracht na te bootsen en hoe dit wordt bewerkstelligd. In het huidige voorbeeld werd fibrose nagebootst door uitgebreide MFB proliferatie, hetgeen een kenmerk is van *in vivo* fibrose en zelfs in afwezigheid van de eveneens bekende excessieve matrix depositie een zeer pro-aritmisch model produceerde. *In vitro* hypertrofie werd behaald door behandeling van CMCs met fenylefrine, een α1-agonist waarvan het belang voor *in vivo* inductie van hypertrofie bekend is. Hypertrofie kan echter ook worden geïnduceerd door andere stoffen en is *in vivo* vaak een resultaat van veranderde druk- en volumebelasting in combinatie met hormonale veranderingen. Het is daarom moeilijk te bepalen waar *in vitro* hypertrofie past in de schaal van progressieve hypertrofie en hartfalen die wordt geobserveerd gedurende cardiale remodelering *in vivo*. Wegens het sterke pro-aritmische fenotype van het gebruikte model van hypertrofie is het waarschijnlijk dat het overeenkomt met een eindstadium van hypertrofie en is derhalve mogelijk relevant voor de behandeling van aritmiëen in het hartfalen stadium. Omdat fibrose zelfstandig als pro-aritmisch substraat kan functioneren, is het ironisch dat in het hartfalen stadium van cardiale remodelering vaak eveneens fibrose wordt geobserveerd aangezien zowel hypertrofie als fibrose compensatoire mechanismen

zijn tegen cardiale overbelasting. Bovendien kan de uitgebreidheid van fibrose en hypertrofie verschillen tussen patiënten, en daarom varieert mogelijk de betrokkenheid van individuele substraat-specifieke mechanismen in verschillende patiënten tijdens verschillende stadia van cardiale remodelering. Buiten dat het gelijktijdig bestaan van deze twee substraten de initiële motivatie was achter het onderzoek naar de individuele pro-aritmische mechanismen, kan dit tevens een reden zijn voor de keuze van vooral symptomatische anti-aritmische behandelingen wegens de veronderstelde complexiteit. Aangezien beide substraten vrijwel gelijkwaardige pro-aritmische kenmerken bezitten kan behandeling van slechts één substraat mogelijk onvoldoende anti-aritmisch effect behalen wegens het bestaan van een ander, minder gevoelig pro-aritmisch substraat. Derhalve is het mogelijk meer haalbaar om een gemeenschappelijk pro-aritmisch kenmerk te behandelen wanneer meerdere pro-aritmische mechanismen werkzaam zijn, dan te trachten verschillende pro-aritmische substraten te behandelen in proportie tot de aanwezigheid in een hart op moment van behandeling. In het voorbeeld van de gebruikte modellen van hypertrofie en fibrose behaalt het aanpakken van de gemeenschappelijke APD verlenging in zulke substraten mogelijk positieve resultaten. De complexiteit van gecombineerde pro-aritmische substraten leidt echter ook tot een behoefte aan uitgebreider onderzoek van pro-aritmische substraten teneinde anti-aritmische drug-regimes te optimaliseren.

Het concept van substraat-specifieke interventie past binnen het opkomende paradigma van patiëntenzorg als maatwerk, waarin de complexiteit van ziekten steeds meer wordt erkend en wordt beantwoord met het onderzoek en gebruik van mechanisme-specifieke interventies. De erkenning van de complexiteit van niet slechts aritmiën maar humane ziekte in het algemeen is een drijfveer geweest voor het onderzoek naar de mogelijkheid tot patiënt-specifieke medicijn-testen middels induced pluripotent stem cells (iPS cellen).[5] Met behulp van genetisch modificatie van somatische cellen middels enkele transcriptiefactoren dedifferentiëren deze cellen tot een op embryonale stamcel gelijkend fenotype, waarna deze kunnen differentiëren naar verschillende patiënt-specifieke cellijnen waaronder cardiomyocyten. Hoewel de uitrijping en puurheid van iPS-afgeleide cardiomyocyten obstakels zijn die overkomen dienen te worden voor daadwerkelijke klinische relevantie, is deze aanpak veelbelovend voor het biologische onderzoeksveld.[6] Als alternatief wordt er gestreefd naar de mogelijkheid van het direct reprogrammeren van eenvoudig verkrijgbare somatische cellen tot CMCs.[7] Met dergelijke technieken kunnen patient-specifieke celtypen zoals cardiomyocyten, die normaliter moeilijk te verkrijgen zijn, worden gekweekt en kan de respons op verschillende farmaca

worden getest.[8] Zodoende kan optimale medicijn selectie worden gerealiseerd op patiënt-specifieke wijze, hetgeen de therapeutische werkzaamheid van farmacologische behandeling kan optimaliseren. Door deze techniek te combineren met reeds bestaande *in vitro* modellen van verschillende pro-aritmische substraten, kan ons begrip van aritmiën uiteindelijk toereikend zijn om alle patiënten farmacologisch optimaal te behandelen door op maat gemaakte anti-aritmische patiënt-specifieke drug regimes.

Het aanpakken van de MFB in vivo als anti-aritmische strategie

De werkzaamheid van anti-aritmica is vooral gebaseerd op symptomatische verlichting. Hierdoor worden onderliggende pro-aritmische substraten zoals cardiale remodelering niet gemodificeerd ondanks de prominente rol in aritmogenese. Het is daarom mogelijk dat het bewerkstelligen van intrinsieke veranderingen van pro-aritmische substraten door ziekte-modificerende medicijnen, genetische modificatie of celtherapie kan leiden tot meer optimale en langdurige resultaten dan wat behaald kan worden met farmacologische behandeling. In het geval van fibrose genieten MFBs sinds recentelijk steeds meer aandacht als potentiële hoofdrolspelers in fibrose-geassocieerde aritmieën. Hoewel deze cellen initieel werden verondersteld een nagenoeg latent te zijn en gedacht werd dat zij slechts de extracellulaire matrix onderhielden, is recentelijk ontdekt dat MFBs functioneel kunnen koppelen met CMCs hetgeen impliceert dat deze cellen een actieve rol kunnen spelen in de context van fibrose-geassocieerde aritmieën.[9] Sindsdien is gebleken dat heterocellulaire koppeling tussen CMCs en MFBs op dosis-afhankelijke wijze geleiding vertraagt,[10] ectopische activiteit verhoogt[11] en de neiging tot het vormen van reentry aritmieën vergroot.[12] Alhoewel deze *in vitro* experimenten, gesteund door *in silico* simulaties,[13] veelbelovende concepten aan de orde brengen die ons begrip van aritmiën verbeteren is een vertaling naar *in vivo* situaties moeilijk. Daarom is de klinische relevantie van dergelijke bevindingen een voorspelbaar onderwerp van discussie. Een voorbeeld van een dergelijke discussie betreft de klinische relevantie van heterocellulaire koppeling tussen MFBs en CMCs, hetgeen tot op heden niet duidelijk is aangetoond *in vivo*.[14-16] Functionele koppeling tussen toegediende, genetisch gelabelde cellen en myocard is aangetoond in vivo,[17] maar onomstotelijk bewijs van koppeling tussen endogeen aanwezige en daardoor ongelabelde cellen is moeilijk te realiseren vanuit technisch oogpunt. Alhoewel het bewijzen van het bestaan van functionele heterocellulaire koppeling *in vivo* een technische uitdaging vormt, is het vele malen uitdagender om met onomstotelijk bewijs het bestaan van dergelijke mechanismen uit te sluiten. Een verder

complicerende factor van MFB-geïnduceerde aritmieën is het gegeven dat tevens mechanische koppeling en paracriene mechanismen een mogelijke rol spelen.[18,19] Aangezien deze bevindingen in lijn liggen met het slechts gedeeltelijke herstel van elektrofysiologische functie na heterocellulaire ontkoppeling *in vitro* (Hoofdstuk III), is het mogelijk dat, om fibrose-geassocieerde aritmiëen effectief te behandelen *in vivo,* het gehele fenotype van de MFB aangepast moet worden in plaats van ieder afzonderlijk pro-aritmisch mechanisme te behandelen. Bovendien zou een interventie die de gehele MFB modificeert ook de extracellulaire matrix depositie kunnen aantasten, een belangrijk pro-aritmisch kenmerk van fibrose *in vivo* dat tot op heden nauwelijks te onderzoeken is *in vitro*.[20] Een mogelijk haalbare aanpak van de gehele MFB werd gedemonstreerd in Hoofdstuk II, waarin remming van MFB proliferatie sterke anti-aritmische effecten teweeg bracht. Omdat MFBs pro-aritmische effecten op een dosis-afhankelijke wijze, zal het verlagen van de hoeveelheid aanwezige MFBs indirect de pro-aritmische effecten van alle bekende en onbekende pro-aritmische mechanismen tegengaan. Het verminderen van de proliferatieve capaciteit van MFBs voorkomt excessieve littekenformatie in non-cardiaal weefsel, waarbij tevens extracellulaire matrix depositie is verminderd.[21] Het is te verwachten dat in toenemende mate bewijs wordt geleverd dat een dergelijke strategie tevens anti-aritmische effecten teweeg kan brengen *in vivo*.[22,23] Echter is het van groot belang te erkennen dat proliferatie-remmende stoffen berucht zijn wegens ernstige, vaak systemische neveneffecten en ongewenste binding aan gevoelige, perifere celtypen. De meerwaarde die genetische modificatie kan bieden boven farmacologische behandeling is substantieel, zoals langere werkzaamheidsduur en verminderde neveneffecten door selectieve transductie van specifieke cel- en weefseltypen door gebruik te maken van celtype-specifieke promotors en virussen met weefsel-specifiek tropisme. Hierdoor is het preferabel het gedrag van MFBs te moduleren middels genetische modificatie. Een voorbeeld hiervan is het verlagen van myocardin-related transcription factor-a, waardoor myofibroblast activatie wordt verhinderd hetgeen resulteert in een sterk verlaagde pro-fibrotische respons van deze cellen *in vivo*.[24]

Een gelijksoortige anti-aritmische benadering die de gehele MFB modificeert is cellulaire herprogrammering, met als doel de MFB te forceren zich te gedragen als een celtype met minder schadelijke gevolgen voor de hartfunctie, zoals stamcellen of zelfs CMCs. Hoewel cellulaire herprogrammering initieel werd gerealiseerd door nucleaire herprogrammering[25] wordt cellulaire herprogrammering van MFBs tot stamcellen of CMCs tegenwoordig bewerkstelligd door genetische modificatie met enkele transcriptie factoren, alhoewel deze aanpak vooralsnog als inefficiënt wordt

beschouwd.[7] In deze context zou geforceerde heterocellulaire fusie zoals onderzocht in dit proefschrift een toekomstige alternatieve route kunnen bieden voor anti-aritmische MFB herprogrammering, aangezien fusie kan worden gebruikt voor genetische herprogrammering van cellen.[25] Als alternatief kunnen MFBs genetisch worden gemodificeerd om qua elektrofysiologie een CMC gedeeltelijk na te bootsen door expressie te forceren van Cx43 en de ionkanalen Kir2.1 en Nav1.5, hetgeen ook voorspelbare anti-aritmische effecten heeft.[26,27] Een nieuwe methode van genetische modificatie is optogenetica, waarmee transgen activiteit kan worden gereguleerd door middel van blootstelling aan licht. Recentelijk is zelf optische controle over eiwitactiviteit gedemonstreerd.[28] Dergelijke verfijnde methoden laten het toe om een genetische interventie precies te richten en timen, hetgeen wegens de complexiteit van aritmische substraten een krachtige mogelijkheid is voor het onderzoek en de toekomstige behandeling van pro-aritmische mechanismen. Optogenetica is gebaseerd op de lichtgevoelige rhodopsines en is binnen neurologisch onderzoek inmiddels een bewezen krachtige techniek die in de toekomst mogelijk gebruikt kan worden om CMCs danwel MFBs te modificeren.[29] Ongeacht de wijze waarop MFBs zullen worden aangepakt in toekomstig *in vivo* onderzoek zullen de voortschrijdende inzichten in de pro-aritmische mechanismen van MFBs alsmede de vooruitgang in biotechnologie blijven leiden tot nieuwe anti-aritmische strategiëen voor de voorzienbare toekomst, die uiteindelijk kunnen resulteren in optimale substraat-georiënteerde behandeling van fibrose-geassocieerde aritmiëen.

Het modificeren van een substraat voorbij de pro-aritmische mechanismen als de ultieme anti-aritmische strategie

Sinds de ontdekking van de microscoop persisteert binnen de wetenschap het idee dat het nader bekijken van bepaalde fenomenen de beste wijze is om de onderliggende mechanismen te begrijpen. Zoals reeds besproken, worden pro-aritmische mechanismen als aangrijpingspunt gezien voor meer adequate toekomstige anti-aritmische behandeling. Daarom zullen voorlopig experimenten die diep gelegen pro-aritmische mechanismen onderzoeken nodig blijven om aritmiëen tot in de diepste details te kunnen begrijpen. De snel uitbreidende kennis betreffende verschillende pro-aritmische mechanismen wijst er echter op dat de complexiteit van het behandelen van deze mechanismen in alle substraten te hoog is om in de nabije toekomst optimale anti-aritmische therapieën te realiseren. Wegens de huidige uitbreidende epidemie van atriumfibrilleren en structurele hartziekte is het nodig tijdig actie te ondernemen tegen pro-aritmische substraten.

Ondanks dat het behandelen van pro-aritmische mechanismen van individuele substraten zoals fibrose en hypertrofie uiteindelijk kunnen leiden tot een geoptimaliseerde anti-aritmische behandeling, zijn deze pro-aritmische substraten tevens geassocieerd met verminderde mechanische hartfunctie die vervolgens systemische co-morbiditeit kan veroorzaken zoals thrombus-vorming met embolisatie en vermoeidheid. Waar cardiale hypertrofie erop is gericht om cardiale output te handhaven, is cardiale fibrose een respons op drukoverbelasting om zo de structurele integriteit van het hart te behouden. Dit resulteert in veranderde contractiliteit en cardiale stijfheid, het geen op zichzelf pro-aritmische consequenties kan hebben. Daarom zou het nodig kunnen zijn het gehele structurele substraat te modificeren om de gehele aritmogeniteit te behandelen. Een dergelijke strategie is stamceltherapie, waarvan wordt verondersteld dat het meerdere nadelige aspecten van structurele hartziekten positief beïnvloedt of zelfs kan omkeren waardoor het mogelijk anti-aritmische effecten kan bewerkstelligen op een hoger organisatieniveau dan individuele pro-aritmische mechanismen. Initieel was de rationale achter cardiale stamceltherapie het vervangen van verloren exciteerbare cardiomyocyten in fibrotisch myocard door middel van toediening van cellen die in staat waren tot cardiale differentiatie om zodoende aritmiëen tegen te gaan. Het potentieel tot cardiale differentiatie van dergelijke cellen is echter teleurstellend laag.[30] De laatste jaren wordt verondersteld dat het kleine maar significante therapeutische effect van stamceltherapie berust op paracriene effecten die structurele hartziekte ten goede beïnvloeden.[31] Wegens de lage hoeveelheid stamcellen die achterblijft bij stamceltherapie, is het huidige streven binnen stamcelonderzoek om de werkzaamheid van deze therapie te verhogen door meer stamcellen in het myocard achter te laten middels verschillende technieken waaronder tissue engineering en genetische of magnetische modificatie van cellen.[32-34] Echter, zoals gedemonstreerd in dit proefschrift, kunnen dergelijke strategieën pro-aritmische effecten hebben, aangezien mesenchymale stamcellen middels heterocelulaire koppeling en non-exosomale paracriene activiteit pro-aritmische effecten hebben op CMCs op dosisafhankelijke wijze. In deze context moet worden verhelderd of de voordelige effecten van stamceltherapie berusten op de afgifte van exosomen, hetgeen kleine lipide vesikels zijn die mRNA, miRNA en eiwit bevatten.[35,36] Aangezien exosomen in onze studie geen significante pro-aritmische effecten liet zien, kunnen deze componenten van het MSC secretoom een toekomstig, veilig alternatief voor celtherapie vormen dat mogelijk het substraat positief beïnvloed zonder de pro-aritmische effecten. Behalve stamceltherapie zijn er methoden als angiotensine-II blokkade waarmee fibrose in het geheel wordt tegengegaan, waardoor indirecte anti-aritmische effecten kunnen worden bereikt

op een organisatieniveau boven individuele pro-aritmische mechanismen.[37] Als alternatief kan anti-fibrotische reprogrammering door verlaging van transcriptiefactor expressive in MFBs een haalbare anti-aritmische strategie zijn die tevens mechanische cardiale functie zou kunnen verbeteren.[24] Zulke benaderingen profiteren van vorderingen in selectieve genetische modificatie waarin specifieke celtypen worden aangepakt middels AAV technologie zoals beschreven in dit proefschrift. Bovendien wordt behandeling middels AAVs mogelijk relatief spoedig opgenomen in de kliniek, aangezien fase-I en fase-II klinische trials die het succes van dergelijke strategieën demonstreren inmiddels worden beschreven.[38,39] Samenvattend vragen alle strategieën die nu of in de nabije toekomst beschikbaar zijn om pro-aritmische mechanismen te onderzoeken en te behandelen meer aandacht, toewijding en onderzoek door de wetenschappelijke gemeenschap, hetgeen uiteindelijk kan leiden tot de beste anti-aritmische strategie die kan worden bereikt: het genezen van een pro-aritmisch substraat in plaats van het slechts te behandelen.

References

1. The 'Sicilian Gambit'. A new approach to the classification of antiarrhythmic drugs based on their actions on arrhythmogenic mechanisms. The Task Force of the Working Group on Arrhythmias of the European Society of Cardiology. *Eur Heart J*. 1991;12:1112-1131.

2. Rosen MR and Janse MJ. Concept of the vulnerable parameter: the Sicilian Gambit revisited. *J Cardiovasc Pharmacol*. 2010;55:428-437.

3. Chang MG, Zhang Y, Chang CY, Xu L, Emokpae R, Tung L, Marban E, Abraham MR. Spiral waves and reentry dynamics in an in vitro model of the healed infarct border zone. *Circ Res*. 2009;105:1062-1071.

4. Jalil JE, Doering CW, Janicki JS, Pick R, Shroff SG, Weber KT. Fibrillar collagen and myocardial stiffness in the intact hypertrophied rat left ventricle. *Circ Res*. 1989;64:1041-1050.

5. Takahashi K, Tanabe K, Ohnuki M, Narita M, Ichisaka T, Tomoda K, Yamanaka S. Induction of pluripotent stem cells from adult human fibroblasts by defined factors. *Cell*. 2007;131:861-872.

6. Lin B, Kim J, Li Y, Pan H, Carvajal-Vergara X, Salama G, Cheng T, Li Y, Lo CW, Yang L. High-purity enrichment of functional cardiovascular cells from human iPS cells. *Cardiovasc Res*. 2012;95:327-335.

7. Chen JX, Krane M, Deutsch MA, Wang L, Rav-Acha M, Gregoire S, Engels MC, Rajarajan K, Karra R, Abel ED, Wu JC, Milan D, Wu SM. Inefficient reprogramming of fibroblasts into cardiomyocytes using Gata4, Mef2c, and Tbx5. *Circ Res*. 2012;111:50-55.

8. Malan D, Friedrichs S, Fleischmann BK, Sasse P. Cardiomyocytes obtained from induced pluripotent stem cells with long-QT syndrome 3 recapitulate typical disease-specific features in vitro. *Circ Res*. 2011;109:841-847.

9. Rook MB, Jongsma HJ, de JB. Single channel currents of homo- and heterologous gap junctions between cardiac fibroblasts and myocytes. *Pflugers Arch*. 1989;414:95-98.

10. Miragoli M, Gaudesius G, Rohr S. Electrotonic modulation of cardiac impulse conduction by myofibroblasts. *Circ Res*. 2006;98:801-810.

11. Miragoli M, Salvarani N, Rohr S. Myofibroblasts induce ectopic activity in cardiac tissue. *Circ Res*. 2007;101:755-758.

12. Zlochiver S, Munoz V, Vikstrom KL, Taffet SM, Berenfeld O, Jalife J. Electrotonic myofibroblast-to-myocyte coupling increases propensity to reentrant arrhythmias in two-dimensional cardiac monolayers. *Biophys J*. 2008;95:4469-4480.

13. Xie Y, Garfinkel A, Camelliti P, Kohl P, Weiss JN, Qu Z. Effects of fibroblast-myocyte coupling on cardiac conduction and vulnerability to reentry: A computational study. *Heart Rhythm*. 2009;6:1641-1649.

14. Baum JR, Long B, Cabo C, Duffy HS. Myofibroblasts cause heterogeneous Cx43 reduction and are unlikely to be coupled to myocytes in the healing canine infarct. *Am J Physiol Heart Circ Physiol*. 2012;302:H790-H800.

15. Camelliti P, Green CR, Kohl P. Structural and functional coupling of cardiac myocytes and fibroblasts. *Adv Cardiol*. 2006;42:132-149.

16. Camelliti P, Green CR, LeGrice I, Kohl P. Fibroblast network in rabbit sinoatrial node: structural and functional identification of homogeneous and heterogeneous cell coupling. *Circ Res*. 2004;94:828-835.

17. Shiba Y, Fernandes S, Zhu WZ, Filice D, Muskheli V, Kim J, Palpant NJ, Gantz J, Moyes KW, Reinecke H, Van BB, Dardas T, Mignone JL, Izawa A, Hanna R, Viswanathan M, Gold JD, Kotlikoff MI, Sarvazyan N, Kay MW, Murry CE, Laflamme MA. Human ES-cell-derived cardiomyocytes electrically couple and suppress arrhythmias in injured hearts. *Nature*. 2012;489:322-325.

18. Pedrotty DM, Klinger RY, Kirkton RD, Bursac N. Cardiac fibroblast paracrine factors alter impulse conduction and ion channel expression of neonatal rat cardiomyocytes. *Cardiovasc Res*. 2009;83:688-697.

19. Thompson SA, Copeland CR, Reich DH, Tung L. Mechanical coupling between myofibroblasts and cardiomyocytes slows electric conduction in fibrotic cell monolayers. *Circulation*. 2011;123:2083-2093.

20. de Bakker JM, van Capelle FJ, Janse MJ, Tasseron S, Vermeulen JT, de JN, Lahpor JR. Slow conduction in the infarcted human heart. 'Zigzag' course of activation. *Circulation*. 1993;88:915-926.

21. Min J, Lukowski ZL, Levine MA, Meyers CA, Beattie AR, Schultz GS, Samuelson DA, Sherwood MB. Prevention of ocular scarring post glaucoma filtration surgery using the inflammatory cell and platelet binding modulator saratin in a rabbit model. *PLoS One*. 2012;7:e35627.

22. Lin X, Yu M, Wu K, Yuan H, Zhong H. Effects of pirfenidone on proliferation, migration, and collagen contraction of human Tenon's fibroblasts in vitro. *Invest Ophthalmol Vis Sci*. 2009;50:3763-3770.

23. Nguyen DT, Ding C, Wilson E, Marcus GM, Olgin JE. Pirfenidone mitigates left ventricular fibrosis and dysfunction after myocardial infarction and reduces arrhythmias. *Heart Rhythm*. 2010;7:1438-1445.

24. Small EM, Thatcher JE, Sutherland LB, Kinoshita H, Gerard RD, Richardson JA, Dimaio JM, Sadek H, Kuwahara K, Olson EN. Myocardin-related transcription factor-a controls myofibroblast activation and fibrosis in response to myocardial infarction. *Circ Res*. 2010;107:294-304.

25. Cowan CA, Atienza J, Melton DA, Eggan K. Nuclear reprogramming of somatic cells after fusion with human embryonic stem cells. *Science*. 2005;309:1369-1373.

26. Kirkton RD and Bursac N. Engineering biosynthetic excitable tissues from unexcitable cells for electrophysiological and cell therapy studies. *Nat Commun*. 2011;2:300.

27. Kirkton RD and Bursac N. Genetic engineering of somatic cells to study and improve cardiac function. *Europace*. 2012;14 Suppl 5:v40-v49.

28. Zhou XX, Chung HK, Lam AJ, Lin MZ. Optical control of protein activity by fluorescent protein domains. *Science*. 2012;338:810-814.

29. Galvan A, Hu X, Smith Y, Wichmann T. In vivo optogenetic control of striatal and thalamic neurons in non-human primates. *PLoS One*. 2012;7:e50808.

30. Ramkisoensing AA, Pijnappels DA, Askar SF, Passier R, Swildens J, Goumans MJ, Schutte CI, de Vries AA, Scherjon S, Mummery CL, Schalij MJ, Atsma DE. Human embryonic and fetal mesenchymal stem cells differentiate toward three different cardiac lineages in contrast to their adult counterparts. *PLoS One*. 2011;6:e24164.

31. van RJ, Bax JJ, Beeres SL, Dibbets-Schneider P, Roes SD, Stokkel MP, de RA, Fibbe WE, Zwaginga JJ, Boersma E, Schalij MJ, Atsma DE. Intramyocardial bone marrow cell injection for chronic myocardial ischemia: a randomized controlled trial. *JAMA*. 2009;301:1997-2004.

32. Cheng K, Li TS, Malliaras K, Davis DR, Zhang Y, Marban E. Magnetic targeting enhances engraftment and functional benefit of iron-labeled cardiosphere-derived cells in myocardial infarction. *Circ Res*. 2010;106:1570-1581.

33. Cheng K, Malliaras K, Li TS, Sun B, Houde C, Galang G, Smith J, Matsushita N, Marban E. Magnetic enhancement of cell retention, engraftment and functional benefit after intracoronary delivery of cardiac-derived stem cells in a rat model of ischemia/reperfusion. *Cell Transplant*. 2012.

34. Terrovitis J, Lautamaki R, Bonios M, Fox J, Engles JM, Yu J, Leppo MK, Pomper MG, Wahl RL, Seidel J, Tsui BM, Bengel FM, Abraham MR, Marban E. Noninvasive quantification and optimization of acute cell retention by in vivo positron emission tomography after intramyocardial cardiac-derived stem cell delivery. *J Am Coll Cardiol*. 2009;54:1619-1626.

35. Lai RC, Chen TS, Lim SK. Mesenchymal stem cell exosome: a novel stem cell-based therapy for cardiovascular disease. *Regen Med*. 2011;6:481-492.

36. Lai RC, Arslan F, Lee MM, Sze NS, Choo A, Chen TS, Salto-Tellez M, Timmers L, Lee CN, El Oakley RM, Pasterkamp G, de Kleijn DP, Lim SK. Exosome secreted by MSC reduces myocardial ischemia/reperfusion injury. *Stem Cell Res*. 2010;4:214-222.

37. van Kats JP, Duncker DJ, Haitsma DB, Schuijt MP, Niebuur R, Stubenitsky R, Boomsma F, Schalekamp MA, Verdouw PD, Danser AH. Angiotensin-converting enzyme inhibition and angiotensin II type 1 receptor blockade prevent cardiac remodeling in pigs after myocardial infarction: role of tissue angiotensin II. *Circulation*. 2000;102:1556-1563.

38. Nathwani AC, Tuddenham EG, Rangarajan S, Rosales C, McIntosh J, Linch DC, Chowdary P, Riddell A, Pie AJ, Harrington C, O'Beirne J, Smith K, Pasi J, Glader B, Rustagi P, Ng CY, Kay MA, Zhou J, Spence Y, Morton CL, Allay J, Coleman J, Sleep S, Cunningham JM, Srivastava D, Basner-Tschakarjan E, Mingozzi F, High KA, Gray JT, Reiss UM, Nienhuis AW, Davidoff AM. Adenovirus-associated virus vector-mediated gene transfer in hemophilia B. *N Engl J Med*. 2011;365:2357-2365.

39. Flotte TR, Trapnell BC, Humphries M, Carey B, Calcedo R, Rouhani F, Campbell-Thompson M, Yachnis AT, Sandhaus RA, McElvaney NG, Mueller C, Messina LM, Wilson JM, Brantly M, Knop DR, Ye GJ, Chulay JD. Phase 2 clinical trial of a recombinant adeno-associated viral vector expressing alpha1-antitrypsin: interim results. *Hum Gene Ther*. 2011;22:1239-1247.

Cellular and Molecular Mechanisms of Arrhythmias in Cardiac Fibrosis and Beyond:
From Symptoms to Substrates towards Solutions

List of Publications

Full papers

Vicente Steijn R, Kolditz DP, Mahtab EA, **Askar SF**, Bax NA, van der Graaf LM, Wisse LJ, Passier R, Pijnappels DA, Schalij MJ, Poelmann RE, Gittenberger-de Groot AC, Jongbloed MR. *Electrical activation of sinus venosus myocardium and expression patterns of RhoA and Isl-1 in the chick embryo.* J Cardiovasc Electrophysiol 2010:21;1284-92

Askar SF, Ramkisoensing AA, Schalij MJ, Bingen BO, Swildens J, van der Laarse A, Atsma DE, de Vries AA, Ypey DL, Pijnappels DA. *Antiproliferative treatment of myofibroblasts prevents arrhythmias in vitro by limiting myofibroblast-induced depolarization*. Cardiovascular research 2011:90;295-304.

Ramkisoensing AA, Pijnappels DA, **Askar SF**, Passier R, Swildens J, Goumans MJ, Schutte CI, De Vries AA, Scherjon S, Mummery CL, Schalij MJ, Atsma DE. *Human embryonic and fetal mesenchymal stem cells differentiate toward three different cardiac lineages in contrast to their adult counterparts*. PLoS One. 2011;6:e24164

Askar SF, Bingen BO, Swildens J, Ypey DL, van der Laarse A, Atsma DE, Zeppenfeld K, Schalij MJ, de Vries AA, Pijnappels DA. *Connexin43 silencing in myofibroblasts prevents arrhythmias in myocardial cultures: Role of maximal diastolic potential.* Cardiovasc Res 2012;93:434-44

Askar SF, Bingen BO, Schalij MJ, Swildens J, Atsma DE, Schutte CI, de Vries AA, Zeppenfeld K, Ypey DL, Pijnappels DA. *Similar Arrhythmicity in Hypertrophic and Fibrotic culures caused by distinct substrate-specific mechanisms.* Cardiovasc Res 2013;97:171-181.

Bingen BO, **Askar SF**, Schalij MJ, Kazbanov IV, Ypey DL, Panfilov AV, Pijnappels DA. *Prolongation of Minimal Action Potential Duration in Sustained Fibrillation Decreases Complexity by transient Destabilization.* Cardiovasc Res 2013;97:161-170.

Askar SF, Ramkisoensing AA. DE Atsma, MJ Schalij, AAF de Vries, DA Pijnappels. *Engraftment patterns of Human Adult Mesenchymal Stem Cells Expose Electrotonic and Paracrine Pro-arrhythmic Mechanisms in Myocardial Cell Cultures.* Circ Arrhythm Electrophysiol 2013;6:380-391.

Piers SR, van Huls van Taxis CF, Tao Q, van der Geest RJ, **Askar SF**, Siebelink HM, Schalij MJ, Zeppenfeld K *Epicardial Substrate Mapping for ventricular tachycardia ablation in patients with non-ischaemic cardiomyopathy: a new algorithm to differentiate between scar and viable myocardium developed by simultaneous integration of computed tomography and contrast-enhanced magnetic resonance imaging.* Eur Heart J 2013;34:586-96.

Bingen BO, Neshati ZN, **Askar SF**, Kazbanov IV, Ypey DL, Panfilov AV, Schalij MJ, de Vries AAF, Pijnappels DA. *Atrium-specific Kir3.x determines inducibility, dynamics and termination of fibrillation by regulating restitution-driven alternans in atrial cardiomyocyte monolayers*. Circulation 2013 in press.

Letters

Bingen BO, **Askar SF**, Schalij MJ, de Vries AA, Pijnappels DA. *Prolongation of minimal action potential duration in sustained fibrillation decreases complexity by transient destabilization: reply*. Cardiovasc Res 2013;98:156-157

Selected peer-reviewed abstracts

Askar SF, AA Ramkisoensing, MJ Schalij, BO Bingen, A van der Laarse, DE Atsma, DL Ypey, DA Pijnappels. *Antiproliferative Treatment of Endogenous Myofibroblasts Prevents Spontaneous Reentrant Tachyarrhythmias in Rat Myocardial Cultures by Limiting Myofibroblast-Induced Depolarization.* Published in Circulation. 2010;122:A16897

Askar SF, Ramkisoensing AA, Schalij MJ, Bingen BO, van der Laarse A, Atsma DE, Ypey DL, Pijnappels DA. *Myofibroblast-associated abnormalities in impulse generation and conduction studied in an in vitro model of cardiac fibrosis*. Published in Europace 2011;13:S3

Askar SF, Bingen BO, Swildens, A van der Laarse, DE Atsma, AAF de Vries, MJ Schalij, DA Pijnappels. *Targeting of heterocellular coupling in fibrotic neonatal rat myocardial cultures by lentiviral connexin43 knockdown is anti-arrhythmic*. Published in Circulation. 2011;124:A13066.

Askar SF, Bingen BO, Swildens, A van der Laarse, DE Atsma, AAF de Vries, MJ Schalij, DA Pijnappels. *Targeting of heterocellular coupling in fibrotic neonatal rat myocardial cultures by lentiviral connexin43 knockdown is anti-arrhythmic*. Published in Eur Heart J 2011;32:930.

Askar SF, Piers SRD, Zeppenfeld K, Schalij MJ, Pijnappels DA. *An in vitro Model of Early- and No-Reperfusion-Scars to Understand Differences in Reentrant Arrhythmia Characteristics and Potential Therapeutic Interventions.* Published in Circulation. 2012;126:A14844

Askar SF, Ramkisoensing AA, Atsma DE, Schalij MJ, de Vries AAF, Pijnappels DA. *Engraftment Characteristics of Human Adult Mesenchymal Stem Cells Expose Electronic and Paracrine Pro-Arrhythmic Mechanisms in Myocardial Cultures.* Published in Circulation. 2012;126:A14805

Askar SF, Bingen BO, Schalij MJ, Neshati ZN, Klautz RJM, de Vries AAF, Pijnappels DA. *Forced cellular fusion of human ventricular scar cells with neonatal rat cardiomyocytes ameliorates their arrhythmicity*. Published in Europace 2013;15:S2-S1

Cellular and Molecular Mechanisms of Arrhythmias in Cardiac Fibrosis and Beyond:
From Symptoms to Substrates towards Solutions

Acknowledgements

Acknowledgements – Dankwoord

Hoewel promoveren in opzet een taak voor één persoon is, wordt deze nooit alleen volbracht. Ik zou iedereen die bij de totstandkoming van dit boekje betrokken is geweest dan ook hartelijk willen bedanken, te beginnen bij iedereen van het laboratorium Experimentele Cardiologie. Daniël, ik heb veel van je mogen leren en altijd kon ik bij je terecht voor discussies ongeacht het tijdstip: bedankt voor de begeleiding, je capaciteit te motiveren, je begrip en doorzettingsvermogen. Twan, de waarde van jouw grote hoeveelheid moleculair biologische kennis wordt slechts overtroffen door je enthousiasme voor wetenschap; ik vind je een groot voorbeeld. Dick, dank voor alle wijsheden en adviezen. Wilbert, dank voor alle interessante discussies. Minka, je bent altijd behulpzaam en vriendelijk geweest, dankjewel. Margreet, dank voor de samenwerking en de gezelligheid. Cindy, je hulp bij veel proeven was onmisbaar, maar de gezelligheid bij het uitvoeren daarvan maakt de samenwerking onvergetelijk.

Aan behulpzame en gezellige collega promovendi is er geen gebrek geweest in het lab. Melina, je wist het lab altijd meer ontspannen achter te laten dan dat je het aantrof. Vanessa, dankjewel voor de gezelligheid. Zeinab and Iolanda, I wish you the best of luck in completing your theses, it was nice working with you. Jim, bedankt voor de moeite die je hebt gestoken in de virale constructen. Arti, dankjewel voor de laboratorium-opvoeding die niet beperkt is gebleven tot het (inmiddels meestal) opruimen van lab-apparatuur, maar zich ook uitte in de mentale steun die je bent geweest tijdens de vele ups en downs van een promotie. Mark, je hebt hart voor de zaak en ik heb er vertrouwen in dat je iets moois maakt van je promotie. Brian, als je middels dit dankwoord moet merken dat ik je waardeer zowel als vriend als collega, heb je niet goed opgelet de laatste paar jaar. Tijdens mijn promotie was zowel je vriendschappelijke als je wetenschappelijke bijdrage van zeer groot belang, ik ben dan ook blij dat je mijn paranimf wilt zijn. Graag wil ik ook alle klinische collega-promovendi bedanken. In het bijzonder Sebastiaan, Gijs, Mihaly, Jeffrey, Maurits en Marieke: zowel de wetenschappelijke discussies als de gezellige congressen waren een verrijking van mijn promotietijd, bedankt!

Zonder de hulp van de afdeling Instrumentele Zaken waren broodnodige nieuwe gereedschappen het ideeën stadium nooit gepasseerd. Alex, Jerry, Michael en Sander bedankt voor jullie inzet. In het bijzonder moet Huybert in het zonnetje worden gezet; ik kon altijd bij je terecht voor allerlei verzoekjes voor nieuwe gadgets en discussies over technologische hoogstandjes. Zonder jou was mijn onderzoek nooit zo voorspoedig gelopen, dankjewel.

Hoewel de meeste tijd is doorgebracht binnen de muren van het LUMC, zijn mensen daarbuiten ook van groot belang geweest tijdens mijn promotieonderzoek. Leden van de BMC; Russ, Kerem, Mariët, Wouter, Brian (deja vu) en Femke: alhoewel onze ambities frequent contact bemoeilijken zijn de etentjes steeds weer gezellig en ik ben dan ook blij dat ik jullie tot mijn vrienden mag rekenen. Navin, onze meetings zorgden altijd voor zeer welkome ontspanning, dankjewel. Tim, nu het boekje af is kunnen we hopelijk vaker afspreken. Marcel, dank voor je inzet bij instrumentele zaken en de altijd gezellige intermezzo's. Tenslotte wil ik graag mijn familie bedanken. Fathy and Tamer, thank you for all your efforts. Youssry, dankjewel voor alle emotionele steun, de wetenschappelijke discussies die we hopelijk nog lang kunnen voeren en dat je mijn paranimf wilt zijn; je bent het beste broertje dat ik me kan wensen. Samira, het is fijn een nieuw zusje erbij te hebben, zeker als ze zo'n mooie omslag voor mijn proefschrift weet te maken, bedankt! Lieve pappa en mamma, bedankt voor alle mentale, emotionele en andere vormen van steun die jullie mij hebben gegeven. Jullie vertrouwen in mijn capaciteiten hebben in grote mate bijgedragen aan mijn eerdere en toekomstige prestaties. Bedankt!

Cellular and Molecular Mechanisms of Arrhythmias in Cardiac Fibrosis and Beyond:
From Symptoms to Substrates towards Solutions

Curriculum Vitae

Curriculum Vitae

Saïd Fathy Abbas Askar was born on March 12th, 1986 in The Hague. In 2004, he graduated from secondary school (IMC, Rijswijk), after which he started his medical studies in Leiden. During the course of the study, he became increasingly interested in cardiovascular subjects as well as basic science. The research internship at the department of Vascular Surgery in Leiden University Medical Center is a prime example of this interest, during which he investigated the presence of an inflammatory component of thoracic aortic aneurysms of Marfan patients. Due to his then discovered affinity with research, Saïd decided to start his PhD traineeship in 2009 under Dr. Daniel Pijnappels and Prof. dr. Martin Schalij, even before finishing his medical studies. The results of his research are described in this thesis. During his research, the author won several awards and prizes. Since januari 2013, the author has resumed his medical studies and will graduate medical school by the end of 2014 while remaining active as a researcher at the Laboratory of Experimental Cardiology in Leiden.

Scientific Awards:

2011: Young Investigator Award at EHRA Europace 2011, Madrid, Spain

2012: Dr. Snellen Poster Prize for best Poster Presentation, Dutch Society of Cardiology congress, Noordwijkerhout, the Netherlands

2012: Best Speaker, NHRA congress, Ermelo, the Netherlands